



PROMOTING ENDOGENOUS REPAIR IN OSTEOCHONDRAL DEFECTS

Exploring therapeutic strategies and the impact of inflammation

M.A. WESDORP

Promoting Endogenous Repair in Osteochondral Defects:

Exploring therapeutic strategies and the impact of inflammation

M.A. Wesdorp

Colophon

ISBN: 978-94-6361-950-9

Cover design: Erwin Timmerman

Layout and printing: Optima Grafische Communicatie, Rotterdam, the Netherlands

© Copyright M.A. Wesdorp, Rotterdam, The Netherlands, 2024

All rights reserved. No part of this thesis may be reproduced, stored in a retrieval system or transmitted in any form or by any means without prior written permission of the author or, when appropriate, of the scientific journal in which parts of this thesis have been published.

The printing of this thesis was financially supported by:

- The department of Orthopaedics and Sports Medicine, Erasmus MC University Medical Center, Rotterdam
- Nederlandse Orthopedische Vereniging (NOV), 's Hertogenbosch
- Erasmus University Rotterdam, Rotterdam
- ABN Amro, Den Haag
- Centrum Orthopedie, Ridderkerk
- Anna Fonds, Leiden
- ChipSoft, Amsterdam
- Medical Delta, Delft

De digitale versie van dit proefschrift is online te vinden via onderstaande QR-code.



Promoting Endogenous Repair in Osteochondral Defects:

Exploring therapeutic strategies and the impact of inflammation

Het bevorderen van endogeen herstel in osteochondrale defecten:
Behandelstrategieën en de impact van ontsteking

Proefschrift

ter verkrijging van de graad van doctor aan de
Erasmus Universiteit Rotterdam
op gezag van de
rector magnificus

Prof. dr. A.L. Bredenoord

en volgens besluit van het College voor Promoties.

De openbare verdediging zal plaatsvinden op
dinsdag 30 januari 2024 om 15:30 uur

door

Marinus Anthonie Wesdorp
geboren te Bergen op Zoom

Promotiecommissie

Promotoren: Prof. dr. G.J.V.M. van Osch
Prof. dr. J.A.N. Verhaar

Overige leden: Prof. dr. C.V.C. Bouten
Prof. dr. R.J.E.M. Dolhain
Prof. dr. H.B.J. Karperien

Copromotor: Dr. R. Narcisi

Voor mijn ouders

CONTENTS

Chapter 1	General introduction, thesis aim and outline	9
Chapter 2	Modulation of inflamed synovium improves migration of mesenchymal stromal cells <i>in vitro</i> through anti-inflammatory macrophages	31
Chapter 3	Intra-articular administration of triamcinolone acetonide in a murine cartilage defect model reduces inflammation but inhibits endogenous cartilage repair	55
Chapter 4	Modulating design parameters to drive cell invasion into hydrogels for osteochondral tissue formation	79
Chapter 5	Effectiveness of BMP-2 and PDGF-BB adsorption onto a collagen/collagen-magnesium-hydroxyapatite scaffold in weight-bearing and non-weight-bearing osteochondral defect bone repair: <i>in vitro</i> , <i>ex vivo</i> and <i>in vivo</i> evaluation	115
Chapter 6	A culture model to analyze the acute biomaterial-dependent reaction of human primary neutrophils <i>in vitro</i>	155
Chapter 7	Discussion	191
Chapter 8	Summary	219
Chapter 9	Nederlandse samenvatting	225
Appendices	List of publications	233
	PhD portfolio	239
	Dankwoord	245
	Curriculum Vitae	253

1

General introduction, thesis aim and outline

INTRODUCTION

Osteochondral defects: clinical challenges and tissue engineering approaches

Osteochondral defects, a focal area of damage which involves both the articular cartilage and the subchondral bone, have long presented a significant clinical challenge. As early as 1743, Hunter recognized the difficulty of treating these defects, stating that “ulcerated cartilage is a troublesome disease; when destroyed, it is not recovered”¹. In 1856, Monro first reported the presence of loose osteochondral bodies in the ankle joint², and in 1888, König coined the term osteochondritis dissecans to describe loose bodies in the knee joint, theorizing that they were caused by spontaneous necrosis of bone or an inflammatory process³. Osteochondral damage can be caused by a variety of causes such as trauma and joint diseases like osteochondritis dissecans (OCD), and is a major contributor to disability in the aging population, resulting in a corresponding increase in economic burden worldwide⁴. The incidence of articular cartilage defects is high, with rates of 19-40% in knee arthroscopies and more than 60% in patients with a meniscus tear and anterior cruciate ligament rupture⁵⁻⁸. Between 1996 and 2011, the incidence of these defects nearly tripled⁹. Untreated articular cartilage defects have been identified as a risk factor for the development of early-onset osteoarthritis^{10,11}. Osteoarthritis is a degenerative joint disease characterized by the breakdown of cartilage, the formation of osteophytes, and inflammation of the surrounding tissues¹².

The osteochondral unit is made up of articular cartilage, calcified cartilage, and subchondral bone¹³. The non-calcified cartilage layer can be divided into three zones based on the morphology and orientation of chondrocytes. These layers include the superficial zone (top 10-20%), the middle zone (next 40-50%), and the deep zone (last 30-40%). The cartilage serves as a low-friction surface and acts as a shock absorber to reduce the forces on the subchondral bone^{14,15}. Articular cartilage is an unusual tissue because the cells, called chondrocytes, make up only 1-2% of the total volume and are dispersed in a dense extracellular matrix (ECM) without blood vessels or nerves¹⁶. The ECM is made up of collagen fibers and proteoglycan (mainly aggrecan), which is composed of a core protein and hydrophilic glycosaminoglycan side chains. These components help the tissue retain water, giving it resilience under compression¹⁷. The ECM also contains small amounts of other proteins, such as lubricin, which helps the tissue move smoothly. Tissue engineering approaches aim to recreate this layered structure to repair damaged tissue, but it is not yet clear if this is necessary in the early stages of repair¹⁸.

Located beneath the non-calcified cartilage there is the calcified cartilage layer, a mineralized transition zone that acts as a stress buffer between the stiffer bone and cartilage, transmitting force and limiting diffusion to the deeper cartilage layer ¹⁹. The subchondral bone, situated under the calcified cartilage, plays a vital role in mechanical support ²⁰. It also consists of the subchondral bone plate, which is formed by bony lamella that separate the cartilage from the marrow cavity. These lamella converge underneath into the subarticular spongiosa region, which is made up of porous trabecular bone containing blood vessels and innervation ²¹. Recognizing the subchondral bone as an integral part of the tissue to be repaired provides several advantages, as it is closely intertwined with the overlying cartilage to form a functional unit. This approach is important because unlike cartilage tissue, the subchondral bone is rich in osteochondral progenitor cells within the bone marrow and has a good nutrient supply thanks to its vascular system, which can naturally provide the required nutrients.

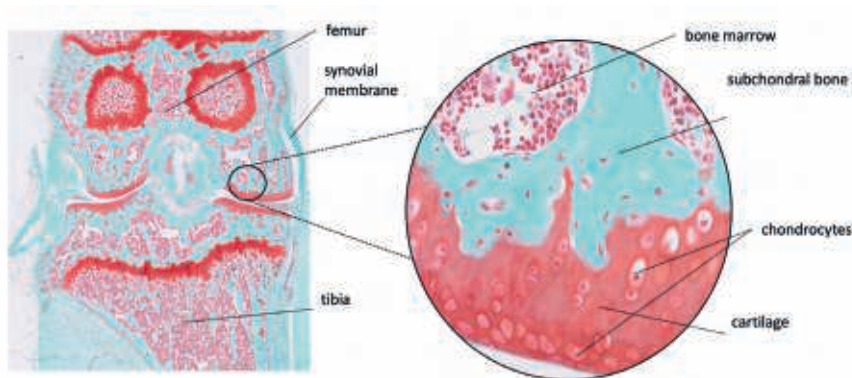


Figure 1. An overview of the osteochondral unit in a mouse knee. Left the representation of the knee joint containing the femur, tibia and synovial membrane. Right a zoomed in section of the knee joint showing the composition of the osteochondral unit that consists of the cartilage layer and subchondral bone. A safranin-O staining representing the cartilage in red and bone in light blue.

Exploring options for osteochondral repair: current approaches and their challenges

Osteochondral defects are a significant clinical challenge in the field of orthopedics, as they can cause pain and lead to the development of early-onset osteoarthritis if left untreated. In order to repair osteochondral defects, various treatment methods have been developed. One approach to repair is the use of bone marrow stimulation techniques such as microfracture, which creates access to the bone marrow and allows for the migration of bone marrow-derived Mesenchymal Stromal Cells (MSC) to the site of the defect ²². MSC migration is an important step in the repair process,

as MSCs must first migrate to the site of the defect before they can begin the process of cartilage formation ²³. MSCs have the ability to differentiate into cells from the adipogenic, osteogenic, and chondrogenic lineages, making it a potential cell source for osteochondral repair ²⁴. However, a drawback of this method is that the newly formed tissue often consists of fibrocartilage, which has inferior mechanical and biological properties compared to native cartilage ²⁵. It appears difficult to regenerate hyaline cartilage through bone marrow stimulation. Another challenge in using the osteochondral approach to repair joints involve the regeneration of two different tissue types, bone and cartilage. Ensuring that these tissue types remain separate and preventing endochondral ossification in the cartilage layer are crucial aspects of this approach. There is a need to regenerate more durable osteochondral tissue.

Another approach to osteochondral repair is the transplantation of (multiple) osteochondral plugs. Osteochondral autograft transfer system (OATS) and osteochondral allograft transplantation are used to repair damaged cartilage and bone in joints. In OATS, a small plug of healthy cartilage and bone is transferred from a non-weight bearing area of the joint to the damaged area ²⁶. In osteochondral allograft transplantation, healthy cartilage and bone from a donor is transplanted to the damaged area ²⁷. One of the main challenges in osteochondral transplantation is the difficulty in achieving long-term integration of the transplanted tissue with the surrounding host tissue ²⁸. Another challenge is the variation in thickness of the cartilage that differs based on the location in the joint. This can all lead to a lack of stability and functional improvement in the affected joint. The migration of MSCs and chondrocytes from the surrounding host tissue into the osteochondral transplant can contribute to the stability and functional improvement of the transplanted tissue.

A third approach is the use of cell-based therapies, which involve the transplantation of cells into the site of the defect. These cells can be autologous (derived from the patient) or allogeneic (derived from a donor) and can include chondrocytes or MSCs. Autologous chondrocyte implantation (ACI) is a common treatment modality that involves the removal of healthy cartilage from a non-weight bearing area of the joint, followed by the isolation and multiplication of chondrocytes in a laboratory ²⁹. These chondrocytes are then implanted into the damaged area. Matrix-induced autologous chondrocyte implantation (MACI) is a further development of ACI, in which the isolated chondrocytes are embedded in a biocompatible matrix before being implanted into the damaged area. ACI and MACI require a two-step surgical procedure involving the isolation, expansion, and reimplantation of cells under a periosteal flap or scaffold, while subchondral drilling and transplantation can be performed in a single step procedure. Furthermore, cell-based and transplantation therapies can

be costly and face regulatory issues ³⁰. In contrast, these issues are avoided with techniques that do not require the harvesting of autologous cells or tissues.

One of the main goals in osteochondral repair is to stimulate the body's natural healing abilities in order to restore native tissue properties. While current approaches such as microfracture and autologous matrix-induced chondrogenesis have shown some success in stimulating the body's own cells to regenerate damaged tissue ^{31,32}, there is still a need to explore new and more effective options for promoting regeneration and repair of osteochondral tissue. Regenerative medicine and tissue engineering are promising fields that may provide alternative or additional approaches for repairing damaged osteochondral tissue. The experts in cartilage repair share the common belief that the future of cartilage repair lies in the use of single-stage procedures using autologous chondrogenic cells ³³. In this context, understanding and promoting the migration of the body's own cells to the site of the defect is a key aspect for the success of cartilage repair procedures.

Inflammation and osteochondral defects: a complex interplay in tissue repair

In joints affected by osteochondral defects, elevated levels of pro-inflammatory cytokines such as TNF- α , IL-1, and IL-6 have been found in the synovial fluid ³⁴⁻³⁶. Inflammatory cytokines have been identified as crucial regulators of the chemotactic migration and homing of MSCs towards sites of injury ^{37,38}. Nevertheless, these mediators can have a detrimental effect on tissue repair, and their presence can be exacerbated by surgical interventions ³⁹. The precise mechanisms by which inflammation impacts cartilage repair are not fully understood. It is known that inflammation is a necessary step in the wound healing process and that the absence of pro-inflammatory mediators have been shown to impede bone healing ⁴⁰. However, it is crucial for the inflammatory response to be resolved in order to prevent negative effects such as impaired wound healing and scar formation ⁴¹. Treatment of older cartilage defects, which tend to be associated with a more chronic inflammatory state, results in a poorer quality repair tissue ^{42,43}. These findings suggest that inflammation is initially required for tissue repair, but its resolution or reduction is necessary for optimal repair to occur.

The synovial membrane, also referred to as synovium, is a highly vascularized lining of the joint that produces synovial fluid that lubricates and nourishes the cartilage. It plays a critical role in inflammation and wound healing in injured or osteoarthritic joints ^{44,45}. Under normal conditions, the synovium of a healthy joint comprises macrophages and synovial fibroblasts. However, during joint inflammation, other immune cells such

as neutrophils, T cells, and dendritic cells, can infiltrate the synovium ⁴⁶. Neutrophils and macrophages are key players in inflammation and wound healing ⁴⁷. Neutrophils, which are also known as polymorphonuclear leukocytes (PMN), are the most abundant immune cells in the human body. They are the first responders to a site of injury and initiate the inflammatory response through the secretion of chemokines, reactive oxygen species (ROS), and neutrophil extracellular traps (NETs) ⁴⁸⁻⁵¹. Later on, recruitment and differentiation of monocytes and macrophages occur ⁵². In the field of tissue engineering, macrophages have attracted significant attention because of their contribution to tissue repair and regeneration ⁵³. These cells can adapt their phenotype depending on the microenvironment, polarizing to pro-inflammatory-, repair-, or anti-inflammatory macrophages ⁵⁴. It has been demonstrated that the presence of pro-inflammatory macrophages can negatively impact the process of chondrogenesis ⁵⁵. Moreover, *in vitro* models of chondrogenesis have indicated that the addition of pro-inflammatory factors can impede the formation of cartilage tissue ⁵⁶. In contrast, the presence of anti-inflammatory macrophages, those with a repair-promoting phenotype, and anti-inflammatory factors, such as transforming growth factor beta (TGF-beta) and corticosteroids, have been shown to stimulate chondrogenesis in *in vitro* studies ⁵⁶⁻⁵⁹. As a potential therapeutic option for osteochondral defect repair, inhibition or reduction of inflammation may improve cartilage repair, however, it is unknown whether this would affect the migration of MSCs to the defect site in the early phase of the repair process. A better understanding of the role of inflammation in osteochondral repair might lead to the development of more effective treatments.

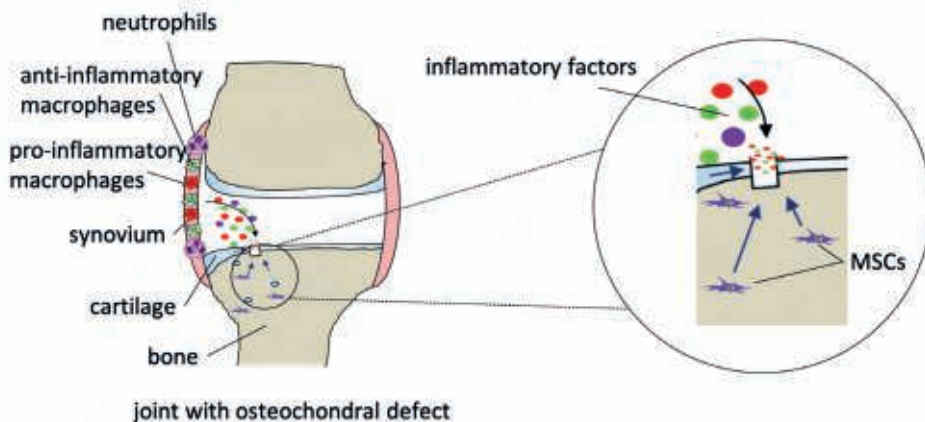


Figure 2. A schematic overview of inflammation in osteochondral defect repair. On the left is shown some of the inflammatory cells (macrophages in red and green, neutrophils in purple) in the synovium that secrete inflammatory factors into the joint and eventual repair environment. Right is a zoomed in image of the defect with MSCs migrating towards the defect and the local presence of the inflammatory factors that might influence this process.

Anti-inflammatory drugs, such as corticosteroids, are widely used clinically to reduce inflammation ⁶⁰. The corticosteroid triamcinolone acetonide (TAA) is frequently used to reduce the symptoms of osteoarthritis (OA) ⁶¹. However, the potential catabolic effects of TAA on cartilage remain a topic of ongoing debate and ongoing research. Clinical studies have yielded conflicting results, with some finding no detrimental effects of TAA on radiologic progression of joint space narrowing after 2 years ⁶², while others have reported greater cartilage volume loss in patients treated with TAA ⁶³. A systematic review that combined clinical, *in vitro*, and *in vivo* studies, suggested that the effects of corticosteroids on articular cartilage are time- and dose-dependent, with low doses and short durations showing a beneficial effect while higher doses and longer durations were associated with detrimental effects ⁶⁴. Furthermore, animal and *in vitro* studies have raised concerns about the use of TAA ^{65,66}, with some studies finding an increase in degenerative changes in response to TAA ⁶⁷, while others reported favorable effects ⁶⁸. These contradictions underscore the need for further research to understand under which conditions TAA may be beneficial or harmful for cartilage repair. The increasing interest in the use of anti-inflammatory drugs immediately after various intra-articular pathologies is driven by the potential to reduce joint inflammation and mitigate long-term effects such as post-traumatic osteoarthritis ^{69,70}. Despite extensive research on the effects of anti-inflammatory medication on the synovium, cartilage, and bone, the impact on the migration of repair cells remains an area of ongoing investigation and further clarification is needed ^{71,72}.

Biomaterial-guided tissue healing in osteochondral repair: navigating challenges in cell migration

The utilization of biomaterials for guiding tissue healing in cartilage repair is a promising strategy ⁷³. This approach leverages the use of a matrix to promote growth and tissue formation, which should lead to improved mechanical properties and increased structural integrity of the repaired tissue. Commercially available biomaterials have been used in a variety of clinical applications, including cardiovascular devices and orthopedic implants ^{74,75}. When biomaterials were first introduced, the focus was on the *replacement* of human tissue or function without inciting adverse reactions. Over time the focus shifted to the application of biomaterials to *repair* diseased or damaged tissue ⁷⁶. The ultimate goal of biomaterial-guided tissue healing is the development of biomaterials that can effectively mobilize the body's own cells and stimulate regenerative processes to achieve functional healing.

Biomaterials play multiple roles in tissue engineering, including serving as templates for stem cells to form new tissue. They provide temporary mechanical support,

promote cell adhesion, proliferation, and differentiation, and help control the size and shape of regenerated tissue ⁷⁷. Biomaterials can also present physical and chemical signals that accurately modulate cell function and guide tissue regeneration ⁷⁸. The design of these materials is based on the recognition that mimicking the extracellular matrix's structural, mechanical, and biochemical properties will encourage niche cells to behave like their *in vivo* counterparts ⁷⁹. Ideally, a scaffold should be a temporary structure that is degraded or reabsorbed in a controlled manner as new tissue regrows ⁸⁰. Biomaterial templates can influence cell behavior and function and positively affect desired tissue formation. Now and in the past several commercially available scaffolds such as TruFit® BGS Plugs (Smith & Nephew), MaioRegen (FinceraMica) and Agili-C™ (CartiHeal) have been used in clinics. However, limited success was reported as none of these scaffolds have achieved satisfactory durable clinical results and the TruFit® was even withdrawn from the market for the questionable results ⁸¹. This highlights the importance of exploring new templates for osteochondral tissue engineering.

Hydrogels have been investigated as a potential to provide this template and are a class of biomaterials that can be a suitable option for minimal invasive filling of complex defects ^{82,83}. Despite substantial *in vitro* research on the chondrogenic properties of hydrogels, these biomaterials have demonstrated a tendency to fail upon implantation *in vivo*. This failure is often attributed to challenges in maintaining the position of the material within the defect because of insufficient fixation, which hinders integration and limits the potential for cellular invasion ⁸⁴. Integration of the biomaterial into the surrounding tissue is primarily achieved through infiltration of host cells and subsequent matrix deposition ⁸⁵. As such, cell migration plays a crucial role in the early phase of an integrative defect repair strategy ⁸⁶. This concept applies not only to acellular treatment approaches but also to cell-based or tissue engineering repair strategies in which cells are encapsulated within a hydrogel ⁸⁷. In these cases, migration of cells (from the host or the implant) is necessary for integration of the repair tissue to the host tissue via matrix deposition ⁸⁸. This underscores the importance of understanding how to enhance cell migration into hydrogels to improve functional tissue repair.

Hydrogels are often composed of components derived from connective tissue such as collagen or glycosaminoglycan. Collagen and hyaluronic acid-based hydrogels, such as gelatin methacryloyl (GelMA), norbornene hyaluronic acid (norHA), and Tyramine functionalized HA (THA), have attracted attention for their potential use in cartilage tissue engineering and for the treatment of osteochondral defects ⁸⁹. These hydrogel biomaterials possess chondrogenic potential, making them well-suited for cartilage

repair⁹⁰⁻⁹³. However, these materials have shown limited cell migration into the gel^{94,95}, which has hindered their clinical success for cell free use in tissue repair. In an effort to address this limitation, several strategies have been developed. One such strategy involves changing the crosslinking density of the gel⁹⁶. The degree of functionalization (number of crosslinks formed) of a material, has been found to impact its ability to support capillary-like network formation in endothelial cells⁹⁷. Another strategy is to use a degradable crosslinker, specifically a matrix metalloproteinase (MMP) cleavable crosslinker, which would enable degradation of the material and has indeed been shown to promote migration of MSCs embedded in a hydrogel⁹⁸. A third strategy is to add cell adhesion sites to the hydrogel, which can be achieved by incorporating collagen or their RGD sites that cells use to adhere to, into hyaluronan-based hydrogels⁹⁹⁻¹⁰¹. Despite these efforts, it is still not entirely clear which physicochemical properties and modifications of hydrogels are most effective for improving cell migration for the repair of osteochondral defects. This is in part due to the fact that most studies have focused on a single material or modification, and different groups use different models for their studies. More research is necessary to fully understand the factors that promote effective cell migration and hydrogel integration for osteochondral repair.

Another promising template is a prefabricated scaffold, which can be engineered to induce specific cellular responses by incorporating biochemical signals that promote cell ingrowth⁸⁶. This can be achieved by encapsulating chemical attractants and growth factors for sustained release, to enhance cell migration and/or to influence matrix deposition. Fibroblasts, endothelial cells, MSCs, and chondrocytes can migrate towards a variety of biomolecules including bone morphogenetic protein 2 (BMP-2) and platelet-derived growth factor BB (PDGF-BB)^{102,103}. Therefore, it may be advantageous to adsorb BMP-2 and/or PDGF-BB onto scaffolds to improve cell migration and enhance the success of strategies for repairing osteochondral defects. This approach, of using chemical attractants and growth factors to induce migration of cells to scaffold material, could be a viable strategy in osteochondral repair.

Understanding the immune response to biomaterials

The outcome of biomaterial-guided tissue repair is closely tied to the body's innate immune response, as biomaterials are initially recognized as foreign bodies¹⁰⁴. Biomaterials have been observed to elicit a wide range of responses, with various design factors that can modulate this response to foster functional tissue healing or regeneration¹⁰⁵. Following implantation, the biomaterial comes into contact with blood and tissue, and proteins from the blood stick to the surface of the biomaterial,

which activates the innate immune system. These coating proteins mediate the material's interaction with the host's immune system, particularly in recruiting neutrophils¹⁰⁴. The early inflammatory response in biomaterial-mediated tissue repair is characterized by a peak in neutrophil recruitment within the first 24-48 hours post-implantation. Subsequent stages, including monocyte and macrophage recruitment and differentiation, occur at later timepoints⁵². Macrophages have been the subject of considerable attention in the field of biomaterial-guided tissue repair, particularly regarding their role in tissue healing⁵³. However, the number of macrophages correlates with the levels of neutrophils present, indicating that neutrophils are important in the recruitment of macrophages and subsequent stages of the wound healing response¹⁰⁶. Furthermore, neutrophils play an important role in the transition from pro-inflammatory to anti-inflammatory macrophages and the resolution of inflammation¹⁰⁷. This highlights the need of better understanding of the role of neutrophils in biomaterial-guided tissue regeneration, and the potential for targeting these cells in order to achieve successful repair.

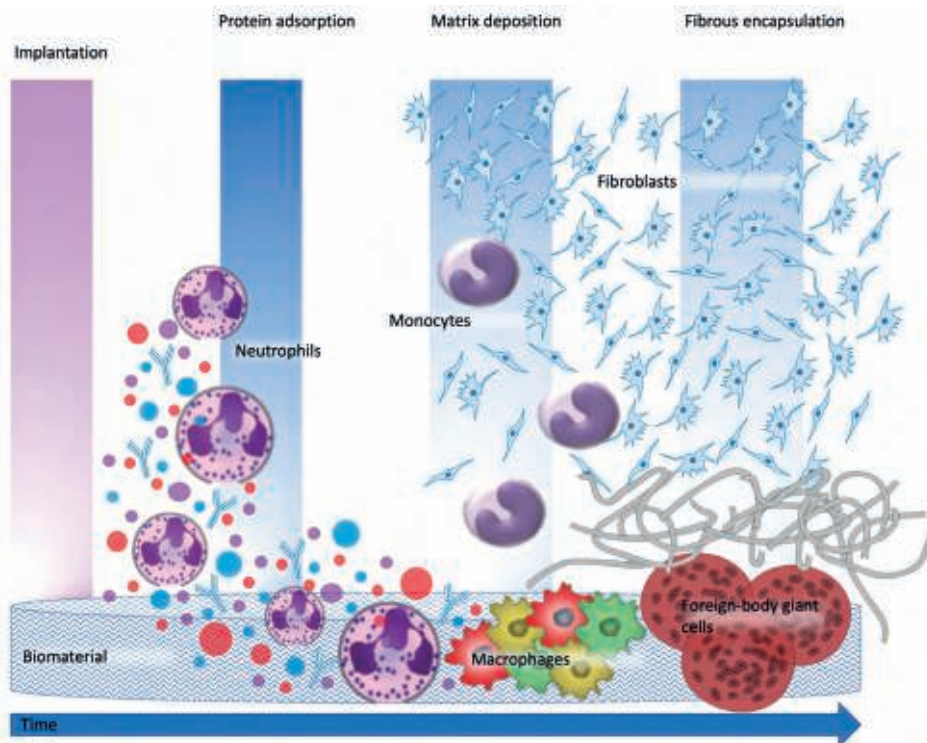


Figure 3. A schematic representation of the immune response to biomaterials. Neutrophils are first recruited to the implantation site, then monocytes are recruited and differentiate into different macrophage phenotypes. Neutrophils play a role in this polarization into different macrophage phenotypes.

Aim and outline of the thesis

This thesis focuses on the use of an endogenous approach to stimulate repair of osteochondral defects. In order to achieve successful repair of the defect, it is important for mesenchymal stromal cells (MSCs) to migrate to the defect area (or, in the case of a biomaterial-assisted approach, into the scaffold) and deposit extracellular matrix (ECM). However, the inflammatory environment present at the defect site influences MSC migration and ECM synthesis. Biomaterials, which provide a scaffold for MSC migration and ECM deposition, can also affect the repair process through the induction of an inflammatory response. Understanding the relationship between MSC migration, inflammation, and biomaterials is crucial for the optimization of endogenous repair strategies.

In **Chapter 2**, we investigate how synovial inflammation, which is often present in osteochondral defects, influences the migration of bone marrow-derived MSCs and whether modulating inflammation can improve migration using human *in vitro* models. We specifically aim to identify the role of macrophages in MSC migration. Overall, with this knowledge, we evaluate the potential of incorporating inflammation modulation into current and future techniques for osteochondral defect repair. In **Chapter 3**, we assess the effect of using a corticosteroid as modulator of inflammation to improve osteochondral repair in a mouse model.

The use of a biomaterial, such as a hydrogel or a scaffold as a support for MSC migration and matrix deposition, can enhance endogenous repair of osteochondral defects. However, the introduction of such a “foreign body” can also trigger an inflammatory response, which can influence MSC migration and the repair process. In **Chapter 4**, we study the effect of different hydrogel modifications to enhance cell migration and tissue formation using a range of *in vitro*, *ex vivo*, and *in vivo* experiments. To further improve cell migration into a biomaterial a chemoattractant or growth factor can be used. In **Chapter 5**, we use a clinically applied porous scaffold and investigate the effect of adding platelet-derived growth factor (PDGF) and bone morphogenetic protein 2 (BMP2) to this scaffold on MSC migration and tissue formation using different *ex vivo* and *in vivo* models.

In addition, we examine the inflammatory response triggered by the implantation of this scaffold. In the inflammatory response caused by a foreign body, such as a hydrogel or scaffold, both macrophages and neutrophils play an important role. While macrophages are known to recognize and phagocytose foreign materials, as well as produce pro-inflammatory cytokines and growth factors, neutrophils have a key role in transitioning from a pro-inflammatory to an anti-inflammatory/repair

microenvironment. Since our understanding of the effect of biomaterials on the functions and regulation of neutrophils is limited, in **Chapter 6**, we evaluate the neutrophil response to various biomaterials that can be used for osteochondral repair using multiple *in vitro* assays to comprehensively assess the main neutrophil functions.

This thesis concludes with **Chapter 7**, which discusses the broader implications of our findings and consider future directions for improving osteochondral defect repair using biomaterials through the rational control of inflammation. **Chapter 8 and 9** contain a summary in English and Dutch.

REFERENCES

1. Hunter W. Of the structure and disease of articulating cartilages. 1743. *Clin Orthop Relat Res.* 1995(317):3-6.
2. Monro A. Part of the cartilage of the joint, separated and ossified. . *Eddinburgh: Ruddimans.* 1856:236.
3. König. Ueber freie Körper in den Gelenken. *Deutsche Zeitschrift f Chirurgie.* 27(1-2):90-109.
4. Martín AR, Patel JM, Zlotnick HM, Carey JL, Mauck RL. Emerging therapies for cartilage regeneration in currently excluded ‘red knee’populations. *NPJ Regenerative medicine.* 2019;4(1):1-11.
5. Aroen A, Loken S, Heir S, Alvik E, Ekeland A, Granlund OG, Engebretsen L. Articular cartilage lesions in 993 consecutive knee arthroscopies. *The American journal of sports medicine.* 2004;32(1):211-215.
6. Curl WW, Krome J, Gordon ES, Rushing J, Smith BP, Poehling GG. Cartilage injuries: A review of 31,516 knee arthroscopies. *Arthroscopy.* 1997;13(4):456-460.
7. Hjellev K, Solheim E, Strand T, Muri R, Brittberg M. Articular cartilage defects in 1,000 knee arthroscopies. *Arthroscopy.* 2002;18(7):730-734.
8. Widuchowski W, Widuchowski J, Trzaska T. Articular cartilage defects: study of 25,124 knee arthroscopies. *Knee.* 2007;14(3):177-182.
9. Mor A, Grijsa M, Nørgaard M, Munthe J, Lind M, Déruaz A, Pedersen A. Trends in arthroscopy-documented cartilage injuries of the knee and repair procedures among 15-60-year-old patients. *Scandinavian Journal of Medicine & Science in Sports.* 2015;25(4):e400-e407.
10. Cicuttini F, Ding C, Wluka A, Davis S, Ebeling PR, Jones G. Association of cartilage defects with loss of knee cartilage in healthy, middle-age adults: a prospective study. *Arthritis and rheumatism.* 2005;52(7):2033-2039.
11. Sowers M, Karvonen-Gutierrez CA, Jacobson JA, Jiang Y, Yosef M. Associations of anatomical measures from MRI with radiographically defined knee osteoarthritis score, pain, and physical functioning. *J Bone Joint Surg Am.* 2011;93(3):241-251.
12. Loeser RF, Goldring SR, Scanzello CR, Goldring MB. Osteoarthritis: a disease of the joint as an organ. *Arthritis and rheumatism.* 2012;64(6):1697.
13. Gomoll AH, Madry H, Knutsen G, van Dijk N, Seil R, Brittberg M, Kon E. The subchondral bone in articular cartilage repair: current problems in the surgical management. *Knee surgery, sports traumatology, arthroscopy : official journal of the ESSKA.* 2010;18(4):434-447.
14. Buckwalter JA, Mankin HJ. Instructional Course Lectures, The American Academy of Orthopaedic Surgeons - Articular Cartilage. Part I: Tissue Design and Chondrocyte-Matrix Interactions*†. *JBJS.* 1997;79(4):600-611.
15. Buckwalter JA, Mankin HJ. Instructional Course Lectures, The American Academy of Orthopaedic Surgeons - Articular Cartilage. Part II: Degeneration and Osteoarthritis, Repair, Regeneration, and Transplantation*†. *JBJS.* 1997;79(4):612-632.
16. Eyre D. Collagen of articular cartilage. *Arthritis Res.* 2002;4(1):30-35.

17. Buckwalter JA. Articular cartilage: injuries and potential for healing. *J Orthop Sports Phys Ther.* 1998;28(4):192-202.
18. Schuurman W, Klein T, Dhert W, Van Weeren P, Hutmacher D, Malda J. Cartilage regeneration using zonal chondrocyte subpopulations: a promising approach or an overcomplicated strategy? *Journal of tissue engineering and regenerative medicine.* 2015;9(6):669-678.
19. Oegema TR, Jr., Carpenter RJ, Hofmeister F, Thompson RC, Jr. The interaction of the zone of calcified cartilage and subchondral bone in osteoarthritis. *Microsc Res Tech.* 1997;37(4):324-332.
20. Goldring SR, Goldring MB. Changes in the osteochondral unit during osteoarthritis: structure, function and cartilage-bone crosstalk. *Nat Rev Rheumatol.* 2016;12(11):632-644.
21. Oláh T, Madry H. The Osteochondral Unit: The Importance of the Underlying Subchondral Bone. In: Farr J, Gomoll AH, eds. *Cartilage Restoration: Practical Clinical Applications.* Cham: Springer International Publishing; 2018:13-22.
22. Steinwachs M, Guggi T, Kreuz P. Marrow stimulation techniques. *Injury.* 2008;39(1):26-31.
23. Caplan AL. Mesenchymal stem cells. *J Orthop Res.* 1991;9(5):641-650.
24. Arthur A, Zannettino A, Gronthos S. The therapeutic applications of multipotential mesenchymal/stromal stem cells in skeletal tissue repair. *Journal of cellular physiology.* 2009;218(2):237-245.
25. Dai L, He Z, Zhang X, Hu X, Yuan L, Qiang M, Zhu J, Shao Z, Zhou C, Ao Y. One-step repair for cartilage defects in a rabbit model: a technique combining the perforated decalcified cortical-cancellous bone matrix scaffold with microfracture. *Am J Sports Med.* 2014;42(3):583-591.
26. Hangody L, Kish G, Karpati Z, Szerb I, Udvarhelyi I. Arthroscopic autogenous osteochondral mosaicplasty for the treatment of femoral condylar articular defects A preliminary report. *Knee Surgery, Sports Traumatology, Arthroscopy.* 1997;5(4):262-267.
27. Bugbee WD, Convery FR. Osteochondral allograft transplantation. *Clinics in sports medicine.* 1999;18(1):67-75.
28. Mollon B, Kandel R, Chahal J, Theodoropoulos J. The clinical status of cartilage tissue regeneration in humans. *Osteoarthritis and Cartilage.* 2013;21(12):1824-1833.
29. Brittberg M, Lindahl A, Nilsson A, Ohlsson C, Isaksson O, Peterson L. Treatment of deep cartilage defects in the knee with autologous chondrocyte transplantation. *New england journal of medicine.* 1994;331(14):889-895.
30. Krych AJ, Gobbi A, Lattermann C, Nakamura N. Articular cartilage solutions for the knee: present challenges and future direction. *Journal of ISAKOS.* 2016;1(2):93-104.
31. Vanlauwe J, Saris DB, Victor J, Almqvist KF, Bellemans J, Luyten FP, TIG/ACT/01/, Group ES. Five-year outcome of characterized chondrocyte implantation versus microfracture for symptomatic cartilage defects of the knee: early treatment matters. *The American journal of sports medicine.* 2011;39(12):2566-2574.
32. Kraeutler MJ, Belk JW, Purcell JM, McCarty EC. Microfracture Versus Autologous Chondrocyte Implantation for Articular Cartilage Lesions in the Knee: A Systematic Review of 5-Year Outcomes. *Am J Sports Med.* 2018;46(4):995-999.

33. Brittberg M. New frontiers for cartilage repair, joint preservation and prevention. *Journal of Cartilage & Joint Preservation*. 2022;2(2):100060.
34. Swärd P, Frobell R, Englund M, Roos H, Struglics A. Cartilage and bone markers and inflammatory cytokines are increased in synovial fluid in the acute phase of knee injury (hemarthrosis)-a cross-sectional analysis. *Osteoarthritis and cartilage*. 2012;20(11):1302-1308.
35. Sward P, Struglics A, Englund M, Roos HP, Frobell RB. Soft tissue knee injury with concomitant osteochondral fracture is associated with higher degree of acute joint inflammation. *The American journal of sports medicine*. 2014;42(5):1096-1102.
36. Tsuchida AI, Beekhuizen M, t Hart MC, Radstake TR, Dhert WJ, Saris DB, van Osch GJ, Creemers LB. Cytokine profiles in the joint depend on pathology, but are different between synovial fluid, cartilage tissue and cultured chondrocytes. *Arthritis research & therapy*. 2014;16(5):441.
37. Zhang S, Hu B, Liu W, Wang P, Lv X, Chen S, Liu H, Shao Z. Articular cartilage regeneration: The role of endogenous mesenchymal stem/progenitor cell recruitment and migration. *Seminars in Arthritis and Rheumatism*. 2020;50(2):198-208.
38. Su P, Tian Y, Yang C, Ma X, Wang X, Pei J, Qian A. Mesenchymal Stem Cell Migration during Bone Formation and Bone Diseases Therapy. *Int J Mol Sci*. 2018;19(8).
39. Yang KG, Saris DB, Verbout AJ, Creemers LB, Dhert WJ. The effect of synovial fluid from injured knee joints on in vitro chondrogenesis. *Tissue engineering*. 2006;12(10):2957-2964.
40. van der Kraan PM. The Interaction between Joint Inflammation and Cartilage Repair. *Tissue Engineering and Regenerative Medicine*. 2019;16(4):327-334.
41. Eming SA, Krieg T, Davidson JM. Inflammation in wound repair: molecular and cellular mechanisms. *Journal of Investigative Dermatology*. 2007;127(3):514-525.
42. Saris D, Dhert WJ, Verbout A. Joint homeostasis: the discrepancy between old and fresh defects in cartilage repair. *The Journal of bone and joint surgery British volume*. 2003;85(7):1067-1076.
43. Rodrigo JJ, Steadman JR, Syftestad G, Benton H, Silliman J. Effects of human knee synovial fluid on chondrogenesis in vitro. *The American journal of knee surgery*. 1995;8(4):124-129.
44. Smith MD. Suppl 1: the normal synovium. *The open rheumatology journal*. 2011;5:100.
45. Sellam J, Berenbaum F. The role of synovitis in pathophysiology and clinical symptoms of osteoarthritis. *Nature Reviews Rheumatology*. 2010;6(11):625.
46. Asif Amin M, Fox DA, Ruth JH. Synovial cellular and molecular markers in rheumatoid arthritis. *Semin Immunopathol*. 2017;39(4):385-393.
47. Fernandes TL, Gomoll AH, Lattermann C, Hernandez AJ, Bueno DF, Amano MT. Macrophage: A Potential Target on Cartilage Regeneration. *Front Immunol*. 2020;11:111.
48. Summers C, Rankin SM, Condliffe AM, Singh N, Peters AM, Chilvers ER. Neutrophil kinetics in health and disease. *Trends Immunol*. 2010;31(8):318-324.

49. Wright HL, Lyon M, Chapman EA, Moots RJ, Edwards SW. Rheumatoid Arthritis Synovial Fluid Neutrophils Drive Inflammation Through Production of Chemokines, Reactive Oxygen Species, and Neutrophil Extracellular Traps. *Front Immunol.* 2020;11:584116.
50. Fetz AE, Radic MZ, Bowlin GL. Neutrophils in Biomaterial-Guided Tissue Regeneration: Matrix Reprogramming for Angiogenesis. *Tissue Eng Part B Rev.* 2021;27(2):95-106.
51. Toumi H, F'Guyer S, Best TM. The role of neutrophils in injury and repair following muscle stretch. *J Anat.* 2006;208(4):459-470.
52. Franz S, Rammelt S, Scharnweber D, Simon JC. Immune responses to implants-a review of the implications for the design of immunomodulatory biomaterials. *Biomaterials.* 2011;32(28):6692-6709.
53. Sridharan R, Cameron AR, Kelly DJ, Kearney CJ, O'Brien FJ. Biomaterial based modulation of macrophage polarization: a review and suggested design principles. *Materials Today.* 2015;18(6):313-325.
54. Park JE, Barbul A. Understanding the role of immune regulation in wound healing. *Am J Surg.* 2004;187(5a):11s-16s.
55. Sesia SB, Duhr R, Medeiros da Cunha C, Todorov A, Schaeren S, Padovan E, Spagnoli G, Martin I, Barbero A. Anti-inflammatory/tissue repair macrophages enhance the cartilage-forming capacity of human bone marrow-derived mesenchymal stromal cells. *J Cell Physiol.* 2015;230(6):1258-1269.
56. Heldens GT, Blaney Davidson EN, Vitters EL, Schreurs BW, Piek E, van den Berg WB, van der Kraan PM. Catabolic factors and osteoarthritis-conditioned medium inhibit chondrogenesis of human mesenchymal stem cells. *Tissue Eng Part A.* 2012;18(1-2):45-54.
57. Fahy N, de Vries-van Melle ML, Lehmann J, Wei W, Grotenhuis N, Farrell E, van der Kraan PM, Murphy JM, Bastiaansen-Jenniskens YM, van Osch GJ. Human osteoarthritic synovium impacts chondrogenic differentiation of mesenchymal stem cells via macrophage polarisation state. *Osteoarthritis Cartilage.* 2014;22(8):1167-1175.
58. Derfoul A, Perkins GL, Hall DJ, Tuan RS. Glucocorticoids promote chondrogenic differentiation of adult human mesenchymal stem cells by enhancing expression of cartilage extracellular matrix genes. *Stem cells.* 2006;24(6):1487-1495.
59. Johnstone B, Hering TM, Caplan AI, Goldberg VM, Yoo JU. In vitro chondrogenesis of bone marrow-derived mesenchymal progenitor cells. *Experimental cell research.* 1998;238(1):265-272.
60. Barnes PJ. Anti-inflammatory actions of glucocorticoids: molecular mechanisms. *Clin Sci (Lond).* 1998;94(6):557-572.
61. Bannuru RR, Schmid CH, Kent DM, Vaysbrot EE, Wong JB, McAlindon TE. Comparative effectiveness of pharmacologic interventions for knee osteoarthritis: a systematic review and network meta-analysis. *Ann Intern Med.* 2015;162(1):46-54.
62. Raynauld JP, Buckland-Wright C, Ward R, Choquette D, Haraoui B, Martel-Pelletier J, Uthman I, Khy V, Tremblay JL, Bertrand C, Pelletier JP. Safety and efficacy of long-term intraarticular steroid injections in osteoarthritis of the knee: a randomized, double-blind, placebo-controlled trial. *Arthritis and rheumatism.* 2003;48(2):370-377.

63. McAlindon TE, LaValley MP, Harvey WF, Price LL, Driban JB, Zhang M, Ward RJ. Effect of Intra-articular Triamcinolone vs Saline on Knee Cartilage Volume and Pain in Patients With Knee Osteoarthritis: A Randomized Clinical Trial. *Jama*. 2017;317(19):1967-1975.
64. Wernecke C, Braun HJ, Dragoo JL. The Effect of Intra-articular Corticosteroids on Articular Cartilage: A Systematic Review. *Orthop J Sports Med*. 2015;3(5):2325967115581163.
65. Jansen I, Tellegen A, Tryfonidou M, Öner C, Saris D, Woike N, Berard J, Messier K, Creemers L. Brief exposure to triamcinolone acetonide, but not its continuous presence, strongly inhibits cartilage regeneration by chondrocytes. *Osteoarthritis and cartilage*. 2016;24:S337.
66. Beekhuizen M, Bastiaansen-Jenniskens Y, Koevoet JLM, Saris DBF, Dhert W, Creemers L, Osch G. Osteoarthritic Synovial Tissue Inhibition of Proteoglycan Production in Human Osteoarthritic Knee Cartilage Establishment and Characterization of a Long-Term Cartilage Synovium-Coculture. *Arthritis and rheumatism*. 2011;63:1918-1927.
67. Moskowitz RW, Davis W, Sammarco J, Mast W, Chase SW. Experimentally induced corticosteroid arthropathy. *Arthritis & Rheumatism: Official Journal of the American College of Rheumatology*. 1970;13(3):236-243.
68. Frisbie DD, Kawcak CE, Trotter GW, Powers BE, Walton RM, McIlwraith CW. Effects of triamcinolone acetonide on an in vivo equine osteochondral fragment exercise model. *Equine Vet J*. 1997;29(5):349-359.
69. Grodzinsky AJ, Wang Y, Kakar S, Vrahas MS, Evans CH. Intra-articular dexamethasone to inhibit the development of post-traumatic osteoarthritis. *J Orthop Res*. 2017;35(3):406-411.
70. Sieker JT, Ayturk UM, Proffen BL, Weissenberger MH, Kiapour AM, Murray MM. Immediate Administration of Intraarticular Triamcinolone Acetonide After Joint Injury Modulates Molecular Outcomes Associated With Early Synovitis. *Arthritis Rheumatol*. 2016;68(7):1637-1647.
71. Evans CH, Kraus VB, Setton LA. Progress in intra-articular therapy. *Nat Rev Rheumatol*. 2014;10(1):11-22.
72. Scotti C, Gobbi A, Karnatzikos G, Martin I, Shimomura K, Lane JG, Peretti GM, Nakamura N. Cartilage Repair in the Inflamed Joint: Considerations for Biological Augmentation Toward Tissue Regeneration. *Tissue Eng Part B Rev*. 2016;22(2):149-159.
73. Zhang L, Hu J, Athanasiou KA. The role of tissue engineering in articular cartilage repair and regeneration. *Crit Rev Biomed Eng*. 2009;37(1-2):1-57.
74. Navarro M, Michiardi A, Castaño O, Planell JA. Biomaterials in orthopaedics. *J R Soc Interface*. 2008;5(27):1137-1158.
75. Lam MT, Wu JC. Biomaterial applications in cardiovascular tissue repair and regeneration. *Expert Rev Cardiovasc Ther*. 2012;10(8):1039-1049.
76. Hench LL, Thompson I. Twenty-first century challenges for biomaterials. *J R Soc Interface*. 2010;7 Suppl 4(Suppl 4):S379-391.
77. Hollister SJ. Porous scaffold design for tissue engineering. *Nature materials*. 2005;4(7):518-524.

78. Kim B-S, Park I-K, Hoshiba T, Jiang H-L, Choi Y-J, Akaike T, Cho C-S. Design of artificial extracellular matrices for tissue engineering. *Progress in Polymer Science*. 2011;36(2):238-268.
79. Dutta RC, Dutta AK. Cell-interactive 3D-scaffold; advances and applications. *Biotechnology advances*. 2009;27(4):334-339.
80. Lu L, Peter SJ, Lyman MD, Lai H-L, Leite SM, Tamada JA, Uyama S, Vacanti JP, Langer R, Mikos AG. In vitro and in vivo degradation of porous poly (DL-lactic-co-glycolic acid) foams. *Biomaterials*. 2000;21(18):1837-1845.
81. Verhaegen J, Clockaerts S, Van Osch GJ, Somville J, Verdonk P, Mertens P. TruFit Plug for Repair of Osteochondral Defects-Where Is the Evidence? Systematic Review of Literature. *Cartilage*. 2015;6(1):12-19.
82. Spector M, Lim TC. Injectable biomaterials: a perspective on the next wave of injectable therapeutics. *Biomed Mater*. 2016;11(1):014110.
83. Jeon O, Lee YB, Lee SJ, Guliyeva N, Lee J, Alsberg E. Stem cell-laden hydrogel bioink for generation of high resolution and fidelity engineered tissues with complex geometries. *Bioact Mater*. 2022;15:185-193.
84. Sennett ML, Friedman JM, Ashley BS, Stoeckl BD, Patel JM, Alini M, Cucchiari M, Eglin D, Madry H, Mata A, Semino C, Stoddart MJ, Johnstone B, Moutos FT, Estes BT, Guilak F, Mauck RL, Dodge GR. Long term outcomes of biomaterial-mediated repair of focal cartilage defects in a large animal model. *Eur Cell Mater*. 2021;41:40-51.
85. Wei F, Liu S, Chen M, Tian G, Zha K, Yang Z, Jiang S, Li M, Sui X, Chen Z, Guo Q. Host Response to Biomaterials for Cartilage Tissue Engineering: Key to Remodeling. *Front Bioeng Biotechnol*. 2021;9:664592.
86. Qu F, Guilak F, Mauck RL. Cell migration: implications for repair and regeneration in joint disease. *Nat Rev Rheumatol*. 2019;15(3):167-179.
87. Pabbruwe MB, Esfandiari E, Kafienah W, Tarlton JF, Hollander AP. Induction of cartilage integration by a chondrocyte/collagen-scaffold implant. *Biomaterials*. 2009;30(26):4277-4286.
88. Moroni L, Elisseeff JH. Biomaterials engineered for integration. *Materials Today*. 2008;11(5):44-51.
89. Zhang Z, Schon L. The Current Status of Clinical Trials on Biologics for Cartilage Repair and Osteoarthritis Treatment: An Analysis of ClinicalTrials.gov Data. *Cartilage*. 2022;13(2):19476035221093065.
90. Petta D, Armiento AR, Grijpma D, Alini M, Eglin D, D'Este M. 3D bioprinting of a hyaluronan bioink through enzymatic-and visible light-crosslinking. *Biofabrication*. 2018;10(4):044104.
91. Galarraga JH, Kwon MY, Burdick JA. 3D bioprinting via an in situ crosslinking technique towards engineering cartilage tissue. *Sci Rep*. 2019;9(1):19987.
92. Mouser VH, Melchels FP, Visser J, Dhert WJ, Gawlitta D, Malda J. Yield stress determines bioprintability of hydrogels based on gelatin-methacryloyl and gellan gum for cartilage bioprinting. *Biofabrication*. 2016;8(3):035003.

93. Behrendt P, Ladner Y, Stoddart MJ, Lippross S, Alini M, Eglin D, Armiento AR. Articular Joint-Simulating Mechanical Load Activates Endogenous TGF-beta in a Highly Cellularized Bioadhesive Hydrogel for Cartilage Repair. *Am J Sports Med.* 2020;48(1):210-221.
94. Vainieri ML, Lolli A, Kops N, D'Atri D, Eglin D, Yayon A, Alini M, Grad S, Sivasubramaniyan K, van Osch G. Evaluation of biomimetic hyaluronic-based hydrogels with enhanced endogenous cell recruitment and cartilage matrix formation. *Acta Biomater.* 2020;101:293-303.
95. Berger AJ, Linsmeier KM, Kreeger PK, Masters KS. Decoupling the effects of stiffness and fiber density on cellular behaviors via an interpenetrating network of gelatin-methacrylate and collagen. *Biomaterials.* 2017;141:125-135.
96. Nguyen AH, McKinney J, Miller T, Bongiorno T, McDevitt TC. Gelatin methacrylate microspheres for controlled growth factor release. *Acta Biomater.* 2015;13:101-110.
97. Klotz BJ, Lim KS, Chang YX, Soliman BG, Pennings I, Melchels FPW, Woodfield TBF, Rosenberg AJ, Malda J, Gawlitta D. Engineering of a complex bone tissue model with endothelialised channels and capillary-like networks. *Eur Cell Mater.* 2018;35:335-348.
98. Caliarì SR, Vega SL, Kwon M, Soulas EM, Burdick JA. Dimensionality and spreading influence MSC YAP/TAZ signaling in hydrogel environments. *Biomaterials.* 2016;103:314-323.
99. Shu XZ, Ghosh K, Liu Y, Palumbo FS, Luo Y, Clark RA, Prestwich GD. Attachment and spreading of fibroblasts on an RGD peptide-modified injectable hyaluronan hydrogel. *J Biomed Mater Res A.* 2004;68(2):365-375.
100. Heino J. The collagen family members as cell adhesion proteins. *Bioessays.* 2007;29(10):1001-1010.
101. Davis GE. Affinity of integrins for damaged extracellular matrix: α v β 3 binds to denatured collagen type I through RGD sites. *Biochemical and biophysical research communications.* 1992;182(3):1025-1031.
102. Zhang W, Zhu C, Wu Y, Ye D, Wang S, Zou D, Zhang X, Kaplan DL, Jiang X. VEGF and BMP-2 promote bone regeneration by facilitating bone marrow stem cell homing and differentiation. *Eur Cell Mater.* 2014;27:1-11; discussion 11-12.
103. Phipps MC, Xu Y, Bellis SL. Delivery of platelet-derived growth factor as a chemotactic factor for mesenchymal stem cells by bone-mimetic electrospun scaffolds. *PLoS One.* 2012;7(7):e40831.
104. Anderson JM, Rodriguez A, Chang DT. Foreign body reaction to biomaterials. *Seminars in Immunology.* 2008;20(2):86-100.
105. Dziki JL, Badylak SF. Immunomodulatory biomaterials. *Current Opinion in Biomedical Engineering.* 2018;6:51-57.
106. Dancey JT, Deubelbeiss KA, Harker LA, Finch CA. Neutrophil kinetics in man. *J Clin Invest.* 1976;58(3):705-715.
107. Kohno K, Koya-Miyata S, Harashima A, Tsukuda T, Katakami M, Ariyasu T, Ushio S, Iwaki K. Inflammatory M1-like macrophages polarized by NK-4 undergo enhanced phenotypic switching to an anti-inflammatory M2-like phenotype upon co-culture with apoptotic cells. *J Inflamm (Lond).* 2021;18(1):2.

2

Modulation of inflamed synovium improves migration of mesenchymal stromal cells *in vitro* through anti-inflammatory macrophages

Marinus A. Wesdorp

Yvonne M. Bastiaansen-Jenniskens

Serdar Capar

Jan A.N. Verhaar

Roberto Narcisi

Gerjo J.V.M. van Osch

Cartilage. 2022 Jan-Mar;13(1)

ABSTRACT

OBJECTIVE: Inflammation is known to negatively affect cartilage repair. However, it is unclear how inflammation influences the migration of mesenchymal stromal cells (MSCs) from the underlying bone marrow into the defect. We therefore aimed to investigate how synovial inflammation influences MSC migration, and whether modulation of inflammation with triamcinolone acetonide (TAA) may influence migration.

DESIGN: Inflamed human osteoarthritic synovium, M(IFN γ +TNF α) pro-inflammatory macrophages, M(IL4) repair macrophages, M(IL10) anti-inflammatory macrophages or synovial fibroblasts were cultured with/without TAA. Conditioned medium (CM) was harvested after 24 hours, and the effect on MSC migration was studied using a Boyden chamber assay. Inflammation was evaluated with gene expression and flow cytometry analysis.

RESULTS: Synovium CM increased MSC migration. Modulation of synovial inflammation with TAA further increased migration 1.5-fold ($p < 0.01$). TAA significantly decreased *TNFA*, *IL1B*, and *IL6* gene-expression in synovium explants, and increased *CD163*, a gene associated with anti-inflammatory macrophages. TAA treatment decreased the percentage of CD14+/CD80+ and CD14+/CD86+ pro-inflammatory macrophages and increased the percentage of CD14+/CD163+ anti-inflammatory macrophages in synovium explants. Interestingly, MSC migration was specifically enhanced by medium conditioned by M(IL4) macrophages and by M(IL10) macrophages treated with TAA, and unaffected by conditioned medium from M(IFN γ +TNF α) macrophages and synovial fibroblasts.

CONCLUSION: Macrophages secrete factors that stimulate the migration of MSCs. Modulation with TAA increased specifically the ability of anti-inflammatory macrophages to stimulate migration, indicating that they play an important role in secreting factors to attract MSCs. Modulating inflammation and thereby improving migration could be used in approaches based on endogenous repair of full-thickness cartilage defects.

Keywords: macrophages, synovial inflammation, MSC, cartilage repair

INTRODUCTION

Articular cartilage defects pose a significant clinical challenge in the orthopaedic field. Cartilage defects of the joint are common and if left untreated can lead to the development of early-onset osteoarthritis ^{1,2}. Cartilage defects have a limited regenerative capacity, as the articular cartilage is avascular ³, combined with an impaired migration capacity of cartilage cells through the dense extracellular matrix ^{4,5}. Therapies involving bone marrow stimulation techniques can partially overcome this problem by creating access to the bone marrow reservoir. Bone Marrow derived Stromal Cells (MSCs) are considered as a promising cell type for the repair of damaged cartilage due to their chondrogenic differentiation potential ^{6,7}. However, the migration of MSCs from the underlying bone marrow and the chondrogenic differentiation will often have to occur in a chronic inflamed joint environment.

Joint inflammation may inhibit successful cartilage defect repair and without successful repair cartilage defects can eventually lead to the development of osteoarthritis (OA) ^{8,9}. Inflammatory cytokines are produced by the synovium ¹⁰, the highly vascularized mucosal lining of the knee joint that is responsible for the production of synovial fluid that lubricates and nourishes the cartilage ^{10,11}. The synovium contains macrophages that are key players in inflammation and wound healing in injured or osteoarthritic joints ¹². Depending on the stimuli they receive from their microenvironment, macrophages can polarize to distinct phenotypes, referred to as pro-inflammatory macrophages, repair macrophages, and anti-inflammatory macrophages ¹³. Pro-inflammatory macrophages inhibit the formation of cartilage *in vitro* while anti-inflammatory macrophages or repair macrophages stimulate the formation of cartilage *in vitro* ¹⁴. A potential therapeutic option could be to inhibit or reduce inflammation to improve cartilage repair. However, it is unknown what the effects of modulating inflammation would be on the migration of MSCs towards the defect site in an earlier phase of the repair process.

MSC migration is an essential step in the repair process, because MSCs first need to migrate into the defect before starting the process of cartilage formation ¹⁵. Clinically, migration of MSCs into the defect can be enabled by techniques such as microfracture ¹⁶. With this technique, a direct connection is created between the cartilage defect and the underlying bone marrow that contains MSCs. This not only connects MSCs with the defect site, but also with the inflamed intra-articular joint environment. Inflammation is known to play an important role in the migration of MSCs towards an injured site ^{17,18}. Studies have shown that the migration of MSCs to injured sites is regulated by chemokines, cytokines and growth factors. These factors have been

widely investigated and overall have a stimulatory effect on the migration capacity of MSCs ¹⁹. However, in higher concentrations these factors inhibit MSC migration ²⁰. In the case of joint inflammation, however, the situation is even more complex due to the presence of a 'cocktail' of pro-inflammatory-, but also antagonistic anti-inflammatory factors. Therefore, migration cannot be attributed to one specific factor and it is unknown what reducing joint inflammation would mean for MSC migration.

Anti-inflammatory drugs such as triamcinolone acetonide are used to reduce inflammation and reduce the symptoms of OA ²¹. Over the years there has been an increasing interest in the use of anti-inflammatory drugs immediately after various intra-articular pathologies to reduce joint inflammation, synovitis and longer-term post-traumatic osteoarthritis ^{22,23}. The effect of anti-inflammatory medication on the synovium, cartilage and bone have been studied extensively ^{24,25}. However, the effect it has on the migration of repair cells remains unclear. In the current study, we investigated how MSC migration is influenced by conditioned medium produced by inflamed synovium focusing on the influence of modulating inflammation with glucocorticoid triamcinolone acetonide (TAA). We hypothesized that the anti-inflammatory effects of TAA treatment would enhance MSC migration. Further, we investigated which cell types present in the synovium might be responsible for the effect.

MATERIALS AND METHODS

Generation of conditioned medium from synovium and synovial fibroblasts

Synovial tissue was obtained from 9 patients with knee OA (4 female, 5 male, 63 ± 8.3 years old) undergoing total knee arthroplasty (**Table S1**). The synovium samples were obtained with implicit consent as waste material from patients undergoing knee replacement surgery (approved by the local ethical committee; MEC2004-322). The patients had the right to refuse as stated by the guidelines of the Dutch Federation of Biomedical Scientific Societies (www.federa.org). Synovium tissue was washed two times with 0.9% NaCl (Sigma Aldrich, St. Louis, USA), separated from the underlying fat, cut into small pieces of approximately 50 mg wet weight. Dulbecco's Modified Eagle Medium, low glucose (DMEM-LG; Gibco, Carlsbad, USA) supplemented with 1% Insulin-Transferrin-Selenium (ITS Premix, Corning, Tewksbury, USA), 50 mg/mL gentamicin (Gibco), 1.5 mg/mL amphotericin B (Fungizone; Gibco) was used to culture the synovial tissue for 24h, using one ml of media per 200 mg of tissue.

Explants were cultured with or without 1 μM of the anti-inflammatory drug triamcinolone acetate (TAA; Sigma Aldrich) at 37 °C. The concentration for TAA was based on previous studies we performed with human synovium^{26,27}. Prior to starting our study, we used two dosages of TAA (1 μM and 10 μM) and confirmed that they were both effective (data not shown). We selected to lowest effective dose of 1 μM . Dimethyl sulfoxide (DMSO; Sigma Aldrich) was used as vehicle control for TAA and the final DMSO concentration in the cultures was 0.01%. After 24 hours, synovium was harvested, and either snap-frozen in liquid nitrogen for later RNA isolation, or digested for flow cytometric analysis. Also, the CM was harvested, centrifuged at 300 g for 8 min to remove the debris, and stored at -80 °C for subsequent Boyden chamber migration assay (**Figure 1**). Unconditioned control medium was generated by incubation of DMEM-LG with 1% ITS, 50mg/ml gentamicin and 1.5 mg/mL amphotericin B for 24 h at 37 °C, centrifuged at 300 g for 8 minutes, and stored at -80 °C.

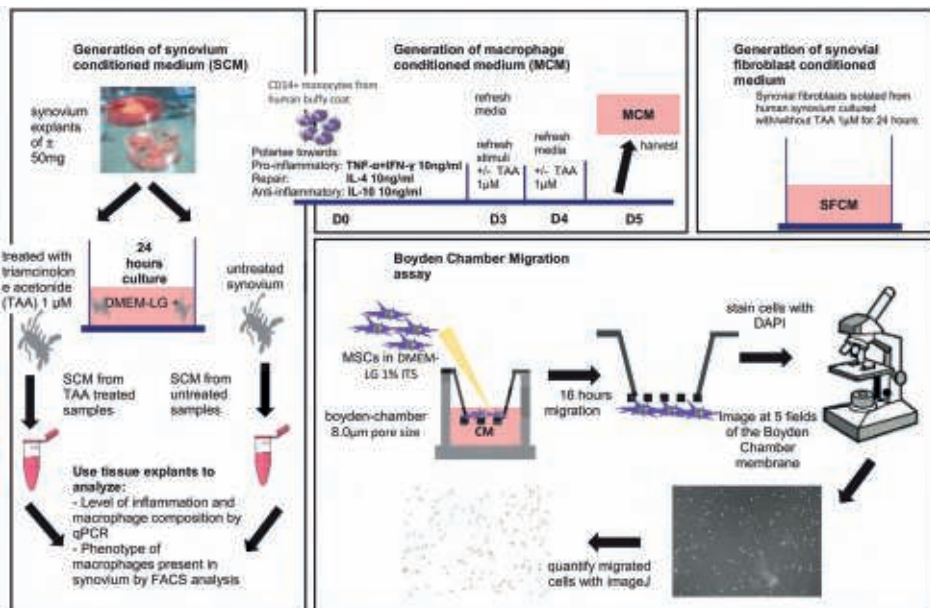


Figure 1. Experimental design on generation of conditioned media and their use in MSC migration assay. **Conditioned medium** from 9 synovium donors of which 6 were treated with TAA and DMSO as vehicle control, 4 monocyte donors and 3 synovial fibroblast donors were generated. Abbreviations: MSC, bone marrow-derived mesenchymal stem/stromal cell; SCM, synovium conditioned medium; MCM, macrophage conditioned medium; SFCM, synovial fibroblast conditioned medium; CM, conditioned medium; TAA, triamcinolone acetate.

Fibroblast-like synoviocytes were isolated from the synovium as described before²⁸. Passage 3 cells were seeded at a density of 50,000 cells/cm² in culture medium. After attachment overnight, the culture medium was removed, cells were washed 3

times with saline and fresh medium was added containing DMEM-LG (Gibco), 1% ITS (Corning), 50 mg/mL gentamicin (Gibco), 1.5 mg/mL amphotericin B (Gibco). The fibroblast-like synoviocytes were cultured for 24 hours in the presence of 1 μ M TAA (Sigma-Aldrich) or 0.01% DMSO as vehicle control. After 24 hours the conditioned medium was harvested, centrifuged for 8 minutes at 300 g and stored at -80°C until further use in the Boyden chamber migration assay (**Figure 1**).

MSC migration assay

Human MSCs (1 female, 2 male, 54.3 \pm 15.7 years old) were isolated by using bone marrow aspirates from patients with hip OA, undergoing total hip arthroplasty after written informed consent and with approval by the local ethical committee (Erasmus MC University Medical Center, The Netherlands, MEC 2015-644 and Albert Schweitzer Hospital: protocol 2011.07) (**Table S2**). Nucleated cells from the heparinized bone marrow aspirates were seeded at the density of 300,000 to 600,000 cells/cm² in Minimum Essential Medium-Alpha expansion medium (α -MEM; Gibco™) supplemented with 10% heat inactivated fetal bovine serum (FCS; Lonza), 50 mg/mL gentamicin (Gibco), 1.5 mg/mL amphotericin B (Fungizone; Gibco), 1 ng/mL fibroblast growth factor 2 (FGF2; R&D Systems) and 25 μ g/mL ascorbic acid-2-phosphate (Sigma-Aldrich). After 24 hours, non-adherent cells were washed away with PBS containing 2% FCS and adherent cells were further expanded in expansion medium, trypsinized at sub-confluence and seeded again at a density of 2,300 cells/cm². Cells were refreshed twice a week and trypsinized in case of sub confluency and passage-3 (P3) cells were used for the migration assays. Viability assessed with trypan blue using a hemocytometer revealed >95% of the MSCs were viable.

Migration assays were performed using a 24-well Boyden chamber setup with cell culture inserts of 8.0 μ m pore size (Corning, Tewksbury, USA). For each cell culture insert 15,000 MSCs were used, suspended in 200 μ L DMEM-LG (Gibco, Carlsbad, USA) supplemented with 1% ITS, 50 mg/mL gentamicin (Gibco), 1.5 mg/mL amphotericin B (Fungizone; Gibco) and seeded on top of the insert membrane. Conditioned medium (CM) was thawed on ice and mixed prior to use with a predetermined volume of DMEM-LG (Gibco, Carlsbad, USA) medium containing 1% ITS Premix (Corning, Tewksbury, USA), 50 mg/mL gentamicin (Gibco) and 1.5 mg/mL amphotericin B (Gibco) corresponding to a percentage of CM in the final medium (**Figure 1**). In total 600 μ L of medium containing CM was added in the lower chamber. After 16 hours of incubation in a humidified incubator of 37°C and 5% CO₂, transwell inserts were carefully removed from the plate as well as the medium inside the insert. The inserts were then washed with PBS, fixed by 4% formaldehyde for 20 minutes and the non-migrated cells from the upper part of the membrane were removed with a cotton swab. The cells that

had migrated to the other side of the membrane were immediately stained with 4',6-diamidino-2-phenylindole (DAPI, ThermoFisher). Images of the migrated cells on the lower part of the membrane were taken at 5 non-overlapping fields of 0.017 cm² from the center, top, bottom, right, and left part of the membrane with a fluorescent microscope (Leica SP5). For each image, the cell number was counted using Image-J software utilizing the analyze particles tool. The cell numbers of the 5 fields covered 25% of the total area of the membrane. The cell numbers of each field were added and this number was converted to match the entire area of the Boyden chamber membrane (0.33 cm²). The cell number of each membrane was normalized to the average of the number of cells that migrated in the control conditions. The average of the unstimulated control conditions was set to 1. Since we had 3-5 samples of unstimulated conditions for each experiment, we also normalised these unstimulated control conditions for the average and thus show the variation in this condition.

RNA isolation and quantitative real-time PCR

Snap frozen synovium explants were pulverized with a Mikro Dismembrator (Braun Biotech International GmbH, Melsungen, Germany) at 3,000 rpm for 30 seconds. The samples were resuspended in 1 ml RNA-Bee (TelTest, Friendswood, Texas, USA). Chloroform (Sigma-Aldrich) was added to all samples in a concentration of 200 µL/mL RNA-Bee. Total RNA from synovium explants was purified by using RNeasy Micro Kit (Qiagen, Hilden, Germany) according to the manufacturer's instructions. RNA yield and purity of samples were determined using NanoDrop ND1000 UV-Vis Spectrophotometer (Isogen Life Science, Veldzicht, The Netherlands) at 260/280 nm. Purified RNA was reverse-transcribed to complementary DNA (cDNA) using the RevertAid First Strand cDNA Synthesis Kit (Fermentas GmbH, Leon-Rot, Germany) according to the manufacturer's instructions. Quantitative real-time polymerase chain reaction (qRT-PCR) was performed with 10 µL of the sample with TaqMan® Universal PCR Master Mix (Applied Biosystems) or Mastermix Plus for SYBR® Green I (Eurogentec) using the CFX96 Touch™ Real-Time PCR Detection System (Biorad, Hercules, California, USA). Expression of genes encoding for glyceraldehyde-3-phosphate dehydrogenase (*GAPDH*), hypoxanthine phosphoribosyltransferase 1 (*HPRT*), ubiquitin C (*UBC*), tumor necrosis factor-α (*TNFA*), interleukin-1β (*IL1B*), IL6 (*IL6*), chemokine (C-C motif) ligand 18 (*CCL18*), mannose receptor C-type 1 (*MRC1*), coding for CD206, and CD163 (*CD163*) was assessed with qRT-PCR (Table 1). The geometric mean of the genes *GAPDH*, *HPRT* and *UBC* was used to calculate the BestKeeper index (BKI). There were no significant differences between the conditions: 0.01% DMSO and treatment with medication did not interfere with best housekeeper gene levels (data not shown). The relative gene expression of genes of interest was calculated according to the $2^{-\Delta CT}$ formula.

Table 1. List of primers used to detect mRNA levels by qRT-PCR

Gene name	Forward	Reverse	Probe
<i>GAPDH</i>	GTCAACGGATTTGGTCGTATTGGG	TGCCATGGGTGGAATCATATTGG	CGCCCAATACGACCAAATCCGTTGAC
<i>HPRT</i>	TATGGACAGGACTGAACGTCTTG	CACACAGAGGGCTACAATGTG	AGATGTGATGAAGGAGATGGGAGGCCA
<i>UBC</i>	ATTTGGGTCGCGGTTCTTG	TGCCTTGACATTCTCGATGGT	n.a.
<i>TNFA</i>	GCCGCATCGCCGTCTCCTAC	GCGCTGAGTCGGTCACCCCT	n.a.
<i>IL1B</i>	CTAAACA-GATGAAGTGCTCCT	TAGCTGGATGCCGCCAT	n.a.
<i>IL6</i>	TCGAGCCACCGGGAACGAA	GCAGGGAAGGCAGCAGGCAA	n.a.
<i>CCL18</i>	GCACCATGGCCCTCTGCTCC	GGGCACTGGGGCTGGTTTC	n.a.
<i>MRC1</i>	TGGCCGTATGCCGGTCACTGTTA	ACTTGTGAGGTCACCGCCTTCCT	n.a.
<i>CD163</i>	GCAATGGGGTGACTTACCT	TCACCATGCTTCACTTCAACAC	n.a.

Fluorescence activated cell sorting (FACS) of macrophage phenotypes

Synovial explants were digested for 3 hours at 37° C in Hanks’ Balanced Salt solution (Gibco) with Ca2+ and Mg2+, containing 2 mg/ml Collagenase IV (Gibco) and 0.2 mg/ml Dispase II (Roche, Penzberg, Upper Bavaria, Germany). At the end of digestion FCS was added to a final concentration of 5% and the cell suspension was filtered first using a 100 µm filter, and then twice through a 40 µm filter. Cells were then centrifuged for 8 minutes at 250 g, re-suspended in FACSflow (#342003 BD Biosciences) and counted. Approximately 200,000 cells were stained for each condition. Cells were re-suspended in 40 µL of FACSflow and incubated for 15 minutes at room temperature in the dark with surface antibody (Ab) solutions containing mixes of the following Abs; CD14 (APC-H7, #561384), CD206 (FITC, #551135), CD163 (PerCP-Cy™5.5, #563887), CD80 (PECy™7, #561135), and CD86 (PE, #560957) all purchased from BD Biosciences with dilutions according to manufacturer’s instructions. Cells were fixed in 1.8% paraformaldehyde for 20 minutes in the dark. Subsequently, cells were re-suspended in FACSflow and analyzed with FACSJazz (BD Biosciences) and FlowJo Software (Tree Star, Palo Alto, CA, USA).

Monocyte isolation, polarization and modulation of macrophages

Monocytes were obtained from four healthy male buffy coat donors (Sanquin, Rotterdam) as previously described ²⁹. After Ficoll (GE Healthcare, Little Chalfont, United Kingdom) density gradient centrifugation, peripheral blood mononuclear cells (PBMCs) were labeled with anti-CD14 magnetic beads (MACS; Miltenyi, Bergisch Gladbach, Germany) and isolated by MACS. Monocytes were seeded at a density of 500,000 monocytes/cm² in X-VIVO™ medium (Lonza, Verviers, Belgium) supplemented with 20% heat-inactivated fetal calf serum (FCS; Lonza), 50 µg/mL gentamicin (Gibco) and 1.5 µg/mL amphotericin B (Gibco). Monocytes were polarized with 10 ng/mL Tumor

Necrosis Factor- α (TNF- α ; PeproTech) and Interferon- γ (INF- γ ; PeproTech) towards a pro-inflammatory M(TNF α +INF γ) macrophage phenotype, with 10 ng/mL Interleukin-4 (IL-4; PeproTech) toward a repair M(IL-4) phenotype or with Interleukin-10 (IL-10; PeproTech) towards an anti-inflammatory M(IL-10) phenotype. After 72 hours the medium with the stimuli was removed and refreshed for another 24 hours with the addition of 1 μ M TAA (Sigma-Aldrich) to modulate their phenotype or 0.01% DMSO as vehicle control. After this polarization period, the different macrophage phenotypes were cultured for an additional 24 hours in Dulbecco's Modified Eagle Medium, low glucose (DMEM-LG; Gibco) supplemented with 1% ITS Premix (Corning), 50 mg/mL gentamicin (Gibco), 1.5 mg/mL amphotericin B (Fungizone; Gibco) in the presence of 1 μ M TAA (Sigma-Aldrich) or 0.01% DMSO as a control. We decided on this set-up to mimic the situation in the joint where inflammatory factors that polarize macrophages will be present initially when TAA is added. For these last 24h we removed the polarization stimuli since they would have an effect on BMSC migration, but kept TAA after we confirmed that the selected dose of TAA did not affect migration. The macrophage conditioned medium (MCM) was harvested, centrifuged for 8 minutes at 300 g and stored at -80°C until used in the Boyden chamber migration assay (Figure 1).

Statistical analysis

Per each group and donor, 3 to 6 biological replicates have been included, each of them measured in technical duplicates. The values of the technical duplicates were averaged before statistical analysis was applied. Gene expression, FACS and Boyden-chamber migration assay data were analyzed using a hierarchical statistical model; the linear mixed model. The different conditions were considered a fixed parameter and the donors (experiments), with the related biological replicates, as a random factor. Dose-response Boyden chamber migration assay data were analyzed with a Kruskal-Wallis test with Dunn's multiple comparison test to analyze the different doses'. Correlation coefficients were calculated using a Spearman rho test for non-parametric data and a Pearson rho test for normally distributed data. All statistical analysis included two-tailed tests. A *P* value of < 0.05 was considered to indicate statistical significance. SPSS statistics package version 27.0 for MAC (SPSS Inc., Chicago, IL, USA) was used for all analyses.

RESULTS

Synovium conditioned medium stimulated MSC migration in a dose and donor dependent way

The effect of factors secreted by synovium on the migration of MSCs was investigated by using the conditioned medium of synovium explants (SCM). MSC migration was significantly stimulated by both 50% and 100% SCM compared to the unconditioned medium, whereas 10% SCM failed to stimulate migration (**Figure 2A**). Since there was no incremental difference between 50% and 100% conditioned medium ($P = 0.38$) (**Figure 2A**), 50% was used for all further experiments described in this paper. SCM resulted in a donor-dependent increase of MSC migration that varied between 3.5-fold and 18.4-fold (**Figure 2B**). To evaluate whether this difference between synovium donors was dependent on the level of inflammation, we analyzed inflammation-related gene expression levels. Similar to the migration of MSCs in response to SCM, the level of inflammation in the synovium explants varied between donors. The expression levels of *TNFA* ($r = -0.46$, $P = 0.21$), *IL1B* ($r = -0.55$, $P = 0.13$), *IL6* ($r = -0.63$, $P = 0.076$), *CCL18* ($r = -0.37$, $P = 0.33$), *CD206* ($r = -0.40$, $P = 0.29$), and *CD163* ($r = 0.60$, $P = 0.09$) were not correlated the number of MSCs for these individual cytokines (**Figure 2C**).

Inflammation of the synovial explants was reduced in response to anti-inflammatory treatment and this increased MSC migration

To further study the relation between synovial inflammation and the number of migrating MSCs, TAA was used to investigate how modulation of inflammation would influence MSC migration. TAA's efficiency was confirmed by a significant reduction of the expression of the inflammation-related genes *TNFA*, *IL1B* and *IL6* in the synovium (**Figure 3A**). Then, we investigated MSC migration in response to conditioned medium from synovium modulated with TAA. First, we showed that the presence of TAA did not influence the effect of SCM on MSC migration, independent of the dose of both SCM and TAA (**Supplementary Figure 1**). We therefore kept TAA in the conditioned medium for all further experiments. MSC migration was higher in response to medium conditioned by synovium modulated with TAA compared to unmodulated synovium (**Supplementary Figure 2**), resulting on average in a 1.5-fold increase in migration (95% CI 0.04-0.94, $P = 0.03$) (**Figure 3B**).

Modulation of synovial inflammation with TAA increased MSC migration through repair- and anti-inflammatory macrophages

To further investigate the contribution of the cell types present in the synovium, we investigated whether TAA alters the phenotype of the macrophages. Next to the downregulation of *TNFA*, *IL1B* and *IL6*, pro-inflammatory macrophage markers

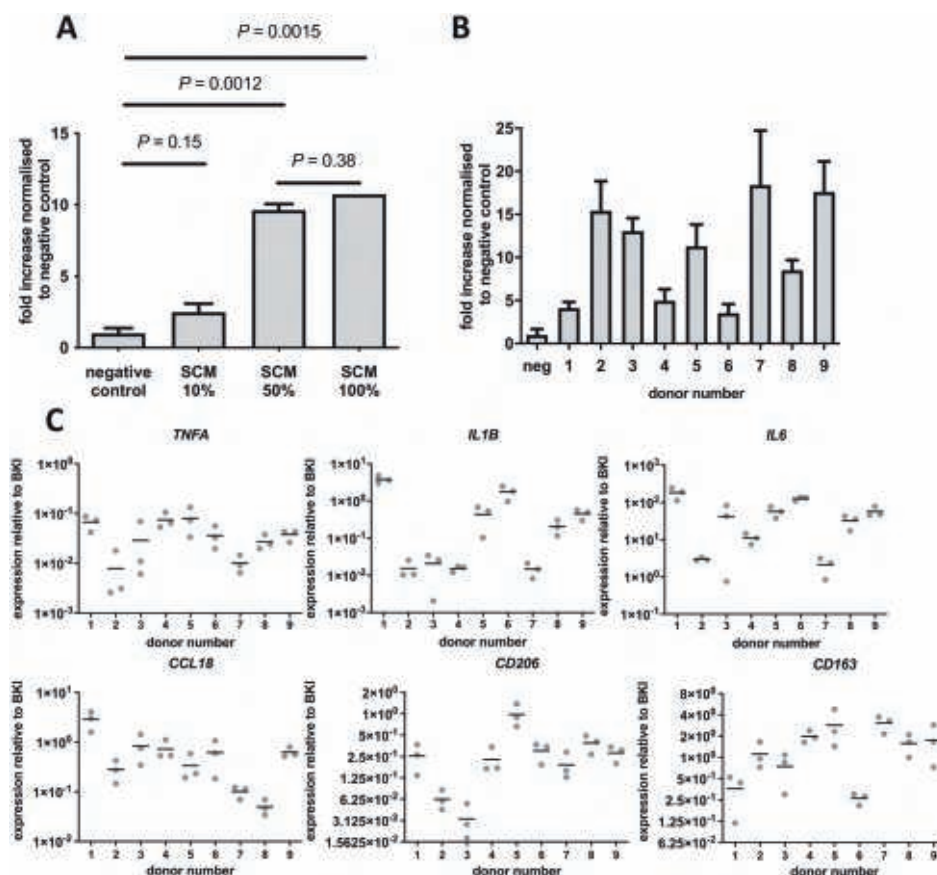


Figure 2. Synovium conditioned medium resulted in a dose- and donor-dependent increase in MSC migration. **A)** MSC migration in response to different SCM doses from 3 pooled donors normalized to unconditioned medium (=negative control). The average number of cells that migrated in the control condition was 279. **B)** MSC migration in response to 9 different SCM donors. Each bar represents the fold increase normalized to the negative control (unconditioned DMEM-LG 1%ITS) + SD. The average number of cells that migrated in the control condition was 233. $n = 9$ donors in quintuplicate. **C)** Gene expression level of *TNFA*, *IL1B*, *IL6*, *CCL18*, *CD206*, and *CD163* relative to the BKI (*GAPDH*, *HPRT*, *UBC*). Each dot represents 1 of 3 explants from 9 synovium donors. Abbreviations: SCM, synovium conditioned medium; MSC, mesenchymal stromal cell; BKI, BestKeeper index.

(**Figure 3A**), *CCL18* and *CD206*, two repair macrophage markers, were not affected by TAA treatment (**Figure 4A**) and the anti-inflammatory macrophage marker *CD163*, was increased (**Figure 4A**). We then evaluated the effect of TAA on the composition of macrophages in the synovium and observed that TAA treatment resulted in a significantly lower percentage of $CD14^+/CD80^+$ (95% CI -7.63 to -4.48, $P < 0.0001$) and $CD14^+/CD86^+$ (95% CI -5.22 to -3.57, $P < 0.0001$) pro-inflammatory macrophages in the synovium. On the other hand, the percentage of $CD14^+/CD163^+$ (95% CI 0.42 - 2.64, P

= 0.008) anti-inflammatory macrophages was significantly higher in synovial explants modulated with TAA (**Figure 4B**). This indicates that treating synovial samples with TAA decreased pro-inflammatory macrophages and increased anti-inflammatory macrophages.

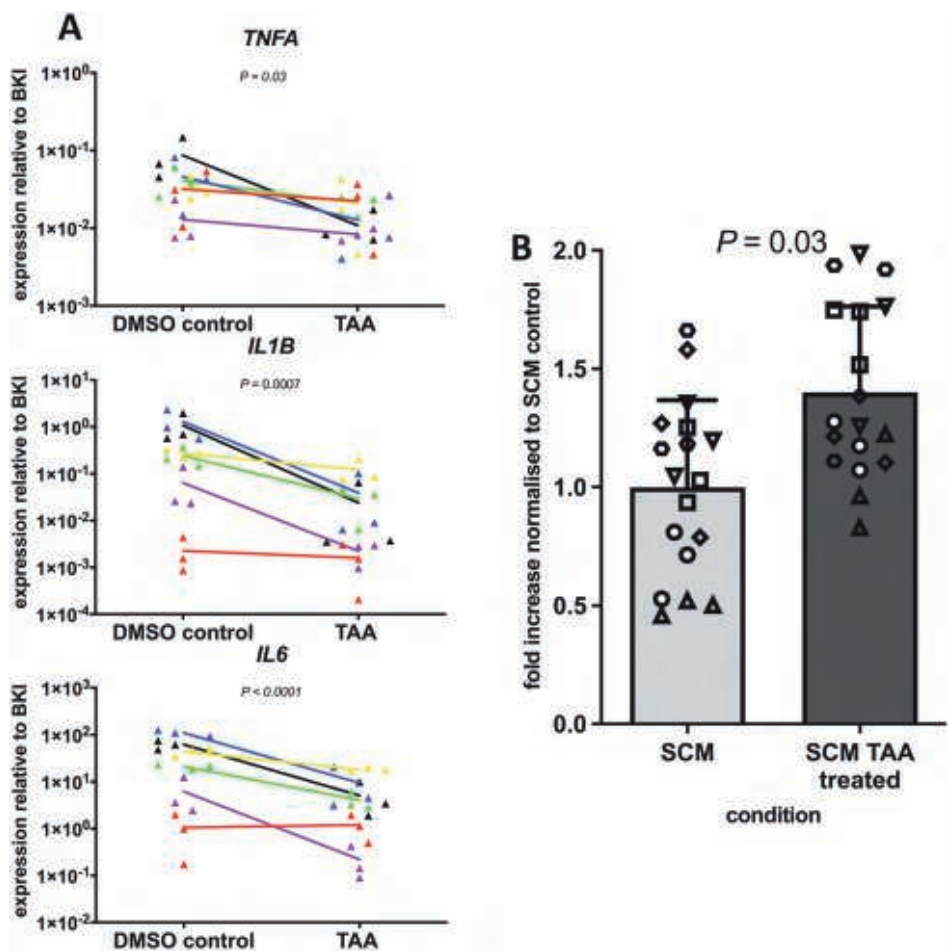


Figure 3. Reduced synovial inflammation increased MSC migration.

A) Gene expression level of *TNFA*, *IL1B* and *IL6* relative to the BKI (*GAPDH*, *HPRT*, *UBC*). Each triangle represents one sample of 3 explants. Each color represents a different donor ($n=6$ in total). The line between the dots represents the difference between the mean of the biological triplicates for the conditions without and with 1 μM TAA for each donor. B) MSC migration in response to conditioned medium from synovium explants modulated without and with 1 μM TAA. To normalize the data of the different experiments, the average of the conditioned control condition (SCM) in each experiment was set to 1. The average number of cells that migrated in the control condition was 3783. The bars represent the mean increase + SD. $n = 6$ synovium donors in triplicate. Each synovium donor is represented by a different symbol. Abbreviations: BKI, BestKeeper index; TAA, triamcinolone acetate; SCM, synovium conditioned medium; MSC, bone marrow-derived mesenchymal stromal cell.

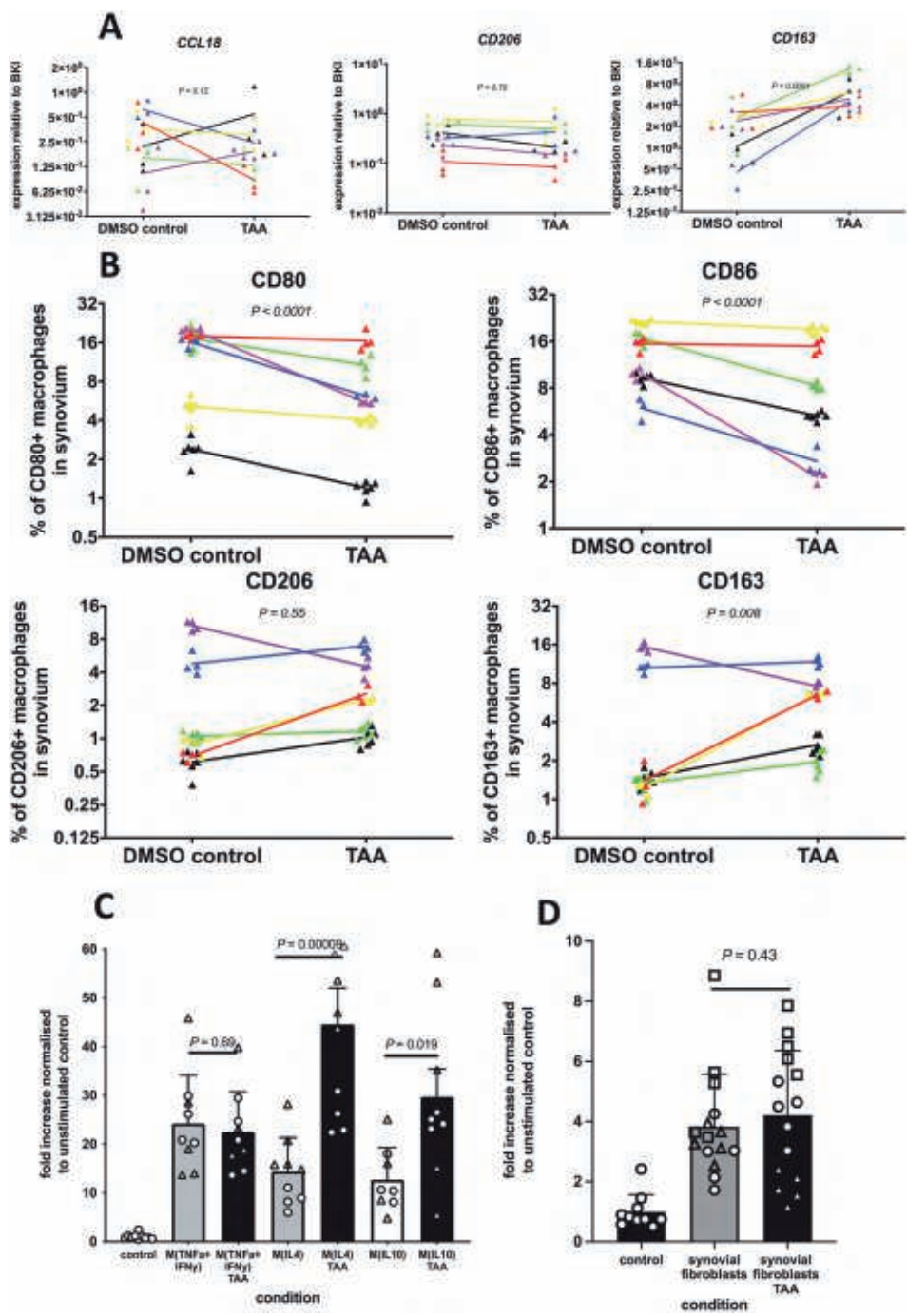


Figure 4. Modulation of synovial inflammation by TAA increased MSC migration through repair M(IL4) and anti-inflammatory M(IL10) macrophages treated with TAA.

A) Expression of repair/anti-inflammatory macrophage-related genes *CCL18*, *CD206* and *CD163* is shown relative to the BKL. Each dot represents one sample of 3 explants. Each color represents a different synovium donor (n=6). B) The percentages of pro-inflammatory (CD80 and CD86) and anti-inflammatory surface markers (CD163 and CD206) among CD14+ macrophages in the synovium are shown. Each dot represents one sample of 5 explants. Each color represents a separate donor (n=6). The lines indicate the difference in the mean of the explants with and without 1 μ M TAA for each individual donor. C) MSC migration in response to conditioned medium from pro-inflammatory M(TNF α +IFN γ), repair M(IL4) macrophages, and anti-inflammatory M(IL10) macrophages compared to conditioned medium from 1 μ M TAA modulated macrophage phenotypes. The average number of cells that migrated in the control condition was 142. n = 2 batches of 2 pooled monocyte donors (4 donors in total), first batch in quadruplicate, second batch in quintuplicate. Each batch of 2 donors is represented by a different symbol. D) MSC migration in response to conditioned medium from synovial fibroblasts and conditioned medium from 1 μ M TAA modulated synovial fibroblasts. The average number of cells that migrated in the control condition was 150. Each bar represents the fold increase normalized to the negative control (unconditioned DMEM-LG 1% ITS) + SD. n = 3 synovial fibroblast donors in quintuplicate. Each synovial fibroblast donor is represented by a different symbol. Abbreviations: BKL, BestKeeper index; TAA, triamcinolone acetone; MSC, bone marrow-derived mesenchymal stromal cell.

To investigate whether this shift in macrophage phenotype could be responsible for the increase in MSC migration in response to synovium explants treated with TAA, we analyzed MSC migration in response to macrophage conditioned medium. Conditioned medium from all macrophage phenotypes, derived from peripheral blood monocytes, stimulated MSC migration (**Figure 4C**). Then we treated macrophages with different phenotypes with TAA and evaluated the effect of their conditioned medium on MSC migration. Conditioned medium from repair M(IL4) and anti-inflammatory M(IL10) macrophages treated with TAA increased MSC migration 2 to 3-fold compared to untreated macrophages (95% CI 18.10 - 42.28, $P = 0.00009$ and 95% CI 3.19 - 30.80, $P = 0.019$) (**Figure 4C**). Modulation of pro-inflammatory macrophages M(TNF α +IFN γ) with TAA did not result in a change in MSC migration (**Figure 4C**). In addition, modulation of synovial fibroblasts (the other main cell type of synovium) with TAA did not increase MSC migration (**Figure 4D**). These results indicate that the increase in MSC migration in modulated synovial samples is probably through the specific role of repair M(IL4) and anti-inflammatory M(IL10) macrophages.

DISCUSSION

The first step in endogenous cartilage repair strategies is the recruitment of progenitor cells that can generate the repair tissue. In joints with a cartilage defect, the intraarticular joint environment is often disturbed and characterized by synovial inflammation³⁰. In this study, we assessed how modulation of synovial inflammation influences MSC migration and elucidated the role of different cell types present in the inflamed synovium. We found that reducing synovial inflammation with TAA increased MSC migration *in vitro*, and that this stimulatory effect appears to be mediated by repair- and anti-inflammatory macrophages.

In our study, conditioned media from all macrophage phenotypes dose-dependently increased MSC migration, indicating that the macrophages secrete factors that can stimulate MSC migration. Since macrophages are the most abundant cell type in the synovium, they play an important role in the disturbed homeostasis in a joint with a cartilage defect. To drive the joint environment to a more favorable cartilage repair environment we modulated the macrophages with TAA. To our knowledge, this is the first study that shows how modulation of synovial inflammation may enhance progenitor cell recruitment to the defect site, with a proposed key role for anti-inflammatory macrophages. The observation that TAA increases repair- and anti-inflammatory macrophages present in the synovium is in line with a study showing that the phenotype of macrophages in the synovium can be modulated towards an anti-inflammatory phenotype upon using dexamethasone ²⁷ and a study on an acute lung injury mouse model that showed that methylprednisolone reduced the number of pro-inflammatory macrophages and increased the number of anti-inflammatory and repair macrophages ³¹. Since these studies used a different glucocorticoid, this indicates that the overall effect of glucocorticoids on macrophage phenotype is similar.

An increase in anti-inflammatory and repair macrophages can occur through a change in the polarization state of pro-inflammatory macrophages into a more anti-inflammatory phenotype. We observed a decrease in the percentage of pro-inflammatory macrophages and at the same time an increase in anti-inflammatory macrophages, indicating that the polarization state of the macrophages might have changed. Our results are supported by a study that reported a decrease in CD80+ cells and an increase in CD163+ cells upon treatment with TAA ³². In addition, glucocorticoids may stimulate the differentiation from naïve monocytes into an anti-inflammatory macrophage phenotype ³³. We cannot discriminate between the mechanisms that could be responsible for the increase in anti-inflammatory macrophages in the synovium and decrease in pro-inflammatory macrophages, and it will most likely be a combination of these two. Whether these mechanisms play a role when glucocorticoids are applied to the joint *in vivo*, remains to be investigated. Moreover, glucocorticoids have been shown to inhibit the migration of pro-inflammatory macrophages and stimulate the migration of anti-inflammatory macrophages ^{33,34}, which can play an additional role when glucocorticoids are applied *in vivo*.

Mesenchymal stromal cells have been shown to be attracted to sites of inflammation, in studies ranging from skin wounds to tumor environments ^{35,36}. Many of the factors present in a joint with a cartilage defect have been widely investigated on an individual basis and overall have a stimulatory effect on the migration capacity of

MSCs¹⁹. However, joint inflammation cannot be attributed to a single factor, but is much more complex and most likely a 'cocktail' of factors that contain both pro-inflammatory and anti-inflammatory factors. Therefore, it might not be the best option to focus on the inhibition or stimulation of one specific cytokine, but rather on modulating this 'cocktail' of factors. By using TAA we demonstrated to inhibit multiple pro-inflammatory markers and stimulated anti-inflammatory markers. This effect is likely to alter the 'cocktail' of factors, which is supported by a study showing that intraarticular glucocorticoid treatment reduced synovial cell infiltration and proinflammatory cytokine expression in chronic arthritis³⁷. The change in pro-inflammatory and anti-inflammatory factors could contribute to a more favorable joint environment that in turn might attract more MSCs from the bone marrow.

TAA itself had no direct effect on the migration of MSCs from bone marrow. This data is at odds with the previous findings that described TAA inhibited cell migration of tenocytes and outgrowth of ligament and synovial capsule cells^{38,39}. However, in those studies, the exposure to TAA varied from 4 to 14 days and was thereby much longer than the 16 hours in our study and the shorter exposure to TAA of 4 days was shown to give less inhibition of cell migration³⁸. Nevertheless, this knowledge should be considered when using TAA in a clinical setting, since after intra-articular injection TAA could be detected up to 15 days⁴⁰. Moreover, a recent case report suggested that high dose of steroids injected intra-articular could transiently compromise the chondrogenic capacity of MSCs from synovium⁴¹. Also, there is an ongoing debate amongst the effect TAA has on the articular cartilage. The current evidence is conflicting and shows both beneficial and detrimental effects on the cartilage⁴². Therefore, it might be of value to explore whether other drugs can also successfully reduce inflammation and improve MSC migration.

After stimulation of migration of bone marrow derived MSCs by surgically making holes from the cartilage defect into the subchondral bone, chondrogenesis and subsequent cartilage tissue formation should take place in endogenous cartilage repair procedures⁴³. Progenitor cells from synovium can also play a role in cartilage repair too⁴⁴. Although it was shown that bone marrow derived MSCs migrate roughly 3x more than synovium derived MSCs in response to 10% FCS. This difference in migration capacity indicates that bone marrow derived MSCs might be more important in migration towards the defect site than MSCs from the synovium⁴⁵, future studies should explore whether the difference in migration capacity also exists in response to synovium secreted factors. Pro-inflammatory factors are known to inhibit the chondrogenic capacity of MSCs *in vitro*^{46,47}. Further, the conditioned medium obtained from inflamed osteoarthritic synovium reduced the chondrogenic capacity of MSCs, and this effect was assigned

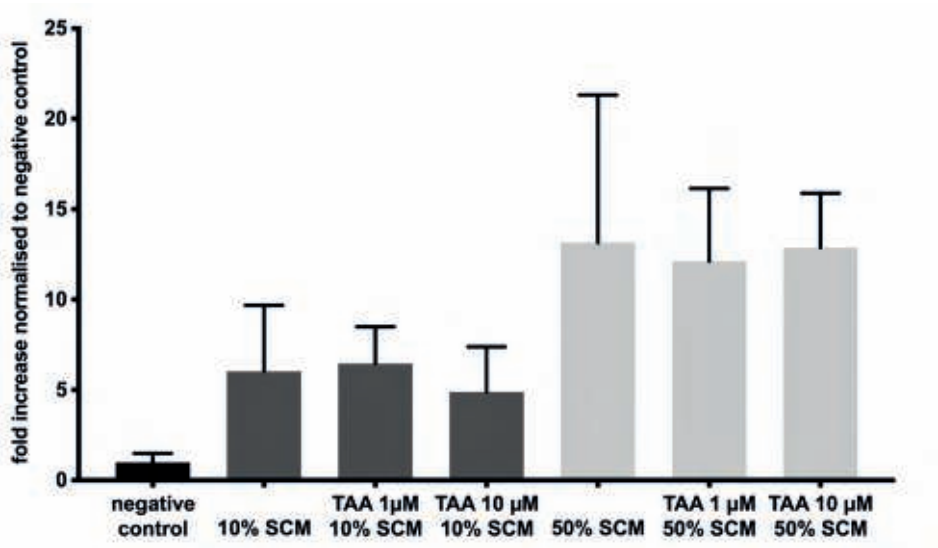
predominantly to proinflammatory macrophages in the synovium ⁴⁸. The transition from pro-inflammatory macrophages towards anti-inflammatory macrophages might, besides increasing the migration of MSCs, also be beneficial for the cartilage formation capacity. Moreover, anti-inflammatory/repair macrophages might even enhance the cartilage forming capacity of MSCs ¹⁴. This implicates that modulating pro-inflammatory macrophages towards a more anti-inflammatory phenotype could be a promising tool to improve the success of endogenous cartilage repair strategies.

Table S1. List of synovium donors

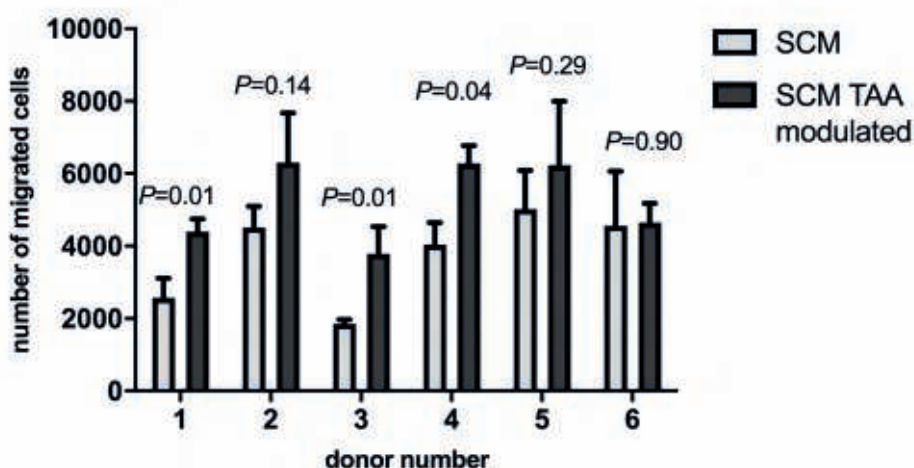
Donor	Sex	Age (years)
1	F	57
2	F	73
3	F	69
4	M	72
5	M	53
6	M	68
7	M	62
8	M	50
9	F	63

Table S2. List of MSC donors

Donor	Sex	Age (years)
1	M	23
2	F	69
3	M	71



Supplementary Figure 1. The presence of TAA in SCM did not affect MSC migration. MSC migration in response to 3 different SCM donors. Each bar represents the fold increase normalized to the negative control (unconditioned DMEM-LG 1% ITS) + SD. Abbreviations: SCM, synovium conditioned medium; TAA, triamcinolone acetone; MSC, mesenchymal stromal cell.



Supplementary Figure 2. MSC migration increased when synovial explants were treated with TAA.

A) MSC migration in response to 6 different SCM donors compared to conditioned medium from the same donor modulated with 1 μ M TAA. The bars represent the mean increase + SD. n = 6 donors in triplicate. Abbreviations: SCM, synovium conditioned medium; TAA, triamcinolone acetonide; MSC, mesenchymal stromal cell.

REFERENCES

1. Widuchowski W, Widuchowski J, Trzaska T. Articular cartilage defects: study of 25,124 knee arthroscopies. *Knee*. 2007;14(3):177-182.
2. Smith GD, Knutsen G, Richardson JB. A clinical review of cartilage repair techniques. *J Bone Joint Surg Br*. 2005;87(4):445-449.
3. Mobasheri A, Csaki C, Clutterbuck AL, Rahmanzadeh M, Shakibaei M. Mesenchymal stem cells in connective tissue engineering and regenerative medicine: applications in cartilage repair and osteoarthritis therapy. *Histol Histopathol*. 2009;24(3):347-366.
4. Verwoerd-Verhoef HL, ten Koppel PG, van Osch GJ, Meeuwis CA, Verwoerd CD. Wound healing of cartilage structures in the head and neck region. *Int J Pediatr Otorhinolaryngol*. 1998;43(3):241-251.
5. Bos PK, van Osch GJ, Frenz DA, Verhaar JA, Verwoerd-Verhoef HL. Growth factor expression in cartilage wound healing: temporal and spatial immunolocalization in a rabbit auricular cartilage wound model. *Osteoarthritis Cartilage*. 2001;9(4):382-389.
6. Djouad F, Bouffi C, Ghannam S, Noël D, Jorgensen C. Mesenchymal stem cells: innovative therapeutic tools for rheumatic diseases. *Nat Rev Rheumatol*. 2009;5(7):392-399.
7. Goldberg A, Mitchell K, Soans J, Kim L, Zaidi R. The use of mesenchymal stem cells for cartilage repair and regeneration: a systematic review. *Journal of orthopaedic surgery and research*. 2017;12(1):1-30.
8. Widuchowski W, Widuchowski J, Faltus R, Lukasik P, Kwiatkowski G, Szyluk K, et al. Long-term clinical and radiological assessment of untreated severe cartilage damage in the knee: a natural history study. *Scand J Med Sci Sports*. 2011;21(1):106-110.
9. van der Kraan PM. The Interaction between Joint Inflammation and Cartilage Repair. *Tissue Eng Regen Med*. 2019;16(4):327-334.
10. Sellam J, Berenbaum F. The role of synovitis in pathophysiology and clinical symptoms of osteoarthritis. *Nature Reviews Rheumatology*. 2010;6(11):625.
11. Smith MD. Suppl 1: the normal synovium. *The open rheumatology journal*. 2011;5:100.
12. Fernandes TL, Gomoll AH, Lattermann C, Hernandez AJ, Bueno DF, Amano MT. Macrophage: A Potential Target on Cartilage Regeneration. *Front Immunol*. 2020;11:111.
13. Park JE, Barbul A. Understanding the role of immune regulation in wound healing. *Am J Surg*. 2004;187(5a):11s-16s.
14. Sesia SB, Duhr R, Medeiros da Cunha C, Todorov A, Schaeren S, Padovan E et al. Anti-inflammatory/tissue repair macrophages enhance the cartilage-forming capacity of human bone marrow-derived mesenchymal stromal cells. *J Cell Physiol*. 2015;230(6):1258-1269.
15. Caplan AI. Mesenchymal stem cells. *J Orthop Res*. 1991;9(5):641-650.
16. Steinwachs M, Guggi T, Kreuz P. Marrow stimulation techniques. *Injury*. 2008;39(1):26-31.
17. Zhang S, Hu B, Liu W, Wang P, Lv X, Chen S et al. Articular cartilage regeneration: The role of endogenous mesenchymal stem/progenitor cell recruitment and migration. *Seminars in Arthritis and Rheumatism*. 2020;50(2):198-208.
18. Su P, Tian Y, Yang C, Ma X, Wang X, Pei J et al. Mesenchymal Stem Cell Migration during Bone Formation and Bone Diseases Therapy. *Int J Mol Sci*. 2018;19(8).

19. Fu X, Liu G, Halim A, Ju Y, Luo Q, Song AG. Mesenchymal Stem Cell Migration and Tissue Repair. *Cells*. 2019;8(8).
20. Schmidt A, Ladage D, Schinköthe T, Klausmann U, Ulrichs C, Klinz FJ et al. Basic fibroblast growth factor controls migration in human mesenchymal stem cells. *Stem Cells*. 2006;24(7):1750-1758.
21. Bannuru RR, Schmid CH, Kent DM, Vaysbrot EE, Wong JB, McAlindon TE. Comparative effectiveness of pharmacologic interventions for knee osteoarthritis: a systematic review and network meta-analysis. *Ann Intern Med*. 2015;162(1):46-54.
22. Grodzinsky AJ, Wang Y, Kakar S, Vrahas MS, Evans CH. Intra-articular dexamethasone to inhibit the development of post-traumatic osteoarthritis. *J Orthop Res*. 2017;35(3):406-411.
23. Sieker JT, Ayturk UM, Proffen BL, Weissenberger MH, Kiapour AM, Murray MM. Immediate Administration of Intraarticular Triamcinolone Acetonide After Joint Injury Modulates Molecular Outcomes Associated With Early Synovitis. *Arthritis Rheumatol*. 2016;68(7):1637-1647.
24. Evans CH, Kraus VB, Setton LA. Progress in intra-articular therapy. *Nat Rev Rheumatol*. 2014;10(1):11-22.
25. Scotti C, Gobbi A, Karnatzikos G, Martin I, Shimomura K, Lane JG et al. Cartilage Repair in the Inflamed Joint: Considerations for Biological Augmentation Toward Tissue Regeneration. *Tissue Eng Part B Rev*. 2016;22(2):149-159.
26. Beekhuizen M, Bastiaansen-Jenniskens YM, Koevoet W, Saris DB, Dhert WJ, Creemers LB et al. Osteoarthritic synovial tissue inhibition of proteoglycan production in human osteoarthritic knee cartilage: establishment and characterization of a long-term cartilage-synovium coculture. *Arthritis Rheum*. 2011;63(7):1918-1927.
27. Utomo L, van Osch GJ, Bayon Y, Verhaar JA, Bastiaansen-Jenniskens YM. Guiding synovial inflammation by macrophage phenotype modulation: an in vitro study towards a therapy for osteoarthritis. *Osteoarthritis Cartilage*. 2016;24(9):1629-1638.
28. Bastiaansen-Jenniskens YM, Wei W, Feijt C, Waarsing JH, Verhaar JA, Zuurmond AM et al. Stimulation of fibrotic processes by the infrapatellar fat pad in cultured synoviocytes from patients with osteoarthritis: a possible role for prostaglandin f2α. *Arthritis Rheum*. 2013;65(8):2070-2080.
29. Grotenhuis N, Bayon Y, Lange JF, Van Osch GJ, Bastiaansen-Jenniskens YM. A culture model to analyze the acute biomaterial-dependent reaction of human primary macrophages. *Biochemical and biophysical research communications*. 2013;433(1):115-120.
30. Tsuchida AI, Beekhuizen M, t Hart MC, Radstake TRDJ, Dhert WJA, Saris DBF et al. Cytokine profiles in the joint depend on pathology, but are different between synovial fluid, cartilage tissue and cultured chondrocytes. *Arthritis Research & Therapy*. 2014;16(5):441.
31. Tu GW, Shi Y, Zheng YJ, Ju MJ, He HY, Ma GG, et al. Glucocorticoid attenuates acute lung injury through induction of type 2 macrophage. *J Transl Med*. 2017;15(1):181.
32. Siebelt M, Korthagen N, Wei W, Groen H, Bastiaansen-Jenniskens Y, Müller C et al. Triamcinolone acetonide activates an anti-inflammatory and folate receptor-positive macrophage that prevents osteophytosis in vivo. *Arthritis Res Ther*. 2015;17:352.

33. Yona S, Gordon S. Inflammation: Glucocorticoids turn the monocyte switch. *Immunol Cell Biol.* 2007;85(2):81-82.
34. Ehrchen JM, Roth J, Barczyk-Kahlert K. More Than Suppression: Glucocorticoid Action on Monocytes and Macrophages. *Front Immunol.* 2019;10:2028.
35. Rustad KC, Gurtner GC. Mesenchymal Stem Cells Home to Sites of Injury and Inflammation. *Adv Wound Care (New Rochelle).* 2012;1(4):147-152.
36. Spaeth E, Klopp A, Dembinski J, Andreeff M, Marini F. Inflammation and tumor microenvironments: defining the migratory itinerary of mesenchymal stem cells. *Gene Ther.* 2008;15(10):730-738.
37. af Klint E, Grundtman C, Engström M, Catrina AI, Makrygiannakis D, Klareskog L et al. Intraarticular glucocorticoid treatment reduces inflammation in synovial cell infiltrations more efficiently than in synovial blood vessels. *Arthritis Rheum.* 2005;52(12):3880-3889.
38. Rudnik-Jansen I, Tellegen AR, Pouran B, Schrijver K, Meij BP, Emans PJ et al. Local controlled release of corticosteroids extends surgically induced joint instability by inhibiting tissue healing. *Br J Pharmacol.* 2019;176(20):4050-4064.
39. Tempfer H, Gehwolf R, Lehner C, Wagner A, Mtsariashvili M, Bauer HC et al. Effects of crystalline glucocorticoid triamcinolone acetonide on cultered human supraspinatus tendon cells. *Acta Orthop.* 2009;80(3):357-362.
40. Soma LR, Uboh CE, You Y, Guan F, Boston RC. Pharmacokinetics of intra-articular, intravenous, and intramuscular administration of triamcinolone acetonide and its effect on endogenous plasma hydrocortisone and cortisone concentrations in horses. *Am J Vet Res.* 2011;72(9):1234-1242.
41. Yasui Y, Hart DA, Sugita N, Chijimatsu R, Koizumi K, Ando W et al. Time-Dependent Recovery of Human Synovial Membrane Mesenchymal Stem Cell Function After High-Dose Steroid Therapy: Case Report and Laboratory Study. *Am J Sports Med.* 2018;46(3):695-701.
42. Wernecke C, Braun HJ, Dragoo JL. The Effect of Intra-articular Corticosteroids on Articular Cartilage: A Systematic Review. *Orthop J Sports Med.* 2015;3(5):2325967115581163.
43. Im G-I. Endogenous cartilage repair by recruitment of stem cells. *Tissue Engineering Part B: Reviews.* 2016;22(2):160-171.
44. McGonagle D, Baboolal TG, Jones E. Native joint-resident mesenchymal stem cells for cartilage repair in osteoarthritis. *Nat Rev Rheumatol.* 2017;13(12):719-730.
45. Arévalo-Turrubiarte M, Olmeo C, Accornero P, Baratta M, Martignani E. Analysis of mesenchymal cells (MSCs) from bone marrow, synovial fluid and mesenteric, neck and tail adipose tissue sources from equines. *Stem Cell Res.* 2019;37:101442.
46. Wehling N, Palmer GD, Pilapil C, Liu F, Wells JW, Muller PE et al. Interleukin-1beta and tumor necrosis factor alpha inhibit chondrogenesis by human mesenchymal stem cells through NF-kappaB-dependent pathways. *Arthritis Rheum.* 2009;60(3):801-812.
47. Harris Q, Seto J, O'Brien K, Lee PS, Kondo C, Heard BJ et al. Monocyte chemotactic protein-1 inhibits chondrogenesis of synovial mesenchymal progenitor cells: an in vitro study. *Stem Cells.* 2013;31(10):2253-2265.

48. Fahy N, de Vries-van Melle ML, Lehmann J, Wei W, Grotenhuis N, Farrell E et al. Human osteoarthritic synovium impacts chondrogenic differentiation of mesenchymal stem cells via macrophage polarisation state. *Osteoarthritis Cartilage*. 2014;22(8):1167-1175.

Intra-articular administration of triamcinolone acetonide in a murine cartilage defect model reduces inflammation but inhibits endogenous cartilage repair

Marinus A. Wesdorp

Serdar Capar

Yvonne M. Bastiaansen-Jenniskens

Nicole Kops

Laura B. Creemers

Jan A.N. Verhaar

Gerjo J.V.M. van Osch *

Wu Wei*

*both authors contributed equally

ABSTRACT

BACKGROUND: Cartilage defects result in joint inflammation. The presence of pro-inflammatory factors has been described to negatively affect cartilage formation.

PURPOSE: We aimed to evaluate the effect and timing of administration of triamcinolone acetonide (TAA), an anti-inflammatory drug, on cartilage repair using a mouse model.

STUDY DESIGN: Controlled laboratory study

MATERIALS & METHODS: A full-thickness cartilage defect was created in the trochlear groove of 10-week-old male DBA/1 mice (n=80). Mice received an intra-articular injection of TAA or saline on day 1 or 7 after induction of the defect. Mice were killed on day 10 and day 28 for histological evaluation of cartilage defect repair, synovial inflammation and synovial membrane thickness.

RESULTS: Mice injected with TAA had significantly less synovial inflammation at day 10 than saline-injected mice independent of the time of administration. At day 28, the levels of synovitis dropped towards healthy levels, nevertheless the synovial membrane was thinner in TAA than in saline-injected mice, reaching statistical significance in animals injected on day 1 ($70.1\mu\text{m}\pm 31.9$ vs. 111.9 ± 30.9 , $P=0.01$) but not in animals injected on day 7 ($68.2\mu\text{m}\pm 21.86$ vs. $90.2\mu\text{m}\pm 21.29$, $P=0.26$). A thinner synovial membrane was moderately associated with less filling of the defect after 10 and 28 days ($r=0.42$ and $r=0.47$, $P=0.02$ and $P=0.01$). Whereas ten days after surgery, there was no difference in the area of the defect filled and the cell density in the defect area between saline and TAA-injected knees, filling of the defect at day 28 was lower in TAA than in saline-injected knees for both injection time points (day 1 injection $P=0.04$, day 7 injection $P=0.01$). Moreover, there was less collagen type II staining in the filled defect area in TAA than in saline injected knees after 28 days, reaching statistical significance in day 1-injected knees (2.6%vs.18.5%, $P=0.01$), but not in day 7-injected knees (7.4%vs.15.8%, $P=0.27$).

CONCLUSION: Intra-articular injection of TAA reduced synovial inflammation, but negatively affected cartilage repair. This implies that inhibition of inflammation may inhibit cartilage repair or that TAA has a direct negative effect on cartilage formation.

CLINICAL RELEVANCE: Our findings show that TAA can inhibit cartilage defect repair. Therefore, we suggest not to use TAA to reduce inflammation in a cartilage repair setting.

Keywords

cartilage defect, inflammation, corticosteroids, anti-inflammatory agents

What is known about the subject

Cartilage defects result in joint inflammation. The presence of pro-inflammatory factors has been described to negatively affect cartilage formation. However, the effect of reducing inflammation on cartilage defect repair, has not well been investigated. Corticosteroids are used to inhibit inflammation in OA. The effect of TAA, a clinically approved corticosteroid, on endogenous repair of a cartilage defect *in vivo* is not clear.

What this study adds to existing knowledge

This study describes the effect TAA has on repair of a cartilage defect *in vivo* and whether it is useful to augment cartilage defect repair techniques with an anti-inflammatory component. Although TAA inhibits inflammation associated with the presence of cartilage defects, tissue repair is compromised. Caution is advised in the use of corticosteroids to reduce inflammation with the aim to improve cartilage repair.

INTRODUCTION

Articular cartilage is a highly specialized tissue that serves as a low-friction gliding surface and acts as a shock absorber to minimize peak pressures on the subchondral bone^{3,4}. Cartilage damage can occur during degenerative joint diseases or as a result of trauma^{1,7,18,50}. As articular cartilage has a limited capacity for self-repair, untreated cartilage defects have been implicated as a risk factor for the development of early-onset osteoarthritis^{6,14}. Furthermore, cartilage injuries evoke an inflammatory response that can remain for a long time^{19,41}.

High levels of pro-inflammatory cytokines, such as TNF- α , IL-1, and IL-6, are found in joints with cartilage defects^{40,41}. The presence of these mediators can negatively affect cartilage formation^{12,17}; however, it is not only the injury itself, but also the surgery involved in cartilage repair strategies that will lead to an inflammatory response in the joint⁵³. Yet, the role of inflammation in cartilage repair is not completely understood. In wound healing, inflammation is the first step in the repair process, and in fracture repair, the absence of pro-inflammatory mediators leads to impaired bone healing⁴⁵. On the other hand, prolonged inflammation results in impaired wound healing and increased scar formation¹¹. Furthermore, a selective pro-inflammatory cytokine inhibitor (IL-1Ra) reduced cartilage degeneration and synovitis in an intra-articular fracture model²⁴, and knee pain and dysfunction in a clinical study in ACL patients²⁶. These findings have led to the view that inflammation is initially needed, but then needs to be resolved to achieve optimal tissue repair.

To reduce inflammation, an anti-inflammatory drug can be used. Triamcinolone acetonide (TAA) is a corticosteroid and a potent anti-inflammatory drug. It is often injected intra-articularly to reduce the symptoms of knee osteoarthritis (OA)³². Also, it is acknowledged that glucocorticoids promote chondrogenic differentiation of human bMSCs by enhancing the expression of cartilage extracellular matrix genes⁸. However, there is controversy about its potential catabolic effects on the cartilage²² as TAA might increase cartilage loss in knee OA³⁰, inhibit glycosaminoglycan (GAG) production^{2,21}, and be chondrotoxic to chondrocytes^{9,42}. Moreover, Wernecke *et al* concluded in their systematic review that corticosteroids seem to have a time- and dose-dependent effect on articular cartilage. They suggested that a beneficial effect on cartilage has been described at a low dose and shorter duration, whereas detrimental effects were found with higher doses and longer duration⁴⁹. This highlights the need to understand clearly under what conditions TAA may be beneficial or harmful in endogenous cartilage defect repair.

In the current study, we investigated the effect of the anti-inflammatory drug TAA on endogenous cartilage repair in a murine cartilage defect model. Moreover, we investigated whether the timing of TAA treatment would influence inflammation and cartilage defect repair.

MATERIALS & METHODS

Animals

Male DBA/10IaHsd mice were purchased from Envigo, part of Jackson Laboratory (Horst, The Netherlands). After transportation, mice were allowed a seven-day acclimatization period. All mice regained normal behavior within 24 hours after transportation. Mice were housed under specific pathogen-free (SPF) conditions in groups of three or four per individually ventilated cage (IVC). They were maintained under a 12 hours light-dark cycle at 21 °C and fed a standard rodent diet with food and water ad libitum.

The study was carried out following the ARRIVE guidelines. Animal protocols and surgical procedures in this study were approved by the Institutional Animal Care and Use Committee (Erasmus MC University Medical Center, The Netherlands, AVD101002016991, AEC 16-691-01).

Experimental outline

Full-thickness cartilage defects were surgically created as described below on day zero in the left knee of ten-week-old male DBA/1 mice (n=80) with a mean weight of $21.3\text{g} \pm 1.8$. Young mice were chosen because of their ability for consistent healing of the articular cartilage, whereas older mice could not repair cartilage¹⁰. Cartilage repair was evaluated by histology after four weeks. Injections with TAA or saline (control) were either administered one day or seven days postoperatively to investigate the effect of timing of anti-inflammatory therapy resulting in four experimental groups (**Figure 1**). To obtain further insight in the repair process cellularity and early tissue formation were assessed after 10 days. Here, all animals received an intra-articular injection on both day one and seven; in the experimental groups with one of them being TAA, in the control group both with saline. This set-up gave a 50% reduction of the number of animals in the control group. Mice were randomly allocated to experimental groups. The number of animals per group was determined using a power calculation based on previous results⁴⁷. The time points for injection at one and seven days postoperatively were chosen based on previous research. Synovitis levels were found to peak after 7-14 days after induction by an inflammatory stimulus²⁰.

The chosen time points therefore represent two phases of inflammation, a very early stage of inflammation (1 day after defect creation) and around the peak (7 days after defect creation).

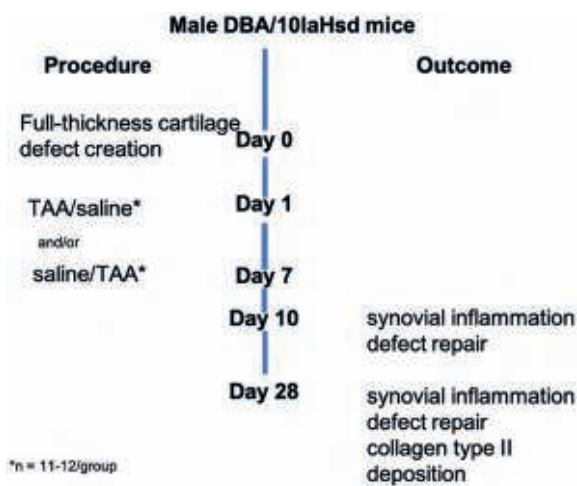


Figure 1. Overview of the experimental setup

Surgical procedure

The procedure was performed during day time in the animal facility operative theatre. One hour before surgery, all mice received a subcutaneous injection of buprenorphine hydrochloride 0.05 mg/kg (Temgesic; Indivior Europe Limited) for analgesia. Mice were anesthetized with an isoflurane/O₂ mixture, positioned on a warmed plate, and a full-thickness cartilage defect was surgically created as previously described by one experienced surgeon (WW) that was blinded to the treatment group^{10,47}. In short, a full-thickness cartilage defect of 250µm in length and 150µm in width was made in the intercondylar notch along the patellar groove using a 25 gauge (25G) hypodermic needle (BD Bioscience). The procedure was regarded as successful when evident bleeding of the subchondral bone was observed. The joint capsule was closed with two resorbable 6-0 Vicryl (Ethicon; Johnson&Johnson) and checked for patellar stability during flexion and extension motion. Full weight-bearing was allowed after recovery from anesthesia. All mice recovered quickly from the anesthesia.

Intra-articular injection

Intra-articular injections of 25 µg TAA suspended in sterile 0.9% saline (Kenacort; Bristol Myers Squibb), or sterile 0.9% saline (as vehicle control) were infused into the operated knee one day and/or seven days post-surgery. The concentration was based on previous rodent studies^{28,35,38}. Under isoflurane/O₂ anesthesia with the mouse in

a supine position, the knee was fully extended and kept in place by surgical forceps. A small skin cut was made to expose the patellar tendon and joint capsule sutures. A 30µL precision glass syringe (Hamilton Company) with a 30G needle (BD Bioscience) was used to inject 6µL into the joint space. In each experiment all injections were performed by one person who was blinded to the treatment group. A second person assisted the injections by preparing all mice and injection fluids for the author performing the injections to ensure blinding of the injecting person.

Tissue processing

At the experimental end-point, animals were euthanized under anesthesia by cervical dislocation. Directly after euthanizing and removal of the skin, both hind legs were dissected below the hip and above the ankle. After removal of the subcutaneous fat and muscles, the knees were fixed in 4% formaldehyde for seven days, followed by two weeks of decalcification in 10% ethylenediaminetetraacetic acid (EDTA), pH 7.4. Samples were further processed by dehydration and infiltration with paraffin. The femoral axis was adjusted to be upright against the embedding surface according to the method by Eltawil *et al.*¹⁰. Subsequently, 6 µm-sections were cut using a microtome (Leica RM-2135; Leica Microsystems). Per knee, six sections at a distance of 100µm were used. As a landmark for section level, cross-section of the growth plate in four points was used. Each section was stained with hematoxylin and eosin (H&E, Sigma-Aldrich) to assess cell morphology and reconstitution of the osteochondral junction. Additionally, a Thionine staining (0.04%, Sigma-Aldrich) was used to analyze the filling of the defect and matrix staining intensity, representative of the amount and distribution of glycosaminoglycan (GAG). Sections from the day 28 endpoint were immunostained with a primary antibody against the cartilage matrix protein collagen type II (mouse anti-human, 1:100 dilution, II-II/II6B3; Developmental Studies Hybridoma Bank). In short, antigen retrieval was performed using pronase 1mg/mL (Sigma-Aldrich) PBS (Sigma-Aldrich), followed by hyaluronidase 10mg/mL PBS (Sigma-Aldrich). To prevent cross-reaction with mouse antigens the primary coll-II antibody was pre-incubated overnight with a biotin-SP F(ab)₂-labeled goat anti-mouse antibody (#115-066-062; Jackson ImmunoResearch Europe). After incubation an alkaline-phosphatase-avidin labeled antibody was used (Biogenex Laboratories, CA, USA), which combined with the Neu Fuchsin substrate resulted in pink staining. An isotype IgG1 monoclonal antibody was used as a negative control. All sections were stained in one batch to reduce staining variation between different samples. Slides were imaged using a 40x objective on a slide scanner (NanoZoomer C9600-12; Hamamatsu Photonics) and processed using NanoZoomer Digital Pathology Image software (Hamamatsu Photonics). Knees with a patella dislocation (determined on histology) were excluded from the analysis.

Evaluation of cartilage repair

All knees were scored using the validated semiquantitative histological scoring system for articular cartilage repair developed by Pineda *et al.*³³. The Pineda score contains the following subdomains: filling of the defect, reconstitution of the osteochondral junction, matrix staining, and cell morphology. A score ranging from 0-4 is given to the subdomains filling of the defect, matrix staining, and cell morphology. Reconstitution of the osteochondral junction is scored between 0 and 2, resulting in a total histologic score ranging from 0-14, where 0 is the best repair, and 14 the worst. Scoring was performed independently by two authors (MW & NK), blinded to the experimental group. Per knee, three different representative sections were scored, resulting in an average score per knee. The average of the two observer scores was used per animal. Inter-observer reliability for cartilage repair scores based on absolute agreement was excellent (interclass correlation coefficient (ICC) 0.96, 95% confidence interval (CI) 0.92-0.98). The filling of the original defect area was measured using NanoZoomer Digital Pathology Image software (Hamamatsu Photonics). Collagen type II deposition was measured by the area stained positive for collagen type II, divided by the total filled area of the defect. The percentages were averaged as described above.

Evaluation of joint inflammation

Joint inflammation was measured by the synovial membrane thickness and Krenn-scores²⁷ on the lateral side of the patella-femoral joint using NanoZoomer Digital Pathology Image software (Hamamatsu Photonics). The lateral side was chosen to be most representative, because of the arthrotomy and sutures on the medial side. Per knee, the synovial thickness was measured in three different sections at three different positions and the average of these nine measurements was calculated. Per mouse the average of two observers was used for further statistical analyses.

Statistical analysis

Pineda scores were considered as non-parametric data. Differences between groups were assessed using a Kruskal-Wallis test with post hoc Dunn non-parametric comparison analysis. Filling of the defect and synovial thickness data were tested for normality using a Shapiro-Wilk test. All data were normally distributed, described as mean · SD, and assessed using a one-way ANOVA, followed by post hoc Tukey honestly significant difference analysis. Correlation values were calculated using the Pearson rho test in case of normal data distribution. A Spearman rho test was used for non-parametric data. Inter-observer reliability of all measurements is expressed as (ICC). A two-way mixed model based on absolute agreement for single measures was used. ICC > 0.75 is regarded as excellent²⁵. All statistical tests were two-tailed. A *P* value

of < 0.05 was considered statistically significant. SPSS statistics package 24.0 for Mac (SPSS Inc) was used for all analyses.

RESULTS

Seventy nine out of 80 animals reached the end-point without signs of infection or abnormal behavior. One animal was lethargic, non-responsive, and had a ruffled fur one day after surgery. Based on these signs and in consultation with the Animal Board, the animal was euthanized. In some of the operated mice, a limping gait pattern was observed in the first three days that resolved in all mice within 7 days. Some mice had a patella dislocation (determined by histology) and were excluded from further histological analyses. Interestingly the dislocations were not equally distributed over the groups. For the 28-day time point, six out of 11 mice injected with TAA at day one had a patella dislocation compared to one out of 11 mice in the saline group ($P = 0.02$). Also, six out of 11 mice injected with TAA at day seven had a patella dislocation compared to two out of 11 mice in the saline group. At the 10-day time point only one mouse (injected with TAA one day after creating the defect) had a patella dislocation, indicating dislocations most likely developed after this time point.

Intra-articular triamcinolone acetone injection reduced synovial inflammation and synovial membrane thickening

To evaluate the effect of TAA on local inflammation in the joint, the thickness of the synovial membrane and the Krenn-scores were evaluated at days 10 and 28 after surgery. The synovium was thicker in knees that underwent full-thickness cartilage defect induction surgery than in non-operated knees (**Figure 2**). Mice injected with TAA one day after surgery had a significantly thinner synovial membrane than control saline-injected mice at day 28 ($70.1\mu\text{m} \pm 31.9$ vs. $111.9\mu\text{m} \pm 30.9$, $P = 0.01$, **Figure 2**), but not at day 10 ($124.7\mu\text{m} \pm 20.0$ vs. $131.3\mu\text{m} \pm 22.0$, $P = 0.80$, **Figure 2**). The Krenn-scores of the mice injected one day after surgery were lower in mice injected with TAA than in saline-injected control mice at day 10 ($P = 0.017$), but not at 28 days ($P = 0.67$). Mice injected with TAA seven days after surgery had a thinner synovial membrane than saline-injected mice at day 10 ($103.1\mu\text{m} \pm 25.2$ vs. $131.3\mu\text{m} \pm 22.0$, $P = 0.02$, **Figure 2A**), and at day 28 ($68.2\mu\text{m} \pm 21.86$ vs. $90.2\mu\text{m} \pm 21.29$, $P = 0.26$, **Figure 2B**), although this did not reach statistical significance. The Krenn-scores in the mice injected 7 days after surgery were significantly lower in the TAA injected than in the saline-injected mice at day 10 ($P < 0.0001$), and at day 28 ($P = 0.005$).

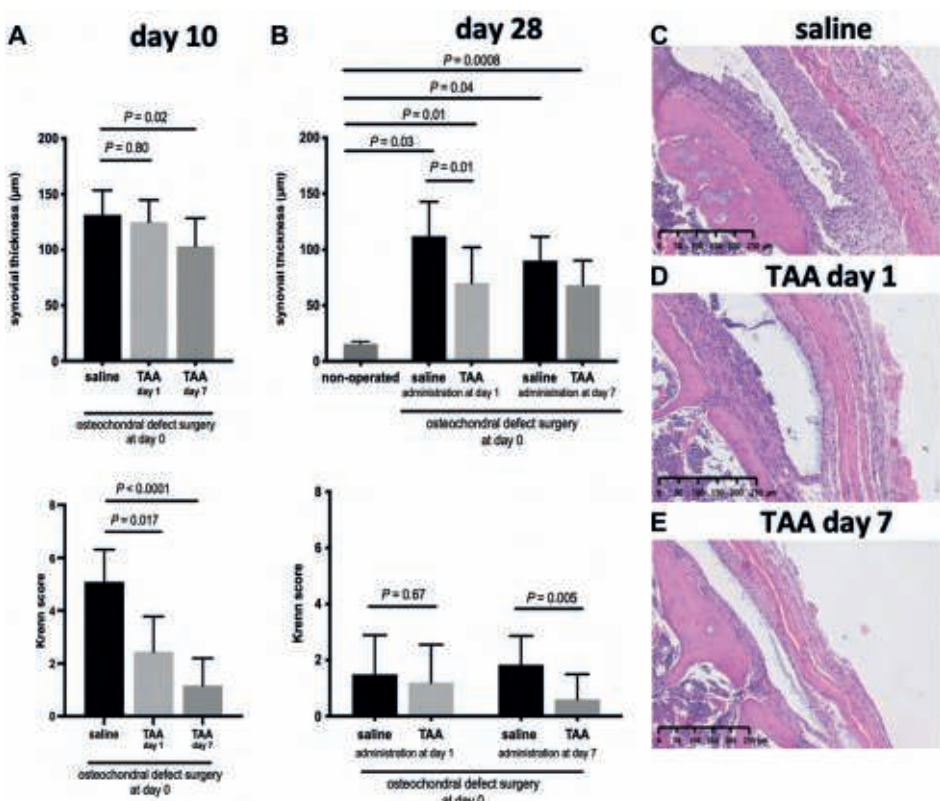


Figure 2. Triamcinolone acetate reduced synovial inflammation. A) The thickness of the synovium and the Krenn-score on the lateral side of the patella-femoral joint at day 10 after full-thickness cartilage defect induction surgery. B) The thickness of the synovium and the Krenn-score on the lateral side of the patella-femoral joint at day 28 after full-thickness cartilage defect induction surgery. C-E) Representative images of the Krenn scores at day 10 in each group. Mice were injected with TAA or saline 1 and/or 7 days after surgery. Each bar represents the mean of all defects in the respective group \pm SD. n=5-10 mice per group. Abbreviations: TAA, triamcinolone acetate; μ m, micrometer.

Cell ingrowth was not inhibited by triamcinolone acetate administration

At day 10, the defect was filled with undifferentiated cells with a spindle-shaped morphology (Figure 3A). There was no difference in the area of the defect filled between the saline and TAA groups at day 10 (Figure 3B). Also, the timing of TAA injection did not affect the filling of the defect (Figure 3B). In addition, the cell density in the defect area was similar in all groups (Figure 3C). This suggests that TAA did not affect migration and/or proliferation of cells in the defect.

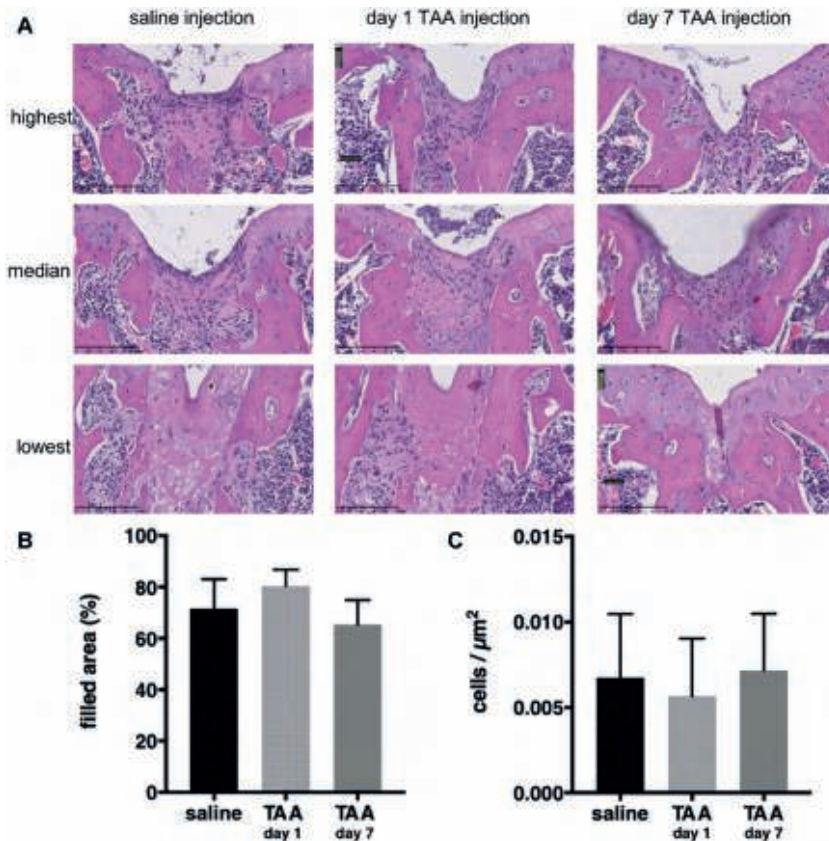


Figure 3. Cellularity was not affected by triamcinolone acetone.

A) Representative images of the highest, median and lowest cell density in the defect at day 10 stratified per group. B) Area filled relative to the original size of the defect. C) Number of cells per squared micrometer. Each bar represents the mean of all defects in the respective group \pm SD. $n=11-12$ mice per group. Abbreviations: μm , micrometer; SD, standard deviation.

Cartilage repair was inhibited by triamcinolone acetone treatment

The effect of TAA injection on cartilage repair was evaluated with histology. Twenty-eight days after generation of the full-thickness defect, the tissue filling the defect consisted of chondrocyte-like cells surrounded by thionine-stained matrix (**Figure 4A**). The median Pineda cartilage repair score was similar in mice treated after one day with TAA and in control mice that received a saline injection (8.9 (IQR 5.9 - 8.9) vs. 8.3 (IQR 5.0-8.7), $P > 0.99$, **Figure 4B**). There were no differences between mice injected with saline, TAA at day one, or TAA at day seven on subdomains of the Pineda cartilage repair score; restoration of the osteochondral junction, matrix staining intensity, or cell morphology (**Supplementary Figure 1**). However, a significantly

lower percentage of the defect area was filled in mice treated with TAA after one day than in control mice injected with saline ($76.4\% \pm 7.0$ vs. $90.4\% \pm 7.4$, $P = 0.04$, **Figure 4C**). Moreover, a significantly lower percentage of the filled defect area stained positive for collagen type II in mice treated with TAA after one day than in control mice injected with saline ($2.6\% \pm 1.5$ vs. $18.5\% \pm 9.6$, $P = 0.01$, **Figure 4D and Figure 5 A,B**). In mice treated with TAA after seven days, median cartilage repair scores at day 28 were similar to control mice injected with saline (8.3 (IQR $6.5 - 11.3$) vs. 7.0 (IQR $6 - 8.4$), $P = 0.44$, **Figure 4E**). Here, the percentage of the defect area that was filled was also significantly lower in TAA injected than in saline-injected control mice ($67.8\% \pm 17.6$ vs. $85.55\% \pm 1.5$, $P = 0.01$, **Figure 4F and Figure 5 A,C**). Also, a seemingly lower percentage of the filled defect area stained positive for collagen type II in mice treated with TAA after seven days than in control mice injected with saline ($7.4\% \pm 12.5$ vs. $15.8\% \pm 10.1$, $P = 0.27$, **Figure 4G**), albeit non-significant due to one outlier.

A moderate correlation was observed between synovial membrane thickness and defect filling

To investigate the relationship between inflammation and cartilage repair, we correlated synovium thickness with defect filling. The thickness of the synovial membrane was moderately associated with the defect filling at day 10 ($r\ 0.42$, $P = 0.02$) and day 28 ($r\ 0.47$, $P = 0.01$, **Figure 6**). Thickness of the synovial membrane was not associated with cell density in the filled defect at day 10 ($r\ -0.08$, $P = 0.69$). Also, the thickness of the synovial membrane and cartilage repair scores were not associated at day 28 ($r\ -0.18$, $P = 0.35$) and day 10 ($r\ 0.006$, $P = 0.97$). No associations were found between Krenn score and defect filling, probably due to the limited range and variation of Krenn scores (0-8).

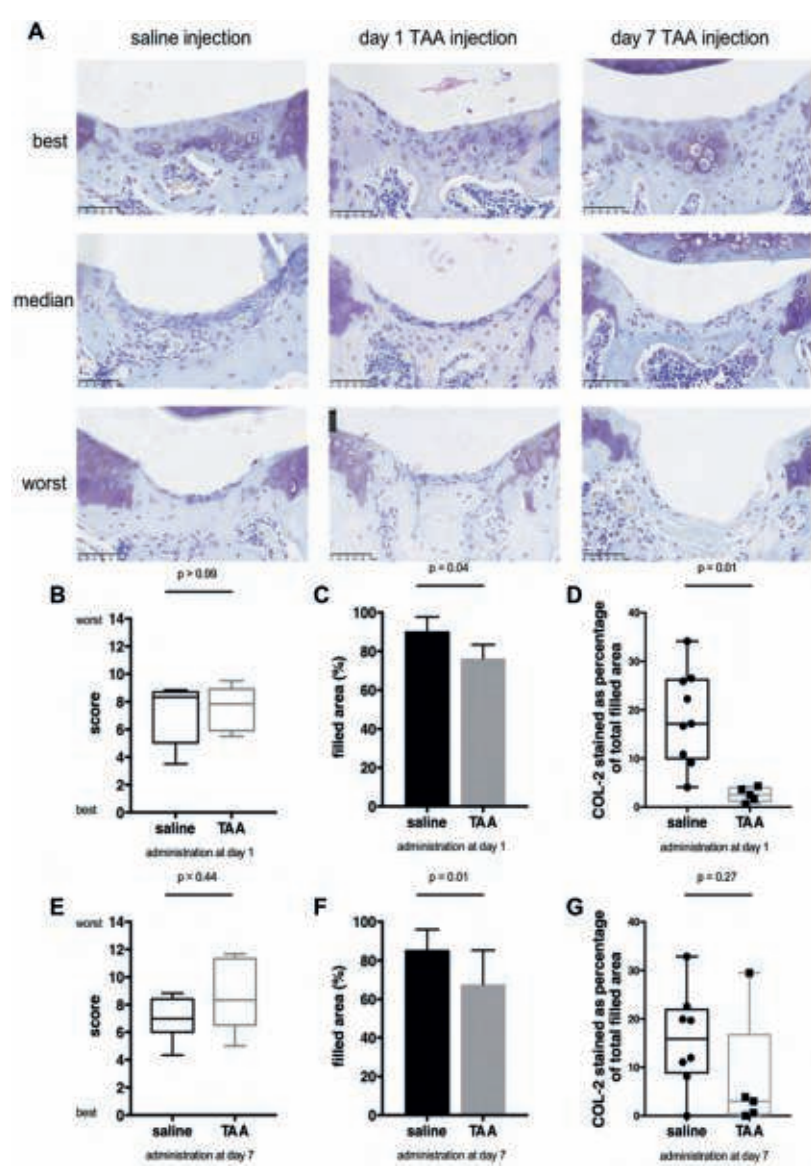


Figure 4. Triamcinolone acetate resulted in less filling and collagen type II deposition in the defect.

A) Representative images of the best, median and worst cartilage repair in the control group treated with saline and groups injected with TAA 1 or 7 days after the creation of a full-thickness defect. The scale bar represents 50 μ m. B) Cartilage repair (Pineda) score at day 28 and injection at day 1. C) Area filled on day 28 relative to the original size of the defect in knees injected on day 1. D) Percentage of collagen type II relative to the filled area at day 28 in knees injected on day 1. E) Cartilage repair (Pineda) score at day 28 and injection at day 7. F) Area filled at day 28 relative to the original size of the defect in knees injected on day 7. G) Percentage of collagen type II relative to the filled area at day 28 in knees injected on day 7. Box plots represent the 25th and 75th percentile with the median, the whiskers indicate the maximum and minimum. Each bar represents the mean of all defects in the respective group. n=5-10 mice per group. \pm SD. Abbreviations: TAA, triamcinolone acetate; μ m, micrometer; SD, standard deviation.

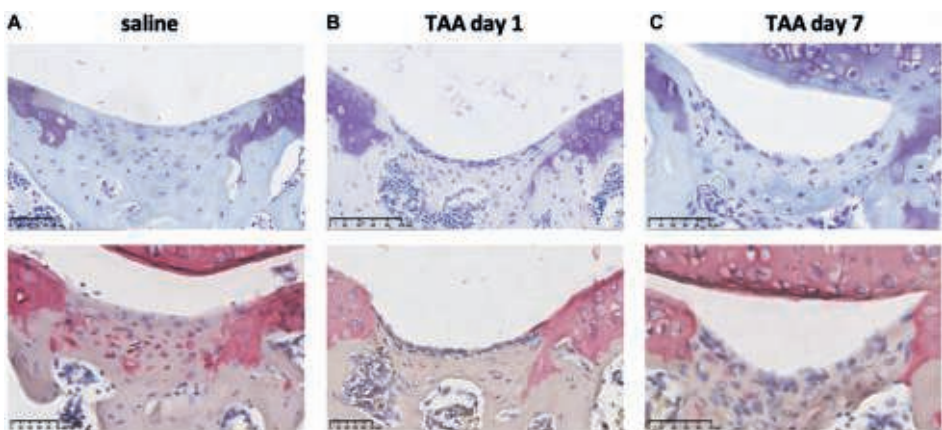


Figure 5. Triamcinolone acetone resulted in less collagen type II deposition in the defect.
A-C) Representative images of thionin (top) and collagen type II (bottom) staining at day 28 in the control group treated with saline and groups injected with TAA at day 1 or 7 after the creation of a full-thickness defect. Thionin and collagen type II staining on the same sample are shown. The scale bar represents 50µm. Abbreviations: TAA, triamcinolone acetone.

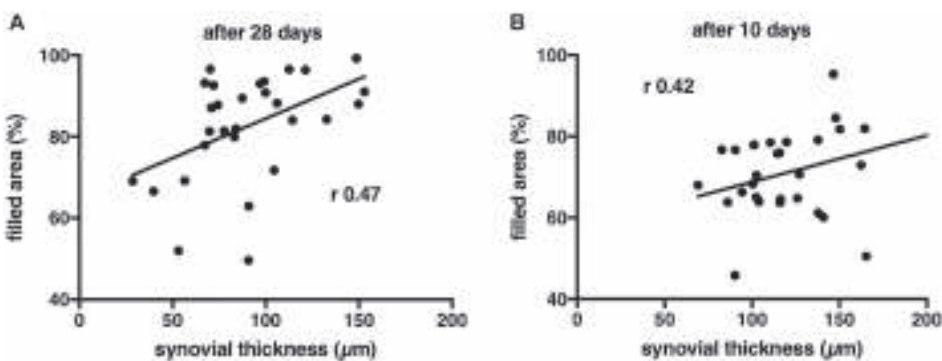


Figure 6. A thinner synovial membrane was moderately associated with less filling of the defect.
A) Scatter plot showing the correlation between synovial thickness and area of the defect filled at day 10. B) Scatter plot showing the correlation between synovial thickness and area of the defect filled at day 28. Each dot represents a unique sample. Abbreviations: µm, micrometer.

DISCUSSION

Previous *in vitro* studies have shown that pro-inflammatory factors inhibit cartilage formation. However, there have only been a few studies exploring the role of anti-inflammatory treatment in cartilage defect repair *in vivo*. Therefore, the purpose of this study was to evaluate the effect of TAA, an anti-inflammatory drug, on endogenous cartilage defect repair. Our main finding was that intra-articular injection with TAA in a murine model for endogenous cartilage repair, reduced synovial inflammation but also inhibited cartilage repair. After 28 days, we observed less filling of the defect in

knees injected with TAA. After ten days, defect filling was not significantly affected by TAA treatment. This observation might suggest that TAA does not affect the influx or proliferation of cells but negatively influences tissue formation in the defect.

To our knowledge, this is the first *in vivo* study evaluating the role of TAA in a model of endogenous cartilage defect repair. We observed less filling of the defect and less collagen type II deposition after 28 days in knees injected with TAA. Although there are no studies on the role of TAA in cartilage defect repair, TAA has been used to study the effect on cartilage in both healthy and OA joints showing conflicting results. One study found dose-dependent degenerative changes in the cartilage of healthy rabbit knees after 2-6 weeks of weekly 3mg TAA injections³¹. Another study found more cartilage degeneration indicated by higher Mankin scores in surgical ACLT and meniscus destabilized rat knees after injection of the extended-release form of TAA³⁶. These findings can be considered in line with the reduced deposition of type II collagen and the reduced filling of the defect we observed. On the other hand, in a collagenase-induced OA rat model, injection of TAA as bolus nor as extended release formulation had an effect on cartilage degeneration³⁴. When Frisbie and colleagues¹³ administered two intra-articular doses of 12mg TAA 13 and 27 days after surgical induction of osteochondral fractures in equine carpal bones, less cartilage degeneration, indicated by lower Mankin scores, was found. Interestingly, the effects were most pronounced if TAA was injected in the contralateral (uninjured) joint rather than the diseased joint, indicating beneficial effects were most pronounced at very low concentrations. The extended presence of TAA in the joint and higher concentrations of TAA in the joint can be detrimental for the cartilage as seen in the study of Rudnik et al.³⁶, although this may depend on the type of pathology present in the joint.

In our study mice injected with TAA had less synovial inflammation than saline-injected mice. This is in line with what is known in literature in arthritis rodent models^{29,34}. Furthermore, in some cases TAA injection even reduced the inflammation to the healthy non-operated situation (as demonstrated by a Krenn score of 1), which is in line with other studies that reported less mononuclear cell infiltration and intimal hyperplasia in response to TAA^{13,27,39}. We found a thicker synovial membrane to be associated with more filling of the defect. This association suggests that inflammation has a positive effect on the filling of the defect. In fracture repair research, knock-out studies in mice have shown that the absence of inflammation-related pro-inflammatory molecules, such as TNF- α and COX-2, lead to a delay in bone healing^{15,52}. This implicates that inflammation is needed to initiate healing. On the contrary, excessive inflammation was shown to inhibit *in vitro* MSC chondrogenesis in a model with inflammatory

factors present from OA joints and from traumatically injured joints^{17,48}. Reducing the inflammation by inhibition of IL-1 α TAK (oxozaenol) or JAK (tofacitinib) could partially restore this inhibitory effect on cartilage formation^{17,44}. However, cartilage formation was shown to be inhibited when anti-inflammatory compounds such as a protein kinase inhibitor or TNF- α inhibitor was used at an early stage of chondrogenesis^{23,44}. This might explain why we observed a decrease in type II collagen deposition, as we administered our anti-inflammatory compound at an early stage of new cartilage formation in the defect site. These findings highlight the challenging balance between inflammation and cartilage defect repair. We acknowledge, though, that inflammation is more comprehensive than synovial thickness and mononuclear cell infiltration only. Serological measurements of the synovial fluid and the composition of inflammatory cells inside the synovial membrane over time could help to better evaluate the role of joint inflammation in cartilage repair.

Cartilage repair scores and filling of the defect were slightly worse when the defect was treated after seven days, albeit non-significant. It is known that the presence of chronic pro-inflammatory factors can impair chondrogenesis and stimulate degeneration of newly formed cartilage^{12,46}. Saris et al. showed in an *in vivo* study in goats that cartilage repair scores were worse in surgical defects treated late compared to defects treated immediately after induction³⁷. After seven days the pro-inflammatory factors may have dropped to a lower level reaching a more chronic inflammatory phase¹⁹. However, it is debatable whether TAA is the right tool to inhibit acute inflammation at these timepoints. Inflammation is a dynamic process that does not only occur between day one and seven, but throughout time. A study in horses that were intra-articularly injected with TAA showed that TAA remained present in the synovial fluid up to 14 days, whereas it was undetectable in serum after 48 hours⁵. This means that TAA administered at day 1 might inhibit inflammation up to 14 days, and thereby not only the acute inflammation phase but also the chronic phase¹⁹. Also, the day 7 injection inhibits this phase resulting in less inflammation after this timepoint. Therefore, it remains uncertain what the effect is if only the acute phase would be inhibited. Future studies should explore the role of selectively inhibiting the acute inflammation phase and the effect on cartilage repair. Based on our results, we can conclude that TAA inhibited cartilage repair regardless of the time of administration and neither early nor late administration is advised.

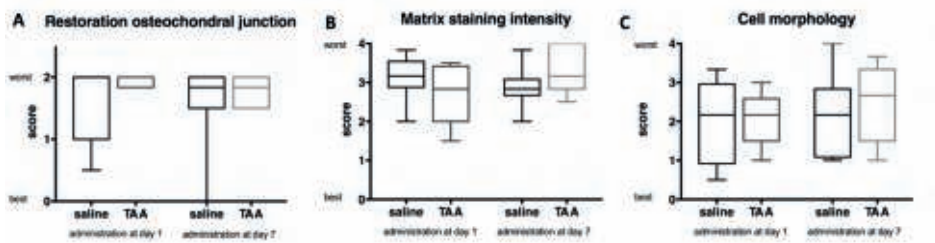
TAA is known to inhibit both tissue outgrowth from ligaments and collagen synthesis in tenocytes, indicating that TAA can impair wound healing in many respects^{43,51}. TAA injection in a rat destabilization-induced OA model (ACL transection and partial meniscectomy) resulted in increased joint instability and subluxations on the longer

term³⁶. Although patella dislocation is relative frequently occurring after surgical procedures in mice⁴⁷, its frequency was significantly higher in TAA-injected animals ($P = 0.004$). Our results indicate that TAA might have a negative effect on wound healing of the arthrotomy site thus resulting in patella dislocations. Interestingly, on day 10 only one out of 24 mice injected with TAA had developed a patella dislocation implicating that patella dislocations develop after this time point. For mice in the 10-day group the endpoint was only 9 or 3 days after TAA injection and most likely the arthrotomy sutures would still provide some support. Hence, this time point might have been too early to observe effects on wound healing. Another explanation might be that TAA reduced pain in the inflamed joint in the time period 1 - 4 weeks after administration¹⁶. This pain reduction might allow mice in the TAA group to move more freely throughout the study period and causing more patellar dislocations than in the saline-injected group.

For translation of these results to clinical practice, some limitations of our study need to be considered. Firstly, with the model chosen we could only study the effect of reducing inflammation on cartilage repair that relies on the body's endogenous repair capacity. It is unclear what the effect will be on procedures like articular chondrocyte implantation (ACI) and/or transplantation strategies, although based on our study it seems that TAA mainly affects the production of extracellular matrix. This indicates that TAA could also negatively influence repair using approaches like ACI. Moreover, for this study we specifically selected DBA mice of 10 weeks of age, as this strain at this age has been shown to be most optimal to study modulation of the endogenous cartilage repair capacity. It is unclear how the results of these young adult mice will translate to a young or middle-aged patient population with a cartilage defect. Additionally, although the dose regimen we tested was consistent and translated from clinical guidelines, we cannot exclude that other dose, timing and or frequency would have generated a different effect. The model furthermore differs from the clinical rehabilitation as the animals were allowed to move freely after surgery. This could potentially affect the stability of the early repair tissue in the defect. In a clinical situation the patient would be non-weight bearing for the first few weeks after a cartilage repair procedure. Finally, our focus was mainly on cartilage repair and inflammation of the joint and we have not measured pain. It would, however, be interesting to see if TAA could play a role in the postoperative care to reduce pain after injuring the articular cartilage.

In conclusion, intra-articular injection of TAA reduced synovial inflammation but inhibited cartilage repair. This implies that inhibition of inflammation with TAA might not be the right direction to move cartilage repair forward. The thin line between

the level of inflammation required and optimal cartilage defect repair underscores the importance of incorporating rational control of inflammation into cartilage repair strategies. The use of TAA to reduce inflammation after cartilage defect treatment to improve cartilage repair is therefore not warranted.



Supplementary Figure 1. Triamcinolone acetate did not affect the subdomains of the cartilage repair score.

A) Restoration of the original osteochondral junction at day 28 scored on a scale of 0 (restored) to 2 (not restored). B) Matrix staining intensity of thionine scored on a scale of 0 (normal) to 4 (no staining). C) Cell morphology scored on a scale of 0 (normal) to 4 (non-chondrocytic cells). Box plots represent the 25th and 75th percentile with the median, the whiskers indicate the maximum and minimum. n=5-10 mice per group. Abbreviations: TAA, triamcinolone acetate.

REFERENCES

1. Aroen A, Loken S, Heir S, et al. Articular cartilage lesions in 993 consecutive knee arthroscopies. *The American journal of sports medicine*. 2004;32(1):211-215.
2. Beekhuizen M, Bastiaansen-Jenniskens Y, Koevoet JLM, et al. Osteoarthritic Synovial Tissue Inhibition of Proteoglycan Production in Human Osteoarthritic Knee Cartilage Establishment and Characterization of a Long-Term Cartilage Synovium-Coculture. *Arthritis and rheumatism*. 2011;63:1918-1927.
3. Buckwalter JA, Mankin HJ. Instructional Course Lectures, The American Academy of Orthopaedic Surgeons - Articular Cartilage. Part I: Tissue Design and Chondrocyte-Matrix Interactions*†. *JBJS*. 1997;79(4):600-611.
4. Buckwalter JA, Mankin HJ. Instructional Course Lectures, The American Academy of Orthopaedic Surgeons - Articular Cartilage. Part II: Degeneration and Osteoarthrosis, Repair, Regeneration, and Transplantation*†. *JBJS*. 1997;79(4):612-632.
5. Chen CL, Sailor JA, Collier J, Wiegand J. Synovial and serum levels of triamcinolone following intra-articular administration of triamcinolone acetone in the horse. *J Vet Pharmacol Ther*. 1992;15(3):240-246.
6. Convery FR, Akeson WH, Keown GH. The repair of large osteochondral defects. An experimental study in horses. *Clinical orthopaedics and related research*. 1972;82:253-262.
7. Curl WW, Krome J, Gordon ES, Rushing J, Smith BP, Poehling GG. Cartilage injuries: A review of 31,516 knee arthroscopies. *Arthroscopy*. 1997;13(4):456-460.
8. Derfoul A, Perkins GL, Hall DJ, Tuan RS. Glucocorticoids promote chondrogenic differentiation of adult human mesenchymal stem cells by enhancing expression of cartilage extracellular matrix genes. *Stem cells*. 2006;24(6):1487-1495.
9. Dragoo JL, Danial CM, Braun HJ, Pouliot MA, Kim HJ. The chondrotoxicity of single-dose corticosteroids. *Knee surgery, sports traumatology, arthroscopy : official journal of the ESSKA*. 2012;20(9):1809-1814.
10. Eltawil NM, De Bari C, Achan P, Pitzalis C, Dell'accio F. A novel in vivo murine model of cartilage regeneration. Age and strain-dependent outcome after joint surface injury. *Osteoarthritis and cartilage*. 2009;17(6):695-704.
11. Eming SA, Krieg T, Davidson JM. Inflammation in wound repair: molecular and cellular mechanisms. *Journal of Investigative Dermatology*. 2007;127(3):514-525.
12. Fahy N, de Vries-van Melle ML, Lehmann J, et al. Human osteoarthritic synovium impacts chondrogenic differentiation of mesenchymal stem cells via macrophage polarisation state. *Osteoarthritis and cartilage*. 2014;22(8):1167-1175.
13. Frisbie DD, Kawcak CE, Trotter GW, Powers BE, Walton RM, McIlwraith CW. Effects of triamcinolone acetone on an in vivo equine osteochondral fragment exercise model. *Equine Vet J*. 1997;29(5):349-359.
14. Fuller JA, Ghadially FN. Ultrastructural observations on surgically produced partial-thickness defects in articular cartilage. *Clinical orthopaedics and related research*. 1972;86:193-205.

15. Gerstenfeld LC, Cho T-J, Kon T, et al. Impaired intramembranous bone formation during bone repair in the absence of tumor necrosis factor-alpha signaling. *Cells Tissues Organs*. 2001;169(3):285-294.
16. Godwin M, Dawes M. Intra-articular steroid injections for painful knees. Systematic review with meta-analysis. *Can Fam Physician*. 2004;50:241-248.
17. Heldens GT, Blaney Davidson EN, Vitters EL, et al. Catabolic factors and osteoarthritis-conditioned medium inhibit chondrogenesis of human mesenchymal stem cells. *Tissue Eng Part A*. 2012;18(1-2):45-54.
18. Hjelle K, Solheim E, Strand T, Muri R, Brittberg M. Articular cartilage defects in 1,000 knee arthroscopies. *Arthroscopy*. 2002;18(7):730-734.
19. Irie K, Uchiyama E, Iwaso H. Intraarticular inflammatory cytokines in acute anterior cruciate ligament injured knee. *The Knee*. 2003;10(1):93-96.
20. Jackson MT, Moradi B, Zaki S, et al. Depletion of protease-activated receptor 2 but not protease-activated receptor 1 may confer protection against osteoarthritis in mice through extracartilaginous mechanisms. *Arthritis Rheumatol*. 2014;66(12):3337-3348.
21. Jansen I, Tellegen A, Tryfonidou M, et al. Brief exposure to triamcinolone acetonide, but not its continuous presence, strongly inhibits cartilage regeneration by chondrocytes. *Osteoarthritis and cartilage*. 2016;24:S337.
22. Jüni P, Hari R, Rutjes AW, et al. Intra-articular corticosteroid for knee osteoarthritis. *Cochrane Database of Systematic Reviews*. 2015(10).
23. Kawaguchi A, Nakaya H, Okabe T, et al. Blocking of tumor necrosis factor activity promotes natural repair of osteochondral defects in rabbit knee. *Acta Orthop*. 2009;80(5):606-611.
24. Kimmerling KA, Furman BD, Mangiapani DS, et al. Sustained intra-articular delivery of IL-1RA from a thermally-responsive elastin-like polypeptide as a therapy for post-traumatic arthritis. *Eur Cell Mater*. 2015;29:124-139; discussion 139-140.
25. Koo TK, Li MY. A Guideline of Selecting and Reporting Intraclass Correlation Coefficients for Reliability Research. *Journal of chiropractic medicine*. 2016;15(2):155-163.
26. Kraus VB, Birmingham J, Stabler TV, et al. Effects of intraarticular IL1-Ra for acute anterior cruciate ligament knee injury: a randomized controlled pilot trial (NCT00332254). *Osteoarthritis and cartilage*. 2012;20(4):271-278.
27. Krenn V, Morawietz L, Burmester GR, et al. Synovitis score: discrimination between chronic low-grade and high-grade synovitis. *Histopathology*. 2006;49(4):358-364.
28. Kroin JS, Kc R, Li X, et al. Intraarticular slow-release triamcinolone acetate reduces allodynia in an experimental mouse knee osteoarthritis model. *Gene*. 2016;591(1):1-5.
29. Kumar A, Bendele AM, Blanks RC, Bodick N. Sustained efficacy of a single intra-articular dose of FX006 in a rat model of repeated localized knee arthritis. *Osteoarthritis and cartilage*. 2015;23(1):151-160.
30. McAlindon TE, LaValley MP, Harvey WF, et al. Effect of Intra-articular Triamcinolone vs Saline on Knee Cartilage Volume and Pain in Patients With Knee Osteoarthritis: A Randomized Clinical Trial. *Jama*. 2017;317(19):1967-1975.
31. Moskowitz RW, Davis W, Sammarco J, Mast W, Chase SW. Experimentally induced corticosteroid arthropathy. *Arthritis and rheumatism*. 1970;13(3):236-243.

32. Paik J, Duggan ST, Keam SJ. Triamcinolone Acetonide Extended-Release: A Review in Osteoarthritis Pain of the Knee. *Drugs*. 2019;79(4):455-462.
33. Pineda S, Pollack A, Stevenson S, Goldberg V, Caplan A. A semiquantitative scale for histologic grading of articular cartilage repair. *Acta anatomica*. 1992;143(4):335-340.
34. Rudnik-Jansen I, Colen S, Berard J, et al. Prolonged inhibition of inflammation in osteoarthritis by triamcinolone acetonide released from a polyester amide microsphere platform. *J Control Release*. 2017;253:64-72.
35. Rudnik-Jansen I, Schrijver K, Woike N, et al. Intra-articular injection of triamcinolone acetonide releasing biomaterial microspheres inhibits pain and inflammation in an acute arthritis model. *Drug delivery*. 2019;26(1):226-236.
36. Rudnik-Jansen I, Tellegen AR, Pouran B, et al. Local controlled release of corticosteroids extends surgically induced joint instability by inhibiting tissue healing. *Br J Pharmacol*. 2019;176(20):4050-4064.
37. Saris D, Dhert WJ, Verbout A. Joint homeostasis: the discrepancy between old and fresh defects in cartilage repair. *The Journal of bone and joint surgery British volume*. 2003;85(7):1067-1076.
38. Siebelt M, Korthagen N, Wei W, et al. Triamcinolone acetonide activates an anti-inflammatory and folate receptor-positive macrophage that prevents osteophytosis in vivo. *Arthritis research & therapy*. 2015;17:352.
39. Sieker JT, Ayturk UM, Proffen BL, Weissenberger MH, Kiapour AM, Murray MM. Immediate Administration of Intraarticular Triamcinolone Acetonide After Joint Injury Modulates Molecular Outcomes Associated With Early Synovitis. *Arthritis Rheumatol*. 2016;68(7):1637-1647.
40. Swärd P, Frobell R, Englund M, Roos H, Struglics A. Cartilage and bone markers and inflammatory cytokines are increased in synovial fluid in the acute phase of knee injury (hemarthrosis)-a cross-sectional analysis. *Osteoarthritis and cartilage*. 2012;20(11):1302-1308.
41. Sward P, Struglics A, Englund M, Roos HP, Frobell RB. Soft tissue knee injury with concomitant osteochondral fracture is associated with higher degree of acute joint inflammation. *The American journal of sports medicine*. 2014;42(5):1096-1102.
42. Syed HM, Green L, Bianski B, Jobe CM, Wongworawat MD. Bupivacaine and triamcinolone may be toxic to human chondrocytes: a pilot study. *Clinical orthopaedics and related research*. 2011;469(10):2941-2947.
43. Tempfer H, Gehwolf R, Lehner C, et al. Effects of crystalline glucocorticoid triamcinolone acetonide on cultered human supraspinatus tendon cells. *Acta orthopaedica*. 2009;80(3):357-362.
44. van Beuningen HM, de Vries-van Melle ML, Vitters EL, et al. Inhibition of TAK1 and/or JAK can rescue impaired chondrogenic differentiation of human mesenchymal stem cells in osteoarthritis-like conditions. *Tissue Eng Part A*. 2014;20(15-16):2243-2252.
45. van der Kraan PM. The Interaction between Joint Inflammation and Cartilage Repair. *Tissue Engineering and Regenerative Medicine*. 2019;16(4):327-334.

46. Wehling N, Palmer GD, Pilapil C, et al. Interleukin-1beta and tumor necrosis factor alpha inhibit chondrogenesis by human mesenchymal stem cells through NF-kappaB-dependent pathways. *Arthritis and rheumatism*. 2009;60(3):801-812.
47. Wei W, Bastiaansen-Jenniskens YM, Suijkerbuijk M, et al. High fat diet accelerates cartilage repair in DBA/1 mice. *Journal of orthopaedic research : official publication of the Orthopaedic Research Society*. 2017;35(6):1258-1264.
48. Wei W, Rudjito E, Fahy N, et al. The infrapatellar fat pad from diseased joints inhibits chondrogenesis of mesenchymal stem cells. *Eur Cell Mater*. 2015;30:303-314.
49. Wernecke C, Braun HJ, Dragoo JL. The Effect of Intra-articular Corticosteroids on Articular Cartilage: A Systematic Review. *Orthop J Sports Med*. 2015;3(5):2325967115581163.
50. Widuchowski W, Widuchowski J, Trzaska T. Articular cartilage defects: study of 25,124 knee arthroscopies. *The Knee*. 2007;14(3):177-182.
51. Wong MW, Tang YN, Fu SC, Lee KM, Chan KM. Triamcinolone suppresses human tenocyte cellular activity and collagen synthesis. *Clinical orthopaedics and related research*. 2004(421):277-281.
52. Xie C, Ming X, Wang Q, et al. COX-2 from the injury milieu is critical for the initiation of periosteal progenitor cell mediated bone healing. *Bone*. 2008;43(6):1075-1083.
53. Yang KG, Saris DB, Verbout AJ, Creemers LB, Dhert WJ. The effect of synovial fluid from injured knee joints on in vitro chondrogenesis. *Tissue engineering*. 2006;12(10):2957-2964.

Modulating design parameters to drive cell invasion into hydrogels for osteochondral tissue formation

Andrea Schwab*

Marinus A. Wesdorp*

Jietao Xu

Florencia Abinzano

Marc Falandt

Claudia Loebel

Riccardo Levato

David Eglin

Roberto Narcisi

Martin J. Stoddart

Jos Malda

Jason A. Burdick

Matteo D'Este

Gerjo J.V.M. van Osch

*both authors contributed equally

ABSTRACT

BACKGROUND/OBJECTIVE: The use of acellular hydrogels to repair osteochondral defects requires cells to first invade the biomaterial and then to deposit extracellular matrix for tissue regeneration. Due to the diverse physicochemical properties of engineered hydrogels, the specific properties that allow or even improve the behaviour of cells are not yet clear. The aim of this study was to investigate the influence of various physicochemical properties of hydrogels on cell migration and related tissue formation using *in vitro*, *ex vivo* and *in vivo* models.

METHODS: Three hydrogel platforms were used in the study: Gelatine methacryloyl (GelMA) (5% wt), norbornene hyaluronic acid (norHA) (2% wt) and tyramine functionalised hyaluronic acid (THA) (2.5% wt). GelMA was modified to vary the degree of functionalisation (DoF 50% and 80%), norHA was used with varied degradability via a matrix metalloproteinase (MMP) degradable crosslinker and THA was used with the addition of collagen fibrils. The migration of human mesenchymal stromal cells (hMSC) in hydrogels was studied *in vitro* using a 3D spheroid migration assay over 48h. In addition, chondrocyte migration within and around hydrogels was investigated in an *ex vivo* bovine cartilage ring model (3 weeks). Finally, tissue repair within osteochondral defects was studied in a semi-orthotopic *in vivo* mouse model (six weeks).

RESULTS: A lower DoF of GelMA did not affect migration *in vitro* ($p=0.390$) and led to a higher migration score *ex vivo* ($p<0.001$). The introduction of an MMP degradable crosslinker in norHA hydrogels did not improve cell infiltration *in vitro* or *in vivo*. The addition of collagen to THA resulted in greater hMSC migration *in vitro* ($p=0.031$) and *ex vivo* ($p<0.001$). Hydrogels that exhibited more cell migration *in vitro* or *ex vivo* also showed more tissue formation in the osteochondral defects *in vivo*, except for the norHA group. Whereas norHA with a degradable crosslinker did not improve cell migration *in vitro* or *ex vivo*, it did significantly increase tissue formation *in vivo* compared to the non-degradable crosslinker ($p<0.001$).

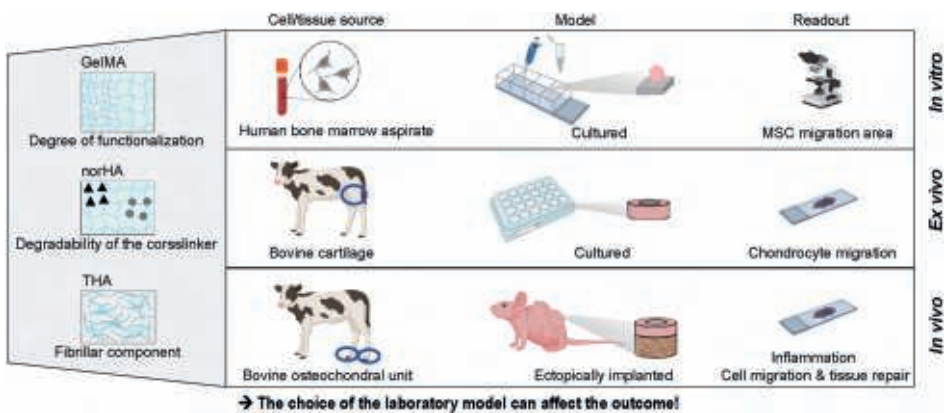
CONCLUSION: The modification of hydrogels by adapting DoF, use of a degradable crosslinker or including fibrillar collagen can control and improve cell migration and tissue formation for osteochondral defect repair. This study also emphasizes the importance of performing both *in vitro* and *in vivo* testing of biomaterials, as, depending on the material, the results might be affected by the model used.

The Translational Potential of this Article

This article highlights the potential of using acellular hydrogels to repair osteochondral defects, which are common injuries in orthopaedics. The study provides a deeper understanding of how to modify the properties of hydrogels to control cell migration and tissue formation for osteochondral defect repair. The results of this article also highlight that the choice of the used laboratory model can affect the outcome. Testing hydrogels in different models is thus advised for successful translation of laboratory results to the clinical application.

Keywords

hydrogels, cartilage, cells, Tissue Engineering, Regenerative Medicine



1 INTRODUCTION

Current matrix-based approaches for the repair of (osteo)chondral defects, like autologous matrix-induced chondrogenesis (AMIC, a combination of microfracture with a collagen scaffold) and matrix-assisted chondrocyte implantation (MACI), have improved clinical outcomes and lowered revision rates when compared to microfracture alone ¹⁻³. Although they lead to improved function and reduced pain, they fail to repair defects fully functional for the long-term ⁴. Acellular biomaterial-assisted approaches are an attractive alternative to cell-based procedures for the treatment of small focal defects, particularly due to the elimination of donor-site morbidity and the possibility of a single-stage procedure ⁵. Importantly, it has been shown that biomaterials help to improve the preservation of the cartilage tissue surrounding the defect ⁶. However, to repair cartilage fully, improved mobilisation and infiltration of cells residing in the knee into the biomaterials are needed ⁷⁻⁹.

Injectable hydrogels are one promising group of biomaterials to fill complex defects of any shape and location through a minimally invasive approach ^{10,11}. Despite the extensive research performed *in vitro* on the chondro-inductive properties of hydrogels, these biomaterials often fail upon implantation *in vivo*. Failure is related to the challenge of retaining the material in the defect area, which limits cell invasion ¹². Integration of the biomaterial with the tissues adjacent to the defect, results mainly from the infiltration of host cells, followed by matrix deposition ¹³. Thus, rapid cell infiltration is an important step in an integrative defect repair strategy ¹⁴. Cell infiltration is not only relevant for acellular hydrogel-assisted repair, but also of interest for approaches where cells are encapsulated within a hydrogel to integrate the repair tissue into the host tissue ¹⁵. This highlights the need to understand how physicochemical properties of hydrogels influence cell migration and which modifications may improve cell migration from surrounding tissues for osteochondral defect repair.

Since collagen and glycosaminoglycan are major components in the ECM of connective tissue, collagen and hyaluronic acid (HA) based hydrogels have attracted interest in cartilage tissue engineering approaches ¹⁶. Gelatine, the product of denatured collagen, modified with methacryloyl groups (GelMA), is an emerging and widely used hydrogel that exhibits tunable material properties while maintaining regions with cell adhesives (e.g. arginine-glycine-aspartate (RGD) and degradable sequences ^{17,18}. The crosslinking density in GelMA hydrogels is controlled by the degree of functionalisation (DoF), which is the extent of functionalisation with methacryloyl groups that alters crosslinking. GelMA at a fixed concentration, but an increase in DoF leads to a higher crosslinking density and thus a smaller mesh size ¹⁹. More recently,

a lower degree of functionalization of the GelMA50 has been associated with a faster enzymatic degradation kinetic ²⁰. For endothelial cells it has been shown that a lower DoF supports greater endothelial cell derived capillary-like-network formation ²¹. Whether this hydrogel modification also improves cell migration in the osteochondral environment and supports tissue repair has not yet been studied.

The most widely used proteoglycan hydrogels in biomedicine are HA and its derivatives. HA-based biomaterials are often functionalised with biochemical cues (e.g., chondroinductive/chondroconductive peptides, the addition of fibrous components) and/or biophysical cues (mechanical properties, mesh size, porosity) to stimulate (endogenous) cell infiltration and cartilaginous matrix deposition ^{14,22,23}. To improve the tunability of mechanical properties, the interaction with the host tissue or the rheological properties and printability, functionalization of HA-based hydrogels (e.g. with thiol-norbornene or tyramine) have been introduced ²⁴⁻²⁶. Norbornene hyaluronic acid (norHA) is an attractive biomaterial due to its excellent printability, tunable properties and the ability for *in situ* crosslinking ²⁷. Tyramine functionalized HA (THA) is characterized by its enhanced binding to the cartilage host tissue via the formation of di-tyrosine bonds between THA and cartilage ECM ²⁸. Together with its tunable properties, THA is also an attractive hydrogel for bioprinting ²⁹⁻³¹. The main limitation of HA-based materials are the limited cell adhesion ^{32,33}. One approach to overcome this is to combine THA with either RGD, collagen or gelatine to increase cell attachment and cell spreading ^{30,34,35}. Beyond the possibility of varying RGD concentration, the use of a degradable crosslinker, specifically the use of a matrix metalloproteinase (MMP) cleavable crosslinker, has allowed MSC spreading and mechano-response when embedded in the hydrogel ³⁶.

The above-introduced hydrogel biomaterials (GelMA, norHA and THA) are attractive for (osteo) chondral repair due to their chondrogenic potential and printability ^{27-30,34,36-41}. Thus, this study aimed to investigate the effect of selected hydrogel modifications on human mesenchymal stromal cells (hMSC) and chondrocyte migration *in vitro* and related tissue formation for (osteo)chondral defect repair *in vivo*. We hypothesised that a lower crosslinking density in GelMA, use of a degradable crosslinker with norHA precursors, as well as the addition of collagen fibrils in THA hydrogels would increase cell migration and improve tissue formation. Cell migration into the hydrogel was investigated using three models: (1) hMSC spheroids seeded within hydrogels for *in vitro* migration, (2) endogenous chondrocyte migration in a cartilage ring model *ex vivo*, and (3) cell migration and tissue formation in a semi-orthotopic mouse model *in vivo*. While the first two models focus on a single cell type, the *in vivo* model was

chosen to study the interplay of multiple cell types within the osteochondral defect environment.

2 MATERIALS AND METHODS

2.1 Biomaterial preparation and characterization

2.1.1 Hydrogel preparation

Two HA-based materials (THA, norHA) and a gelatine-based material (GelMA) were evaluated by MSC cell migration *in vitro*, chondrocyte migration from cartilage explants *ex vivo*, cell migration, and osteochondral defect repair in a semi-orthotopic model *in vivo* (Figure 1). For the *in vitro* migration study, hydrogels were crosslinked in an 8-well plate prior to cell seeding. For the *in vivo* and *ex vivo* model, hydrogel precursors were injected in the defects of either cartilage rings or osteochondral explants and photo-crosslinked.

Gelatine methacryloyl (GelMA)

GelMA was synthesized with a DoF of 50% (GelMA50) and 80% (GelMA80). Based on the protocol described by Melchels *et al.*, 0.6 g methacrylic anhydride (Sigma Aldrich 92%) per g of gelatine (type A from porcine skin, 300 g Bloom, Sigma Aldrich) was used (10% gelatine in PBS, 50°C, 1h) for GelMA80. For GelMA50, 0.036 g methacrylic anhydride per g of gelatine was used^{42,43}. GelMA (50 mg/ml) was reconstituted at 60°C before adding the photo crosslinker ruthenium (0.5 mM) and sodium persulfate (5.0 mM) with subsequent photo-crosslinking (15 min, 3 cm distance, AVIDE lamp). The variable of the two GelMA formulations used in this study were the DoF (50% or 80%).

Norbonene hyaluronic acid (norHA)

NorHA was synthesized as previously described and reconstituted with either a non-degradable 1,4-Dithiothreitol (DTT, 0.22 mg/ml, Sigma Aldrich, Saint Louis, USA) crosslinker or a MMP cleavable crosslinker (2.55 mg/ml, GCNSVPMS↓MRGGSNCG, Lot: U1432DL070-1/PE2401, GenScript, Piscataway Township, USA)^{41,44}. NorHA was reconstituted at a final polymer concentration of 20 mg/ml. NorHA precursors (norHA-DTT and norHA-MMP) contained thiolated RGD sequences (GCGYGRGDSPG, 1.0 mM, U0140DA260-1, Lot: 94230930001/PE8559, GenScript). Photo-crosslinking (20 min, 3 cm distance, AVIDE lamp) was achieved using photo-initiators ruthenium and sodium persulfate (Advanced Biomatrix, 5248-1KIT) followed by hydrogel gelation. The choice of the crosslinker (MMP degradable or non-degradable DTT) was the variable to prepare two norHA formulations.

Tyramine modified hyaluronic acid (THA)

THA with a degree of substitution of 6% was synthesized as described previously⁴⁵. THA was reconstituted (25 mg/ml) and photoinitiator Eosin Y (0.02 mg/ml, Sigma Aldrich) was added. THA (25 mg/ml final concentration) and THA-collagen (THA 12.5 mg/ml and 2.5 mg/ml collagen 1 isolated from rat tails, Corning, Bedford, USA) hydrogels were enzymatically crosslinked using peroxidase from horseradish (0.3 U/ml, Sigma Aldrich) and hydrogen peroxide (120 ppm, Carl Roth, Karlsruhe, Germany) with subsequent photo-crosslinking (10 min, 3 cm distance, AVIDE lamp, Well-Com Vertriebs GmbH, Gelsenkirchen, Germany)³⁴. The variable for the two THA formulations was the addition of the fibrillar component (THA-col) compared to THA alone.

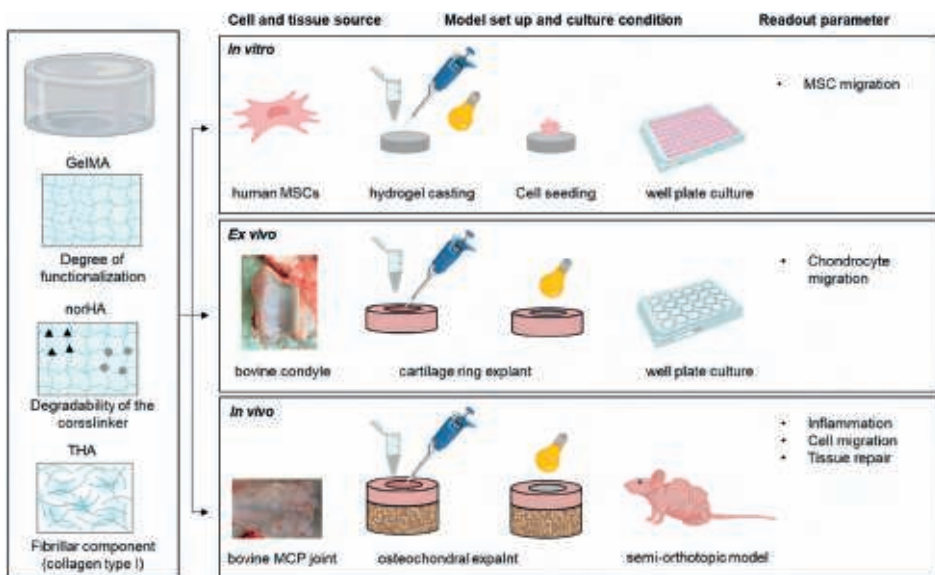


Figure 1: Graphical illustration of the in vitro, ex vivo and in vivo models to evaluate acellular hydrogels for (osteo-) chondral repair.

Three hydrogel types were evaluated for cell migration and tissue formation in osteochondral defects. Comparisons included the degree of functionalization (50% and 80%) for gelatin methacryloyl (GelMA hydrogels), the degradability of matrix metalloprotease (MMP) degradable versus non-degradable(1,4-Dithiothreitol, DTT) crosslinkers for norbornene-modified hyaluronic acid (HA) and the addition of fibrillar collagen on tyramine modified HA (THA) hydrogels. Images created with Biorender.com.

2.1.2 Nuclear magnetic resonance (NMR) spectrum

The ¹H-NMR spectrum of the hydrogel precursor materials were measured by NMR to check the purity and the functionalization of the materials. All materials were dissolved in deuterium oxide (D₂O) and ¹H-NMR spectrum recorded.

2.1.3 *Dynamic mechanical analysis*

Hydrogel mechanical properties were assessed using a dynamic mechanical analyzer (DMA Q800, TA Instruments, The Netherlands). Hydrogels in phosphate buffered saline (PBS, Sigma Aldrich) were analysed in unconfined uniaxial compression test (room temperature, n=5 samples per condition) to measure their compressive moduli. A preload of 0.01 N was applied to the hydrogels, followed by a ramp force of 2 N/m until a maximum force of 8 N was reached. The compressive modulus (Young's modulus) was calculated as the slope of the linear elastic range of the stress/strain curve. To measure the stress-relaxation response, a constant strain was applied (preload of 0.001 N, room temperature, n=5 samples per condition) to hydrogels. After applying a constant strain of 20% for 2 minutes, the hydrogel response was measured over a period of 1 minute. The relaxation of the material was calculated as the ratio of minimum and maximum stress after 2 minutes of 20% strain.

2.1.4 *Rheological characterization*

Photo rheology experiments on the hydrogel precursor solutions (GelMA DOF 50 and DOF80, norHA MMP and norHA DTT) to determine the crosslinking kinetics was measured using a DHR2 rheometer (TA Instruments, The Netherlands). Samples were prepared fresh (100 μ L measuring volume, n = 3) before loaded onto the rheometer for oscillatory time sweep experiments (frequency of 1.0 Hz, angular frequency of 6.28 rad/s, with 5.0% constant strain at 37°C, preset measuring gap size of 300 μ m, 20.0 mm parallel EHP stainless steel plate). After 30 seconds of measuring, the visible light source was turned on to allow photo crosslinking of the hydrogels for the remaining time of the experiment and storage (G') and loss moduli (G'') were recorded.

2.2 *In vitro* hMSC migration assay

2.2.1 *hMSC isolation and expansion*

hMSC were isolated from bone marrow of patients undergoing total hip replacement after informed consent (approved by the local Medical Ethical Committees of Erasmus MC: protocol MEC-2015-644) as described earlier⁴⁶. hMSCs were thawed, and expanded in media composed of alpha-Minimum Essential Medium (α -MEM, Gibco, California, USA) supplemented with 10% fetal bovine serum (FBS, Gibco, California, USA), 50 μ g/mL gentamycin (Gibco), 1.5 μ g/mL fungizone (Gibco), 1 ng/mL fibroblast growth factor 2 (FGF2, AbD Serotec, Puchheim, Germany) and 25 μ g/mL ascorbic acid-2-phosphate (AA-2-P, Sigma-Aldrich) in a humidified atmosphere with media replacement twice per week. Cells at 80-90% confluency were sub-cultured using 0.25% Trypsin/1x EDTA (Gibco). hMSCs were fluorescently labelled according to the

manufacturer's instructions (Vybrant CFDA-SE Cell tracer Kit, Thermo Fisher) to visualize cell location after seeding on the hydrogels (see 2.2.2).

2.2.2 *In vitro migration assay set up*

hMSC migration was evaluated by measuring the migration area of the cells in a 3D migration assay after 48h of culture *in vitro*⁴⁷. Micro-moulds (Micro Tissues 3D Petri Dish, Sigma Aldrich) were casted with agarose to form 256 circular micro-wells. After the micro moulds gelled, they were transferred to a 12-well-plate containing α -MEM (Gibco) supplemented with 10% foetal bovine serum (FBS, Gibco) and 25 μ g/mL ascorbic acid-2-phosphate (Sigma-Aldrich) and incubated in a humidified atmosphere (37°C, 5% CO₂) for 1h. Cell spheroids (500 cells per spheroid) were prepared by dropwise seeding the CFDA labelled cell suspension (0.128×10^6 cells/190 μ L) into the 3D agarose moulds and then cultured in a humidified atmosphere for 24 hours to form spheroids. Spheroid formation was assessed by a standard inverted microscope and irregular sized spheroids were discarded. To harvest the spheroids, the 3D agarose moulds were transferred and inverted into a new 12-well plate containing media and cell centrifuged for five minutes at 120g. The medium containing the spheroids was transferred to a falcon tube and again centrifuged (30 seconds at 300 g). Spheroids were resuspended in the assay media composed of α -MEM supplemented with 1% insulin, transferrin and selenium (ITS+, Sigma Aldrich), and 25 μ g/mL ascorbic acid (Sigma-Aldrich) Next, 125 μ L of each hydrogel precursor was casted in each well of a chamber slide (Nunc cell culture imaging 8-wells, Thermo Fisher), crosslinked and washed three times with serum free α -MEM. Afterwards, 5-10 spheroids were seeded on each hydrogel in each well. Cell spheroids were cultured on the hydrogels for 48h with assay media supplemented with platelet-derived growth factor BB (50 ng/mL, PDGF-BB, Peprotech, NJ, USA) to stimulate cell migration. To quantify cell migration, confocal imaging (Leica SP5, FITC channel, 10x magnification) was performed with the acquisition of z-stacks to monitor the spheroid migration from the top to the bottom of the hydrogel. Cell migration area of hMSC was measured on the different hydrogel compositions (n=6, n=5 for THA-col) using the earlier described macro with Fiji image processing software⁴⁷. The migration area of the migrating cells was calculated to obtain the total migratory area in a radius of 760 μ m.

2.3 *Ex vivo migration assay to assess chondrocyte migration*

2.3.1 *Cartilage ring isolation and ex vivo explant culture*

Cartilage explants were isolated from the patellar groove of bovine knee joints (six months old calves, Angst AG, CH) using a sharp biopsy punch (8mm, KAI medical, Arnold Bott AG, Opfikon, Switzerland). Cartilage was separated from the subchondral

bone with a scalpel. Explants were washed with DMEM HG (Gibco) supplemented with 1% antibiotics (10 U/ml penicillin, 10 µg/ml streptomycin, Gibco). After defect creation (4mm, KAI medical, Arnold Bott AG, Switzerland) in the centre of the explant, the defects were filled with the hydrogel precursors (described in Figure 1), and then gelled in the defect to ensure optimal integration between the hydrogel and the cartilage tissue. All samples were transferred into a 24 well plate (TPP, Trasadingen, Switzerland) containing DMEM HG enriched with 10% FBS, 50 µg/ml ascorbic acid and 1% antibiotics. Samples were cultured *ex vivo* for 21 days (37°C, 5% CO₂) with media change every 2-3 days.

2.3.2 Cell viability staining of ex vivo samples

After 21 days of culture, metabolic activity of cartilage explants was assessed with 3-(4,5-dimethylthiazol-2-yl)-2,5-diphenyltetrazoliumbromid (MTT, 1mg/ml, 1h incubation at 37°C, Sigma Aldrich). Samples were imaged with bright field microscope (Zeiss). Samples were also stained for live-dead assessment (Sigma Aldrich) with Ethidium homodimer (4 µM) and Calcein-AM (2 µM) according to manufacturer's instructions, washed with PBS after 25 min incubation and kept in culture media for microscopic assessment (Zeiss confocal microscope, LSM800).

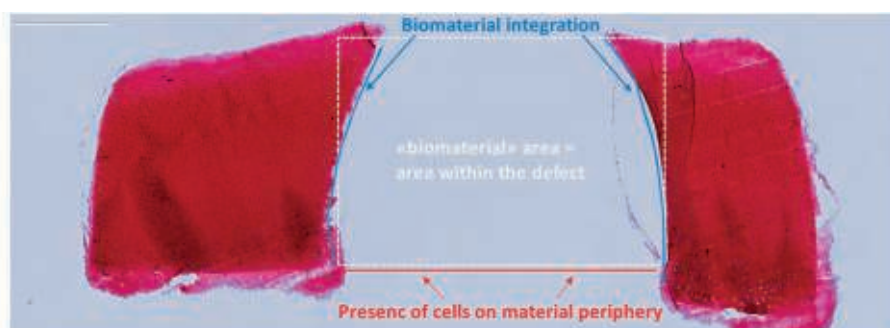
2.3.3 Histological processing, staining and scoring of ex vivo samples

Samples were harvested at day 21, fixed with formalin (4%, Formafix AG, Hittnau, Switzerland), washed with PBS, immersed with sucrose (150 mg/ml and 300 mg/ml, Sigma Aldrich), embedded in freezing media (Leica, Nussloch, Germany) and snap frozen with liquid nitrogen. Sections of 8 µm were cut with a cryostat microtome (HM 500 OM; Zeiss) and stored at -20°C.

Safranin-O staining was performed to visualize proteoglycans. Cryosections were washed with deionized water to remove freezing media, incubated for 10 min with Weigert's hematoxylin (Sigma Aldrich), blued with tap water and incubated with fast green (0.02%, 6 min, Sigma Aldrich). After washing with acetic acid (1%, Fluka), slides were incubated in safranin-O (0.01%, 15 min, Sigma Aldrich) and differentiated with ethanol (70%, Alcosuisse, Rüti bei Büren, Switzerland) with subsequent dehydration (ethanol 96%, ethanol absolute, Xylene) and cover slipping (Eukitt, Sigma Aldrich). Bright-field microscopic images (Olympus BX63, Olympus) were acquired for cell migration analysis.

A migration score was introduced to semi-quantitatively evaluate chondrocyte migration from the explant towards the acellular hydrogels. Safranin-O stained slices of the samples at day 21 (n=3 samples per biomaterial, n=2 samples empty defect

control, n= 2 sections) were scored by three independent observers blinded for the condition (Figure 2). The individual scores were visually inspected and in case of differences, discussed to reach consensus between observers.



Scoring criteria	0	1	2	3
Explant-biomaterial integration	No integration, gaps formed between material and tissue	Limited integration. Material-tissue contact (<25%) less than half	Local integration with cartilage tissue (> 50%)	Nearly full integration, no gaps between material and tissue (>90%)
Presence of cells on material periphery	No cells	Singel cells present (locally)	Parts are covered with cells (>20%)	Full layer of cells on materials (>90%)
Presence of cells within biomaterial	No cells	Few (local) cells	Moderate cell density, inhomogeneous distribution	Many cells, "homogenous" distribution

Figure 2: Scoring criteria to assess chondrocyte migration in the ex vivo cartilage ring model. Safranin O staining of cartilage explant with defect in the centre (white dashed line). The areas of interest are indicated for the biomaterial integration (blue line) and presence of cells (red line).

2.4 Semi-orthotopic model to assess osteochondral defect repair *in vivo*

2.4.1 *In vivo subcutaneous chondral and osteochondral defect model*

To evaluate the capacity of the hydrogels to support endogenous cell migration and osteochondral repair, an *in vivo* semi-orthotopic osteochondral defect model was used, where tissues are implanted subcutaneously in mice⁴⁸. This animal experiment was approved by the ethics committee for laboratory animal use (under license AVD101002016691, protocol #EMC16-691-07) and following the ARRIVE (Animal Research: Reporting of In Vivo Experiments) guidelines. Bovine osteochondral biopsies (8 mm diameter, 5 mm height) were harvested with a dental trephine from metacarpal-phalangeal joints of 3-8 months old calves from a local slaughterhouse and provided by LifeTec Group (Eindhoven, Netherlands). Osteochondral defects (4

mm diameter, 4 mm depth) were created in the centre of the biopsies using a hand drill to avoid thermal damage. The defect created into the subchondral bone will allow bone marrow and subchondral bone hosting cells to infiltrate the defect area. The osteochondral biopsies were kept overnight in α -MEM (Gibco, USA) supplemented with 10% fetal bovine serum (FBS, Gibco), 1.5 μ g/mL fungizone (Gibco), and 50 μ g/mL gentamycin (Gibco) to ensure sterility. The hydrogel precursors were used to fill the defects and then photo crosslinked before implantation. All hydrogel-loaded osteochondral constructs were covered with a circular 8 mm Neuro-Patch membrane (Braun, Melsungen, Germany) on the cartilage to prevent the ingrowth of host cells.

Thirteen 11-week-old female NMRI-Foxn1 nu/nu mice (Janvier Labs, St.Berthevin, France) were used in this study. The mice were allowed to adapt to the conditions of the animal facility for 7 days before implantation surgery. The mice were housed under specific-pathogen-free conditions with a regular day/night light cycle and food and water were available ad libitum. Four osteochondral constructs were randomly implanted subcutaneously on the back of each mouse under 2.5-3.0% isoflurane anaesthesia (Laboratories Karizoo, Barcelona, Spain). To minimise the risk of infection, the mice received 25 mg/kg bodyweight of ampicillin (Dopharma, Raamsdonksveer, Netherlands) subcutaneously during surgery. Staples (AgnTho's, Lidingö, Sweden) were used to close the incisions and were removed 1 week after implantation. To ensure pre- and postoperative analgesia, the mice received a subcutaneous injection of 0.05 mg/kg body weight of buprenorphine (Chr. Olesen & Co, Copenhagen, Denmark) 1 h before surgery and 6 h after surgery. After ten days (n=3 samples per condition) and six weeks (n=5 samples per condition), mice were killed by cervical dislocation and the osteochondral constructs were harvested.

2.4.2 Histological processing, staining and scoring

The osteochondral constructs were fixed in 4% formalin for 1 week, followed by decalcification using 10% ethylenediaminetetraacetic acid (EDTA, pH 7.4, Sigma Aldrich) for up to 4 weeks. Six-week samples were processed for routine paraffin embedding and sectioned (microtome, Leica). Dewaxed slides were stained with hematoxylin and eosin (HE) to study general cell and tissue morphology. Images were taken with a slide scanner (NanoZoomer, Hamamatsu). Ten-week samples were processed for cryo embedding (OCT, Sakura, Nagano, Japan) and cutting (Cryostat, Leica, Nussloch, Germany) after demineralization.

Image analysis using the NDP.View2 software (version 2.8.24, 2020 Hamamatsu Photonics K.K.) was used to assess tissue formation. The area of the newly formed tissue was measured by manually selecting the tissue regions. The percentages of

the defects covered with cartilage-like, bone-like and other tissue were measured separately (**supplementary Figure S4D**), with the defect area set to 100%. The tissue volume of three sections that were taken at depths of 1, 1.5 and 2 mm for each sample was averaged for further analyses. All slides were scored by an investigator blinded to the experimental condition.

2.5 Statistical analysis

Mechanical characterization and *ex vivo* migration are presented as box plots (min to max value with a line presenting the median). *In vitro* MSC migration area and tissue volume in % are presented as mean \pm standard deviation (SD). For each of the hydrogel groups (THA, GelMA, norHA) the results of the two modifications were compared. All statistical analyses were performed using SPSS (version 28.0.1.0, IBM Corporation, USA). Student T-tests were performed for mechanical characterization, *in vitro* MSC migration and *in vivo* tissue formation and two-sided p-values are reported. In case the variances between the two modifications were significantly different, p-value of equal variances not assumed is reported and marked with a *. Mann-Whitney U tests were used to assess statistical significance in the *ex vivo* migration scores. For all statistical analyses, a p-value <0.05 was considered statistically significant and marked with a *.

3 RESULTS

3.1 Lower crosslinking density of GelMA hydrogels increases cell migration

Compression moduli (E-moduli) of GelMA hydrogels with DoF of 50% and 80% crosslinked under the same conditions after equilibrating in PBS were respectively 6.8 ± 1.3 kPa and 7.3 ± 1.7 kPa, $p=0.637$, revealing no significant difference between the two DoF (**Figure 3A**). Stress recovery of GelMA80 (0.8 ± 0.1) was similar to that of GelMA50 (0.7 ± 0.1 , $p=0.236$).

The ^1H NMR spectrum confirms the different DOF (**Supplementary Figure S1**). GelMA50 had slower photo-crosslinking kinetics than GelMA80, both with a final storage modulus around 1 kPa (**Supplementary Figure S2**).

hMSCs migrated out of the spheroid in both GelMA formulations. The migration area (**Figure 3B**) of hMSC seeded in GelMA 50% DoF ($42050 \pm 15335 \mu\text{m}^2$) was similar to the migration in GelMA 80% ($28010 \pm 34241 \mu\text{m}^2$, $p=0.390^*$) trending towards more

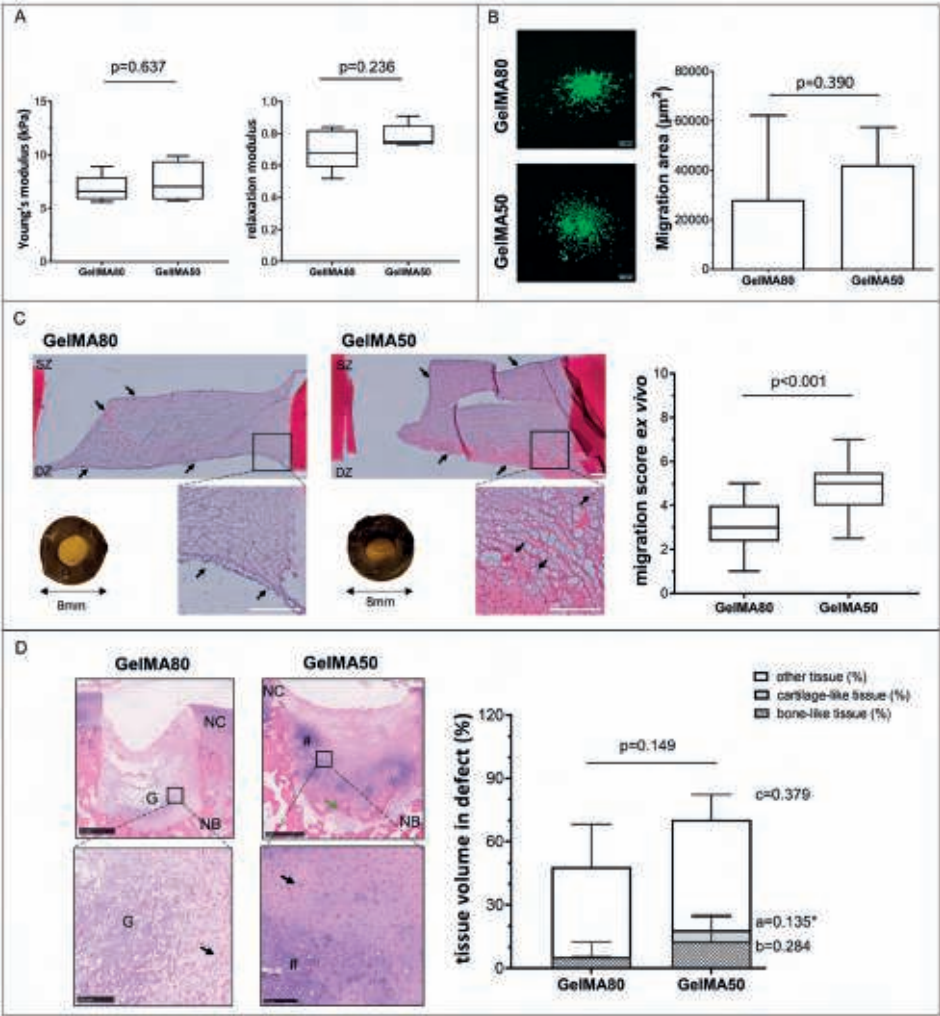


Figure 3: Effect of lowering the degree of functionalization (DoF) from 80% to 50% in gelatin methacryloyl (GelMA) hydrogels on cell migration and tissue formation.

A) the Young's modulus and stress-relaxation to characterize hydrogel recovery after swelling in PBS (n=5 per group). B) In vitro cell migration of hMSCs out of spheroids seeded on top of hydrogels (n=6 per group). hMSC labelled with membrane dye are shown in green. Scale bar 200 μm . C) Chondrocyte migration and migration score in the ex vivo cartilage ring model (min to max score with median). Macroscopic (explant diameter 8 mm) and microscopic image of MTT stained samples, the safranin O-stained section of the hydrogel and migration score with a maximum score of 9 (n=3 samples per group, n=2 slides per sample). Scale bar 200 μm . D) Cell migration and related tissue formation in acellular hydrogels implanted in osteochondral explants in a semi-orthotopic mouse model (n=5 samples per biomaterial). Hematoxylin and eosin-stained cross-sections of one representative sample are shown. Tissue volume in osteochondral defect (OCD) is presented as bone-like tissue, cartilage-like tissue and other tissue (mean \pm SD) relative to total tissue volume. Scale bar low magnification image 1 mm, higher magnification image 100 μm . NC: native cartilage, NB: native bone, G: hydrogel, # indicated newly formed cartilage-like tissue, green arrow indicates newly formed bone-like tissue, black arrow indicates infiltrated cells within the defects, blue arrow indicates the integration of newly formed bone and native bone. Statistical significance comparing means between hydrogel formulations: a: cartilage-like, b: bone-like, c: other tissue, p: total tissue volume. * equal variances not assumed.

migration in the lower DoF. In the *ex vivo* migration assay, the chondrocytes in the cartilage explant remained metabolic active (as indicated by MTT staining **Figure 3C**) and a few metabolically active chondrocytes invaded both GelMA formulations (**supplementary Figure S6A**). Most of the cells were observed on top of the hydrogels. GelMA50 had a significantly higher chondrocyte migration score (min/max:2.5/7, median:5) than GelMA80 (min/max:1/5, median:3, $p<0.001$). The hydrogels with both DoF remained inside the cartilage defect. In general, a slight shrinkage was observed during culture resulting in a gap between the hydrogel and the surrounding defect.

Hydrogels were implanted in the semi-orthotopic *in vivo* model. After ten days, infiltration of a few multinucleated cells was observed in GelMA80 (2 out of 3 samples) and GelMA50 (1 out of 3 samples), indicating a low inflammatory response (**supplementary Figure S3**). After six weeks the average area of remaining hydrogel implanted in the osteochondral defect was $11.3\% \pm 9.7\%$ for GelMA50 and $16.4\% \pm 12.3\%$ for GelMA80 (values calculated relative to respective total defect area). This means that the hydrogel was degraded upon implantation. The infiltration of cells and newly formed osteochondral tissue were mostly present in the deep zone and at the lateral sides of the osteochondral defects (**Figure 3D**). In GelMA80 a cell-free area within the hydrogel was still present, even in the samples with the highest invasion (see **supplementary Figure S4A and S5A**). GelMA50 and GelMA80 both allowed osteochondral defect repair ($70.5\% \pm 21.3\%$ vs $48.0\% \pm 23.0\%$, $p=0.149$). The repair consisted of cartilage-like tissue ($0.04\% \pm 0.09\%$ vs $5.3\% \pm 6.3\%$, $p=0.135^*$), bone-like tissue ($5.4\% \pm 7.1\%$ vs $12.8\% \pm 12.6\%$, $p=0.284$) and other tissues ($52.4\% \pm 11.9\%$ vs $42.6\% \pm 20.2\%$, $p=0.379$).

3.2 MMP cleavable norHA hydrogels limit cell migration in vitro and ex vivo but increase tissue formation in vivo

The two norHA hydrogel formulations differed by the presence of either a MMP degradable crosslinker or a non-degradable (DTT) crosslinker. The modulus of norHA MMP (13.4 ± 3.5 kPa) was significantly lower than the modulus of norHA DTT (36.3 ± 6.8 kPa, $p<0.001$) after swelling and equilibrating in PBS (**Figure 4**). The stress recovery was significantly higher in norHA DTT (0.9 ± 0.0) compared to norHA MMP (0.7 ± 0.1 , $p<0.001$). The ^1H NMR spectrum of norHA confirms the functionalization of HA with norbornene groups (**Supplementary Figure S1**). The results of the photo rheological characterization (**Supplementary Figure S2**) showed a similar trend to the DMA measurement with a higher storage modulus for norHA DTT (1.5 kPa) compared to norHA MMP (0.2 kPa).

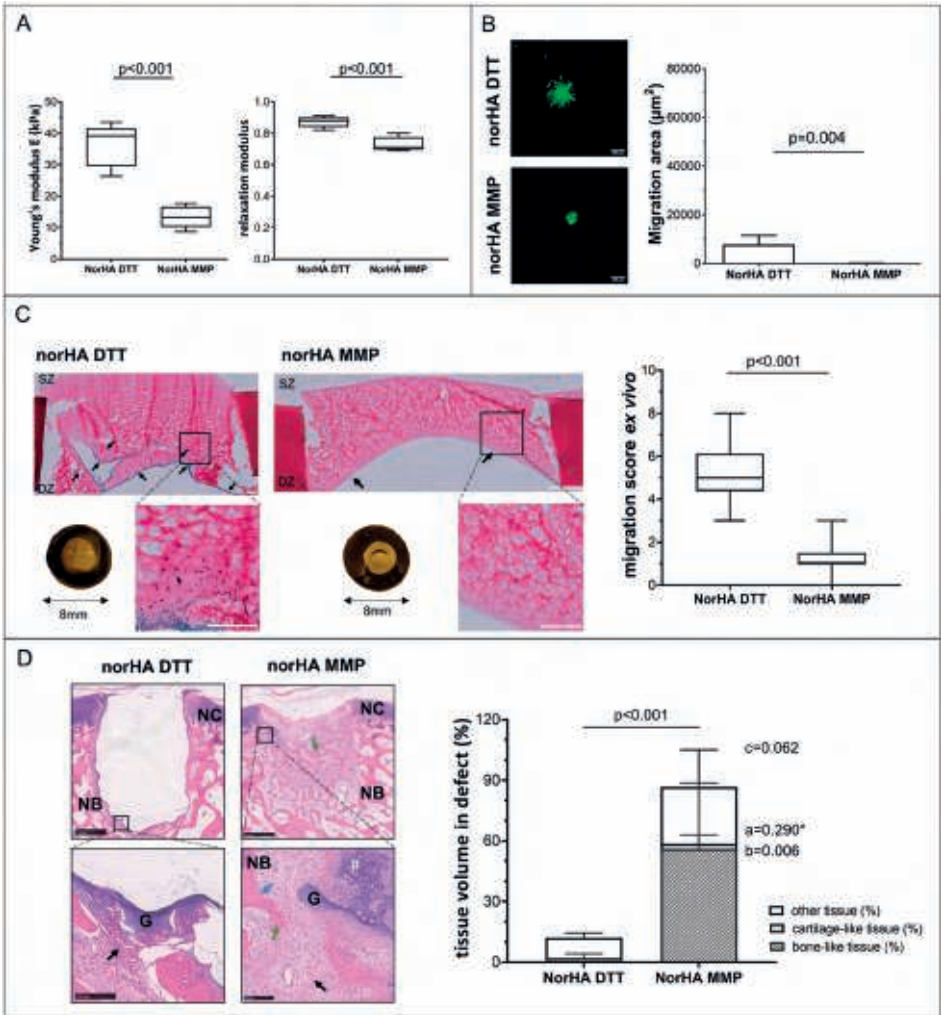


Figure 4: Effect of crosslinker degradability (MMP degradable vs non-degradable DTT) on norbonene modified hyaluronic acid hydrogel (norHA) cell migration and tissue formation.

A) Young's modulus and stress-relaxation to characterize hydrogel recovery after swelling in PBS (n=5 per group) are shown. B) In vitro cell migration of hMSCs out of spheroids seeded on top of hydrogels (n=6 per group). hMSC labelled with membrane dye are shown in green. Scale bar 200 μm . C) Chondrocyte migration and migration score in the ex vivo cartilage ring model (min to max score with median). Macroscopic (explant diameter 8 mm) and microscopic image of MTT stained samples, the safranin O-stained section of the hydrogel and migration score with a maximum score of 9 (n=3 samples per group, n=2 slides per sample). Scale bar 200 μm norHA MMP low magnification 500 μm . D) Cell migration and related tissue formation in acellular hydrogels implanted in osteochondral explants in a semi-orthotopic mouse model (n=5 samples per biomaterial). Hematoxylin and eosin-stained cross-sections of one representative sample are shown. Tissue volume in osteochondral defect (OCD) is presented as bone-like tissue, cartilage-like tissue and other tissue (mean \pm SD) relative to total tissue volume. Scale bar low magnification image 1 mm, higher magnification image 100 μm . NC native cartilage, NB native bone, G: hydrogel, green arrow indicates newly formed bone-like tissue, black arrow indicates infiltrated cells within the defects, blue arrow indicates the integration of newly formed bone and native bone. Statistical significance comparing means between hydrogel formulations: a: cartilage-like, b: bone-like, c: other tissue, , p: total tissue volume. * equal variances not assumed.

Both NorHA hydrogel formulations showed limited migration of MSC into the hydrogel *in vitro*. Less hMSC migration (**Figure 4B**) was observed when a norHA MMP degradable crosslinker ($44 \pm 68 \mu\text{m}^2$) was used, compared to a norHA non-degradable DTT crosslinker ($7742 \pm 3772 \mu\text{m}^2$, $p=0.004$). NorHA MMP was also invaded by less chondrocytes than norHA DTT after three weeks of *ex vivo* culture (**Figure 4C**, **supplementary Figure S8A, B**). A significantly lower migration score was observed for the norHA material with a degradable crosslinker (norHA MMP, min/max: 0/3, median: 1) compared to norHA with a non-degradable crosslinker (norHA DTT, min/max: 3/8, median: 5, $p<0.001$). Both hydrogel formulations remained in the defect during 21 days of culture.

After ten days of implantation *in vivo* (**Figure 4D**) no cell invasion was present in norHA DTT hydrogels (0 out of 3 samples) while the group with the MMP degradable crosslinker exhibited invading cells even in the deeper regions of the hydrogels (3 out of 3 samples (**supplementary Figure S3**)). After six weeks of implantation total tissue formation was significantly higher in norHA MMP than norHA DTT ($86.6\% \pm 15.9\%$ vs. $12.1\% \pm 3.7\%$, $p<0.001$). The average percentage of remaining hydrogel in the defect was $0.7\% \pm 0.5\%$ for norHA MMP and $8.5\% \pm 9.7\%$ for norHADTT (values calculated relative to respective defect area). The infiltrated cells and newly formed tissue were mostly in the deeper parts and at the sides of the osteochondral defects in the periphery of the hydrogels (**Figure 4D**). Cartilage-like tissue ($2.4\% \pm 4.5\%$ vs $0.0\% \pm 0.0\%$, $p=0.290^*$) was observed with areas of proteoglycan-rich matrix (**supplementary Figure S5B**). Significantly more bone-like tissue ($56.1\% \pm 32.6\%$ vs $2.0\% \pm 2.3\%$, $p=0.006$) and a tendency towards more other-like tissue ($28.1\% \pm 18.4\%$ vs $10.1\% \pm 2.4\%$, $p=0.062$) was formed in the norHA MMP compared to norHA DTT.

3.3 The addition of collagen fibres to THA improves cell migration *in vitro* and *ex vivo*

Moduli (**Figure 5A**) of THA-col ($60.4 \pm 24.9 \text{ kPa}$) were similar to THA ($38.3 \pm 8.5 \text{ kPa}$, $p=0.121$). The stress recovery was significantly increased in THA compared to THA-col (0.9 ± 0.1 vs 0.6 ± 0.2 , $p=0.042^*$). The ^1H NMR spectrum of THA confirm the functionalization of HA with tyramine (**Supplementary Figure S1**).

THA-col had significantly more MSC migration *in vitro* (**Figure 5B**) ($37647 \pm 23532 \mu\text{m}^2$) than THA only ($3737 \pm 4243 \mu\text{m}^2$, $p=0.031^*$). Only a few metabolic active chondrocytes were present in the THA hydrogel, and more cells were present in THA-col hydrogel in the *ex vivo* model (**Figure 5C**, **supplementary Figure S6A**). This was also visible from the chondrocyte migration score that was significantly higher in THA-col (chondrocyte migration score min/max; 2/5.5, median 4) than in THA (min/max: 0/5.5, median 1,

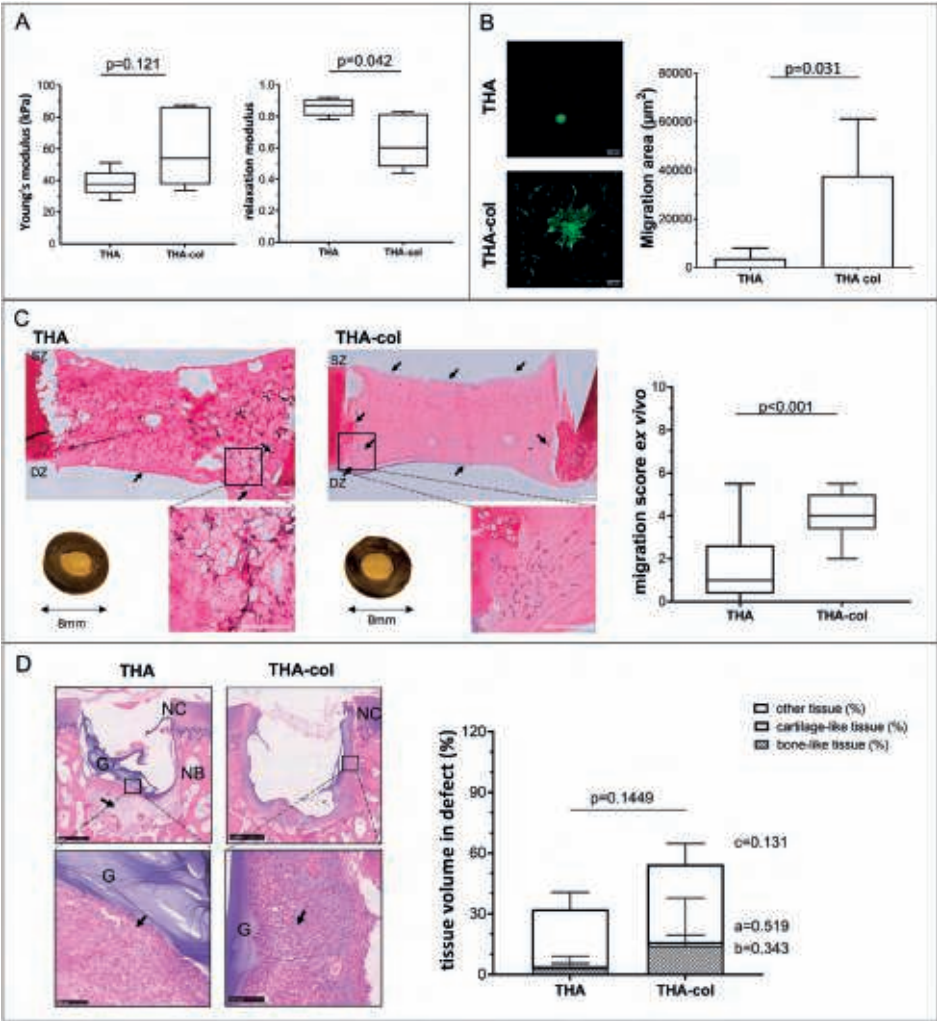


Figure 5: Effect of the addition of fibrillary collagen (col) to tyramine modified hyaluronic acid (THA) hydrogels on cell migration and tissue formation.

A) Young's modulus and stress-relaxation to characterize hydrogel recovery after swelling in PBS (n=5 per group). B) In vitro cell migration of hMSCs out of spheroids seeded on top of hydrogels (n=6 THA, n=5 THA-col). hMSC labelled with membrane dye shown in green. Scale bar 200 μm . C) Chondrocyte migration and migration score in the ex vivo cartilage ring model (min to max score with median). Macroscopic (explant diameter 8 mm) and microscopic image of MTT stained samples, the safranin-O stained section of the hydrogel and migration score with a maximum score of 9 (n=3 samples per group, n=2 slides per sample). Scale bar 200 μm . D) Cell migration and related tissue formation in acellular hydrogels implanted in osteochondral explants in a semi-orthotopic mouse model (n=5 samples per biomaterial). Haematoxylin and eosin-stained cross-sections of one representative sample are shown. Tissue volume in osteochondral defect (OCD) is presented as bone-like tissue, cartilage-like tissue and other tissue (mean \pm SD) relative to total tissue volume. Scale bar low magnification image 1 mm, higher magnification image 100 μm . NC native cartilage, NB native bone, G: hydrogel, black arrow indicates infiltrated cells within the defects, blue arrow indicates the integration of newly formed bone and native bone. Statistical significance comparing means between hydrogel formulations: a: cartilage-like, b: bone-like, c: other tissue, p: total tissue volume. * equal variances not assumed.

$p < 0.001$). Hydrogels of both formulations remained in the cartilage defect during the 21 days of culture.

Ten days after implantation *in vivo*, a few inflammatory cells were observed on the hydrogels (THA 2 out of 3 samples, THA-col 2 out of 3 samples, **supplementary Figure S3**), located at the hydrogel periphery and inside the hydrogels. After six weeks of implantation, the average amount of remaining hydrogel in the defect was $9.7\% \pm 3.0\%$ for THA-col and $15.2\% \pm 9.1\%$ for THA (values calculated relative to respective defect area). For THA materials, limited cell migration and total osteochondral tissue repair (THA-col $54.4\% \pm 26.4\%$ vs. THA $32.3\% \pm 15.4\%$, $p = 0.144$) was observed in the defects of the osteochondral explants. In line with the *in vitro* hMSC migration and *ex vivo* chondrocyte migration, a trend for an increased amount of cartilage-like tissue ($1.8\% \pm 3.5$ vs $0.7\% \pm 1.5\%$, $p = 0.519$), bone-like tissue ($14.3\% \pm 23.6\%$ vs $3.4\% \pm 5.7\%$, $p = 0.343$) and other tissue ($38.3\% \pm 10.3\%$ vs $28.3\% \pm 8.4\%$ $p = 0.131$) were observed in the defects filled with THA-col composite compared to THA alone (**Figure 5D**, **supplementary Figure S4C and S5C**).

4 DISCUSSION

Material-based cell-free approaches to treat cartilage and osteochondral defects have shown promising results^{5,49,50}. These approaches are of interest due to the limited availability of autologous chondrocytes. Infiltration of cells from the adjacent tissues into the biomaterial is a critical step in this approach, as these migrating cells play a pivotal role in depositing the extracellular matrix and facilitating tissue repair¹⁵. However, data on which biomaterial properties influence cell infiltration and related tissue formation is limited since most studies use only one material or modification, and different studies use different models for their evaluation. Focus of this study was to evaluate different materials and modifications in an *in vitro* assay for MSC migration, an *ex vivo* assay for chondrocyte migration and an *in vivo* model to assess cell infiltration, inflammatory response and tissue formation. Our findings indicate significant differences between the three hydrogel groups across the various assays, and the outcomes may be extended to other materials and modifications.

Lowering DoF from 80% to 50% (GelMA 80 vs GelMA50) showed a higher migration index and thus a higher number of chondrocytes migrating into the hydrogel *ex vivo*. It has also been described that the hydraulic permeability and mechanical properties of GelMA can be controlled by the DoF, polymer concentration and crosslinking time⁵¹. The mechanical behaviour of the two formulations during the rheology tests was not

significantly different and did not allow estimation of the permeability of the gels. The lower degree of functionalization of the GelMA50 has been previously associated with a faster enzymatic degradation kinetic ²⁰, which is known to promote cell migration. A higher cell migration and more tissue formation compared to the higher DoF group was only observed in the *ex vivo* migration assay. The MSCs in the *in vitro* assay were spreading and migrating in both, GelMA50 and GelMA80. This partially aligns with a previous *in vitro* study comparing GelMA (5% wt) with different DoF, which showed spreading of encapsulated adipose-derived MSCs in the samples with a DoF of 30% and 50%, but not above 70% ^{21,43}. In the *ex vivo* assay, the difference in migration score between the two DoF was more prominent. Although the chondrocytes retained a round morphology, they seem to prefer invasion into the lower DoF hydrogel. This finding highlights that different models and/or the cell types used, influence migration behaviour. A tendency of overall more tissue formation was observed in GelMA50 compared to GelMA80 after six weeks of implantation. Although GelMA has some potential to stimulate cell migration and cartilage-like-tissue formation, the shrinking of the hydrogel when cultured in the cartilage ring model is a drawback. Nguyen *et al.* described that GelMA with a lower DoF degrades faster by collagenase-loaded micro-particles ¹⁹. This shrinkage leads to limited integration with the surrounding tissue and resulting in gap formation that cells might not be able to bridge.

A different approach to control the degradability of a hydrogel and to increase cell migration is the use of a MMP degradable crosslinker with a norHA hydrogel. In contrast to our original hypothesis, that the use of a MMP cleavable crosslinker would improve cell migration, the addition of the MMP degradable crosslinker did not improve cell migration *in vitro* or in the *ex vivo* setting. It is possible that the proteases secreted by the MSCs and the cartilage explants in these settings were not capable of sufficiently degrading the VPMSMRGG peptide of the crosslinker in our study - it has been investigated before that the VPMSMRGG is most sensitive to MMP 1 ^{52,53}. It is likely that there are more MMPs present in the *in vivo* model that lead to a faster degradation. In addition, it is plausible that the *ex vivo* model prompts the secretion of tissue inhibitors of matrix metalloproteinases, which hinder the activity of MMPs and, as a result, impede the degradation of the hydrogel ^{54,55}. Although no differences in mesenchymal stromal cells ⁴¹, and (lung) epithelial cells ⁵⁶ were observed in previous studies, future studies will need to investigate whether specific MMPs are responsible to degrade these bonds in the norHA-MMP gels. Furthermore, the more than three-fold lower bulk mechanical properties of norHA MMP could have limited cell attachment and thus migration. In the *in vivo* model, however, the MMP-sensitive crosslinker clearly showed more tissue formation in the gels crosslinked with the non-degradable DTT crosslinker. The formation of various tissue types, including cartilage-like and

bone-like tissue, in the semi-orthotopic model aligns with prior literature, which has reported that in norHA hydrogels that incorporate non-degradable crosslinkers, matrix deposition is confined to the pericellular region after 28 days²⁷. Additionally, research on maleimide modified HA (1.2% wt) crosslinked with an MMP-sensitive crosslinker (CRDVPMSQMRGGDRCG) has shown that a greater amount of cartilage-like tissue is formed compared to gels with protease-insensitive DTT crosslinkers⁵⁷. Thus, our study verifies the benefits of using an MMP-cleavable crosslinker to promote the formation of repair tissue and cartilage-like matrix deposition. Furthermore, our study underscores the importance of utilizing multiple assays and selecting an appropriate experimental design to evaluate the performance of a hydrogel.

Besides using a MMP degradable crosslinker, the addition of RGD peptides is another approach to control cell spreading. Collagen type I and, to some extent, GelMA contains natural RGD sites that are characterized by cell-instructive properties⁵⁸. We found that the addition of collagen in a THA hydrogel enhanced the migration of MSCs and chondrocytes in all three models examined. Furthermore, the incorporation of type 1 collagen into the THA hydrogel leads to the development of a fibrillary network, which induces bio-instructive properties sensed by the cells, thereby providing an additional advantage. It has been shown that these micro-structural features in THA-col can be used to orient collagen fibres via 3D bioprinting³⁹. Whether the fibrillar component, the RGD sites or a combination of both are the most driving factor promoting cell migration remains unknown and a focus for future studies. Although THA-col composite did positively influence MSC migration and MSC chondrogenesis *in vitro*^{59,60}, still only 60% of the defect volume was filled with newly formed tissue, and limited cartilage-like tissue was formed in the *in vivo* setting. Further optimization of this hydrogel is needed to achieve more cell invasion and support cartilage-like tissue formation.

Cell-material interaction and thus mechanosensing contributes to cell spreading and migration. The results suggest that cell migration is not primarily controlled by the bulk mechanical properties as it has been proposed in other studies. It is rather a combination of different material properties that control cell behaviour^{47,61,62}. THA and THA-col had similar Young's moduli and the higher cell migration in the THA-col compared to THA is likely due to the presence of RGD sequences. Storage moduli of THA and THA-col have been shown to be similar^{34,39}. GelMA80 and GelMA50 both naturally contain RGD sequences and in this study the young's moduli as well as final storage moduli were comparable⁴³. Yet, migration on GelMA50 was better in the *ex vivo* model compared to GelMA80. This indicates that the lower DOF can have a positive effect on cell migration and tissue formation. Both norHA hydrogels contained RGD for cell adhesion. In the *in vitro* and the *ex vivo* model, more cell invasion was

found in the stiffer norHA DTT hydrogel compared to norHA MMP. Caliri *et al.* have shown that MSC spreading depends on the substrate stiffness of norHA hydrogels, and found that stiffer hydrogels (20 kPa) stimulated MSC spreading in 2D, whereas in 3D cell spreading was seen only in the least stiff hydrogel (1 kPa)³⁶. This discrepancy with our results in norHA gels indicates that the dimensionality of the model and hydrogel stiffness are not the only parameters influencing cell migration. Instead, a complex interplay of multiple parameters might affect cell migration in hydrogels. More research is needed to understand the underlying mechanisms of bioinstructive properties to increase cell infiltration and improve biochemical and biophysical properties of biomaterials for cell free tissue repair.

When evaluating the samples implanted for only ten days in the semi-orthotopic mouse model, we identified only a few inflammatory cells on and within the hydrogels, highlighting that there was no strong foreign body reaction related to any of the hydrogels used. Although a strong foreign body response can cause unwanted effect, inflammation is also known to influence cell migration as well as matrix degradation and therefore can be stimulating the ingrowth of cells in a hydrogel^{7,14,63,64}. In the design and modification of biomaterials such a positive effect of inflammation should be considered as well. To pre-screen biomaterials and modifications on their pro- or anti-inflammatory response, different *in vitro* models are available. Wesdorp *et al.* showed a similar response of neutrophils seeded on THA, THA-col (2.5% wt HA, 0.25% wt col) and GelMA (15% wt, DoF 50%) in terms of myeloperoxidase, neutrophil elastase and cytokine secretion⁶⁵. In light of the 3R principle (refinement, reduction, and replacement), an initial screening may be conducted *in vitro* to assess the potential impact of hydrogel modifications on inflammation, which could alter the cell infiltration behavior of the hydrogel.

Cell type specific differences in response to the materials as a function of the mechanical properties, chemical composition and mesh size have been reported^{26,66,67}. The screening of the hydrogels in the three models covers different cell types, namely MSCs, chondrocytes and cells residing in the subchondral bone and bone marrow of the osteochondral explants. Results of the here reported *in vitro*, *ex vivo* and *in vivo* testing together with findings related to how cells respond to different materials suggest that the specific hydrogel formulations tested in this study were not selective for different mesenchymal cell types present in the osteochondral environment. This study further showed that with a single modification in either an HA or gelatine-based hydrogel, cell invasion can be stimulated. A limitation of the present study is that for each formulation multiple characteristics of the matrices (total polymer concentration, crosslinking density, mesh size) are simultaneously modified, limiting

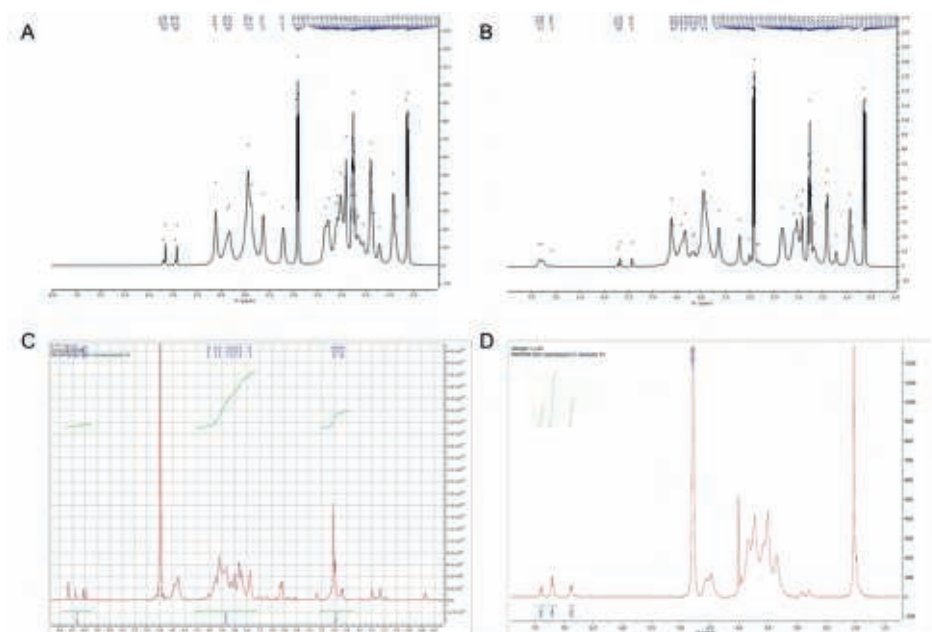
the ability to decouple findings. Since each modification will have different effects on hydrogel swelling, secondary structure, degradation and most likely the cell-biomaterial interaction, a direct comparison would have been not very practical. The current approach prevented this direct comparison and solely demonstrated the possible effects of one specific chemical modification within three selected hydrogel types on cell migration and tissue formation. More fundamental knowledge on how different material properties influence cell behaviour is required to optimize the design of hydrogels for osteochondral tissue repair.

The success of acellular hydrogel approaches to repair (osteo-) chondral defects is limited in treating larger defects. In this case, the relatively low number of cells invading the biomaterial implanted in the defect might not allow for complete defect repair. One approach to increase the invasion distance might be the use of chemotactic factors. If this is not feasible, a combined approach of encapsulating patient-derived cells and a hydrogel stimulating the migration and invasion of cells from surrounding tissue can be considered. Moreover, good bonding and minimal lateral delamination of the hydrogel from the surrounding tissue are a prerequisite allowing for endogenous cell migration and related matrix deposition ⁶⁸. To address this research question, different models including push out tests are available for quantitative measures of integration ^{69,70}. Dynamic mechanical analysis has been proposed to study the adhesion strength between the tissue and hydrogel ⁷¹. Before taking this next step, a more in-depth understanding is needed to improve cell invasion further and to understand the mechanisms driving or limiting cell migration.

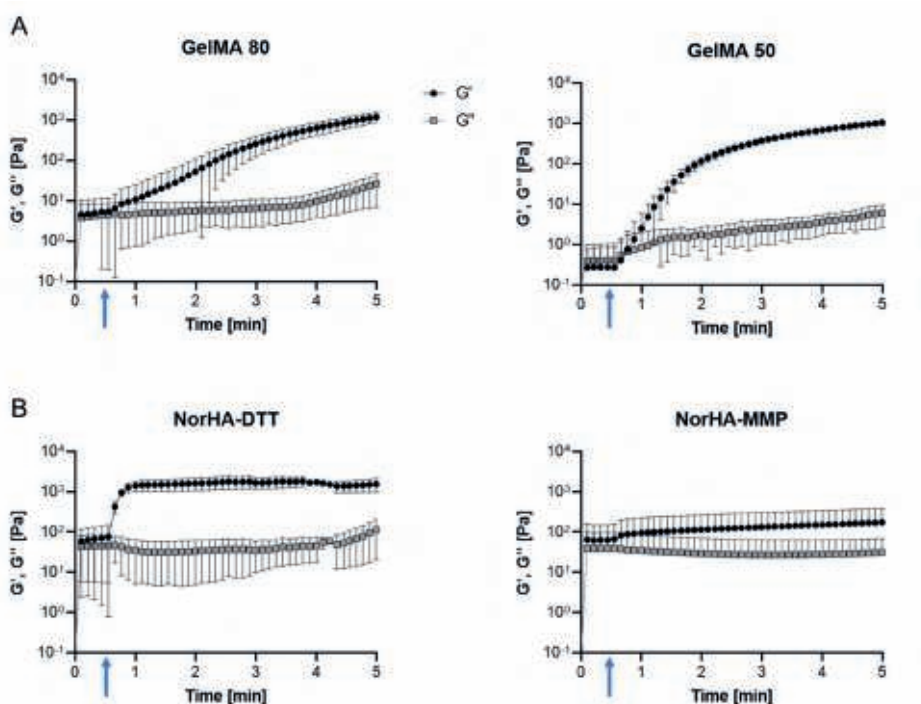
Conclusion

Migration of cells with chondrogenic potential into hydrogels is the first step to improve cell free repair of osteochondral defects. While cell free approaches would fail in the absence of cell invasion, cell-based treatments would also benefit from enhanced integration of the implant to the surrounding tissue. Our study shows that cell migration is dependent on multiple material characteristics, including physicochemical and bio-instructive properties. Moreover, this study also highlights the need for screening biomaterials in different models *in vitro*, *ex vivo* and *in vivo* since results might differ depending on the model used. The three hydrogel groups and modifications screened in this study, do support cartilage-like and bone-like tissue formation making them suitable candidates for further optimization and use in osteochondral repair.

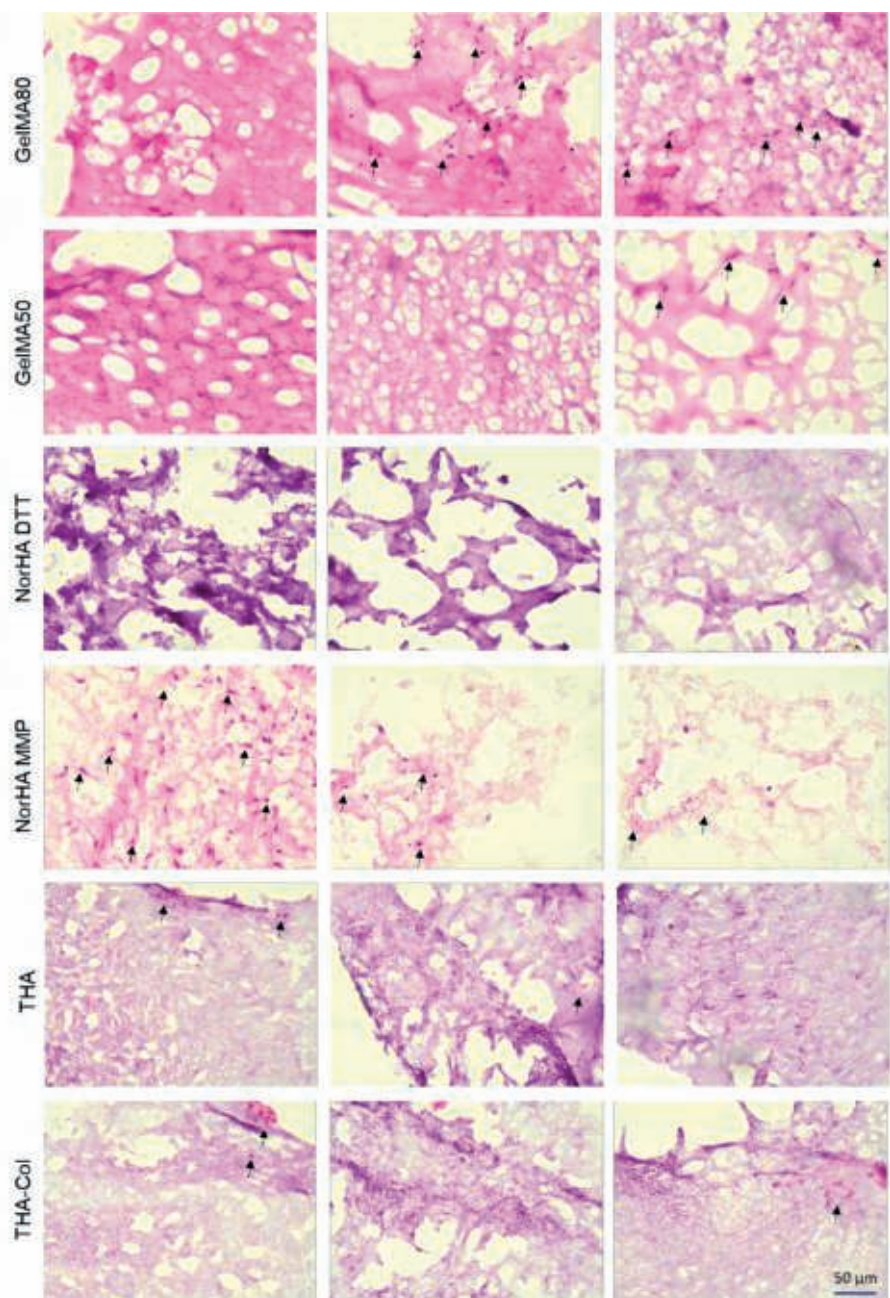
Supplementary Material



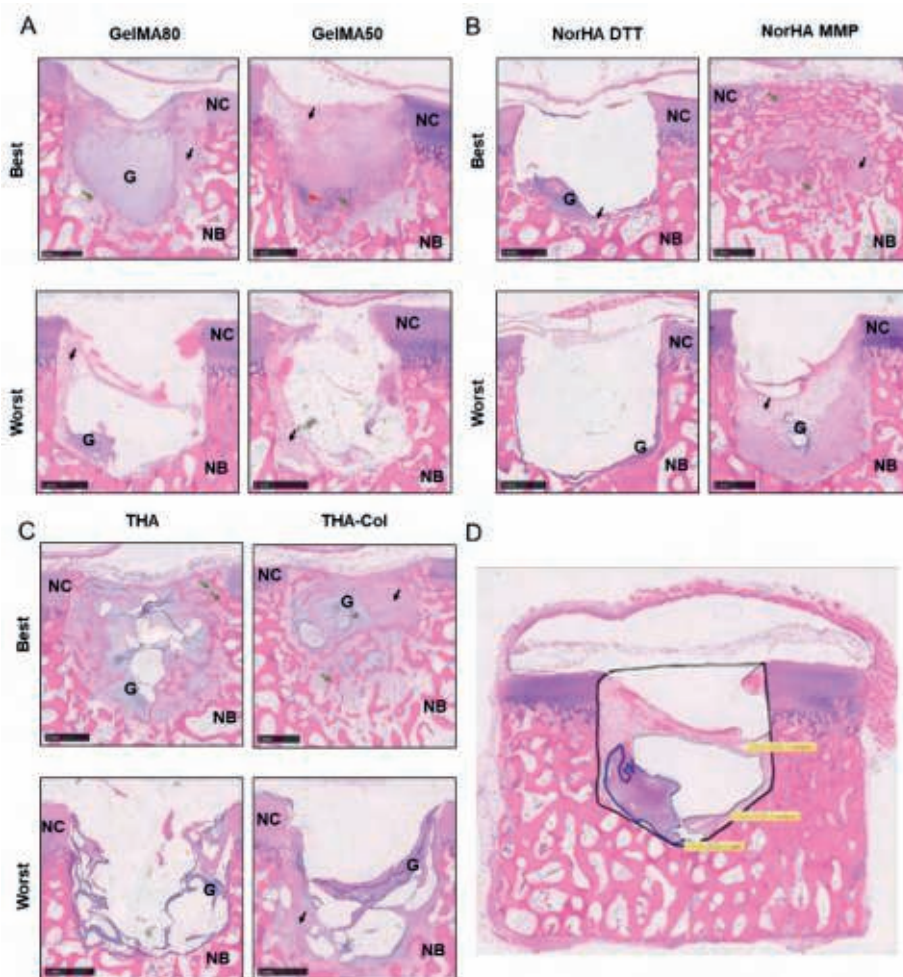
Supplementary figure S1: ^1H NMR spectrum of hydrogel precursors. (A, B) Gelatine methacryloyl (GelMA) in D_2O (4% concentration, with 0.5 mg/ml of 3-(Trimethylsilyl)-1-propanesulfonic acid sodium salt). NMR spectra of (A) GelMA50 and (B) GelMA80 confirm the methacrylation of the gelatine backbone. At 5.5 and 6.0 ppm the peaks corresponding to the protons belonging to the double bond of the methacrylate moiety with a shorter peak in GelMA50 compared to GelMA80. A small peak for lysine at 3.0 ppm was still present on the GelMA50 but it is missing on the GelMA80 sample. (C) Norbornene-functionalized hyaluronic acid (NorHA) in D_2O (5wt%). Modification of HA with norbornene (30%) determined by integration of vinyl protons ($2 \times 2\text{H}$) relative to the sugar ring of HA (10H). NorHA precursor was the same for preparing, norHA-DTT and norHA-MMP. (D) Tyramine functionalized hyaluronic acid (THA) in D_2O (3%w/v in D_2O containing 0.4 mg/ml hyaluronidase). The NMR spectrum conforms to the structure of the tyramine derivative of HA, showing a singlet corresponding to the N-acetyl group around 2 ppm, and a broad multiplet between 3.2 and 4.0 ppm corresponding to various protons on the saccharide rings. The three peaks around 7 ppm corresponding to the aromatic resonances of the tyramine groups are visible (Loebel, Stauber et al. 2017). THA precursor was the same to prepare THA-collagen.



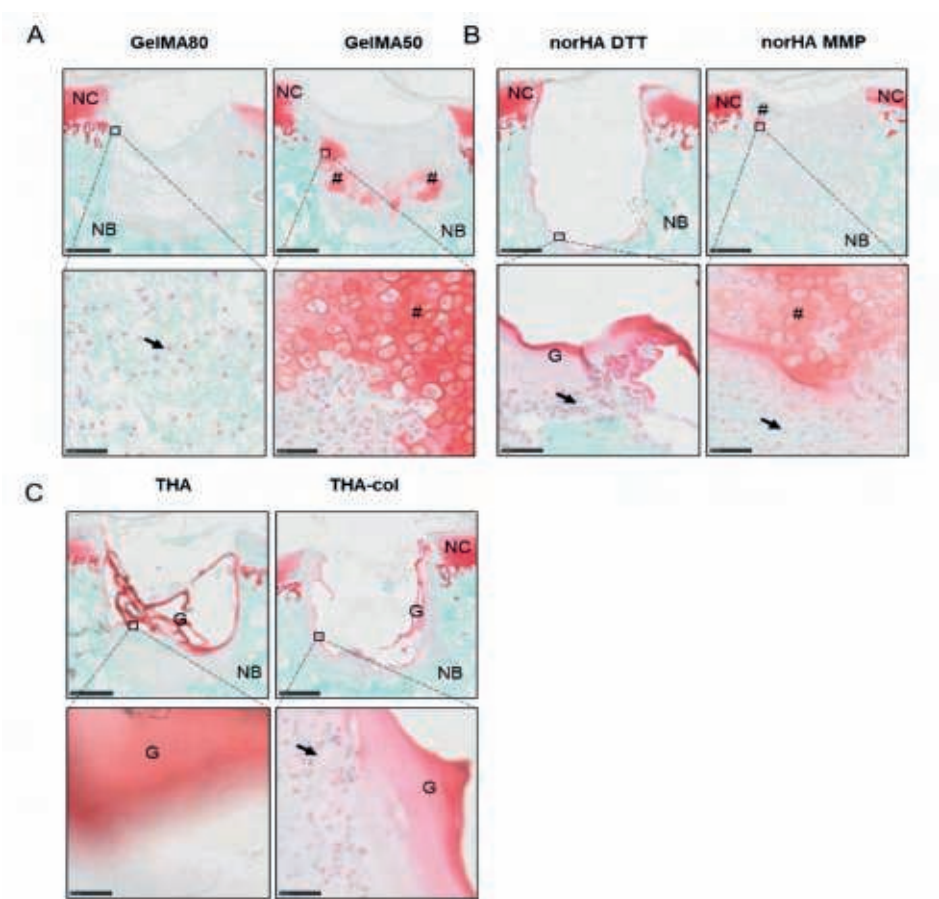
Supplementary figure S2: Photo rheology of gelatine methacryloyl (50% and 80% degree of functionalization, DOF) and norbornene functionalized hyaluronic acid (norHA) crosslinked with either a non-degradable (DTT) or MMP degradable crosslinker. Blue arrow indicates the time (30 sec) when the light was turned on for photo- crosslinking the hydrogel precursors.



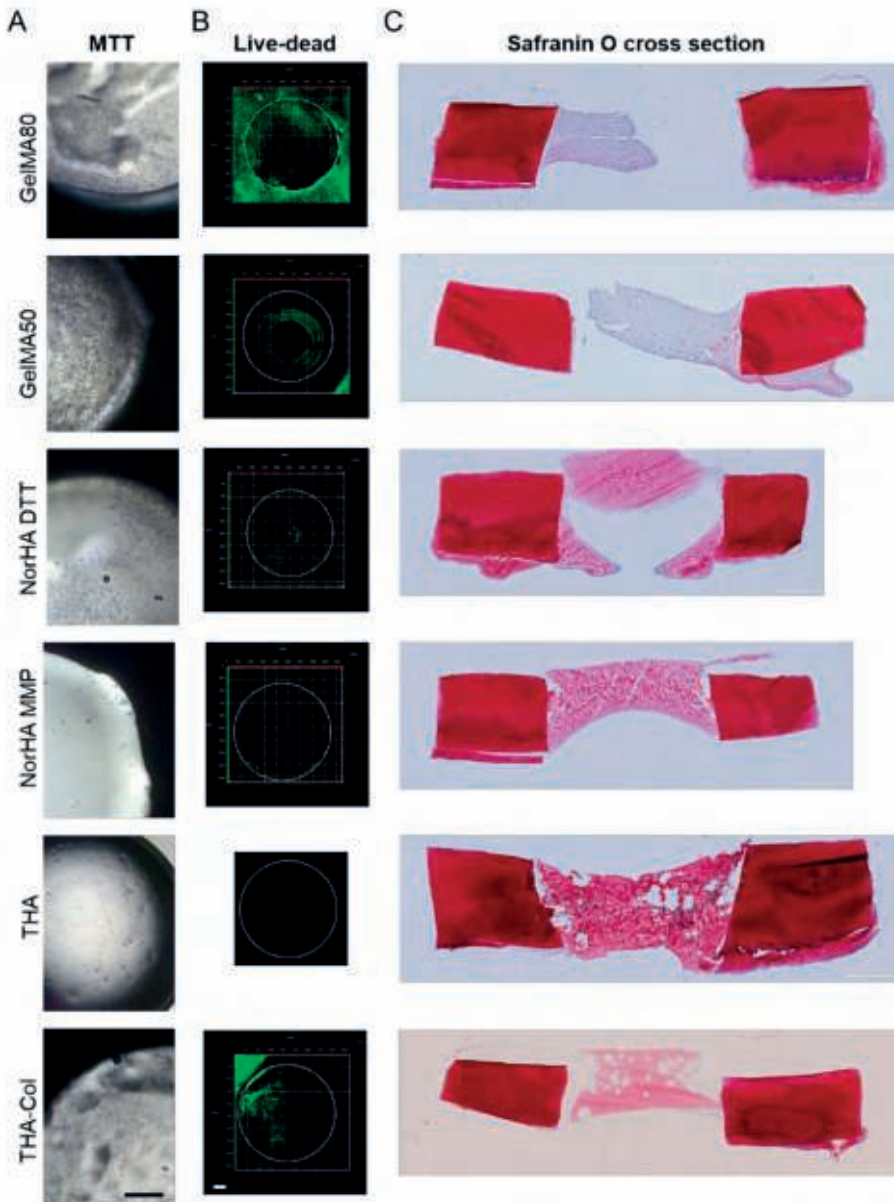
Supplementary figure S3: Cell infiltration into hydrogels after 10 days implantation in semi-orthotopic model. HE staining of acellular hydrogels were polymerized in osteochondral defects and implanted in nude mice (n=3 samples per biomaterial). Most cells were observed in GelMA 80% and 50% as well as norHA MMP gels. Only single cells were present in the other hydrogel groups. Arrows indicate (multinucleated) cells. Scale bar 50 μm.



Supplementary figure S4: Tissue regeneration in osteochondral defects filled with the hydrogels in an in vivo subcutaneous implantation mouse model. The best and worst repair constructs stained with H&E showing the in- situ hydrogels and tissue regeneration within the osteochondral defects after 6 weeks of implantation. A) GelMA degree of functionalization 50% and 80%, B) norHA with protease (MMP) cleavable and non-degradable DTT crosslinker, C) THA and THA-collagen. Scale bars indicate 1 mm. Black arrows indicated infiltrated cells within the defects. Red arrows indicated newly formed cartilage-like tissue. Green arrows indicated newly formed bone-like tissue. NC: native cartilage; NB: native bone; G: hydrogel. D) Example on defining the defect region (black line), hydrogel selection (blue line) and newly formed tissue formation (grey line) for quantification of tissue formation mice (n=5 samples per biomaterial).



Supplementary figure S5: Representative images of the repair constructs stained with Safranin O showing the in- situ hydrogels and tissue regeneration within the osteochondral defects after 6 weeks of implantation. A) GelMA degree of functionalization 50% and 80%, B) norHA with protease (MMP) cleavable and non-degradable DTT crosslinker, C) THA and THA-collagen. Scale bars indicate 1 mm (lower magnification) and 50 μ m (higher magnification). Black squares indicated the magnified areas. Black arrows indicated infiltrated cells within the defects. NC: native cartilage; NB: native bone; G: hydrogel; #: cartilage-like tissue.



Supplementary figure S6: Ex vivo cartilage explant model after 21 days of culture. A) Microscopic image of metabolic active chondrocytes migrating on the biomaterials (MTT staining). Scale bar 500 μm . B) Live-dead staining (green: alive cells, red: dead cells). Scale bar 500 μm . C) Safranin O staining of representative cartilage explants treated with biomaterials. Scale bar 1 mm. THA: tyramine modified hyaluronic acid (HA), THA-col, norHA DTT: norbonene functionalized HA with non-degradable crosslinker, norHA MMP: norHA with Matrix Metalloproteinase degradable crosslinker, GelMA 50: gelatine methacryloyl with 50% degree of functionalization (DoF), GelMA 80: GelMA 80% DoF.

REFERENCES

1. Volz M, Schaumburger J, Frick H, Grifka J, Anders S. A randomized controlled trial demonstrating sustained benefit of Autologous Matrix-Induced Chondrogenesis over microfracture at five years. *Int Orthop* 2017;41(4):797-804.
2. Migliorini F, Maffulli N, Baroncini A, Bell A, Hildebrand F, Schenker H. Autologous matrix-induced chondrogenesis is effective for focal chondral defects of the knee. *Sci Rep* 2022;12(1):9328.
3. Brittberg M. New frontiers for cartilage repair, joint preservation and prevention. *Journal of Cartilage & Joint Preservation* 2022;2(2):100060.
4. Brittberg M, Recker D, Ilgenfritz J, Saris DBF, Group SES. Matrix-Applied Characterized Autologous Cultured Chondrocytes Versus Microfracture: Five-Year Follow-up of a Prospective Randomized Trial. *Am J Sports Med* 2018;46(6):1343-51.
5. Brittberg M. Cellular and Acellular Approaches for Cartilage Repair: A Philosophical Analysis. *Cartilage* 2015;6(2 Suppl):4S-12S.
6. Levinson C, Cavalli E, von Rechenberg B, Zenobi-Wong M, Darwiche SE. Combination of a Collagen Scaffold and an Adhesive Hyaluronan-Based Hydrogel for Cartilage Regeneration: A Proof of Concept in an Ovine Model. *Cartilage* 2021;13(2_suppl):636S-49S.
7. Zhang S, Hu B, Liu W, Wang P, Lv X, Chen S, et al. Articular cartilage regeneration: The role of endogenous mesenchymal stem/progenitor cell recruitment and migration. *Semin Arthritis Rheum* 2020;50(2):198-208.
8. Yang Z, Li H, Yuan Z, Fu L, Jiang S, Gao C, et al. Endogenous cell recruitment strategy for articular cartilage regeneration. *Acta Biomater* 2020;114:31-52.
9. Moroni L, Elisseeff JH. Biomaterials engineered for integration. *Materials Today* 2008;11(5):44-51.
10. Spector M, Lim TC. Injectable biomaterials: a perspective on the next wave of injectable therapeutics. *Biomed Mater* 2016;11(1):014110.
11. Jeon O, Lee YB, Lee SJ, Guliyeva N, Lee J, Alsberg E. Stem cell-laden hydrogel bioink for generation of high resolution and fidelity engineered tissues with complex geometries. *Bioact Mater* 2022;15:185-93.
12. Sennett ML, Friedman JM, Ashley BS, Stoeckl BD, Patel JM, Alini M, et al. Long term outcomes of biomaterial-mediated repair of focal cartilage defects in a large animal model. *Eur Cell Mater* 2021;41:40-51.
13. Wei F, Liu S, Chen M, Tian G, Zha K, Yang Z, et al. Host Response to Biomaterials for Cartilage Tissue Engineering: Key to Remodeling. *Front Bioeng Biotechnol* 2021;9:664592.
14. Qu F, Guilak F, Mauck RL. Cell migration: implications for repair and regeneration in joint disease. *Nat Rev Rheumatol* 2019;15(3):167-79.
15. Pabbruwe MB, Esfandiari E, Kafienah W, Tarlton JF, Hollander AP. Induction of cartilage integration by a chondrocyte/collagen-scaffold implant. *Biomaterials* 2009;30(26):4277-86.

16. Zhang Z, Schon L. The Current Status of Clinical Trials on Biologics for Cartilage Repair and Osteoarthritis Treatment: An Analysis of ClinicalTrials.gov Data. *Cartilage* 2022;13(2):19476035221093065.
17. Sun M, Sun X, Wang Z, Guo S, Yu G, Yang H. Synthesis and Properties of Gelatin Methacryloyl (GelMA) Hydrogels and Their Recent Applications in Load-Bearing Tissue. *Polymers (Basel)* 2018;10(11).
18. Van Den Bulcke AI, Bogdanov B, De Rooze N, Schacht EH, Cornelissen M, Berghmans H. Structural and rheological properties of methacrylamide modified gelatin hydrogels. *Biomacromolecules* 2000;1(1):31-8.
19. Nguyen AH, McKinney J, Miller T, Bongiorno T, McDevitt TC. Gelatin methacrylate microspheres for controlled growth factor release. *Acta Biomater* 2015;13:101-10.
20. Li X, Chen S, Li J, Wang X, Zhang J, Kawazoe N, et al. 3D Culture of Chondrocytes in Gelatin Hydrogels with Different Stiffness. *Polymers (Basel)* 2016;8(8).
21. Klotz BJ, Lim KS, Chang YX, Soliman BG, Pennings I, Melchels FPW, et al. Engineering of a complex bone tissue model with endothelialised channels and capillary-like networks. *Eur Cell Mater* 2018;35:335-48.
22. Nicolas J, Magli S, Rabbachin L, Sampaolesi S, Nicotra F, Russo L. 3D Extracellular Matrix Mimics: Fundamental Concepts and Role of Materials Chemistry to Influence Stem Cell Fate. *Biomacromolecules* 2020;21(6):1968-94.
23. Xia H, Li X, Gao W, Fu X, Fang RH, Zhang L, et al. Tissue repair and regeneration with endogenous stem cells. *Nature Reviews Materials* 2018;3(7):174-93.
24. Kim YS, Guilak F. Engineering Hyaluronic Acid for the Development of New Treatment Strategies for Osteoarthritis. *Int J Mol Sci* 2022;23(15).
25. Kim IL, Mauck RL, Burdick JA. Hydrogel design for cartilage tissue engineering: a case study with hyaluronic acid. *Biomaterials* 2011;32(34):8771-82.
26. Petta D, D'Amora U, Ambrosio L, Grijpma DW, Eglin D, D'Este M. Hyaluronic acid as a bioink for extrusion-based 3D printing. *Biofabrication* 2020;12(3):032001.
27. Galarraga JH, Kwon MY, Burdick JA. 3D bioprinting via an in situ crosslinking technique towards engineering cartilage tissue. *Sci Rep* 2019;9(1):19987.
28. Behrendt P, Ladner Y, Stoddart MJ, Lippross S, Alini M, Eglin D, et al. Articular Joint-Simulating Mechanical Load Activates Endogenous TGF-beta in a Highly Cellularized Bioadhesive Hydrogel for Cartilage Repair. *Am J Sports Med* 2020;48(1):210-21.
29. Petta D, Armiento AR, Grijpma D, Alini M, Eglin D, D'Este M. 3D bioprinting of a hyaluronan bioink through enzymatic-and visible light-crosslinking. *Biofabrication* 2018;10(4):044104.
30. Petta D, Grijpma DW, Alini M, Eglin D, D'Este M. Three-Dimensional Printing of a Tyramine Hyaluronan Derivative with Double Gelation Mechanism for Independent Tuning of Shear Thinning and Postprinting Curing. *ACS Biomater Sci Eng* 2018;4(8):3088-98.
31. Loebel C, Stauber T, D'Este M, Alini M, Zenobi-Wong M, Eglin D. Fabrication of cell-compatible hyaluronan hydrogels with a wide range of biophysical properties through high tyramine functionalization. *Journal of Materials Chemistry B* 2017;5(12):2355-63.

32. Shu XZ, Ghosh K, Liu Y, Palumbo FS, Luo Y, Clark RA, et al. Attachment and spreading of fibroblasts on an RGD peptide-modified injectable hyaluronan hydrogel. *J Biomed Mater Res A* 2004;68(2):365-75.
33. Lam J, Truong NF, Segura T. Design of cell-matrix interactions in hyaluronic acid hydrogel scaffolds. *Acta Biomater* 2014;10(4):1571-80.
34. Staubli F, Stoddart MJ, D'Este M, Schwab A. Pre-culture of human mesenchymal stromal cells in spheroids facilitates chondrogenesis at a low total cell count upon embedding in biomaterials to generate cartilage microtissues. *Acta Biomater* 2022;143:253-65.
35. Lei Y, Gojgini S, Lam J, Segura T. The spreading, migration and proliferation of mouse mesenchymal stem cells cultured inside hyaluronic acid hydrogels. *Biomaterials* 2011;32(1):39-47.
36. Caliarì SR, Vega SL, Kwon M, Soulas EM, Burdick JA. Dimensionality and spreading influence MSC YAP/TAZ signaling in hydrogel environments. *Biomaterials* 2016;103:314-23.
37. Mouser VH, Melchels FP, Visser J, Dhert WJ, Gawlitta D, Malda J. Yield stress determines bioprintability of hydrogels based on gelatin-methacryloyl and gellan gum for cartilage bioprinting. *Biofabrication* 2016;8(3):035003.
38. Loebel C, Szczesny SE, Cosgrove BD, Alini M, Zenobi-Wong M, Mauck RL, et al. Cross-Linking Chemistry of Tyramine-Modified Hyaluronan Hydrogels Alters Mesenchymal Stem Cell Early Attachment and Behavior. *Biomacromolecules* 2017;18(3):855-64.
39. Schwab A, Helary C, Richards RG, Alini M, Eglin D, D'Este M. Tissue mimetic hyaluronan bioink containing collagen fibers with controlled orientation modulating cell migration and alignment. *Mater Today Bio* 2020;7:100058.
40. Loebel C, Kwon MY, Wang C, Han L, Mauck RL, Burdick JA. Metabolic Labeling to Probe the Spatiotemporal Accumulation of Matrix at the Chondrocyte-Hydrogel Interface. *Advanced Functional Materials* 2020;30(44):1909802.
41. Loebel C, Mauck RL, Burdick JA. Local nascent protein deposition and remodelling guide mesenchymal stromal cell mechanosensing and fate in three-dimensional hydrogels. *Nat Mater* 2019;18(8):883-91.
42. Melchels FPW, Dhert WJA, Huttmacher DW, Malda J. Development and characterisation of a new bioink for additive tissue manufacturing. *Journal of Materials Chemistry B* 2014;2(16):2282-89.
43. Pepelanova I, Kruppa K, Scheper T, Lavrentieva A. Gelatin-Methacryloyl (GelMA) Hydrogels with Defined Degree of Functionalization as a Versatile Toolkit for 3D Cell Culture and Extrusion Bioprinting. *Bioengineering (Basel)* 2018;5(3).
44. Gramlich WM, Kim IL, Burdick JA. Synthesis and orthogonal photopatterning of hyaluronic acid hydrogels with thiol-norbornene chemistry. *Biomaterials* 2013;34(38):9803-11.
45. Loebel C, D'Este M, Alini M, Zenobi-Wong M, Eglin D. Precise tailoring of tyramine-based hyaluronan hydrogel properties using DMTMM conjugation. *Carbohydr Polym* 2015;115:325-33.
46. Wesdorp MA, Bastiaansen-Jenniskens YM, Capar S, Verhaar JAN, Narcisi R, Van Osch GJVM. Modulation of Inflamed Synovium Improves Migration of Mesenchymal Stromal Cells in Vitro Through Anti-Inflammatory Macrophages. *Cartilage* 2022;13(1):19476035221085136.

47. Vainieri ML, Lolli A, Kops N, D'Atri D, Eglin D, Yayan A, et al. Evaluation of biomimetic hyaluronic-based hydrogels with enhanced endogenous cell recruitment and cartilage matrix formation. *Acta Biomater* 2020;101:293-303.
48. de Vries-van Melle ML, Tihaya MS, Kops N, Koevoet WJ, Murphy JM, Verhaar JA, et al. Chondrogenic differentiation of human bone marrow-derived mesenchymal stem cells in a simulated osteochondral environment is hydrogel dependent. *Eur Cell Mater* 2014;27:112-23; discussion 23.
49. Ricci M, Tradati D, Maione A, Uboldi FM, Usellini E, Berruto M. Cell-free osteochondral scaffolds provide a substantial clinical benefit in the treatment of osteochondral defects at a minimum follow-up of 5 years. *J Exp Orthop* 2021;8(1):62.
50. Kon E, Filardo G, Perdisa F, Venieri G, Marcacci M. Acellular Matrix-Based Cartilage Regeneration Techniques for Osteochondral Repair. *Operative Techniques in Orthopaedics* 2014;24(1):14-18.
51. Miri AK, Hosseiniabadi HG, Cecen B, Hassan S, Zhang YS. Permeability mapping of gelatin methacryloyl hydrogels. *Acta Biomater* 2018;77:38-47.
52. Chen W, Zhou Z, Chen D, Li Y, Zhang Q, Su J. Bone Regeneration Using MMP-Cleavable Peptides-Based Hydrogels. *Gels* 2021;7(4).
53. Turk BE, Huang LL, Piro ET, Cantley LC. Determination of protease cleavage site motifs using mixture-based oriented peptide libraries. *Nat Biotechnol* 2001;19(7):661-7.
54. Cawston T, Billington C, Cleaver C, Elliott S, Hui W, Koshy P, et al. The regulation of MMPs and TIMPs in cartilage turnover. *Ann N Y Acad Sci* 1999;878:120-9.
55. Raeeszadeh-Sarmazdeh M, Do LD, Hritz BG. Metalloproteinases and Their Inhibitors: Potential for the Development of New Therapeutics. *Cells* 2020;9(5).
56. Loebel C, Weiner AI, Eiken MK, Katzen JB, Morley MP, Bala V, et al. Microstructured Hydrogels to Guide Self-Assembly and Function of Lung Alveolospheres. *Advanced Materials* 2022;34(28):2202992.
57. Feng Q, Zhu M, Wei K, Bian L. Cell-mediated degradation regulates human mesenchymal stem cell chondrogenesis and hypertrophy in MMP-sensitive hyaluronic acid hydrogels. *PLoS One* 2014;9(6):e99587.
58. Gavenis K, Schneider U, Maus U, Mumme T, Muller-Rath R, Schmidt-Rohlfing B, et al. Cell-free repair of small cartilage defects in the Goettinger minipig: which defect size is possible? *Knee Surgery, Sports Traumatology, Arthroscopy* 2012;20(11):2307-14.
59. Heino J. The collagen family members as cell adhesion proteins. *Bioessays* 2007;29(10):1001-10.
60. Davis GE. Affinity of integrins for damaged extracellular matrix: $\alpha v\beta 3$ binds to denatured collagen type I through RGD sites. *Biochemical and Biophysical Research Communications* 1992;182(3):1025-31.
61. Matellan C, del Río Hernández AE. Engineering the cellular mechanical microenvironment - from bulk mechanics to the nanoscale. *Journal of Cell Science* 2019;132(9).
62. Zan F, Wei Q, Fang L, Xian M, Ke Y, Wu G. Role of Stiffness versus Wettability in Regulating Cell Behaviors on Polymeric Surfaces. *ACS Biomaterials Science & Engineering* 2020;6(2):912-22.

63. Li M, Yin H, Yan Z, Li H, Wu J, Wang Y, et al. The immune microenvironment in cartilage injury and repair. *Acta Biomaterialia* 2022;140:23-42.
64. van der Kraan PM. The Interaction between Joint Inflammation and Cartilage Repair. *Tissue Engineering and Regenerative Medicine* 2019;16(4):327-34.
65. Wesdorp MA, Schwab A, Bektas EI, Narcisi R, Eglin D, Stoddart MJ, et al. A culture model to analyze the acute biomaterial-dependent reaction of human primary neutrophils in vitro. *Bioact Mater* 2023;20:627-37.
66. Caliarì SR, Burdick JA. A practical guide to hydrogels for cell culture. *Nature Methods* 2016;13(5):405-14.
67. Levato R, Jungst T, Scheuring RG, Blunk T, Groll J, Malda J. From Shape to Function: The Next Step in Bioprinting. *Advanced Materials* 2020;32(12):1906423.
68. Khan IM, Gilbert SJ, Singhrao SK, Duance VC, Archer CW. Cartilage integration: evaluation of the reasons for failure of integration during cartilage repair. A review. *Eur Cell Mater* 2008;16:26-39.
69. Iseki T, Rothrauff BB, Kihara S, Sasaki H, Yoshiya S, Fu FH, et al. Dynamic Compressive Loading Improves Cartilage Repair in an In Vitro Model of Microfracture: Comparison of 2 Mechanical Loading Regimens on Simulated Microfracture Based on Fibrin Gel Scaffolds Encapsulating Connective Tissue Progenitor Cells. *Am J Sports Med* 2019;47(9):2188-99.
70. van de Breevaart Bravenboer J, In der Maur CD, Bos PK, Feenstra L, Verhaar JAN, Weinans H, et al. Improved cartilage integration and interfacial strength after enzymatic treatment in a cartilage transplantation model. *Arthritis Res Ther* 2004;6(5):R469.
71. Lim KS, Abinzano F, Bernal PN, Albillos Sanchez A, Atienza-Roca P, Otto IA, et al. One-Step Photoactivation of a Dual-Functionalized Bioink as Cell Carrier and Cartilage-Binding Glue for Chondral Regeneration. *Adv Healthc Mater* 2020;9(15):e1901792.

Effectiveness of BMP-2 and PDGF-BB
adsorption onto a collagen/collagen-
magnesium-hydroxyapatite scaffold in
weight-bearing and non-weight-bearing
osteocondral defect bone repair: *in vitro*,
ex vivo and *in vivo* evaluation

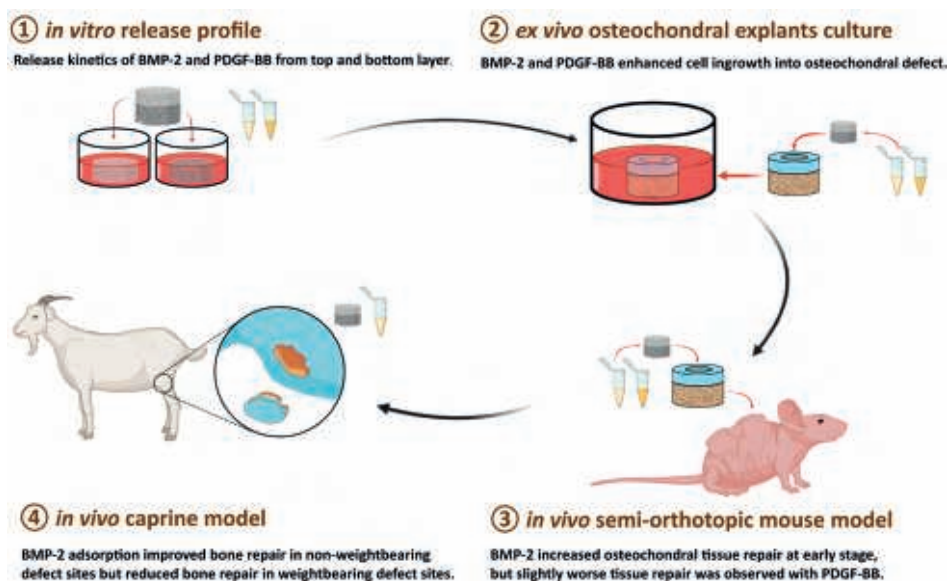
Jietao Xu
Shorouk Fahmy-Garcia
Marinus A. Wesdorp
Nicole Kops
Lucia Forte
Claudio De Luca
Massimiliano M. Misciagna
Laura Dolcini
Giuseppe Filardo

Margot Labberté
Karin Vancíková
Joeri Kok
Bert van Rietbergen
Joachim Nickel
Eric Farrell
Pieter A.J. Brama
Gerjo J.V.M. van Osch

ABSTRACT

Despite promising clinical results in osteochondral defect repair, a recently developed bi-layered collagen/collagen-magnesium-hydroxyapatite scaffold has demonstrated less optimal subchondral bone repair. This study aimed to improve the bone repair potential of this scaffold by adsorbing bone morphogenetic protein 2 (BMP-2) and/or platelet-derived growth factor-BB (PDGF-BB) onto said scaffold. The *in vitro* release kinetics of BMP-2/PDGF-BB demonstrated that PDGF-BB was burst released from the collagen-only layer, whereas BMP-2 was largely retained in both layers. Cell ingrowth was enhanced by BMP-2/PDGF-BB in a bovine osteochondral defect *ex vivo* model. In an *in vivo* semi-orthotopic athymic mouse model, adding BMP-2 or PDGF-BB increased tissue repair after four weeks. After eight weeks, most defects were filled with bone tissue. To further investigate the promising effect of BMP-2, a caprine bilateral stifle osteochondral defect model was used where defects were created in weight-bearing femoral condyle and non-weight-bearing trochlear groove locations. After six months, the adsorption of BMP-2 resulted in significantly less bone repair compared to scaffold-only in the femoral condyle defects and a trend to more bone repair in the trochlear groove. Overall, the adsorption of BMP-2 onto a Col/Col-Mg-HAP scaffold reduced bone formation in weight-bearing osteochondral defects, but not in non-weight-bearing osteochondral defects.

Keywords: tissue engineering; regenerative medicine; osteochondral lesion; biocompatible materials; Bone Morphogenetic Proteins; Platelet-Derived Growth Factor; animal model; weight-bearing



1. INTRODUCTION

Osteochondral tissue is formed by two main tissue types: the articular cartilage, which functions as a low-friction and wear-resistant surface, and the subchondral bone, which plays a crucial mechanically supportive role ¹. Without effective and timely interventions, damage to this osteochondral unit, caused by traumatic injury or disease, may progress to osteoarthritis ^{2,3}. Bi-layered biomaterial-scaffolds have been developed to restore the structural and physiological properties of the entire osteochondral unit and thus to support chondrogenesis and osteogenesis simultaneously ^{4,5}. As a biologically derived protein, collagen is an efficient biomaterial to support cellular activities and promote osteochondral repair ⁶⁻⁸. The addition of hydroxyapatite (HAp) can improve the osteogenic potential of a collagen-based scaffold *in vivo*, and magnesium ions (Mg^{2+}) induce osteogenic differentiation and osteoblast differentiation. Preclinically, bi-layered collagen/collagen-magnesium-HAp (Col/Col-Mg-HAp) scaffolds have successfully reconstructed the articular cartilage and the subchondral bone in animal models ⁹⁻¹¹. Clinical cohort studies also demonstrated the excellent stability of this scaffold and clinical improvement in knee function ¹²⁻¹⁴. However, subchondral bone repair remained suboptimal in some clinical follow-ups in comparison to the cartilage repair capacity of this scaffold ¹⁴, which may lead to altered biomechanical properties of the osteochondral unit and thereby affect the long-term survival of the neo-cartilage ¹⁵. This might subsequently lead to renewed osteochondral damage and joint disease ^{16,17}.

Incorporating factors that stimulate bone formation could be a promising approach to overcome this limitation in bone regeneration capacity ¹⁸. Bone morphogenetic protein 2 (BMP-2) has a vital role in osteogenesis and osteoclastogenesis ^{19,20} and is approved by the Food and Drug Administration (FDA) as an osteogenic protein. The recruitment of stem cells or osteoblasts is necessary for osteogenic initiation, and BMP-2 was reported to facilitate cell ingrowth ²¹. Platelet-derived growth factor (PDGF) is potent in stimulating cell ingrowth, angiogenesis, and osteogenesis ²²⁻²⁵. The delivery of BMP-2 and PDGF onto biomaterials has been shown an improvement in osteoblast function and bone integration ²⁶⁻²⁸. Therefore, it might be promising to adsorb BMP-2 and PDGF-BB onto this Col/Col-Mg-HAp scaffold to improve bone healing.

This study aimed to evaluate the osteogenic effectiveness of BMP-2 or PDGF-BB adsorption onto a Col/Col-Mg-HAp scaffold on bone repair in osteochondral defects. We first assessed the release profiles of BMP-2 and PDGF-BB from the two layers of a Col/Col-Mg-HAp scaffold *in vitro*. Next, an *ex vivo* osteochondral culture model was

used to investigate the added effect of growth factors on cell ingrowth from adjacent tissues. Then, we investigated the effect of BMP-2 or PDGF-BB incorporated into a Col/Col-Mg-HAp scaffold in an *in vivo* semi-orthotopic mouse model for the early phases of tissue repair. Finally, the effect of BMP-2 incorporated into a Col/Col-Mg-HAp scaffold was investigated in both weight-bearing and non-weight-bearing locations of the knee joint in an established preclinical caprine osteochondral defect model.

2. MATERIALS AND METHODS

2.1 Scaffold fabrication and characterization

Col/Col-Mg-HAp scaffold is a biomimetic scaffold that has a porous, 3-Dimensional, composite structure. The scaffold is composed of two layers: the cartilaginous layer, consisting of Type I collagen, to maintain joint congruence and the bone layer consisting of a combination of Type I collagen (60%) and magnesium-hydroxyapatite (40%). Each layer of the scaffold is synthesised separately by a standardised process from an atelocollagen aqueous solution (1% w/w) in acetic acid, isolated from equine tendon. The upper non-mineralised chondral layer of the scaffold is obtained by dissolving an acetic solution of Type I collagen in bi-distilled water by adding NaOH. The bone layer of the scaffold is obtained by nucleating nanostructured hydroxyapatite into self-assembling collagen fibers, as occurs in the natural biological neo-ossification process. To stabilise the scaffold, the fibrous structures were chemically cross-linked for 16hrs at room temperature. After chemical cross-linking, the two layers were superimposed and afterwards they are freeze-dried.

The morphology of the scaffold was evaluated by Scanning Electron Microscopy (SEM) performed on a SEM-LEO 438 VP (Carl Zeiss AG, Oberkochen, Germany). The samples were sputter coated with gold prior to examination. The mineral content of the bone layer was evaluated by thermogravimetric analysis (TGA), performed in alumina crucibles in an air atmosphere with a flow rate of 80 ml/min, between 25 and 700 °C (Mettler Toledo DT-TGA/DSC1 Star System, Columbus, OH, USA). The elemental composition of the mineral phase (Magnesium-Hydroxyapatite) was determined using inductively coupled plasma-optical emission spectrometry (ICP-OES, Thermo Scientific iCAP 7400, Waltham, MA, USA). In particular, the composition is expressed as Ca/P, (Ca+Mg)/P, Mg/Ca% molar ratios. The bone layer was dissolved in hot nitric acid (65 v/v%) in order to completely destroy the collagen matrix and solubilise the inorganic phase. The content (ppm) of magnesium, calcium and phosphorous in the samples is determined by comparison with a predetermined standard curve: Ca/P = $1.5 \pm 0.1\%$; (Ca+Mg)/P = $1.6 \pm 0.1\%$; Mg/Ca% = $1.5 \pm 0.4\%$. The total porosity of the osteochondral

scaffold was determined using Archimedes' principle. The exterior volume (V_s) of the sample was measured using a Vernier caliper. The sample was then immersed in a pycnometer containing 96% ethanol solution. The actual volume (V_a) of the sample is calculated using the formula:

$$V_a = \frac{(W_w - W_o) - (W_t - W_p)}{0.789} \text{ g/cm}^3$$

W_w is the weight of the ethanol and the pycnometer, W_o is the dry weight of the pycnometer, W_t is the combined weight of the ethanol, the pycnometer and the plug sample, W_p is the combined weight of the dry pycnometer and dry plug sample, and 0.789 g/cm^3 is the density of ethanol solution. The porosity of the scaffold was then determined using the following formula:

$$\text{Total Porosity}(\%) = \frac{V_s - V_a}{V_s} * 100$$

2.2 BMP-2 and PDGF-BB release from the different layers of a Col/Col-Mg-HAp scaffold

To investigate the release kinetics of BMP-2 and PDGF-BB from the different layers of the Col/Col-Mg-HAp scaffold, a time course study was performed (Figure S1A). 35 μL (28.5 $\mu\text{g/ml}$) BMP-2 or PDGF-BB (Sigma, Saint Louis, USA) was absorbed into the separated layers (either collagen-only layer or Col-Mg-HAp layer) of a Col/Col-Mg-HAp scaffold. (Osteochondral scaffold, Fincermica, Italy) in a low-affinity binding plate at 37 degrees Celsius for 30 minutes. The concentration of growth factors was determined according to our previous studies^{29,30}. After absorption, the medium was harvested from the plate, and the scaffolds were transferred to a new low-affinity binding plate. 800 μL alpha-Minimum Essential Medium (α -MEM, Gibco, Massachusetts, USA) was added to each scaffold-containing well. At each time point (6, 24, 48, 72, 96, 120, 144, 168 hours, 336 hours only for BMP-2), the medium was collected and replaced by fresh medium. The collected medium was analysed for BMP-2 by recombinant human BMP-2 (Peprotech, NJ, USA) or PDGF-BB by recombinant human PDGF-BB DuoSet ELISA kit (R&D Systems, Minneapolis, USA) according to the manufacturer's instructions.

2.3 Cell recruitment capacity of BMP-2 or PDGF-BB in an ex vivo osteochondral defect culture model

To study the effect of BMP-2 and PDGF-BB adsorbed onto a bi-layered Col/Col-Mg-HAp scaffold on cell recruitment capacity, an ex vivo osteochondral defect culture model, previously developed and validated in our laboratory, was used³¹ (Figure S1B). Briefly, osteochondral defects were created in bovine osteochondral biopsies (8 mm diameter, 5 mm height) harvested from metacarpal-phalangeal joints of 6 to 8 months

old calves (LifeTec, Eindhoven, The Netherlands), in which a 4 mm wide and 4 mm high defect was created. The osteochondral plugs were kept overnight in Dulbecco's Modified Eagle Medium-high glucose (DMEM, 4.5 g/L glucose, Gibco, Massachusetts, USA) supplemented with 10% fetal bovine serum (FBS, Gibco, Massachusetts, USA), 50 µg/mL gentamycin (Gibco, Massachusetts, USA), and 1.5 µg/mL fungizone (Gibco, Massachusetts, USA). The following day, the Col/Col-Mg-HAp scaffolds (diameter: 4 mm, height: 4 mm) with or without adsorbed growth factors (n=4 for each condition) were inserted into the osteochondral defects. Either 4 µg (57.1 µg/mL) BMP-2 solution or 100 ng (1.4 µg/mL) PDGF-BB was adsorbed onto the scaffold. Each construct was cultured in 3.5 mL medium in a new 12-well plate at 37 °C and 5% CO₂. The medium was refreshed on the first day and subsequently every two days. After 3 weeks, the osteochondral constructs were harvested and fixed in 4% formalin for 1 week with subsequent further histological analysis.

2.4 *In vivo* osteochondral defect model in mice

To assess the effect of BMP-2 and PDGF-BB in the Col/Col-Mg-HAp scaffolds on bone repair, an established *in vivo* subcutaneous mouse model developed previously in our laboratory was used (Figure S1C) ³². Osteochondral biopsies were harvested, and the defects were created as described earlier (see under 2.3) and kept overnight in α -MEM medium supplemented with 10% FBS, 50 µg/mL gentamycin, and 1.5 µg/mL fungizone until implantation. 11 12-week-old NMRI-Fox1nu mice (Taconic, New York, USA) were used for this study. The animals were randomly assigned and housed under specific-pathogen-free conditions with a regular day/night light cycle and allowed to adapt to the conditions of the animal facility for 7 days. Food and water were available *ad libitum*. Before implantation, 70 µL of saline, BMP-2 (57.1 µg/mL, 4 µg), or PDGF-BB (28.5 µg/mL, 2 µg or 1.4 µg/mL, 100 ng) solution was added dropwise onto the Col/Col-Mg-HAp scaffolds. All osteochondral plugs were covered with a circular 8-mm Neuro-Patch membrane (Braun, Melsungen, Germany) to prevent the ingrowth of host cells from the top. The osteochondral plugs were randomly implanted in subcutaneous pockets on the back of the mice under 2.5-3% isoflurane anaesthesia (1000 mg/g, Laboratorios Karizoo, Maharashtra, India). One osteochondral plug was implanted per pocket, and four osteochondral plugs were implanted per mouse. The incisions were closed with staples (Fine Science Tools, Vancouver, Canada). 1 h before surgery and 6-8 h after surgery, 0.05 mg/kg body weight of buprenorphine (Chr. Olesen & Co, Copenhagen, Denmark) was injected subcutaneously to ensure pre- and postoperative analgesia. Mice received a subcutaneous prophylactic antibiotic injection of 25 mg/kg body weight of Amoxicillin (Dopharma, Raamsdonksveer, Netherlands).

After 4 or 8 weeks, mice were euthanised by cervical dislocation under 2.5-3% isoflurane anaesthesia, and the osteochondral plugs were harvested. All samples were fixed in 4% formalin for 1 week for further analysis. This animal experiment was approved by the ethics committee for laboratory animal use (AVD101002016991; protocol #EMC 16-691-05).

2.5 *In vivo* osteochondral defect caprine model

A validated bilateral osteochondral defect caprine model was used to assess the osteochondral defect repair capacity of BMP-2 supplemented scaffolds in a preclinical large animal model (Figure S1D). An experimental unit of 11 skeletally mature female Saanen goats (age: 3 years, weight: 37.9 ± 7.3 kg) was subjected to a bilateral arthrotomy under general anaesthesia as described before³³⁻³⁵. In short: all animals received a prophylactic antibiotic injection with amoxycillin clavulanic acid 8.75mg/kg intramuscular (Noroclav, Norbrook, Ireland) and were intravenously sedated with butorphanol (0.2 mg/kg, Butador, Chanelle Pharma, Ireland) and diazepam (0.2 mg/kg, Diazemuls; Accord Healthcare, UK). A lumbosacral epidural block with lidocaine (2 mg/kg, Lidocaine HCl 2%, B.Braun Medical Inc., EU) and morphine (0.2 mg/kg, Morphine Sulphate 10mg/ml, Kalceks, Latvia) was performed with the animal in sternal recumbency. Anaesthesia was induced with propofol IV to effect (max. 6 mg/kg, Propofol-Lipuro 1%, B. Braun Medical Inc., EU) and was maintained with isoflurane (Vetflurane, Virbac Animal Health, UK) in 100% oxygen via a circle rebreathing system. All animals received analgesia with meloxicam IV (0.5 mg/kg, Rheumocam, Chanelle, Ireland); and morphine IV (0.2 mg/kg, Morphine sulphate, Mercury Pharmaceuticals, Ireland) 90 min after the epidural block.

An arthrotomy of each stifle joint was performed in dorsal recumbency using a lateral parapatellar approach. Under constant irrigation with saline, a pointed 6 mm drill bit was used to drill an approximate 3-4 mm deep non-weight-bearing defect in the transition of the distal 1/3 to the middle 1/3 of the trochlear groove and in the weight-bearing part of the medial femoral condyle. Subsequently, a custom-made flattened drill bit and a depth guide were used to create an exact flat 6 mm deep by 6 mm wide circular critical-sized osteochondral defect in a non-weight-bearing and a weight-bearing location. The joint was flushed with saline to remove any debris, and the defects were press fit with a similar-sized selected scaffold before surgical closure as described before. Each stifle joint was randomly assigned to one of the two treatment groups (Figure S1D): 1) Col/Col-Mg-HAp scaffold-only (6 mm diameter, 6 mm height, Osteochondral scaffold, Finceramica, Italy), and 2) Col/Col-Mg-HAp scaffold adsorbed with BMP-2 (57.1 µg/mL).

Following surgery, postoperative analgesia was provided (meloxicam 5 days) and goats were housed in indoor pens for daily postoperative welfare monitoring and scoring. Two weeks postoperatively, following the removal of skin sutures, animals were released to pasture or loose housing (weather dependent) for the remainder of the study period with daily health checks. An orthopedic assessment (Table S1) was performed on the day of humane euthanasia under sedation with a barbiturate overdose at the predetermined endpoint 6 months after surgery. Subsequently, all the joints, surrounding joint tissues, and synovial fluids were scored (Table S2), dissected, and photographed (Body Canon EOS R5, lens: Canon EF 100mm f/2.8L Macro IS USM, flash: Macro Ring lite MR-14EX II). Biopsies 1 cm by 1 cm square containing the entire defects were harvested with an oscillating saw.

Ethical evaluation and approval were provided by the Health Products Regulatory Authority of Ireland (AE1898217/P032), The Animal Research Ethics Committee of University College Dublin (AREC-P-12-71) and the Lyons Animal Welfare Board (Health, Husbandry and Monitoring plans).

2.6 Macroscopic assessment of the defect repair in caprine model

The quality of the cartilage repair in the caprine samples was assessed semi-quantitatively using the International Cartilage Repair Society (ICRS) macroscopic evaluation system (Table S3) and a macroscopic scoring system (Table S4) developed by Goebel et al.³⁶. The ICRS scoring system evaluates the macroscopic appearance of cartilage repair tissue as Grade IV (severely abnormal), Grade III (abnormal), Grade II (nearly normal) or Grade I (normal). The Goebel Score describes macroscopic articular cartilage repair with five major evaluation categories. The quality of defect repair was scored on fresh samples by two independent assessors, and the scores were averaged for further analysis. All the samples were fixed in 4% formalin for 10 days after macroscopic assessment for further analysis.

2.7 Micro-computed tomography

From the mouse model, the retrieved bovine osteochondral plugs were scanned (Quantum GX, Perkin Elmer, USA) with the following settings after fixation in 4% formalin: energy 90 KV, intensity 88 μ A, 18 mm FOV, 36 μ m isotropic voxel size. All the scans above were under an X-ray filter of Cu (thickness = 0.06 mm) and Al (thickness = 0.5 mm) and were calibrated using a phantom with a known density of 0.75 g/cm³, which was additionally scanned before and after each scan. A high-resolution mode was set, and a scan time of 4 minutes was used.

The caprine samples were scanned with the same settings except for 36 mm FOV, 72 μm isotropic voxel size. Image processing included modest Gauss filtering ($\sigma=0.8$ voxel, width=1 voxel) and segmentation using a single threshold. A cylindrical region (4 mm diameter and 5 mm height) within the original defect (6 mm diameter and 6 mm height) was selected as a volume of interest (VOI) for the caprine samples. In this VOI the following morphometric parameters were measured: bone volume per total volume (BV/TV), trabecular thickness (Tb.Th), trabecular number (Tb.N), and trabecular separation (Tb.Sp). Morphological analyses were performed using IPL (Scanco Medical AG, Bruettisellen, Switzerland).

2.8 Histology and immunohistochemistry

The bovine osteochondral plugs cultured *ex vivo* were decalcified for 2 weeks using 10% formic acid (Sigma, Saint Louis, USA). After micro-CT scanning, the bovine osteochondral plugs harvested from mice were decalcified using 10% ethylenediaminetetraacetic acid (EDTA, Sigma, Saint Louis, USA) for 4 weeks. The caprine samples were decalcified for 3 weeks using 10% formic acid. Subsequently, all samples were embedded in paraffin and sectioned at 6 μm . Following dewaxing, H&E staining was performed with Hematoxylin (Sigma, Saint Louis, USA) and Eosin Y (Merck, Kenilworth, USA) to study general cell and tissue morphology. To visualise glycosaminoglycans in the extracellular matrix (ECM), dewaxed sections were stained with Safranin O (Fluka, Buchs, Switzerland) and Light green (Fluka, Buchs, Switzerland). To study the regenerated tissue type in the osteochondral defects, RGB staining was performed (Proteoglycans/hyaline cartilage appears blue, mineralised cartilage matrix appears pink/greenish, collagen fibers/uncalcified bone appears red, and mineralised bone appears green) using Alcian Blue (Sigma, Saint Louis, USA), Fast Green (Sigma, Saint Louis, USA), and Picrosirius Red (Sigma, Saint Louis, USA)³⁷. The cell number in the scaffolds was counted under microscopy. NDP View2 software (version 2.8.24, 2020 Hamamatsu Photonics K.K.) was used to measure the tissue volume in the defect at three sections that were taken at the middle, 0.5 mm and 1 mm further away for bovine samples or at the middle for caprine samples (Figure S2). The percentage of the defect covered with newly formed osteochondral tissue (100% indicated that the defect was fully filled with newly formed tissue) was calculated (Figure S3). All slides were independently scored by two investigators blinded to the experimental condition. The measurements of the two investigators were averaged for each section.

To investigate the presentation of neutrophils in the defect, immunohistochemistry for myeloperoxidase (MPO) was performed on retrieved bovine osteochondral samples from the mouse study. After dewaxing, antigen retrieval was performed by placing the

slides with Tris/EDTA (pH9) in a water bath at 95 °C for 20 minutes. Then the slides were pre-incubated with 10% normal rabbit serum (NRS, Invitrogen, Massachusetts, USA) in PBS containing 1% bovine serum albumin (BSA, Sigma, Saint Louis, USA) and 1% milk powder (ELK, Campina, Amersfoort, Netherlands). The slides were incubated by the first antibody against MPO (Thermo Scientific, Massachusetts, USA, 1:200 dilution) or rabbit IgG antibody (DakoCytomation, California, USA, 1:10000 dilution) as the negative control in PBS containing 1% BSA for 1 hour. Next, the slides were incubated by biotinylated goat- α -rabbit (Biogenex, California, USA, 1:50 dilution in PBS containing 1% BSA and 5% mouse serum of total volume) for 30 min. Then, the reaction was amplified by streptavidin-labeled alkaline-phosphatase (Biogenex, California, USA) diluted 1:50 in PBS containing 1% BSA and visualized by subsequent incubation of Neu Fuchsin substrate. Slides were counterstained with Hematoxylin.

To evaluate the infiltration of macrophages in the defect, immunohistochemistry for F4/80 was performed on bovine osteochondral plugs retrieved from the *in vivo* mouse study. For antigen retrieval, each dewaxed slide was treated with 300 μ L proteinase K (20 μ g/ml, Thermo Scientific, Massachusetts, USA) solution and incubated at 37 °C for 30 min. Then the slides were pre-incubated with 10% NRS in PBS containing 1% BSA and 1% milk powder. The following steps were similar to the immunohistochemistry for F4/80, with the first antibody against F4/80 (eBioscience, San Diego, USA, 1 μ g/ml) or rat IgG2a (eBioscience, San Diego, USA, 1 μ g/ml) as the negative control in PBS containing 1% BSA; the second antibody: biotinylated rabbit-anti-rat IgG (6 μ g/ml in PBS containing 1% BSA and 5% mouse serum of total volume), and third antibody: streptavidin-labeled alkaline-phosphatase (Biogenex, California, USA) diluted 1:50 in PBS containing 1% BSA. To distinguish between pro-inflammatory (M1) and anti-inflammatory/tissue-repair (M2) macrophages, immunohistochemistry for inducible Nitric Oxide Synthase (iNOS, as an indicator for pro-inflammatory M1 macrophages) was performed. The steps were similar to the immunohistochemistry for MPO, with the first antibody against iNOS (2 μ g/ml, Abcam, Cambridge, UK).

The slides were ranked according to the positive degree of immunohistochemical staining, and all negatively stained sections were ranked 0. Only areas that were also stained for F4/80 were taken into account when the iNOS staining was ranked.

2.9 Statistical analysis

All statistical tests were performed using SPSS software 28.0 (SPSS inc., Chicago, USA). The repair tissue volume was expressed as mean \pm standard deviation (SD). The rankings of immunohistochemical MPO, F4/80, and iNOS staining were presented as column plots in graphs. Multiple comparisons between scaffold-only, BMP-2 and PDGF

groups in bovine osteochondral plug samples were analysed by a Kruskal-Wallis test. Statistically significant differences between scaffold-only and scaffold+BMP-2 groups, or between trochlear groove and femoral condyle groups, in caprine samples were determined by a Mann-Whitney U test. A P value ≤ 0.05 was considered statistically significant.

3. RESULTS

3.1 Scaffold characterization

SEM images show the detailed morphology of the cartilaginous layer (collagen, **Figure 1A**) and the bone layer (60% collagen and 40% magnesium-hydroxyapatite, **Figure 1B**) of the scaffolds. The ratio between collagen and magnesium-hydroxyapatite is 69/31 w/w%. The mineral phase is composed of non-stoichiometric, calcium deficient, Magnesium-substituted hydroxyapatite. The total porosity of the osteochondral scaffold was $83 \pm 1\%$.

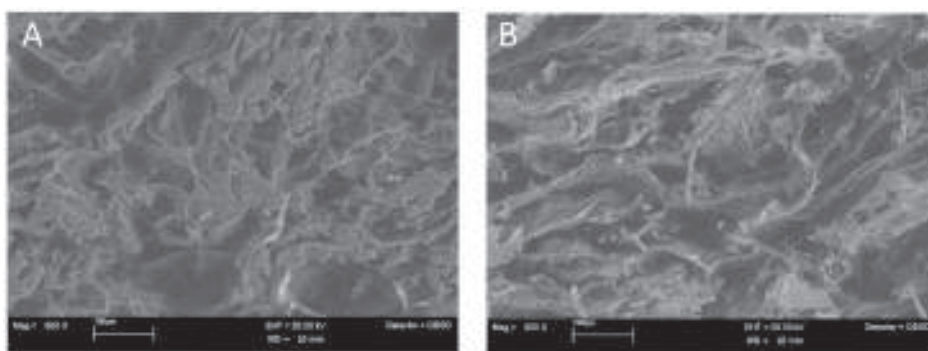


Figure 1. SEM images of (A) the cartilaginous layer (collagen) and (B) the bone layer (60% collagen and 40% magnesium-hydroxyapatite).

3.2 The release profiles of BMP-2 and PDGF-BB *in vitro*

0.6% of the added BMP-2 was detected in the medium after adsorption for the collagen-only layer and 3.0% for the Col-Mg-HAp layer, indicating that most BMP-2 was indeed adsorbed, and both layers had a similar adsorption capacity at the tested volume. Over 14 days, only 48.8 ± 14.8 ng and 22.1 ± 3.4 ng of adsorbed BMP-2 was released from collagen-only layers or Col-Mg-HAp layers, respectively (**Figure 2A**). BMP-2 was largely retained within the scaffolds. A similar release pattern was observed for both layers, although the collagen-only layer released (2-fold) more over the 14 days period (**Figure 2A**).

Of the added PDGF-BB, 3.9% was detected in the medium after adsorption for the collagen-only layer and 5.9% for the Col-Mg-HAp layer, indicating most was adsorbed and both layers and a similar adsorption capacity. In contrast to BMP-2, a rapid release of PDGF-BB from the collagen-only layer was observed, and 600.4 ± 273.6 ng was released within 6 hours (Figure 2B). Interestingly, almost no release was observed from the Col-Mg-HAp layer; Only 33.8 ± 11.8 ng PDGF-BB cumulatively released from the Col-Mg-HAp layer over 7 days.

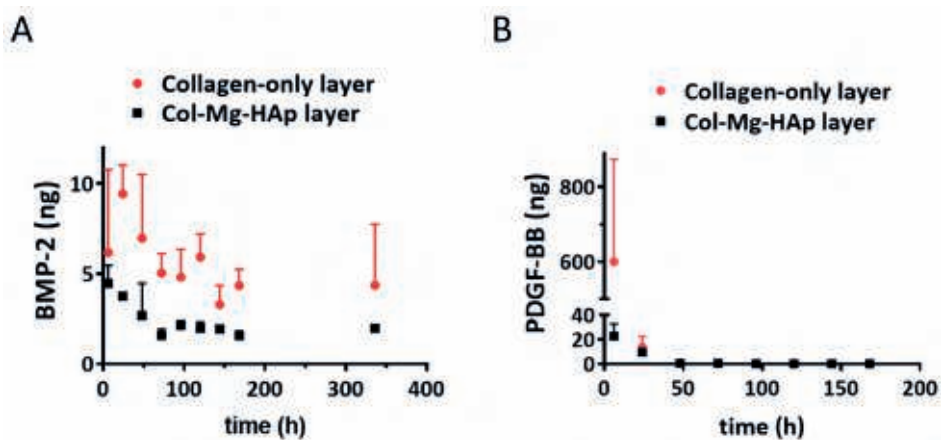


Figure 2. Bone morphogenetic protein 2 (BMP-2) and Platelet-derived growth factor-BB (PDGF-BB) released from the different layers of the Col/Col-Mg-HAp scaffold.

(A) *In vitro* release of BMP-2 from the different layers of Col/Col-Mg-HAp scaffold over a 14-day period. (B) *In vitro* release of PDGF-BB from the different layers of the Col/Col-Mg-HAp scaffold over a 7-day period. The release of BMP-2 and PDGF-BB is presented as the released dose at each time point. Data points indicate the mean \pm SD of 3 samples per time point.

3.3 Effect of BMP-2 and PDGF-BB on cell ingrowth in an *ex vivo* culture model

To evaluate the effect of BMP-2 or PDGF-BB addition onto the scaffold on cell recruitment from adjacent osteochondral tissues, an *ex vivo* model was used. After 3 weeks, the scaffolds filled the osteochondral defects, and cells infiltrated the scaffolds. In the scaffold without growth factors, cells were mostly located at the periphery of the scaffold (Figure 3A). Interestingly, when BMP-2 or PDGF-BB were added, cell infiltration was also observed in the center, particularly in the collagen-only layer (Figure 3A). Almost no cells were found in the Col-Mg-HAp layer. Overall, the addition of growth factors significantly increased cell infiltration into the scaffolds (Figure 3B).

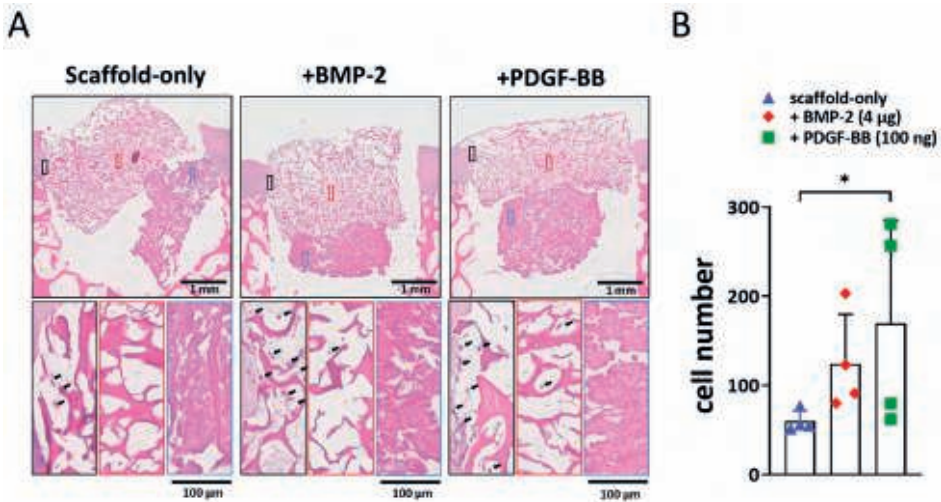


Figure 3. Adsorption of BMP-2 or PDGF-BB might improve the cell recruitment property *ex vivo*.

(A) Representative images of the 3-week constructs stained with H&E. Scale bars indicate 1 mm and 100 μm, respectively. Magnified images showed cell infiltration at the periphery (black square), in the center (red square) of the collagen-only layer, and in the Col-Mg-HAp layer (blue square) of the scaffold. Black arrows indicate infiltrated cells. (B) The number of cells infiltrated into the scaffolds. Each bar indicates the mean ± SD of 4 samples per condition. * $P < 0.05$ analysed by a Kruskal-Wallis test.

3.4 Effect of BMP-2 and PDGF-BB at the early phases of bone repair in an *in vivo* semi-orthotopic osteochondral defect model in mice

One dose of BMP-2 (4 μg) and two doses of PDGF-BB (100 ng and 2 μg) were tested in order to investigate their potential effect on the early stages of bone repair. After 4 weeks, neither cartilage nor bone formation were observed in any of the samples with scaffold-only (**Figure 4A**). When BMP-2 or PDGF-BB was adsorbed into the scaffold, cartilage-like tissue was found in 1 out of 4 samples with 100 ng PDGF-BB, 2 out of 4 samples with 2 μg PDGF-BB and 2 out of 4 samples with 4 μg BMP-2 (**Figure 4B**). Interestingly, the scaffolds adsorbed with either 4 μg BMP-2 or 2 μg PDGF-BB showed less MPO (as an indicator for neutrophils) and iNOS (as an indicator for pro-inflammatory macrophages) staining, albeit this did not reach statistical significance due to the relatively low sample size (**Figure S4**).

The effect of 4 μg BMP-2, 2 μg PDGF-BB or the combination of the two were further investigated in the semi-orthotopic mouse model after 8 weeks. Inflammation was largely resolved in all samples. Immunohistochemical staining for MPO and iNOS was negative in all but one defect that was from the scaffold-only group. No difference was found between the different groups. All the defects were filled with bone tissue and

blood vessels were observed, independent of the presence of growth factors (Figure 4C). Overall, there was slightly more tissue repair in BMP-2-adsorbed scaffolds ($78.9 \pm 23.1\%$ of the defect filled) compared to PDGF-BB-adsorbed scaffolds ($50.9 \pm 28.0\%$) or scaffold-only ($68.8 \pm 36.2\%$) (Figure 4D). Partially repaired bone defects were found in 5 out of 7 defects fitted with PDGF-BB-adsorbed scaffolds, while only in 3 out of 7 in the scaffold-only group and 2 out of 7 in the group of BMP-2 adsorbed scaffolds.

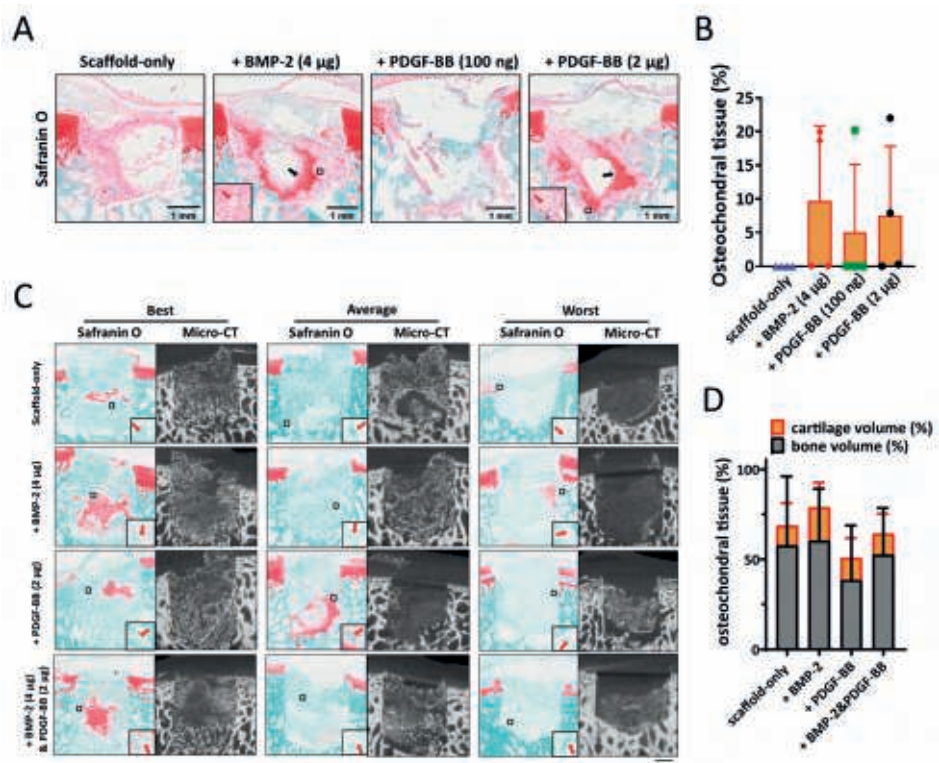


Figure 4. The effect of BMP-2 or PDGF-BB adsorption onto Col/Col-Mg-HAP scaffolds on osteochondral defect repair in a semi-orthotopic model *in vivo*. (A) Representative images of the 4-week repair constructs stained with safranin-O. Scale bars indicate 1 mm. Black arrows indicate cartilage-like tissue. Red arrows indicate blood vessels. (B) The percentage of the defect filled with osteochondral tissue (%) in the osteochondral defects at 4 weeks. (C) Representative images of the 8-week repair constructs stained with safranin-O, and the 8-week CT images. The best, average and worst repaired samples are presented based on osteochondral tissue volume (%). Scale bars indicate 1 mm. Red arrows indicate blood vessels. (D) The percentage of the defect filled with osteochondral tissue (%) in the osteochondral defects at 8 weeks. Scale bars indicate 1 mm.

3.5 Effect of BMP-2 on bone repair in an *in vivo* caprine model

3.5.1 Scaffold implantation and clinical observations

Most osteochondral tissue was regenerated in the osteochondral defects when 4 µg BMP-2 was adsorbed to the Col/Col-Mg-HAP scaffold in the mouse model. Therefore, BMP-2 was selected to be further investigated in an established bilateral preclinical caprine osteochondral defect model. Two differently loaded locations were selected in this caprine model: a weight-bearing region of the medial femoral condyle and a non-weight-bearing area in the trochlear groove. During surgery, scaffolds were successfully press fit into osteochondral defects flush with the surrounding cartilage. All defects bled after drilling and scaffolds became saturated with fresh blood upon implantation, as observed by a change in colour of the implanted scaffold.

Recovery was uneventful and no postoperative complications occurred except for the unforeseen death of one animal 3 days post-surgery due to ruminal acidosis caused by overeating of concentrates, unrelated to the experimental procedure. Macroscopic appearance after 3 days in the unforeseen dead animal showed that scaffolds were stable in the osteochondral defects (**Figure S5A**). The two layers of the scaffold were clearly visible in the defects (**Figure S5B**).

Clinical examination of animals daily for 14 days post-surgery and weekly until the endpoint at 6 months demonstrated excellent recovery from surgery and a normal pain-free range of movement and normal locomotion from 3-10 days post-surgery. After 6 months, there were no signs of inflammation or cartilage abnormalities found during post-mortem evaluation of the joints. No signs of joint swelling, effusion, abnormal mobility, synovial adhesions, synovial fluid and membrane abnormalities, abnormal wound healing, patellar luxation, erosions or lesions on the opposite cartilage surface were found in any of the animals.

3.5.2 Tissue repair in the non-weight-bearing trochlear groove osteochondral defects

To quantify the subchondral bone formation within the bone defect, micro-CT analysis was performed. Well-repaired subchondral bone was observed in the images of the trochlear groove treated with both the scaffold-only and BMP-2-adsorbed scaffold at 6 months (**Figure 5A**). A slightly higher Tb.N was found in the defects with BMP-2-adsorbed scaffolds. No significant differences in the BV/TV, Tb.Th, Tb.N and Tb.Sp were found between the groups (**Figure 5B**).

Macroscopical and histological evaluation of the cross sections of the defect supported the micro-CT quantification (**Figure 5C**). Overall, the scaffolds were completely

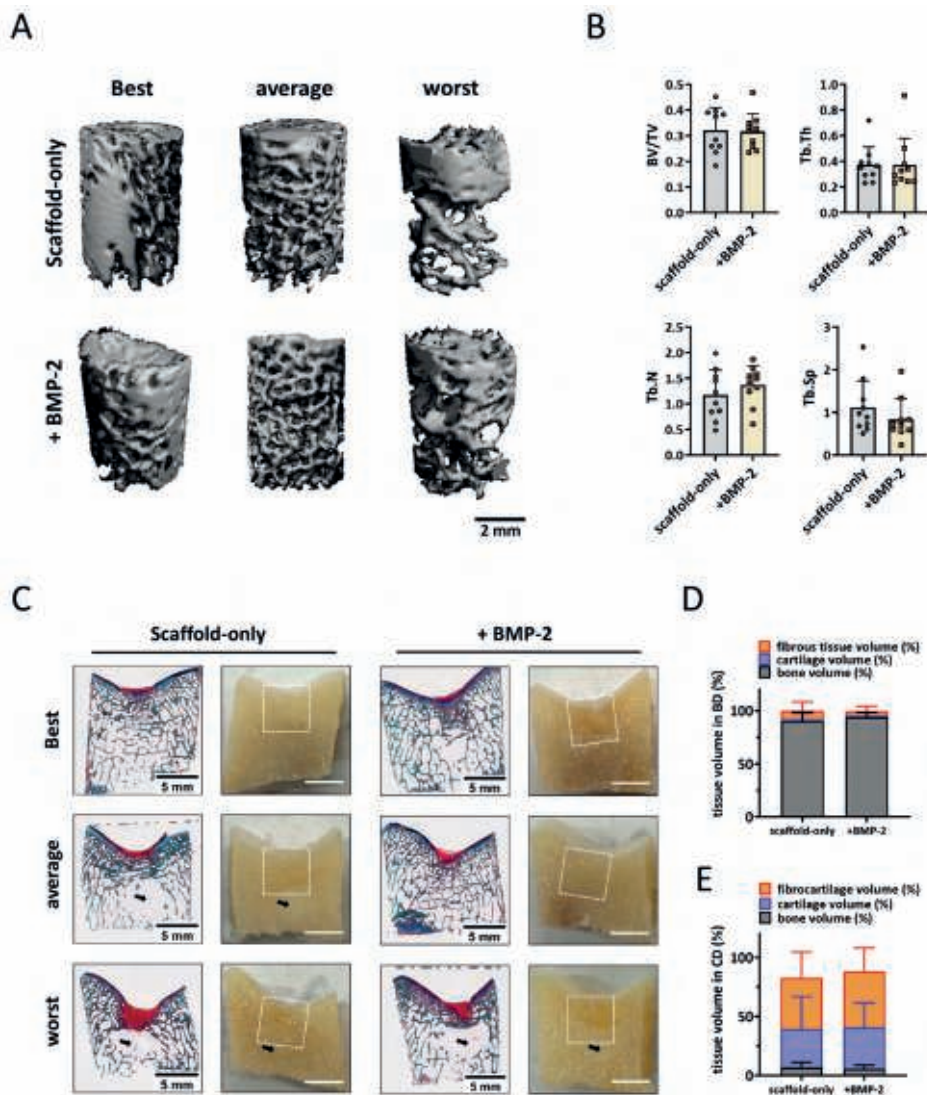


Figure 5. Tissue repair in non-weight-bearing trochlear groove defects.

(A) Representative Micro-CT reconstructions treated with either scaffold-only or scaffold adsorbed with BMP-2. The best, average and worst repaired samples are presented based on BV/TV. The scale bar indicates 2 mm. (B) BV/TV, trabecular thickness (Tb.Th [mm]), trabecular number (Tb.N [1/mm]), and trabecular separation (Tb.Sp [mm]) in the bone defects after 6 months. (C) RGB (Alcian Blue, Fast Green, and Picrosirius Red) staining and macroscopic cross-sectional view of osteochondral defects treated with either scaffold-only or scaffold adsorbed with BMP-2. The best, average and worst repaired samples are presented. White squares indicate 6*6 mm osteochondral defects. Black arrows indicate the structure with only bone marrow. The scale bar indicates 5 mm. (D) The percentage of tissue volume calculated in the bone defects (BD). (E) The percentage of tissue volume calculated in the cartilage defects (CD).

degraded, and a well-structured subchondral trabecular bone was observed in most bone defects after 6 months (**Figure 5C**). Slightly more bone tissue ($93.9 \pm 4.4\%$ vs. $90.1 \pm 8.4\%$) and less fibrous tissue ($4.0 \pm 4.5\%$ vs. $7.8 \pm 8.4\%$) was found in the bone defects when the scaffolds were adsorbed with BMP-2 compared to the scaffold-only, although no significant difference was reached (**Figure 5D**). Notably, a structure without trabecular bone but with only bone marrow was observed underneath some defects, independent of the condition.

Macroscopically, defects were covered with newly formed cartilage with good integration into the surrounding native tissue. Small, scattered fissures or cracks were observed on the surfaces of some defects, and no noticeable depressions were observed (**Figure S6A**). The ICRS and Goebel scores for the scaffold-only group had a median score of 11.3 ± 0.5 and 19.0 ± 0.7 , respectively (**Figure S6B**). For the scaffold + BMP-2 group, the macroscopic ICRS and Goebel scores were 11.6 ± 0.6 and 19.3 ± 0.5 , respectively (**Fig. S6B**). All the trochlear groove samples were classified as normal (grade I) or nearly normal (grade II) cartilage. Overall, no significant difference was observed in cartilage repair between scaffold-only and BMP-2-adsorbed scaffold. On histology, $43.2 \pm 22.1\%$ (scaffold-only) and $47.4 \pm 19.8\%$ (scaffold + BMP-2) of the newly formed tissue generated in the cartilage defects was fibrous tissue after 6 months as indicated by predominantly Picrosirius red instead of Alcian blue staining in RGB staining (**Fig. 4E**). And only $32.4 \pm 27.6\%$ (scaffold-only) and $35.2 \pm 20.6\%$ (scaffold + BMP-2) of the repaired tissue in the cartilage region was Alcian blue positive, indicating hyaline cartilage (**Figure 5E**).

3.5.3 Tissue repair in the weight-bearing femoral condyle osteochondral defects

For the femoral condyle, micro-CT analysis was performed in the same manner as for the trochlear groove. In the weight-bearing femoral condyle, well-structured subchondral bone was formed after 6 months in defects treated with the scaffold-only or BMP-2 adsorbed scaffold (**Figure 6A**), no significant difference was found in the BV/TV and Tb.Th parameters (**Figure 6B**). Surprisingly, a slightly lower BV/TV was found in defects with BMP-2-adsorbed scaffolds, indicating relatively worse bone repair when BMP-2 was adsorbed. Significantly less Tb.N (1.1 ± 0.4 vs. 1.5 ± 0.2 , $P=0.019$, **Figure 6B**) and higher Tb.Sp (1.2 ± 0.6 vs. 0.7 ± 0.1 , $P=0.015$, **Figure 5B**) were observed in the femoral condyle bone defects fitted with BMP-2-adsorbed scaffolds, suggesting a relatively courser bone structure when BMP-2 was adsorbed.

Macroscopic and histological evaluation of the cross sections through the defect supported the micro-CT quantification (**Figure 6C**). Newly formed hyaline cartilage-

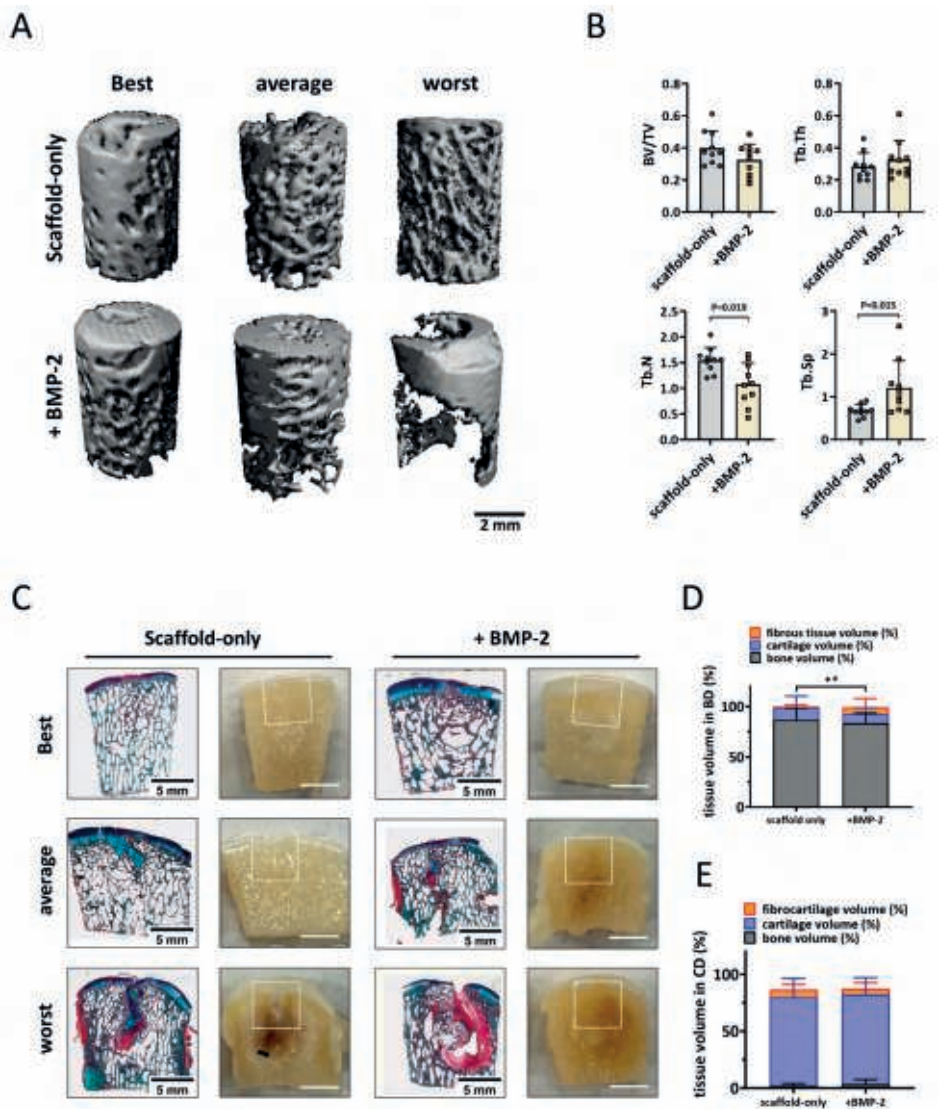


Figure 6. Bone repair in the weight-bearing femoral condyle defects deteriorated with the adsorption of BMP-2 onto the scaffold.

(A) Representative Micro-CT reconstructions treated with either scaffold-only or scaffold adsorbed with BMP-2. The best, average and worst repaired samples are presented based on BV/TV. The scale bar indicates 2 mm. (B) BV/TV, trabecular thickness (Tb.Th [mm]), trabecular number (Tb.N [1/mm]), and trabecular separation (Tb.Sp [mm]) in the bone defects after 6 months. Tissue repair in the femoral condyle defects. (C) RGB (Alcian Blue, Fast Green, and Picrosirius Red) staining and macroscopic images of osteochondral defects treated with either scaffold-only or scaffold adsorbed with BMP-2. The best, average and worst repaired samples are presented. White squares indicate 6*6 mm osteochondral defects. The scale bar indicates 5 mm. (D) The percentage of tissue volume calculated in the bone defects (BD). * $P < 0.05$ in fibrous tissue, # $P < 0.05$ in osteochondral (cartilage-like and bone-like) tissue. (E) The percentage of tissue volume calculated in the cartilage defects (CD).

like tissues were mostly supported by a well-structured subchondral trabecular bone that was well-integrated in the surrounding native bone (**Figure 6C**). Surprisingly, significantly less cartilage and bone tissue were observed in the bone defects fitted with BMP-2-adsorbed scaffolds compared to the bone defects treated with scaffold-only ($92.7 \pm 9.5\%$ vs. $99.1 \pm 1.7\%$, $P=0.043$, **Figure 6D**). In addition, significantly more fibrous tissue was found in the bone defects when BMP-2 was adsorbed onto the Col/Col-Mg-HAp scaffolds ($6.9 \pm 8.4\%$ vs. $1.0 \pm 1.6\%$, $P=0.035$, **Figure 6D**). Some defects demonstrated cyst like areas without trabecular bone below some of the defects. However, marrow-like tissue was found in these areas.

The defects were mostly covered with hyaline cartilage-like tissue with macroscopically good integration with the surrounding native tissue (**Figure S6C**). Small, scattered fissures or cracks were observed on surfaces of some defects, and no noticeable depressions were observed except for one sample treated with Col/Col-Mg-HAp scaffolds-only. The median ICRS score was 10.8 ± 0.5 out of 12, and the median Goebel score 18.9 ± 0.5 out of 20 (**Figure S6D**) when scaffold-only was placed in the defects. The defects with the scaffold + BMP-2 received median ICRS scores of 10.3 ± 1.8 out of 12, and median Goebel scores of 18.5 ± 1.8 out of 20 (**Figure S6D**). All the samples were classified as normal (grade I) or nearly normal (grade II) cartilage except for one sample treated with BMP-2 (grade III). By histological examination, the scaffolds were completely degraded after 6 months, and round cells residing within lacunae were present in the cartilage region. GAG and collagen were present in the repair tissue in the defects demonstrated by RGB staining (**Figure 6C**), indicating cartilaginous tissue formation. In fact, $77.8 \pm 16.5\%$ (scaffold-only) and $78.8 \pm 14.7\%$ (scaffold + BMP-2) of the newly formed tissue was Alcian blue positive, indicating hyaline-like cartilage (**Figure 6E**).

3.5.4 Different tissue repair in the non-weight-bearing trochlear groove and the weight-bearing femoral condyle osteochondral defects

In trochlear groove bone defects, the trabecular number was lower (1.2 ± 0.5 vs. 1.5 ± 0.2 , $P=0.063$) and the trabecular separation was higher (1.1 ± 0.6 vs. 0.7 ± 0.1 , $P=0.052$) compared to the femoral condyle defects when scaffold-only was implanted, although no significant difference was found. Interestingly, when BMP-2 was adsorbed onto the scaffold, an opposite trend was found in Tb.N (1.4 ± 0.4 in trochlear groove and 1.1 ± 0.4 in femoral condyle, $P=0.143$) and Tb.Sp (0.8 ± 0.5 in trochlear groove and 1.2 ± 0.6 in femoral condyle $P=0.105$). In other words, there was 0.2 ± 0.6 higher Tb.N, 0.3 ± 0.9 lower Tb.Sp in the trochlear groove defect and 0.47 ± 0.6 lower Tb.N ($P=0.029$, compared to trochlear groove), 0.5 ± 0.7 higher Tb.Sp ($P=0.063$, compared to trochlear groove) in the femoral condyle defect when BMP-2 was adsorbed onto

the scaffold, indicating that bone repair was improved in trochlear groove defects and reduced in femoral condyle defects when BMP-2 was added. Histological results further confirmed that significantly more bone-like tissue was regenerated in the trochlear groove defects compared to the femoral condyle defects when BMP-2 was added ($93.9 \pm 4.4\%$ vs. $83.5 \pm 9.8\%$, $P=0.011$), while no difference between weight-bearing and non-weight-bearing sites was observed when scaffold-only was implanted ($90.1 \pm 8.4\%$ vs. $86.7 \pm 11.5\%$, $P=0.579$). For cartilage repair, however, significantly less hyaline cartilage-like tissue was observed in the non-weight-bearing trochlear groove compared to the weight-bearing femoral condyle defects with either scaffold-only ($32.4 \pm 27.6\%$ vs. $77.8 \pm 16.5\%$, $P=0.003$) or BMP-2-adsorbed scaffold ($35.2 \pm 20.6\%$ vs. $78.8 \pm 14.7\%$, $P<0.001$).

4. DISCUSSION

In this study, we evaluated the effectiveness of growth factor adsorption onto a bilayer Col/Col-Mg-HAp scaffold in osteochondral defect repair. *In vitro* release results showed that the Col-Mg-HAp (bone) layer retained more growth factor than the collagen-only (cartilage) layer and that BMP-2 was retained much better than PDGF-BB. In an *ex vivo* osteochondral defect model, cell ingrowth into the scaffold was enhanced by BMP-2 and by PDGF-BB. In a semi-orthotopic non-weight-bearing osteochondral defect mouse model representing the early phase (4 weeks) of defect repair *in vivo*, the addition of growth factors resulted in fewer pro-inflammatory cells and better tissue repair, with BMP-2 showing the most favorable results. Therefore BMP-2 addition was taken forward for testing in an established preclinical large animal osteochondral defect model to study scaffold enhancement by BMP-2 under physiological environment with different loading conditions. After 6 months in goats, both the scaffold-only and the BMP-2 adsorbed scaffold induced good osteochondral defect healing. Surprisingly, the addition of BMP-2 led to worse bone repair in the weight-bearing femoral condyle osteochondral defects, whereas this negative effect of BMP-2 was not seen in the non-weight-bearing trochlear groove osteochondral defect location.

Our approach was based on the sequential use of osteochondral defect models: the first experiments were performed in an *ex vivo* bovine osteochondral explant model, followed by a semi-orthotopic non-weight-bearing model where we implanted bovine osteochondral explants subcutaneously in mice. This took into account the effects of the innate immune system and blood vessel invasion. We then selected the most promising condition to be further evaluated in a preclinical caprine osteochondral

defect model, where we tested both weight-bearing and non-weight-bearing repair conditions simultaneously. All models were developed and used previously to evaluate new osteochondral repair approaches^{33,38}. *In vivo* animal models can closely resemble the human osteochondral microenvironment in the context of the presence of immune cells and tissue repair factors. The mouse model allows the screening of four conditions in one animal, whereas the caprine bilateral osteochondral defect model is a fully immune-competent model using outbred animals. That model also allows animal controls (comparing left and right knees), and provides the opportunity to assess tissue regeneration in both weight-bearing and non-weight-bearing locations within the same joint. These animal models offered the opportunity to investigate the possible effect of incorporating growth factors into a Col/Col-Mg-HAp scaffold for osteochondral repair towards translation into the human patient.

Loading can have a significant effect on tissue repair^{39,40}. Not much is known about the interaction between mechanical loading and growth factors and their effect upon osteochondral tissue repair^{41,42}. To study the effect of mechanical stimuli on osteochondral repair during normal ambulation, we used both a non-weight-bearing location (a distal region in the trochlear groove) and a weight-bearing location (a central region on the medial femoral condyle) in the bilateral stifle caprine osteochondral defect model^{43,44}. Better subchondral bone repair was observed in the non-weight-bearing trochlear groove defects than in the weight-bearing femoral condyle defects when BMP-2 was adsorbed onto the scaffold, while no significant difference in repair was found between locations when the scaffold without additions was evaluated. In the non-weight-bearing trochlear groove defects, there was a trend towards more bone-like tissue being generated in the BMP-2-adsorbed scaffolds compared to the scaffold-only. However, this difference did not reach statistical significance, which might be due to the excellent repair capacity of the scaffold-only. The weight-bearing femoral condyle defects implanted with BMP-2-adsorbed scaffolds appeared to have less bone repair and more fibrous tissues in the bone defect compared to the scaffold-only.

Notably, there was no mechanical loading in the semi-orthotopic mouse model and at the 4-week time point, the addition of BMP-2 to the scaffolds seemed beneficial. Our results reveal the interesting hypothesis that, with a specific dose of BMP-2, the beneficial effect of BMP-2 on bone repair is apparent in non-weight-bearing conditions, whilst BMP-2 addition can be detrimental to bone repair in weight-bearing conditions. Although the effect of BMP-2 on osteochondral defect repair in different loading environments is still unknown, the action of BMP-2 on tibia fractures or femoral bone defect healing was demonstrated to be dependent on the mechanical environment *in*

vivo^{45,46}. This might be due to an interaction between BMP-2 and mechanical loading⁴⁷ and related to the dosage used. Compression and loading affect BMP signalling both immediately and in a long-term manner⁴⁸. Mechanical loading was shown to increase BMP-2 expression⁴⁹, and the effect of BMP-2 can be strongly potentiated by mechanical forces⁴⁷. It is possible that the combination of added and locally produced BMP-2 might lead to an overstimulation of BMP-2 signalling, which is shown to cause inflammation, bone resorption and fibrotic tissue formation⁵⁰⁻⁵². No previous study has reported this potential side effect nor the relationship with mechanical loading. However, the mechanical loading patterns in long bone defects with fixation and osteochondral defects with scaffolds in the femoral condyle (especially with the presence of synovial fluid) are quite distinct from one another. Therefore, further studies are needed to elucidate if and at which step of the BMP signalling cascade the pathway is modulated and by which type of mechanical stimuli.

BMP-2 is, to date, the only FDA-approved and commercially available osteoinductive growth factor used in clinics. The function and application of BMP-2 in promoting bone regeneration and bone remodelling has been widely investigated preclinically and clinically⁵³⁻⁵⁵. Mg²⁺ was incorporated in this scaffold, which might up-regulate the bioactivity of BMP-2 upon calcium phosphate cement via enhanced BMP receptor recognition⁵⁶. Previous studies have demonstrated that BMP-2 accelerated the migration of bone marrow mesenchymal stromal cells (MSCs) *in vitro* and *in vivo*^{57,58}. In the presented study, we also observe the promotion of cell ingrowth by BMP-2 addition in our *ex vivo* culture model. Although the primary expected function of BMP-2 in promoting bone repair is to enhance MSC migration to the sites, differentiation into osteoblasts, and enhancing the osteogenic capacity of osteoblasts, BMP-2-induced osteogenesis may also involve an immunoregulatory role^{59,60}. Macrophages act as immune cells and osteoclast precursors, and are involved in multiple stages of bone healing⁶¹. BMP-2 might diminish the expression of pro-inflammatory phenotypic markers and promote the macrophage transition towards a more tissue repair-like phenotype⁶⁰. Neutrophils and M1 macrophages participate in tissue repair as effector cells in inducing inflammation and M2 macrophages are involved in the resolution of inflammation, promoting angiogenesis and matrix remodelling⁶². In our semi-orthotopic model, fewer M1 macrophages, as well as neutrophils, were found in the BMP-2 condition than in the scaffold-only condition after 4 weeks. Therefore, the regulatory effect of BMP-2 in a local osteoimmune environment might be one of the potential mechanisms for promoting bone healing in the early phase.

Although BMP-2 has been clinically applied because of its osteogenic effect, it is still not widely used due to the adverse events associated with implanted supraphysiological

high doses⁵⁵. The most documented side effect is ectopic ossification. Aulin et al. demonstrated that intra-articular injection of a hyaluronan hydrogel containing BMP-2 (150 µg/mL) resulted in excessive ectopic bone formation on the knee joint surface of rabbits (6-7-month-old females)⁶³. In our study, we used 57.1 µg/mL BMP-2 for both 4*4 mm and 6*6 mm cylindrical osteochondral defects according to our previous *in vivo* results²⁹. HAp was reported to have a high affinity for BMP-2 due to the large surface area and functional groups^{28,64}. Three types of functional groups, -OH, -NH₂, and -COO- allow BMP-2 to adsorb on the HAp surface⁶⁴. This is not the case for all growth factors, where, for example, no functional groups or only one might be present. *In vitro*, we demonstrated that BMP-2 was bound and largely retained in both layers, especially in the Col-Mg-HAp layer. In this way, a sustained release was expected, thereby reducing the adverse events of BMP-2. Over longer periods, however, correlations between the *in vitro* and *in vivo* settings become ever more unreliable since the release *in vivo* will be determined by the degradation of the scaffold as well. In fact, no BMP-2-related ectopic ossification or abnormal inflammation was observed in the knee joints of our experimental goats macroscopically or on Micro-CT. Similarly, no ectopic ossification was reported in a publication that investigated the addition of 625 µg/mL of BMP-2 (adsorbed onto Col/HAp scaffolds) in skeletally mature male rabbits²⁸.

Consistent with other studies, we found that PDGF-BB is an effective chemoattractant of cells *ex vivo*^{65,66}. PDGF-BB was rapidly released from the collagen-only layers within 6 hours, most PDGF-BB was retained in the Col-Mg-HAp layers *in vitro*. This might be due to the capacity of HAp in adsorbing a large quantity of proteins and drugs. At the early repair phase in the *in vivo* mouse model, both dosages (1 µg and 100 ng) of PDGF-BB slightly improved tissue formation. Most of the regenerated tissue was in the bone defect area, which might be related to the sustained release from the Col-Mg-HAp layers, which is aimed at the repair of the bone defect specifically. Lee et al. reported that labeled cells migrated towards the osteochondral defect when defects were treated with PDGF-AA or PDGF-BB loaded heparin-conjugated fibrin⁶⁵. Overall, the chemotactic ability of PDGF-BB might be one of the mechanisms in inducing tissue repair in the early phase. However, after 8 weeks, the defects loaded with PDGF-BB generated slightly less osteochondral tissue compared to scaffold-only. A previous study on osteochondral repair also showed that the addition of 1 µg/mL PDGF-BB worsened the cartilage repair in an *in vivo* subcutaneous mouse model, although cell recruitment was enhanced *in vitro*. The short half-life of PDGF might be one of the reasons for the different results between *in vitro* and *in vivo* studies. Zhang et al. demonstrated that PDGF-BB overexpression improved the osteogenic and angiogenic abilities of MSCs in a critical-sized rat calvaria defect model⁶⁷. We also expected the

combination of BMP-2 and PDGF-BB to further improve bone repair, since PDGF was reported to modulate BMP-2-induced osteogenesis in periosteal progenitor cells ⁶⁸. However, no significant improvement was found after 8 weeks in the semi-orthotopic mouse model *in vivo*. Therefore, PDGF-BB and the combination of BMP-2 and PDGF-BB were not further evaluated in our large animal osteochondral defect model. Suboptimal subchondral bone repair of osteochondral defects might lead to damage of the renewed overlying cartilage in the long term ¹⁵⁻¹⁷. In our caprine large animal model, blinded macroscopic evaluation of repaired cartilage tissue indicated the presence of a smooth white cartilaginous layer that was continuous with surrounding naive cartilage, both with control scaffolds and BMP-2 enhanced scaffolds. Histology further confirmed the presence of hyaline cartilage in the superficial layer, with no significant improvement or deterioration observed when BMP-2 was added. This might be due to that tissue repair was assessed at only one, relatively early, 6-month time-point in the caprine model. A longer 12- or 24-month study might be useful to confirm the potential effectiveness of enhanced bone repair on the long-term survival of the neocartilage.

5. CONCLUSIONS

Adsorption of BMP-2 onto a Col/Col-Mg-HAp scaffold reduced bone formation in weight-bearing osteochondral defects, but not in non-weight-bearing osteochondral defects. Since the application of BMP-2 adsorbed to a Col/Col-Mg-HAp scaffold in osteochondral defects did not lead to adverse effects in the joint of goats, and human patients are not allowed full weight-bearing in the first weeks after the osteochondral repair, further investigation taking into consideration dose of BMP-2, timing and location of application for osteochondral defect repair is warranted.

Supplementary Material

Table S1: Clinical Health Assessment.
This tool is to evaluate the overall health of the caprines.

Parameter	Variables	Score
Feeding behavior	Normal	4
	Somewhat less appetite	3
	Clearly reduced appetite	2
	No food intake	1
Clinical signs	Norm peripheral temp, respiratory, no obvious clinical abnormal	4
	Rect T \pm 0.5° C, Cardiac/Respiratory rates increase > 20 %	3
	Rect T \pm 1° C, Cardiac/Respiratory rates increase > 30 %	2
	Rect T \pm 2° C, Cardiac/Respiratory rates increase > 50 %	1
Natural behavior	Normal	4
	Minor changes (such as less responsiveness)	3
	Less mobile and alert, isolated	2
	Restless or still or not raising	1
Total score		12

Table S2: Clinical Orthopedic Assessment.

This tool is to evaluate the clinical health of caprine joints.

Parameter	Variables	Score
Lameness	Walks normally	5
	Slightly lame when walking	4
	Moderately lame when walking	3
	Severely lame when walking	2
	Reluctant to rise and will not walk more than five paces	1
Joint mobility	Full range of motion	5
	Mild limitation (10-20%) in ROM; no crepitus	4
	Mild limitation (10-20%) in ROM; with crepitus	3
	Moderate limitation (20-50%) in ROM; \pm crepitus	2
	Severe limitation (>50%) in ROM; \pm crepitus	1
Pain on knee palpation and movement	None	5
	Mild signs; Caprine turns head in recognition	4
	Moderate signs; Caprine pulls limb away	3
	Severe signs; Caprine vocalises or becomes aggressive	2
	Caprine will not allow palpation	1
Weight-bearing	Equal on all limbs standing and walking	5
	Normal standing; favours affected limb when walking	4
	Partial weight-bearing standing and walking	3
	Part. weight-bearing standing; non-weight-bearing walk	2
	Non-weight-bearing standing and walking	1
Overall score of clinical condition	Not affected	5
	Mildly affected	4
	Moderately affected	3
	Severely affected	2
	Very severely affected	1
Total score		25

Table S3: Macroscopic joint Assessment.

This tool is to evaluate the macroscopic normalization of caprine joints when the joints were opened.

Parameter	Variables	Score
Wound healing abnormal	Yes	0
	No	1
Swelling of joints area	Yes	0
	No	1
Effusion of the joints	Yes	0
	No	1
Patellar luxation	Yes	0
	No	1
Joint mobility abnormal / Contractures	Yes	0
	No	1
Adhesions of whole joint	Yes	0
	No	1
Erosions of whole joint	Yes	0
	No	1
Synovial fluid abnormal	Yes	0
	No	1
Synovial membrane abnormal	Yes	0
	No	1
lesion on the opposite cartilage surface (trochlear groove vs patella)	Yes	0
	No	1
lesion on the opposite cartilage surface (medial femoral condyle vs meniscus/tibia plateau)	Yes	0
	No	1
Total		0-11

Table S4: International Cartilage Repair Society (ICRS) cartilage repair scoring system³⁰.

Parameter	Variables	scores
Degree of defect repair	In level with surrounding cartilage	4
	75% repair of defect depth	3
	50% repair of defect depth	2
	25% repair of defect depth	1
	0% repair of defect depth	0
Integration to border zone	Complete integration with surrounding cartilage	4
	Demarcating border < 1 mm	3
	¾ of graft integrated, ¼ with a notable border > 1 mm	2
	1/2 of graft integrated with surrounding cartilage, 1/2 with a notable border > 1 mm	1
	From no contact to ¼ of graft integrated with surrounding cartilage	0
Macroscopic appearance	Intact smooth surface	4
	Fibrillated surface	3
	Small, scattered fissures or cracks	2
	Several, small or few but large fissures	1
	Total degeneration of grafted area	0
Overall	Grade I normal	12
	Grade II nearly normal	11-8
	Grade III abnormal	7-4
	Grade IV severely abnormal	3-1

Table S5: A semi-quantitative macroscopic scoring system developed by Goebel et al. ³¹

Parameter	Variables	scores
Color of the repair tissue	Hyaline or white	4
	Predominantly white (>50%)	3
	Predominantly translucent (>50%)	2
	Translucent	1
	No repair tissue	0
Presence of blood vessels in the repair tissue	No	4
	Less than 25% of the repair tissue	3
	25-50% of the repair tissue	2
	50-75% of the repair tissue	1
	More than 75% of the repair tissue	0
Degeneration of adjacent articular cartilage	Normal	4
	Cracks and/or fibrillations in integration zone	3
	Diffuse osteoarthritic changes	2
	Extension of defect into the adjacent cartilage	1
	Subchondral bone damage	0
Surface of the repair tissue	Smooth, homogeneous	4
	Smooth, heterogeneous	3
	Fibrillated	2
	Incomplete new repair tissue (rough)	1
	No repair tissue	0
Percentage defect filling	80-100 %	4
	60-80 %	3
	40-60 %	2
	20-40%	1
	0-20 %	0
Total Scores		20

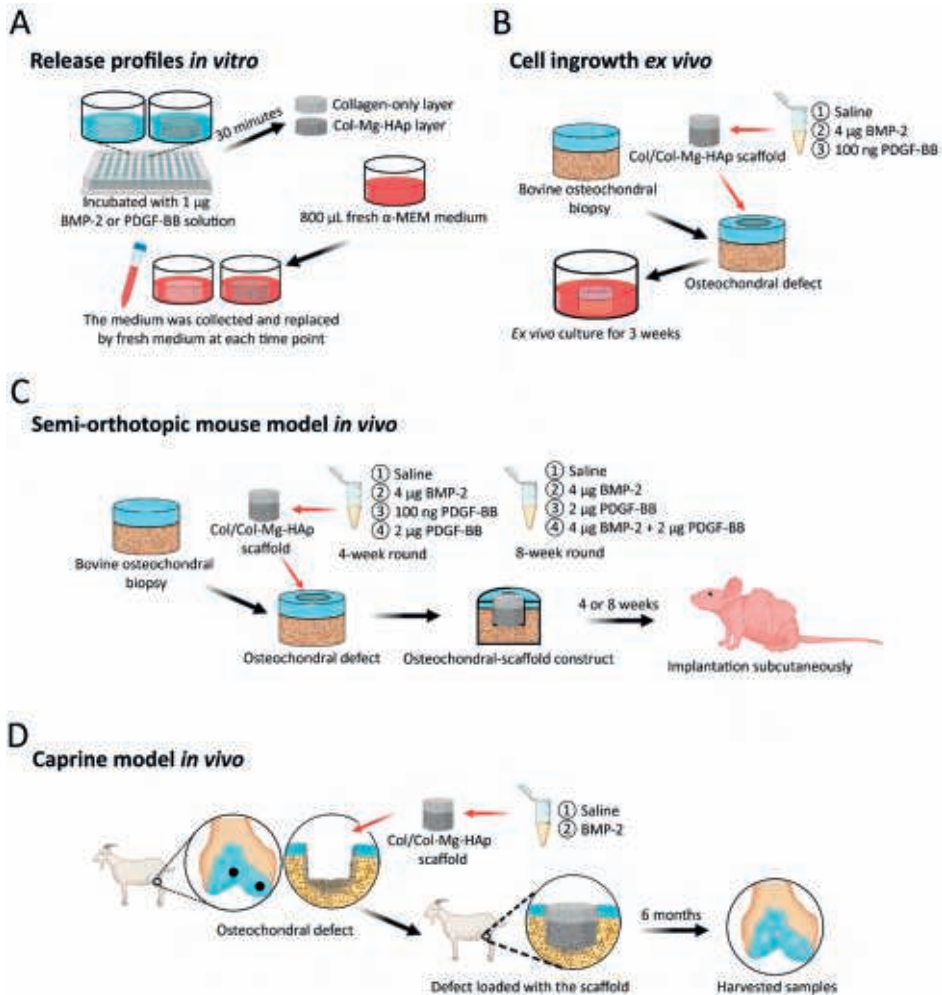


Figure S1. Experiment setup of both *in vitro* and *in vivo* studies

(A) Scheme of the *in vitro* release of BMP-2 and PDGF-BB from the different layers of the Col/Col-Mg-HAP scaffold. (B) Scheme of the *ex vivo* osteochondral defect culture model. (C) Scheme of the *in vivo* osteochondral defect mouse model. (D) Scheme of the *in vivo* osteochondral defect in femoral condyle and trochlear groove defects in caprine model.

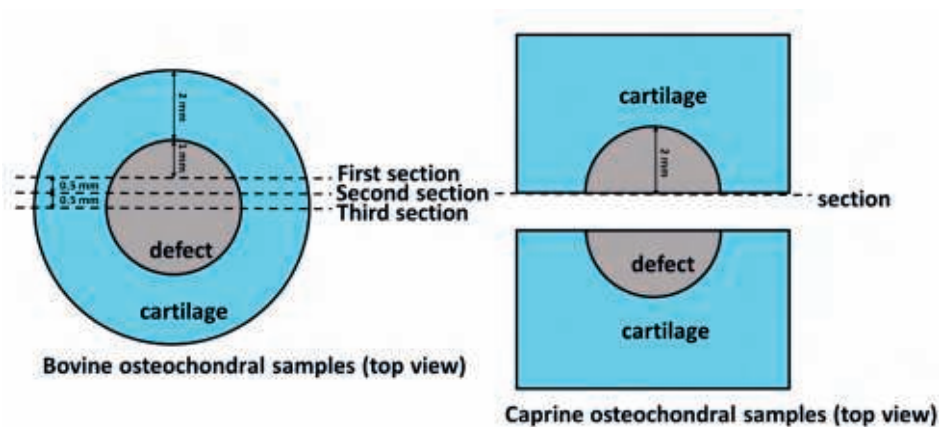


Figure S2. Collection of sections from bovine or caprine samples for histology.

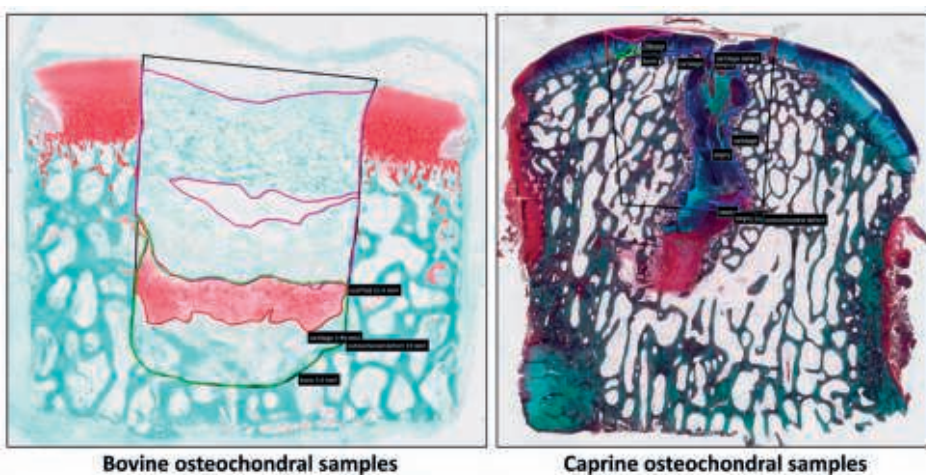


Figure S3. Example on defining the defect region, newly formed cartilage-like tissue formation, bone-like tissue formation, fibrous-like tissue formation, remnants of the scaffold for quantification.

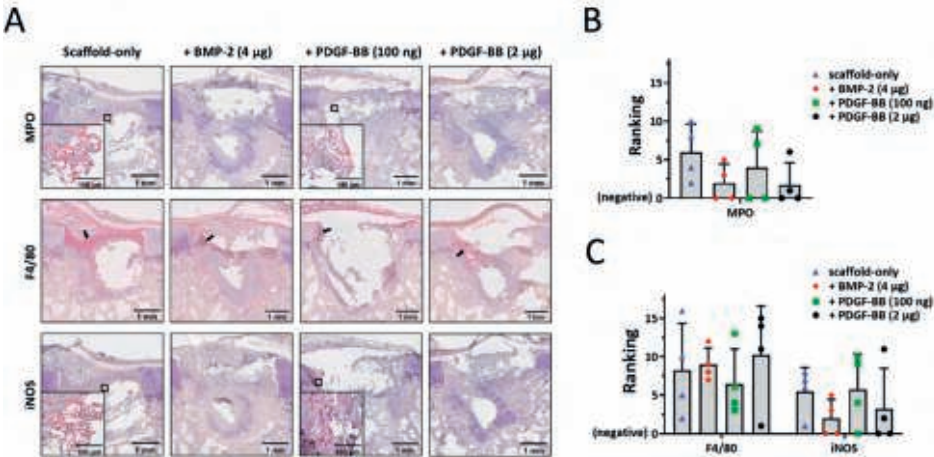


Figure S4. Association between inflammation and tissue repair at the early phase. (A) Representative images of the 4-week repair constructs stained with immunohistochemistry for MPO and iNOS. Scale bars indicate 1 mm and 100 µm respectively. Black arrows indicated positive areas. Ranking of MPO (B), F4/80 and iNOS (C) staining in the 4-week osteochondral defects.

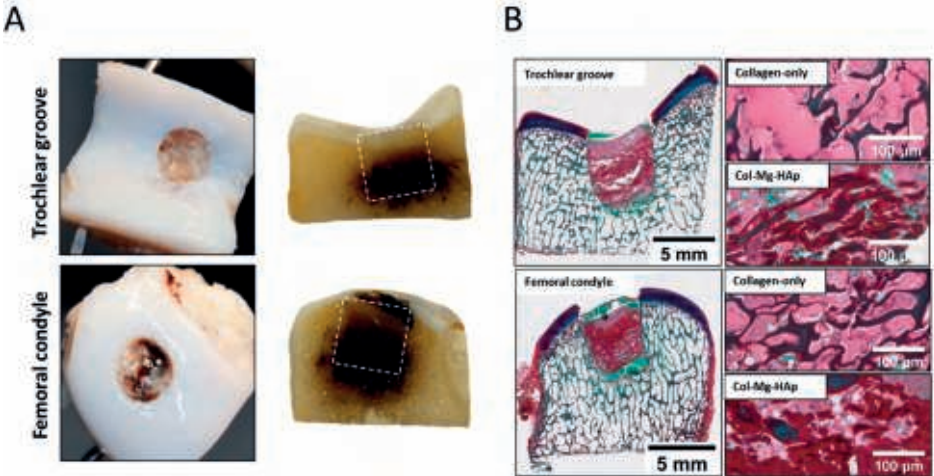


Figure S5. (A) The macroscopic appearance of osteochondral defects 3 days after implantation. The white squares indicated 6*6 mm osteochondral defects. (B) two layers of the scaffold implanted in the femoral condyle defect and trochlear groove defect (stained with Alcian Blue, Fast Green, and Picrosirius Red). The scale bar indicated 5 mm and 100 µm.

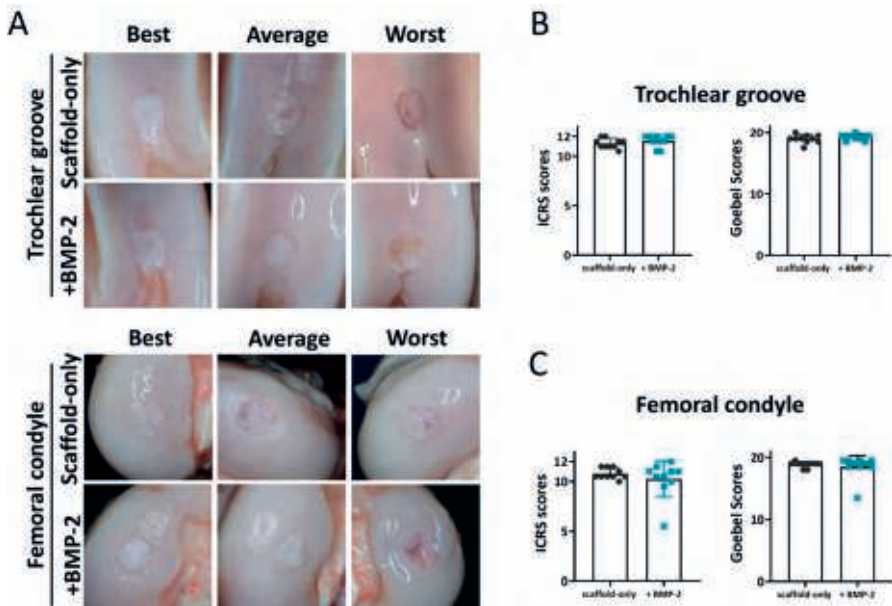


Figure S6. Macroscopic assessment of femoral condyle and trochlear groove defect repair.

(A) representative examples of trochlear groove defect sites treated with scaffold-only or scaffold with BMP-2 after 6 months. Best, average, and worst samples determined according to the ICRS scores, are presented. (B) macroscopic scores (according to ICRS Score and Goebel Score) of repair tissue in the trochlear groove defects. (C) representative examples of femoral condyle defect sites treated with scaffold-only or scaffold with BMP-2 after 6 months. Best, average, and worst samples determined according to the ICRS scores, are presented. (D) macroscopic scores of repair tissue in the femoral condyle defects (according to ICRS score and Goebel Score). The maximum score for ICRS is 12 (indicating the best), and the maximum score for Goebel score is 20 (indicating the best).

REFERENCES

1. Hu, Y.; Chen, X.; Wang, S.; Jing, Y.; Su, J. Subchondral bone microenvironment in osteoarthritis and pain. *Bone Res* **2021**, *9*, 20.
2. Temenoff, J.S.; Mikos, A.G. Review: tissue engineering for regeneration of articular cartilage. *Biomaterials* **2000**, *21*, 431-440, doi:10.1016/s0142-9612(99)00213-6.
3. Mano, J.F.; Reis, R.L. Osteochondral defects: present situation and tissue engineering approaches. *Journal of tissue engineering and regenerative medicine* **2007**, *1*, 261-273, doi:10.1002/term.37.
4. Tamaddon, M.; Gilja, H.; Wang, L.; Oliveira, J.M.; Sun, X.; Tan, R.; Liu, C.; Cl; Mt; Hg; et al. Osteochondral scaffolds for early treatment of cartilage defects in osteoarthritic joints: from bench to clinic. *Biomater Transl* **2020**, *1*, 3-17.
5. Donate, R.; Tamaddon, M.; Ribeiro, V.; Monzón, M.; Oliveira, J.M.; Liu, C. Translation through collaboration: practice applied in BAMOS project in in vivo testing of innovative osteochondral scaffolds. *Biomater Transl* **2022**, *3*, 102-104.
6. Rutgers, M.; Saris, D.B.; Vonk, L.A.; van Rijen, M.H.; Akrum, V.; Langeveld, D.; van Boxtel, A.; Dhert, W.J.; Creemers, L.B. Effect of collagen type I or type II on chondrogenesis by cultured human articular chondrocytes. *Tissue engineering. Part A* **2013**, *19*, 59-65, doi:10.1089/ten.TEA.2011.0416.
7. Ragetly, G.; Griffon, D.J.; Chung, Y.S. The effect of type II collagen coating of chitosan fibrous scaffolds on mesenchymal stem cell adhesion and chondrogenesis. *Acta biomaterialia* **2010**, *6*, 3988-3997, doi:10.1016/j.actbio.2010.05.016.
8. Xue, X.; Hu, Y.; Deng, Y.; Su, J. Recent Advances in Design of Functional Biocompatible Hydrogels for Bone Tissue Engineering. *Advanced Functional Materials* **2021**, *31*, 2009432, doi:https://doi.org/10.1002/adfm.202009432.
9. Tampieri, A.; Sandri, M.; Landi, E.; Pressato, D.; Francioli, S.; Quarto, R.; Martin, I. Design of graded biomimetic osteochondral composite scaffolds. *Biomaterials* **2008**, *29*, 3539-3546, doi:10.1016/j.biomaterials.2008.05.008.
10. Sosio, C.; Di Giancamillo, A.; Deponti, D.; Gervaso, F.; Scalera, F.; Melato, M.; Campagnol, M.; Boschetti, F.; Nonis, A.; Domeneghini, C.; et al. Osteochondral repair by a novel interconnecting collagen-hydroxyapatite substitute: a large-animal study. *Tissue engineering. Part A* **2015**, *21*, 704-715, doi:10.1089/ten.TEA.2014.0129.
11. Levingstone, T.J.; Thompson, E.; Matsiko, A.; Schepens, A.; Gleeson, J.P.; O'Brien, F.J. Multi-layered collagen-based scaffolds for osteochondral defect repair in rabbits. *Acta biomaterialia* **2016**, *32*, 149-160, doi:10.1016/j.actbio.2015.12.034.
12. Kon, E.; Delcogliano, M.; Filardo, G.; Pressato, D.; Busacca, M.; Grigolo, B.; Desando, G.; Marcacci, M. A novel nano-composite multi-layered biomaterial for treatment of osteochondral lesions: technique note and an early stability pilot clinical trial. *Injury* **2010**, *41*, 693-701, doi:10.1016/j.injury.2009.11.014.
13. Perdisa, F.; Filardo, G.; Sessa, A.; Busacca, M.; Zaffagnini, S.; Marcacci, M.; Kon, E. One-Step Treatment for Patellar Cartilage Defects With a Cell-Free Osteochondral Scaffold: A Prospective Clinical and MRI Evaluation. *The American journal of sports medicine* **2017**, *45*, 1581-1588, doi:10.1177/0363546517694159.

14. Di Martino, A.; Perdisa, F.; Filardo, G.; Busacca, M.; Kon, E.; Marcacci, M.; Zaffagnini, S. Cell-Free Biomimetic Osteochondral Scaffold for the Treatment of Knee Lesions: Clinical and Imaging Results at 10-Year Follow-up. *The American journal of sports medicine* **2021**, *49*, 2645-2650, doi:10.1177/03635465211029292.
15. Dhollander, A.A.; Huyse, W.C.; Verdonk, P.C.; Verstraete, K.L.; Verdonk, R.; Verbruggen, G.; Almqvist, K.F. MRI evaluation of a new scaffold-based allogenic chondrocyte implantation for cartilage repair. *European journal of radiology* **2010**, *75*, 72-81, doi:10.1016/j.ejrad.2009.03.056.
16. Brown, T.D.; Pope, D.F.; Hale, J.E.; Buckwalter, J.A.; Brand, R.A. Effects of osteochondral defect size on cartilage contact stress. *Journal of orthopaedic research : official publication of the Orthopaedic Research Society* **1991**, *9*, 559-567, doi:10.1002/jor.1100090412.
17. Christensen, B.B.; Foldager, C.B.; Jensen, J.; Jensen, N.C.; Lind, M. Poor osteochondral repair by a biomimetic collagen scaffold: 1- to 3-year clinical and radiological follow-up. *Knee surgery, sports traumatology, arthroscopy : official journal of the ESSKA* **2016**, *24*, 2380-2387, doi:10.1007/s00167-015-3538-3.
18. Xue, X.; Zhang, H.; Liu, H.; Wang, S.; Li, J.; Zhou, Q.; Chen, X.; Ren, X.; Jing, Y.; Deng, Y.; et al. Rational Design of Multifunctional CuS Nanoparticle-PEG Composite Soft Hydrogel-Coated 3D Hard Polycaprolactone Scaffolds for Efficient Bone Regeneration. *Advanced Functional Materials* **2022**, *32*, 2202470, doi:https://doi.org/10.1002/adfm.202202470.
19. Burkus, J.K.; Transfeldt, E.E.; Kitchel, S.H.; Watkins, R.G.; Balderston, R.A. Clinical and radiographic outcomes of anterior lumbar interbody fusion using recombinant human bone morphogenetic protein-2. *Spine (Phila Pa 1976)* **2002**, *27*, 2396-2408.
20. Burkus, J.K.; Gornet, M.F.; Dickman, C.A.; Zdeblick, T.A. Anterior lumbar interbody fusion using rhBMP-2 with tapered interbody cages. *J Spinal Disord Tech* **2002**, *15*, 337-349.
21. Zhang, W.; Zhu, C.; Wu, Y.; Ye, D.; Wang, S.; Zou, D.; Zhang, X.; Kaplan, D.L.; Jiang, X. VEGF and BMP-2 promote bone regeneration by facilitating bone marrow stem cell homing and differentiation. *European cells & materials* **2014**, *27*, 1-11; discussion 11-12.
22. Nash, T.J.; Howlett, C.R.; Martin, C.; Steele, J.; Johnson, K.A.; Hicklin, D.J. Effect of platelet-derived growth factor on tibial osteotomies in rabbits. *Bone* **1994**, *15*, 203-208.
23. Heldin, C.H.; Westermark, B. Mechanism of action and in vivo role of platelet-derived growth factor. *Physiological reviews* **1999**, *79*, 1283-1316, doi:10.1152/physrev.1999.79.4.1283.
24. Phipps, M.C.; Xu, Y.; Bellis, S.L. Delivery of platelet-derived growth factor as a chemotactic factor for mesenchymal stem cells by bone-mimetic electrospun scaffolds. *PLoS one* **2012**, *7*, e40831, doi:10.1371/journal.pone.0040831.
25. Hankenson, K.D.; Dishowitz, M.; Gray, C.; Schenker, M. Angiogenesis in bone regeneration. *Injury* **2011**, *42*, 556-561.
26. Kim, S.E.; Yun, Y.P.; Lee, J.Y.; Shim, J.S.; Park, K.; Huh, J.B. Co-delivery of platelet-derived growth factor (PDGF-BB) and bone morphogenetic protein (BMP-2) coated onto heparinized titanium for improving osteoblast function and osteointegration. *Journal of tissue engineering and regenerative medicine* **2015**, *9*, E219-228.
27. Keceli, H.G.; Bayram, C.; Celik, E.; Ercan, N.; Demirbilek, M.; Nohutcu, R.M. Dual delivery of platelet-derived growth factor and bone morphogenetic factor-6 on titanium surface

- to enhance the early period of implant osseointegration. *Journal of periodontal research* **2020**, *55*, 694-704, doi:10.1111/jre.12756.
28. Taniyama, T.; Masaoka, T.; Yamada, T.; Wei, X.; Yasuda, H.; Yoshii, T.; Kozaka, Y.; Takayama, T.; Hirano, M.; Okawa, A.; et al. Repair of Osteochondral Defects in a Rabbit Model Using a Porous Hydroxyapatite Collagen Composite Impregnated With Bone Morphogenetic Protein-2. *Artificial Organs* **2015**, *39*, 529-535, doi:https://doi.org/10.1111/aor.12409.
 29. Mumcuoglu, D.; Fahmy-Garcia, S.; Ridwan, Y.; Nicke, J.; Farrell, E.; Kluijtmans, S.G.; van Osch, G.J. Injectable BMP-2 delivery system based on collagen-derived microspheres and alginate induced bone formation in a time- and dose-dependent manner. *European cells & materials* **2018**, *35*, 242-254.
 30. Vainieri, M.L.; Lolli, A.; Kops, N.; D'Atri, D.; Eglin, D.; Yayon, A.; Alini, M.; Grad, S.; Sivasubramanian, K.; van Osch, G. Evaluation of biomimetic hyaluronic-based hydrogels with enhanced endogenous cell recruitment and cartilage matrix formation. *Acta biomaterialia* **2020**, *101*, 293-303, doi:10.1016/j.actbio.2019.11.015.
 31. de Vries-van Melle, M.L.; Narcisi, R.; Kops, N.; Koevoet, W.J.; Bos, P.K.; Murphy, J.M.; Verhaar, J.A.; van der Kraan, P.M.; van Osch, G.J. Chondrogenesis of mesenchymal stem cells in an osteochondral environment is mediated by the subchondral bone. *Tissue engineering. Part A* **2014**, *20*, 23-33, doi:10.1089/ten.TEA.2013.0080.
 32. de Vries-van Melle, M.L.; Tihaya, M.S.; Kops, N.; Koevoet, W.J.; Murphy, J.M.; Verhaar, J.A.; Alini, M.; Eglin, D.; van Osch, G.J. Chondrogenic differentiation of human bone marrow-derived mesenchymal stem cells in a simulated osteochondral environment is hydrogel dependent. *European cells & materials* **2014**, *27*, 112-123; discussion 123.
 33. Levingstone, T.J.; Ramesh, A.; Brady, R.T.; Brama, P.A.J.; Kearney, C.; Gleeson, J.P.; O'Brien, F.J. Cell-free multi-layered collagen-based scaffolds demonstrate layer specific regeneration of functional osteochondral tissue in caprine joints. *Biomaterials* **2016**, *87*, 69-81, doi:10.1016/j.biomaterials.2016.02.006.
 34. Browe, D.C.; Burdis, R.; Díaz-Payno, P.J.; Freeman, F.E.; Nulty, J.M.; Buckley, C.T.; Brama, P.A.J.; Kelly, D.J. Promoting endogenous articular cartilage regeneration using extracellular matrix scaffolds. *Materials Today Bio* **2022**, *16*, 100343, doi:https://doi.org/10.1016/j.mtbio.2022.100343.
 35. Burdis, R.; Chariyev-Prinz, F.; Browe, D.C.; Freeman, F.E.; Nulty, J.; McDonnell, E.E.; Eichholz, K.F.; Wang, B.; Brama, P.; Kelly, D.J. Spatial patterning of phenotypically distinct microtissues to engineer osteochondral grafts for biological joint resurfacing. *Biomaterials* **2022**, *289*, 121750, doi:10.1016/j.biomaterials.2022.121750.
 36. Goebel, L.; Orth, P.; Müller, A.; Zurakowski, D.; Bückner, A.; Cucchiari, M.; Pape, D.; Madry, H. Experimental scoring systems for macroscopic articular cartilage repair correlate with the MOCART score assessed by a high-field MRI at 9.4 T--comparative evaluation of five macroscopic scoring systems in a large animal cartilage defect model. *Osteoarthritis and cartilage* **2012**, *20*, 1046-1055.
 37. Gaytan, F.; Morales, C.; Reymundo, C.; Tena-Sempere, M. A novel RGB-trichrome staining method for routine histological analysis of musculoskeletal tissues. *Scientific Reports* **2020**, *10*, 16659, doi:10.1038/s41598-020-74031-x.

38. de Vries-van Melle, M.L.; Mandl, E.W.; Kops, N.; Koevoet, W.J.; Verhaar, J.A.; van Osch, G.J. An osteochondral culture model to study mechanisms involved in articular cartilage repair. *Tissue engineering. Part C, Methods* **2012**, *18*, 45-53, doi:10.1089/ten.TEC.2011.0339.
39. Rath, B.; Nam, J.; Knobloch, T.J.; Lannutti, J.J.; Agarwal, S. Compressive forces induce osteogenic gene expression in calvarial osteoblasts. *J Biomech* **2008**, *41*, 1095-1103, doi:10.1016/j.jbiomech.2007.11.024.
40. Bergmann, P.; Body, J.J.; Boonen, S.; Boutsen, Y.; Devogelaer, J.P.; Goemaere, S.; Kaufman, J.; Reginster, J.Y.; Rozenberg, S. Loading and skeletal development and maintenance. *J Osteoporos* **2010**, *2011*, 786752, doi:10.4061/2011/786752.
41. Jeppsson, C.; Aspenberg, P. BMP-2 can inhibit bone healing. Bone-chamber study in rabbits. *Acta Orthop Scand* **1996**, *67*, 589-592, doi:10.3109/17453679608997762.
42. Wescott, D.C.; Pinkerton, M.N.; Gaffey, B.J.; Beggs, K.T.; Milne, T.J.; Meikle, M.C. Osteogenic gene expression by human periodontal ligament cells under cyclic tension. *J Dent Res* **2007**, *86*, 1212-1216, doi:10.1177/154405910708601214.
43. Eggli, P.S.; Hunziker, E.B.; Schenk, R.K. Quantitation of structural features characterizing weight-and less-weight-bearing regions in articular cartilage: A stereological analysis of medial femoral condyles in young adult rabbits. *The Anatomical Record* **1988**, *222*, 217-227.
44. Athanasiou, K.A.; Rosenwasser, M.; Buckwalter, J.; Malinin, T.; Mow, V.C. Interspecies comparisons of in situ intrinsic mechanical properties of distal femoral cartilage. *Journal of orthopaedic research* **1991**, *9*, 330-340.
45. Cuenca-López, M.D.; Peris, J.L.; García-Roselló, M.; Atienza, C.; Prat, J.; Becerra, J.; Andrades, J.A. Action of recombinant human BMP-2 on fracture healing in rabbits is dependent on the mechanical environment. *Journal of tissue engineering and regenerative medicine* **2010**, *4*, 543-552, doi:https://doi.org/10.1002/term.271.
46. Boerckel, J.D.; Kolambkar, Y.M.; Stevens, H.Y.; Lin, A.S.P.; Dupont, K.M.; Guldberg, R.E. Effects of in vivo mechanical loading on large bone defect regeneration. *Journal of Orthopaedic Research* **2012**, *30*, 1067-1075, doi:https://doi.org/10.1002/jor.22042.
47. Kopf, J.; Petersen, A.; Duda, G.N.; Knaus, P. BMP2 and mechanical loading cooperatively regulate immediate early signalling events in the BMP pathway. *BMC Biol* **2012**, *10*, 37, doi:10.1186/1741-7007-10-37.
48. da Silva Madaleno, C.; Jatzlau, J.; Knaus, P. BMP signalling in a mechanical context - Implications for bone biology. *Bone* **2020**, *137*, 115416, doi:https://doi.org/10.1016/j.bone.2020.115416.
49. Rui, Y.F.; Lui, P.P.; Ni, M.; Chan, L.S.; Lee, Y.W.; Chan, K.M. Mechanical loading increased BMP-2 expression which promoted osteogenic differentiation of tendon-derived stem cells. *Journal of orthopaedic research : official publication of the Orthopaedic Research Society* **2011**, *29*, 390-396.
50. Kanatani, M.; Sugimoto, T.; Kaji, H.; Kobayashi, T.; Nishiyama, K.; Fukase, M.; Kumegawa, M.; Chihara, K. Stimulatory effect of bone morphogenetic protein-2 on osteoclast-like cell formation and bone-resorbing activity. *J Bone Miner Res* **1995**, *10*, 1681-1690, doi:10.1002/jbmr.5650101110.

51. Kaneko, H.; Arakawa, T.; Mano, H.; Kaneda, T.; Ogasawara, A.; Nakagawa, M.; Toyama, Y.; Yabe, Y.; Kumegawa, M.; Hakeda, Y. Direct stimulation of osteoclastic bone resorption by bone morphogenetic protein (BMP)-2 and expression of BMP receptors in mature osteoclasts. *Bone* **2000**, *27*, 479-486, doi:10.1016/s8756-3282(00)00358-6.
52. Zara, J.N.; Siu, R.K.; Zhang, X.; Shen, J.; Ngo, R.; Lee, M.; Li, W.; Chiang, M.; Chung, J.; Kwak, J.; et al. High doses of bone morphogenetic protein 2 induce structurally abnormal bone and inflammation in vivo. *Tissue engineering. Part A* **2011**, *17*, 1389-1399, doi:10.1089/ten.TEA.2010.0555.
53. Halloran, D.; Durbano, H.W.; Nohe, A. Bone Morphogenetic Protein-2 in Development and Bone Homeostasis. *J Dev Biol* **2020**, *8*, doi:10.3390/jdb8030019.
54. Lo, K.W.; Ulery, B.D.; Ashe, K.M.; Laurencin, C.T. Studies of bone morphogenetic protein-based surgical repair. *Adv Drug Deliv Rev* **2012**, *64*, 1277-1291, doi:10.1016/j.addr.2012.03.014.
55. James, A.W.; LaChaud, G.; Shen, J.; Asatrian, G.; Nguyen, V.; Zhang, X.; Ting, K.; Soo, C. A Review of the Clinical Side Effects of Bone Morphogenetic Protein-2. *Tissue Eng Part B Rev* **2016**, *22*, 284-297, doi:10.1089/ten.TEB.2015.0357.
56. Ding, S.; Zhang, J.; Tian, Y.; Huang, B.; Yuan, Y.; Liu, C. Magnesium modification up-regulates the bioactivity of bone morphogenetic protein-2 upon calcium phosphate cement via enhanced BMP receptor recognition and Smad signaling pathway. *Colloids Surf B Biointerfaces* **2016**, *145*, 140-151.
57. Enhancement of BMP-2 Induced Bone Regeneration by SDF-1 α Mediated Stem Cell Recruitment. *Tissue Engineering Part A* **2014**, *20*, 810-818, doi:10.1089/ten.tea.2013.0222.
58. Liu, S.; Liu, Y.; Jiang, L.; Li, Z.; Lee, S.; Liu, C.; Wang, J.; Zhang, J. Recombinant human BMP-2 accelerates the migration of bone marrow mesenchymal stem cells via the CDC42/PAK1/LIMK1 pathway in vitro and in vivo. *Biomater Sci* **2018**, *7*, 362-372, doi:10.1039/c8bm00846a.
59. The Immunomodulatory Role of BMP-2 on Macrophages to Accelerate Osteogenesis. *Tissue Engineering Part A* **2018**, *24*, 584-594, doi:10.1089/ten.tea.2017.0232.
60. Wu, D.H.; Hatzopoulos, A.K. Bone morphogenetic protein signaling in inflammation. *Exp Biol Med (Maywood)* **2019**, *244*, 147-156, doi:10.1177/1535370219828694.
61. Sinder, B.P.; Pettit, A.R.; McCauley, L.K. Macrophages: Their Emerging Roles in Bone. *J Bone Miner Res* **2015**, *30*, 2140-2149, doi:10.1002/jbmr.2735.
62. Ode Boni, B.; Lamboni, L.; Souho, T.; Gauthier, M.; Yang, G. Immunomodulation and Cellular Response to Biomaterials: The Overriding Role of Neutrophils in Healing. *Materials Horizons* **2019**, *6*, doi:10.1039/C9MH00291J.
63. Aulin, C.; Jensen-Waern, M.; Ekman, S.; Hägglund, M.; Engstrand, T.; Hilborn, J.; Hedenqvist, P. Cartilage repair of experimentally 11 induced osteochondral defects in New Zealand White rabbits. *Laboratory Animals* **2013**, *47*, 58-65.
64. Dong, X.; Wang, Q.; Wu, T.; Pan, H. Understanding Adsorption-Desorption Dynamics of BMP-2 on Hydroxyapatite (001) Surface. *Biophysical Journal* **2007**, *93*, 750-759, doi:https://doi.org/10.1529/biophysj.106.103168.

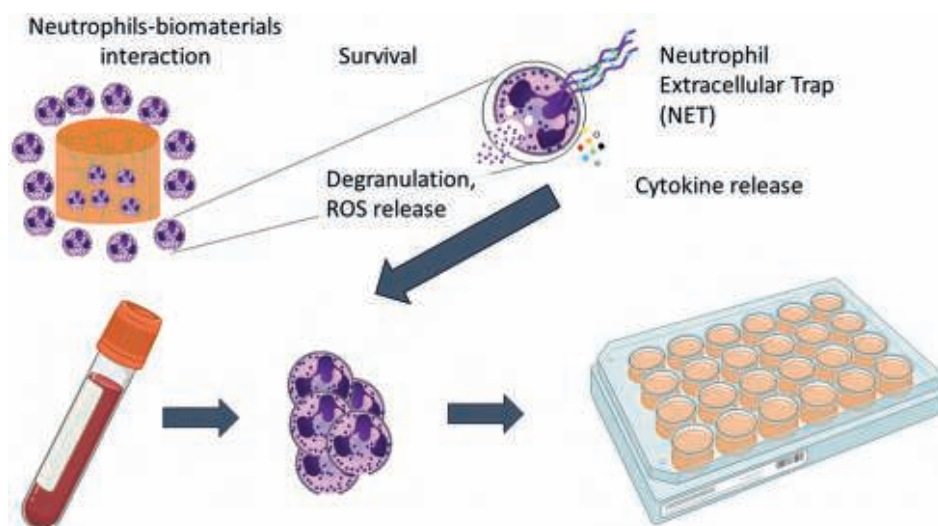
65. Lee, J.M.; Kim, B.-S.; Lee, H.; Im, G.-I. In vivo tracking of mesenchymal stem cells using fluorescent nanoparticles in an osteochondral repair model. *Molecular Therapy* **2012**, *20*, 1434-1442.
66. Vainieri, M.L.; Lolli, A.; Kops, N.; D'atri, D.; Eglin, D.; Yayan, A.; Alini, M.; Grad, S.; Sivasubramanian, K.; Van Osch, G. Evaluation of biomimetic hyaluronic-based hydrogels with enhanced endogenous cell recruitment and cartilage matrix formation. *Acta biomaterialia* **2020**, *101*, 293-303.
67. Zhang, M.; Yu, W.; Niibe, K.; Zhang, W.; Egusa, H.; Tang, T.; Jiang, X. The Effects of Platelet-Derived Growth Factor-BB on Bone Marrow Stromal Cell-Mediated Vascularized Bone Regeneration. *Stem Cells Int* **2018**, *2018*, 3272098, doi:10.1155/2018/3272098.
68. Wang, X.; Matthews, B.G.; Yu, J.; Novak, S.; Grcevic, D.; Sanjay, A.; Kalajzic, I. PDGF Modulates BMP2-Induced Osteogenesis in Periosteal Progenitor Cells. *JBM Plus* **2019**, *3*, e10127, doi:https://doi.org/10.1002/jbm4.10127.

A culture model to analyze the acute
biomaterial-dependent reaction of human
primary neutrophils *in vitro*

Marinus A. Wesdorp
Andrea Schwab
Ezgi I. Bektas
Roberto Narcisi
David Eglin
Martin J. Stoddart
Gerjo J.V.M. van Osch
Matteo D'Este

ABSTRACT

Neutrophils play a pivotal role in orchestrating the immune system response to biomaterials, the onset and resolution of chronic inflammation, and macrophage polarization. However, the neutrophil response to biomaterials and the consequent impact on tissue engineering approaches is still scarcely understood. Here, we report an *in vitro* culture model that comprehensively describes the most important neutrophil functions in the light of tissue repair. We isolated human primary neutrophils from peripheral blood and exposed them to a panel of hard, soft, naturally- and synthetically-derived materials. The overall trend showed increased neutrophil survival on naturally derived constructs, together with higher oxidative burst, decreased myeloperoxidase and neutrophil elastase and decreased cytokine secretion compared to neutrophils on synthetic materials. The culture model is a step to better understand the immune modulation elicited by biomaterials. Further studies are needed to correlate the neutrophil response to tissue healing and to elucidate the mechanism triggering the cell response and their consequences in determining inflammation onset and resolution.



INTRODUCTION

Biomaterial-based implants are widespread in clinics, and subject to intensive research efforts in tissue engineering applications. Commercially available biomaterials are used in different clinical fields ranging from cardiovascular devices to orthopedic implants. At the time when the first biomaterials were introduced in the 50s and 60s, the emphasis was on replacing human tissues or their function without causing undesired reactions. Nowadays, biomaterials are used to repair diseased or damaged tissue by stimulating specific cellular responses at the level of molecular biology ¹. The goal of biomaterial-guided tissue healing is to design biomaterials that mobilize the body's endogenous cells and stimulate regenerative processes to drive functional healing. The biological activity of biomaterials is widely recognized, and biomaterial design parameters are functionally used to achieve successful repair. The development of biomaterials aimed at stimulating regenerative processes necessitates a thorough understanding of the biological responses to the implanted materials. The success of biomaterial-guided tissue repair closely relies on the wound healing response, which is driven by the body's innate immune system as biomaterials are initially recognized as a foreign body ². Today it is widely recognized that biomaterials can trigger a broad spectrum of responses, and even more importantly, there are design factors to modulate this response and foster functional tissue healing or regeneration ³. This interaction between biomaterials and the immune system is being established as a mainstream subject in biomaterials research, and efforts dedicated to elucidating the biological mechanisms which determine the immune response to biomaterials are constantly increasing ⁴.

After implantation, biomaterials are coated with proteins that activate the innate immune system. The proteins that coat the materials mediate the subsequent steps and the interaction of the material with the host's immune system, particularly in attracting neutrophils ². Neutrophils are the most prevalent immune cell in the human blood, and the first cell to encounter a biomaterial upon implantation ⁵. Neutrophils predominate the early inflammatory response as their numbers peak within the first 24 to 48 hours after implantation ⁶. Recruitment and differentiation of monocytes and macrophages occurs at a later stage ⁷. In the field of biomaterials and tissue engineering, macrophages have attracted considerable attention, especially regarding their role in tissue healing ⁸. However, the number of macrophages correlates with the levels of neutrophils present, indicating that neutrophils are important in the recruitment of macrophages and thus the consequent stages of the wound healing response ⁹. Therefore, it is crucial to understand the role of neutrophils in tissue healing and their crosstalk with macrophages. In recent years, cancer research has

shown that neutrophils are important in the progression and regression of tumors ¹⁰. The occurrence of neutrophils driving disease progression is not limited to cancer. Neutrophils also play a role in myocardial infarction, systemic lupus erythematosus (SLE), rheumatoid arthritis, sepsis, psoriasis, human immunodeficiency virus (HIV) infection, asthma, antineutrophil cytoplasmic antibody associated vasculitis, malaria and Chagas' disease ¹¹. Furthermore, neutrophils have also been shown to be essential in bone fracture healing ^{12, 13}. Recent reviews have acknowledged the importance of neutrophils in biomaterial-guided tissue regeneration to achieve successful repair ^{6, 14, 15}. These studies highlight the importance and potential of neutrophils for biomaterial-guided tissue regeneration.

Neutrophils unfold a spectrum of functions in response to biomaterial implantation. The first function is their capacity to survive on the material and eventually die via apoptosis. The apoptosis of neutrophils plays an important role in the transition from pro-inflammatory towards anti-inflammatory macrophages and thereby the resolution of inflammation ¹⁶. The second function is the release of an oxidative burst upon activation. This oxidative burst consists of reactive oxygen species that are critical for killing invaders and degradation of internalized particles, but can also contribute to inflammatory damage of the tissue surrounding the implanted material ¹⁷. The third function is the release of granules with cytokine release and formation of neutrophil extracellular traps (NETs). This function is associated with a strong pro-inflammatory activity that is important in pathogen killing, but when dysregulated it can cause tissue damage, fibrosis and prevent the neutrophils from exerting their function in the wound healing response ⁶. NETs are web like structures that contain decondensed chromatin together with granular proteins such as myeloperoxidase (MPO) and neutrophil elastase. MPO and neutrophil elastase regulate the formation of NETs by digesting histones and promoting chromatin decondensation ¹⁸. The fourth function is the production and secretion of cytokines, chemokines, and angiogenic/fibrogenic factors such as vascular endothelial growth factor (VEGF) and interleukin 8 (IL8). These factors play an important role in the foreign body response to the biomaterial; this response is crucial for the outcome of the tissue repair process ¹⁹. Therefore, the interaction between neutrophils and biomaterials is key to orchestrate inflammation at later phases. Despite the urgent need to obtain a comprehensive understanding of the neutrophil interaction with the biomaterial, there are few studies that have examined the effect of biomaterials on neutrophils *in vitro*. Chang and colleagues found that neutrophils' survival drops on rough compared to smooth surfaces ²⁰. Kaplan and colleagues reported that neutrophils respond with different levels of superoxide release in response to different biomaterials ²¹. Szponder and colleagues showed that neutrophils release different levels of elastase on alginate biomaterials than on

carbon fibers²². Velard and colleagues found that the addition of zinc to hyaluronic acid results in decreased levels of IL8 and matrix metallo-proteinase-9 (MMP9)²³. All the aforementioned studies only focus on one specific neutrophil function. *In vitro* models that exhaustively characterize the neutrophil response to biomaterials are still missing.

We devised an *in vitro* model based on human primary neutrophils to enable comprehensive characterization of the acute neutrophil response to a biomaterial. To provide proof of principle that the model can discriminate the response of neutrophils to different materials, seven polymeric biomaterials were chosen including synthetic and naturally derived biomaterials as well as soft and hard materials to represent a range in physical and chemical properties. The materials investigated were: tyramine functionalized hyaluronic-acid (THA), THA mixed with collagen (THA-col), type I collagen (col), gelatin-methacryloyl (GelMA), polyvinyl alcohol (PVA), tissue culture plastic (TCP) and polycaprolactone (PCL).

We analyzed the activity and survival of neutrophils after seeding them on the biomaterials. The oxidative burst of neutrophils in response to the biomaterials was characterized by analyzing superoxide anion, the amounts of MPO and neutrophil elastase released from the granules, and a large panel of chemokines, cytokines, angiogenic, and fibrogenic factors via OLINK®.

MATERIALS AND METHODS

Biomaterial synthesis and hydrogel formation

A panel of seven naturally derived and synthetic materials was selected as follows: tyramine functionalized hyaluronic-acid (THA), THA mixed with collagen (THA-col), type I collagen (col), gelatin-methacryloyl (GelMA), polyvinyl alcohol (PVA), tissue culture plastic (TCP) and polycaprolactone (PCL). Prior to use, the polymer powders were UV sterilized and all solutions were sterile filtered. The materials were coated (press fit in case of PCL) on the bottom of a cell culture well plate in the desired size for each experiment. The raw materials were processed in a setup to allow cell culture in different well plates. A similar volume ($150\mu\text{l}/\text{cm}^2$) of precursor hydrogels was casted on the bottom of a well plate using a positive displacement pipette (CP1000/CP250; Gilson, Middleton, USA) and polymerized. After casting/fitting all materials into the wells, the materials were washed with PBS 3x before seeding the neutrophils.

THA was synthesized as previously described²⁴. In short, sodium hyaluronate (280-290 kDa, 5mM carboxylic groups) (Contipro Biotech S.R.O, Dolni Dobrouc, Czech Republic) was dissolved in deionized H₂O (1% w/v) and functionalized with tyramine (Sigma-Aldrich, Buchs, Switzerland) via 4-(4,6-dimethoxy-1,3,55-triazin-2-yl)-4-mehtylmorpholinium chloride (DMTMM; TCI Europe, Zwijndrecht, Belgium) amidation by mixing at a stoichiometric ratio of 1:1:1. Functionalization was performed under mild stirring for 24h at 37°C. THA was precipitated by adding 16% v/v of saturated NaCl and 96% ethanol dropwise, isolated using Gooch filter no. 2, washed, and dried under vacuum. The amidation reaction was repeated to increase the degree of substitution (DoS) to 11.3% as determined by absorbance reading at 275nm Multiskan[®] GO Microplate Spectrophotometer (ThermoFisher, Waltham, USA). For each experiment the THA conjugate was reconstituted in phosphate buffered saline (PBS) at 2.5% (w/v) containing 0.6 U/ml HRP (Sigma-Aldrich) and rotated overnight at 4°C. To initiate hydrogel formation, 1.3mM hydrogen peroxide (H₂O₂, Sigma-Aldrich) was added and immediately mixed to provide a homogeneous distribution. The material was casted into the well and incubated at 37°C, 5% CO₂ for 10 minutes to allow enzymatic gelation.

Collagen type I derived from rat tail was bought from Corning (Collagen I rat tail in 0.2 N acetic acid, 10.98 mg/ml). Collagen type I hydrogels were prepared on ice by neutralizing the collagen I solution with a mixture of 10x PBS, dH₂O and 1N sodium hydroxide (NaOH) to a final concentration of 5mg/ml. The hydrogel precursors were incubated at 37°C, 5% CO₂ for 30 minutes until a firm gel was formed.

THA-col composites were prepared by mixing the previously described mixtures of THA and collagen in a 1:1 ratio for a final concentration of 2.5mg/ml collagen and 2.5% (w/v) THA. Enzymatic gelation and neutralization of collagen was initiated simultaneously.

GelMA (type A, 180 g Bloom, Fluka) was synthesized by dissolving gelatin (10% w/v) in phosphate buffered saline (PBS, pH = 7.4) at 60°C²⁵. After dissolving, 0.28% methacrylic anhydride was added to the dissolved gelatin and mixed with the solution. To stop the reaction the mixture was diluted with PBS and transferred in a dialysis membrane (12-14 kDa) to remove unreacted methacrylic anhydride and other side products. After dialysis was complete, ultrapure H₂O was added to the dialyzed solution and subsequently freeze-dried for storage. The DoS of the final GelMA was 50% as determined via NMR analysis. The GelMA macromer 15% (w/v) was fabricated into hydrogels by UV crosslinking after mixing with 0.5% 2-hydroxy-4'-(2-hydroxyethoxy)-2-methylpropiophenone (Irgacure 2959) (Sigma-Aldrich) in PBS.

PVA pellets with a molecular weight (MW) of 70,000 Da were dissolved at 90°C in H₂O (5% w/v) under stirring until a clear solution was obtained. The PVA precursor hydrogel solution was casted in a circular well and frozen at -20°C. To fabricate PVA hydrogels, the solution underwent 7 freeze thawing cycles ensuring complete freezing at -20°C followed by thawing at room temperature.

PCL discs were printed in the respective diameter of the used well plate after melting PCL pellets with a MW of 45,000 Da (Sigma-Aldrich) and press fitted onto the bottom of a well plate ensuring a flat surface. An extrusion-based 3D printer RegenHu 3D Discovery (RegenHU, Villaz-Saint-Pierre, Switzerland) was used with the following parameters: inner diameter nozzle 300 µm, 1 bar, 16 revs/m, writing speed 6 mm/s, temperature tank 75°C, temperature printer head 70°C.

Tissue culture treated polystyrene plates (TCP) were bought from Corning.

Endotoxin analysis

The endotoxin content of each biomaterial was measured using the Pierce™ Chromogenic Endotoxin Quant Kit (Thermo-Fisher) according to the manufacturer's instructions. All polymers were diluted with endotoxin free H₂O (Sigma-Aldrich) at the polymer concentration matching those used in the neutrophil experiments. Due to high viscosity, THA and GelMa hydrogels were cast (250 µl) into a 24 well plate. All materials were incubated with endotoxin free H₂O (1ml) for 1h. An endotoxin standard stock solution was prepared by adding endotoxin free H₂O (Sigma-Aldrich) to the E. coli endotoxin standard vial to create a high standard (0.1-1.0 EU/ml) and a low standard (0.01-0.1 EU/ml). Samples harvested from THA and GelMA were diluted prior to the assay in endotoxin free water and transferred together with the standard curve into the pre-warmed plate at 37°C. The supernatant from all other materials was directly transferred to the pre-warmed plate together with the standard curve. The amoebocyte lysate reagent was added to each well and the plates were incubated for 8 min at 37°C. The reaction of the chromogenic substrate solution was stopped after 6 min at 37°C by adding 25% (v/v) acetic acid to each well and the optical density was measured at 405 nm using the Infinite® 200 Pro plate reader (Tecan, Männedorf, Switzerland). The obtained values were used to calculate the concentration based on the provided standard curve for the aforementioned concentration ranges. The correlation coefficients for the standard curves were between 0.9922 and 0.9953.

Rheological characterization biomaterials

To assess the viscoelastic properties of all hydrogels, rheological measurements at 20°C using the Anton-Paar MCR-302 rheometer equipped with 1° cone-plate geometry

and a gap distance of 0.049 mm were performed ($n=4$ replicates per material). Silicone oil (Sigma-Aldrich) was applied to the external border to prevent drying during the measurement. The amplitude sweep test (frequency = 1 Hz, amplitude = 0.01-100% strain) was performed to characterize the elastic storage modulus (G') and viscous loss modulus (G'') of all hydrogel materials. The moduli were measured at a strain of 1%, which was within the linear viscoelastic region of each hydrogel.

Isolation and culture of human primary neutrophils

Peripheral blood was collected from 5 human healthy volunteers, 3 males and 2 females, average age 26 years, age range 24 to 29 years donating 24 mL of venous whole blood after written informed consent was obtained. Ethical approval was granted by the cantonal ethical committee (BASEC-Nr. 2019-02353). The blood was collected by a venipuncture into potassium EDTA-coated containers (S-Monovette®, Sarstedt, Nümbrecht, Germany). Neutrophils were isolated from whole blood by immunomagnetic negative selection using the EasySep® Direct Human Neutrophil Isolation Kit (STEMCELL Technologies #19666, Vancouver, Canada) following the manufacturer's instructions. After the last separation step, the enriched suspension containing neutrophils was pipetted into a new tube, centrifuged at 300 g for 5 minutes and resuspended in Roswell Park Memorial Institute (RPMI) 1640 medium (26) with HEPES (Gibco, ThermoFisher, Waltham, USA) supplemented with 100 U/ml penicillin (Gibco) and 100 µg/ml streptomycin (Gibco) to a concentration of 1×10^6 cells/mL. Neutrophils were counted using a hemocytometer and viability was confirmed to be > 99% with trypan blue.

For evaluating purity after negative selection, neutrophils were resuspended (1×10^6 cells) in 2 mL of 0.5 % (w/v) bovine serum albumin (BSA) containing phosphate buffered saline (1X PBS) subsequent to isolation. Following the centrifugation step at 300 g for 5 minutes, cells were incubated with 5 µL of Fc Receptor Blocking Solution (BioLegend, USA) in 100 µL 0.5 % (w/v) BSA-PBS for 15 minutes. The cells were stained with anti-human CD 16-APC (10 µL/ 1×10^6 cells) (R&D Systems, Biotechne, USA), FITC mouse anti- human CD66b (20 µL/ 1×10^6 cells) (BD Biosciences, USA) and PE mouse anti-human CD14 (20 µL/ 1×10^6 cells) (BD Biosciences, USA) antibodies for 40 minutes. After washing cells with 0.5 % (w/v) BSA-PBS and centrifugation (300 g for 5 minutes), cells were analyzed to measure the intensity of CD markers via BD FACSAria™ III cytometer (BD Life Sciences, USA).

After isolation, neutrophils were seeded in complete RPMI-1640 medium on top of the materials occupying the well in a density of 1×10^6 cells/mL equal to 263,000 cells/cm². All plates were cultured in a humidified atmosphere with 5% CO₂ at 37°C. At each

culture timepoint the medium was harvested from the well, centrifuged for 8 minutes at 300 g and stored at -80°C until further use. Unconditioned control medium was generated by the incubation of complete RPMI-1640 medium and processed in the same way as earlier described. A complete overview of all the assays and harvesting timepoints is shown in **Figure 1**. The experiment was carried out in 5 independent experiments ($n=5$ donors) with two replicates each.

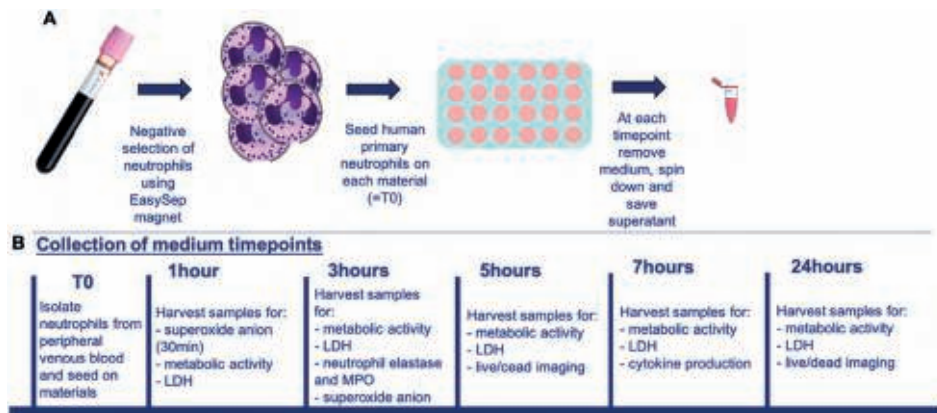


Figure 1. Summary of the assays performed

A) Schematic experimental outline from drawing peripheral blood to collection of media from each material. B) Timeline of the assays that were carried out at each time points ($n=5$ donors, $n=2$ replicates).

Metabolic activity of neutrophils

The metabolic activity, an indicator of cell viability, was measured using the resazurin-based CellTiter-Blue® Cell Viability Assay (Promega, Dübendorf, Switzerland). The CellTiter-Blue® Reagent was added at a concentration of 16.7% in RPMI 1640 medium to each sample 30 minutes prior to each time point (1, 3, 5, 7 and 24 hours). The Fluorescence intensity was measured immediately after transferring the media to a 96 well plate using the Infinite® 200 Pro plate reader (Tecan) at an excitation wavelength (λ_{ex}) of 560 nm and emission wavelength (λ_{em}) of 590-610 nm. The final fluorescence value for each sample was calculated after subtracting the average fluorescence values of the culture medium background.

LDH release

Lactate dehydrogenase (LDH) is rapidly released into the cell culture supernatant in dying cells when the plasma membrane is damaged. The LDH release was measured using the Cytotoxicity Detection Kit^{PLUS} LDH (Roche, Sigma-Aldrich) according to the manufacturer's instructions. The low control value was determined by medium from uncultured cells at the timepoint $t = 0$ h and the high control value was determined by

medium from cultured cells at each timepoint by adding 9% Triton X-100 15 minutes prior to harvest. Unconditioned control medium served as a background control. The absorbance value of the samples was measured at 490 nm using the Infinite® 200 Pro plate reader (Tecan). The percentage of cytotoxicity was calculated according to the following formula: cytotoxicity (%) = $\frac{\text{experimental value} - \text{low control}}{\text{high control} - \text{low control}} \times 100$.

Confocal microscopy based live/dead assay

Neutrophils were stained after 5 and 24 hours with 2 μM Calcein AM (Sigma-Aldrich) and 10 μM ethidium homodimer-1 (Sigma-Aldrich) in culture medium for 30 minutes at 37°C and imaged using the LSM 800 confocal microscope (Zeiss, Oberkochen, Germany). Images were taken at 5 fields per sample to represent the top, lower, central, right and left zone of the material. For each image the alive and dead cells were counted using Image-J software. The percentage of living cells was calculated by the number of alive cells divided by the total number of cells per sample.

Neutrophils oxidative burst

Superoxide anion production was determined from the rate of cytochrome C reduction, measured using the Cytochrome C Assay Kit (Abcam, Cambridge, United Kingdom) according to the manufacturer's instructions. Neutrophils were seeded on the materials and cytochrome C was added. After 30 minutes and 3 hours the medium was centrifuged, and the supernatant was transferred to a 96-well plate and the absorbance value was measured at 550 nm using the Infinite® 200 Pro plate reader (Tecan). Unconditioned, cell free control medium supplemented with cytochrome C served as a background control. After subtracting the background values, superoxide anion production was calculated with the use of the extinction coefficient of 21 $\text{mM}^{-1} \text{cm}^{-1}$ for cytochrome c.

MPO and neutrophil elastase

Medium that was conditioned for 3 hours by the neutrophils seeded on different materials was used to determine MPO and neutrophil elastase. The MPO content was measured using the Meso Scale Discovery (MSD) human myeloperoxidase kit and the MESO QuickPlex SQ 120 (MSD, Kenilworth, USA) according to the manufacturer's instructions. The samples were diluted to allow detection of MPO within the linear range of the standard curve (33-50,000 pg/ml). The MSD Discovery Workbench Software was used to convert relative luminescent units into protein concentrations using interpolation from the standard curve. Neutrophil elastase was measured using the human neutrophil elastase/ELA2 DuoSet ELISA kit (R&D Systems, Minneapolis, USA) according to the manufacturer's instructions of the kit. The absorbance value of each sample was measured at 450 nm using the Infinite® 200 Pro plate reader (Tecan).

and subtracted by the absorbance value at 570 nm. The samples were diluted to allow detection of neutrophil elastase within the linear range of the standard curve (47 - 3000 pg/ml).

Quantification of neutrophil cytokine secretion

A panel of proteins associated with inflammation was measured in the media supernatant using the OLINK® inflammation multiplex immunoassay (OLINK® Proteomics, Uppsala, Sweden). This panel covers 92 established and validated inflammation related markers including pro- and anti-inflammatory cytokines, chemokines, growth factors, receptors and factors involved in acute inflammatory and immune responses. The OLINK® immunoassay panel is based on the proximity extension assay technology that include oligonucleotide-labeled antibody probe pairs that can bind to their respective protein targets in the sample and can be detected and quantified using standard real-time PCR. Data of the 7h timepoint is presented as normalized protein expression values (NPX) which are comparable in their distribution to log2-transformed protein concentrations. The full description of the inflammatory markers is given in **Supplementary Material Table S1**. The data analysis was done using the OLINK®'s Normalized Protein eXpression Manager software. In this OLINK® inflammation panel matrix metalloproteinase 9 (MMP-9), an important regulatory factor in neutrophil migration, angiogenesis and wound repair (27), was not present. For this reason, MMP-9 was quantified in samples of the 7h timepoint by the human MMP-9 DuoSet ELISA kit (R&D Systems) according to the manufacturer's instructions. The absorbance value of each sample was measured at 450 nm using the Infinite® 200 Pro plate reader (Tecan) and subtracted by the absorbance value at 570 nm. The samples were diluted to allow detection of neutrophil elastase within the linear range of the standard curve (31 - 2000 pg/ml).

Statistical analysis

All samples were measured in technical duplicates per each donor (n=10 samples of 5 independent donors in total), group and timepoint. Statistical analysis was performed with Graph Pad Prism (Prism 9, Graphpad Software, San Diego, USA). A one-way analysis of variation (ANOVA) with a post hoc Tukey honestly significant difference analysis was performed to analyze differences between materials and to correct for multiple testing. In case of large donor variability and gaussian distribution of the data, a linear mixed model (LMM) was used. For the LMM, the different materials were considered a fixed parameter and the donors (experiments) as a random factor. For the OLINK® data, the OLINK® Insights Stat Analysis app was used to analyze differences between groups within a protein. All statistical analysis included two tailed tests. A *P* value of < 0.05 was considered as statistically significant. In the manuscript statistical differences

are indicated as follows: a=statistically significant to THA, b=statistically significant to THA-collagen, c= statistically significant to collagen, d= statistically significant to GelMA, e=statistically significant to PVA, f= statistically significant to TCP, g= statistically significant to PCL. All graphs with the exact *P* values are shown in the supplementary materials to allow for better visualization of the graphs in the main paper.

RESULTS

Materials Characterization

Bacterial endotoxins or lipopolysaccharides (LPS) are cell wall constituents of gram negative bacteria which can induce a strong immune response²⁸. Therefore, materials were characterized for their endotoxin levels. For collagen type I, PVA, PCL and TCP endotoxins were on the lower detection limit (**Figure 2B**). The endotoxin levels of THA and GelMA were significantly higher than the other materials ($P < 0.001$), but still relatively low (**Figure 2B**). The other reagents used for the crosslinking displayed values below the lower limit of detection (data not shown). Concentrations of polymers and crosslinkers were selected to achieve a similar shear storage modulus for all hydrogels except collagen, as measured by rheological amplitude sweep. THA, THA-col, GelMA and PVA showed similar shear storage moduli around 5 kPa (**Figure 2C**). The storage modulus of collagen hydrogel was significantly lower than the moduli of all other hydrogels ($P < 0.001$, **Figure 2C**).

Purity, metabolic activity and survival of neutrophils cultured on different biomaterials

Neutrophil purity after negative selection was evaluated via cytometry by assessing the presence of cell surface markers CD66b and CD16 and the absence of CD14 (29). The isolated neutrophils were characterized by 99.7% CD66b, 99% CD16 and 0.2% CD14, confirming a high purity, as expected from immunomagnetic selection (**Figure 3A**). Neutrophil survival and metabolic activity on different materials was evaluated with cell-titer blue assay, LDH and calcein AM/ethidium homodimer staining. Overall, neutrophils showed the highest level of metabolic activity after one hour with a gradual decrease over time. After 24 hours, most neutrophils were no longer metabolically active independent of the material. Clear differences between materials were observed. Neutrophils cultured on TCP and PCL were significantly more metabolically active after 1 and 3 hours than neutrophils cultured on other materials. The difference in activity diminished after 5 hours of culture (**Figure 3B**, **Suppl. Figure 1A**). This

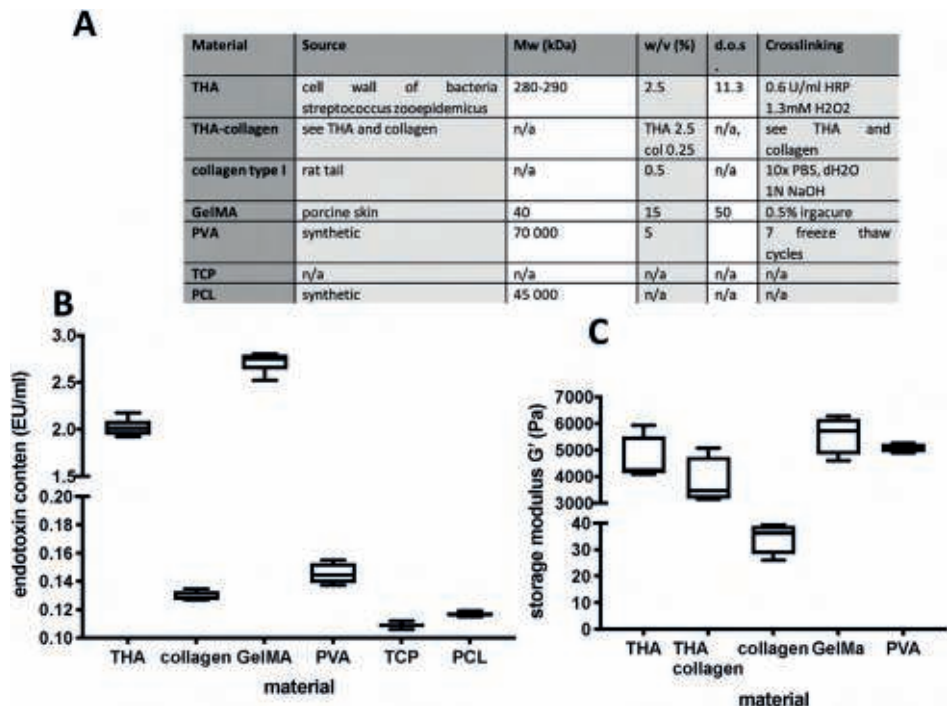


Figure 2. Composition and characterization of the biomaterials

A) Summary of the characteristics of the materials used in this study, including the source, molecular weight, polymer concentration, degree of substitution, and materials used for crosslinking. B) Endotoxin content of different materials (n=2-6) with endotoxins present between 2-3 EU/mL in THA and GelMA. C) Storage moduli of different hydrogels (n=4) ranging between 4-5k Pa for THA, THA-collagen, GelMA and PVA and 35 Pa for collagen. Box plots represent the 25th and 75th percentile with the median, the whiskers indicate the maximum and minimum. Abbreviations: Mw, molecular weight; kDa, kilo Dalton; w/v, weight per volume; d.o.s., degree of substitution.

indicates that neutrophils cultured on hard hydrophobic surfaces have a different activity than neutrophils cultured on softer hydrated substrates.

A similar trend was seen for release of LDH in the medium. After one hour, LDH was only released by neutrophils cultured on PCL, which was approximately 20% of the maximum amount (Triton x1-100 treated high control) and significantly higher than from neutrophils cultured on other materials. The LDH release increased over time. After 24 hours neutrophils cultured on synthetic materials PVA, TCP and PCL released significantly more LDH than neutrophils that were cultured on naturally derived materials like THA, THA-collagen, collagen and GelMA, that released almost no LDH up to 24 hours (Figure 3C, Suppl. Figure 1B).

To visualize the survival of the neutrophils cultured on different materials we performed a live and dead assay, with representative images after 5 and 24 hours

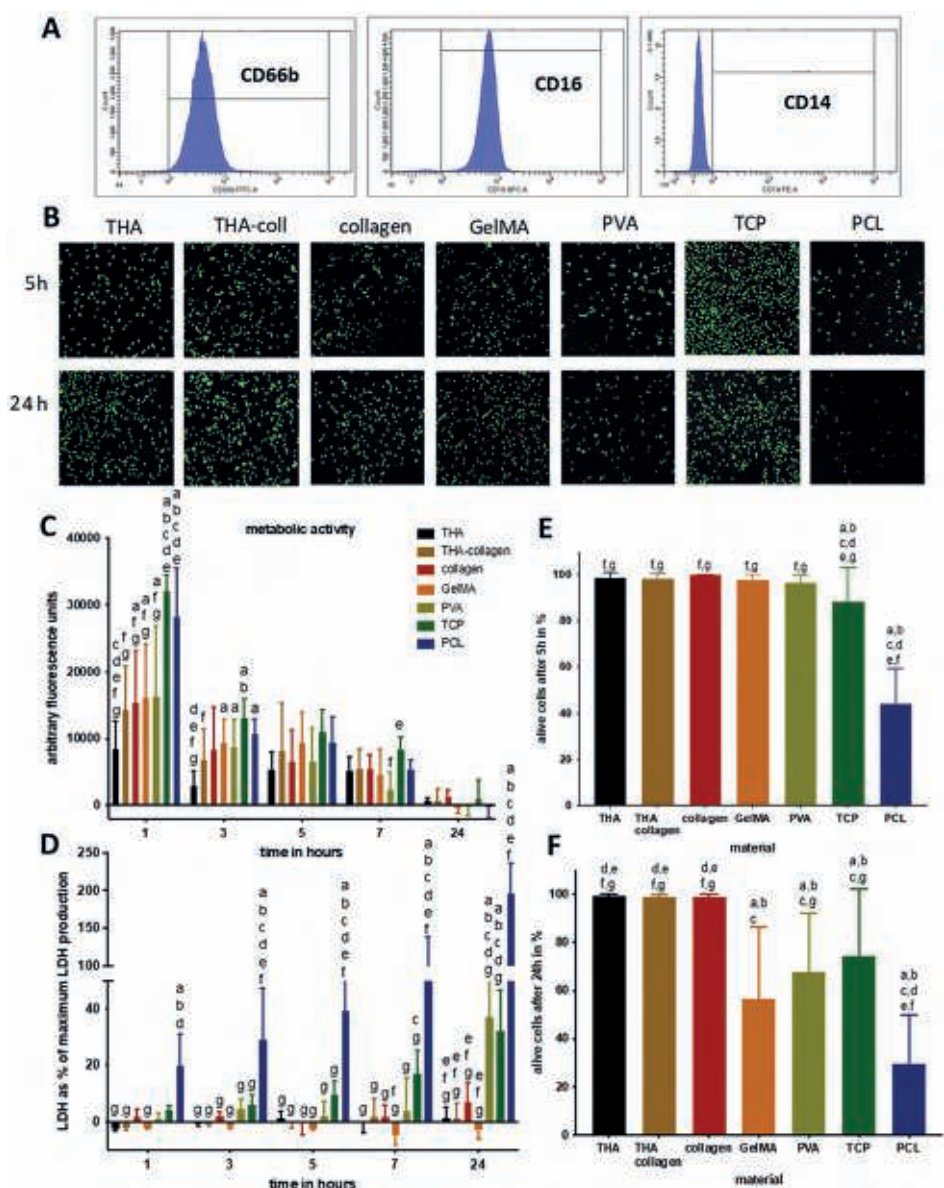


Figure 3. Neutrophil purity assessment, activity and cell survival on different material
A) Flow cytometry histograms showing CD66b and CD16, and CD14 expression on neutrophils. B) Representative images of live/dead staining after 5 and 24 hours showing living cells in green with dead cells in red. C) Metabolic activity of neutrophils measured via cell titer blue assay and expressed as fluorescence units over time for each material. D) LDH release by neutrophils cultured on different materials expressed as a percentage of the maximum amount of LDH release after cell lysis. E) The percentage of living cells after 5 hours. F) The percentage of alive cells after 24 hours. Each bar represents the mean of 5 donors + SD. Abbreviations: LDH, lactate dehydrogenase. a=statistically significant to THA, b=statistically significant to THA-coll, c= statistically significant to coll, d= statistically significant to GelMA, e=statistically significant to PVA, f= statistically significant to TCP, g= statistically significant to PCL.

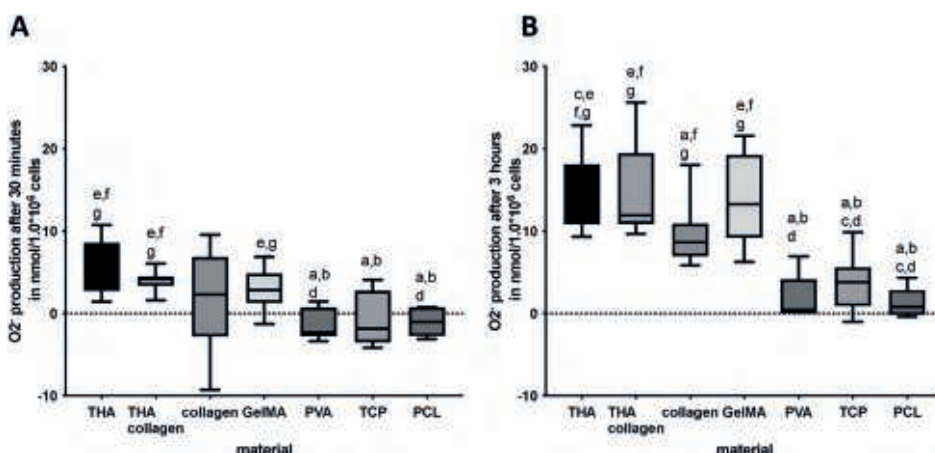


Figure 4. Superoxide anion production by neutrophils cultured on different materials

Superoxide anion production after A) 30 minutes and B) 3 hours of culture. Box plots represent the 25th and 75th percentile with the median, the whiskers indicate the maximum and minimum. a=statistically significant to THA, b=statistically significant to THA-coll, c= statistically significant to coll, d= statistically significant to GelMA, e=statistically significant to PVA, f= statistically significant to TCP, g= statistically significant to PCL.

shown in **Figure 3D**. This assay also showed clear differences between materials. After 5 hours, 44% of the neutrophils cultured on PCL and 88% of the neutrophils on TCP were viable. This was significantly lower than neutrophils cultured on the other hydrogel materials with a viability of more than 96% after 5 hours (**Figure 3E**, **Suppl. Figure 1C**). After 24 hours, more than 98% of the neutrophils cultured on THA, collagen, and THA-collagen were still viable. Neutrophils were significantly less viable on GelMA, PVA, TCP and PCL ranging from 30 to 75% (**Figure 3F**, **Suppl. Figure 1D**).

Release of oxidative burst by means of reactive oxygen species production

To better understand the effect of biomaterials on the ROS production by neutrophils, we measured the amount of superoxide anion released in the culture media. Significantly more superoxide anion was produced by neutrophils cultured on THA, THA-collagen, collagen, GelMA than by neutrophils cultured on PVA, TCP, PCL after 30 minutes (**Figure 4A**, **Suppl. Figure 2A**). After 3 hours, the superoxide anion production increased in all groups. The level of superoxide anion was significantly higher for all naturally derived materials (THA, THA-collagen, collagen, GelMA) than for all synthetic (PVA, TCP, PCL) materials (**Figure 4B**, **Suppl. Figure 2B**) at both time points.

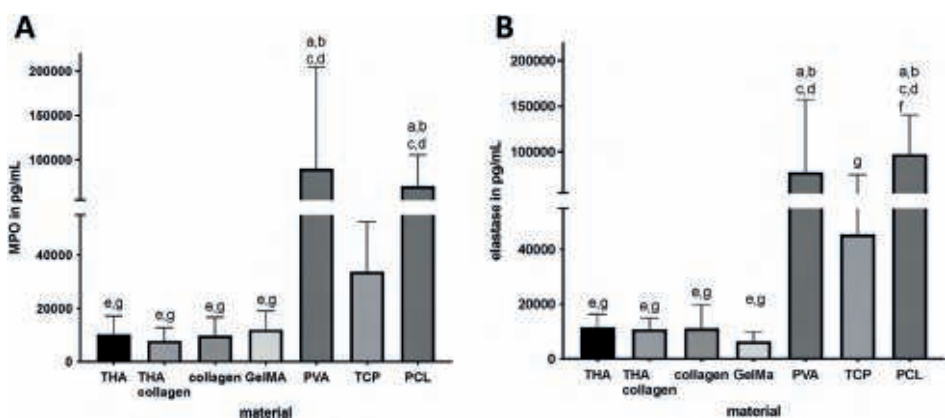


Figure 5. Release of MPO and neutrophil elastase on different materials
The release of A) MPO in pg/ml and B) neutrophil elastase in pg/ml by neutrophils cultured on different materials. Each bar represents the mean level + SD. Abbreviations: MPO, myeloperoxidase. a=statistically significant to THA, b=statistically significant to THA-coll, c= statistically significant to coll, d= statistically significant to GelMA, e=statistically significant to PVA, f= statistically significant to TCP, g= statistically significant to PCL.

Neutrophil elastase and MPO release induced by biomaterials

Neutrophils cultured on PVA and PCL released significantly more MPO and elastase than neutrophils cultured on THA, THA-collagen, collagen and GelMA (Figure 5). Neutrophils cultured on TCP displayed the same trend, albeit non-significant, possibly due to the high variability between donors (Figure 5, Suppl. Figure 3).

Cytokine secretion by neutrophils cultured on different biomaterials

To further understand the response of neutrophils to different biomaterials, proteins which are differentially regulated can be identified. We used the OLINK® technique to analyze a panel of 92 cytokines, chemokines, growth factors and receptors all being related to inflammation (Figure 6). In total, 19 proteins were detected in more than 75% of the samples (Suppl. Table 2). Further analysis showed that most proteins are related to biological processes such as cellular response to cytokine stimulus, chemotaxis, inflammatory response, cell adhesion and secretion (Figure 6).

In a second step we specifically investigated the top-6 most abundant proteins released by the neutrophils: vascular endothelial growth factor A (VEGF-A), hepatocyte growth factor (HGF) urokinase-type plasminogen activator (uPA), extracellular newly identified receptor for advanced glycation end-products binding protein (EN-RAGE), oncostatin M (OSM), and interleukin 8 (IL-8) (Figure 6C-H, Suppl. Figure 4). Neutrophils cultured on PCL and PVA secreted significantly more of the selected proteins than neutrophils

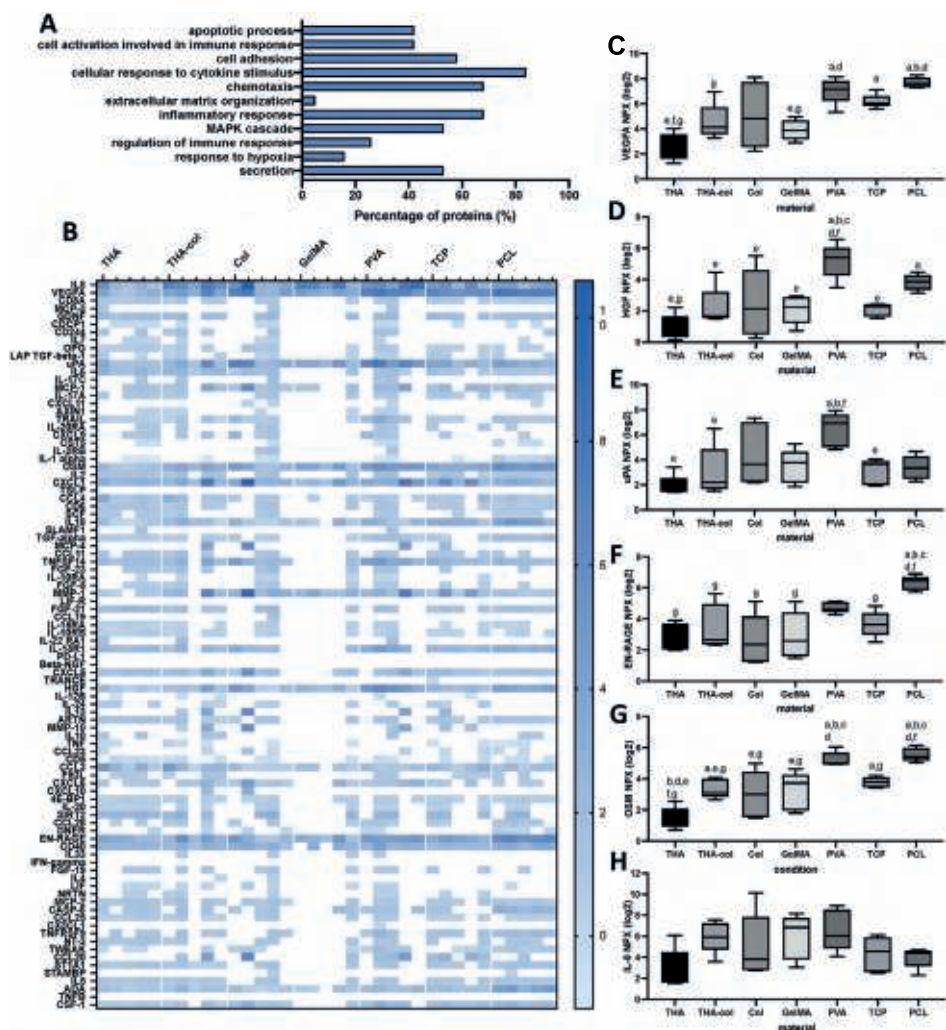


Figure 6. Analysis of cytokine secretion by neutrophils using the OLINK® technology
A) Heatmap of 92 inflammation related proteins that were quantified in NPX on a Log2 scale. Each column within a material represents one donor (5 Donors). The darker the color the higher the protein level. B) Biological analysis to which biological process the detected proteins contribute. C-H) Box plots showing the level of C) VEGF-A, D) HGF, E) uPA, F) EN-RAGE, G) OSM, and H) IL-8. Box plots represent the 25th and 75th percentile with the median, the whiskers indicate the maximum and minimum. a=statistically significant to THA, b=statistically significant to THA-coll, c= statistically significant to coll, d= statistically significant to GelMA, e=statistically significant to PVA, f= statistically significant to TCP, g= statistically significant to PCL.

that were cultured on the naturally derived materials THA, THA-coll, collagen and GelMA. Interestingly, neutrophils cultured on THA tend to secrete less than the neutrophils cultured on other natural materials, reaching statistical significance for OSM. Secretion of IL-8 was not different between neutrophils cultured on the different materials. Since the OLINK® panel did not include the important neutrophil regulator

MMP9, we separately analyzed this enzyme by ELISA. The secretion of MMP9 increased 5-17-fold depending on the material where the neutrophils were cultured, with an overall higher secretion in PVA, TCP and PCL (Suppl. Figure 5).

DISCUSSION

Although neutrophils are the most prevalent immune cells in the human body and the first responders to invaders, their role in triggering and resolving inflammation after biomaterial implantation is still scarcely understood. A first step in unraveling these mechanisms, consists of introducing methods to characterize the interaction of neutrophils with biomaterials. Therefore, we devised an *in vitro* model describing multiple functions of human primary neutrophils and investigated their variation after exposure to biomaterials.

To our knowledge, this is the first *in vitro* study comprehensively evaluating early neutrophil functions in response to a biomaterial. We selected a broad panel of assays to represent different neutrophil functions relevant for tissue repair: (1) survival (live-dead staining, metabolic activity, LDH release), (2) release of oxidative burst (ROS production), (3) MPO and elastase release and (4) the release of granules and inflammation related proteins (OLINK®). Each of these assays could distinguish specific differences in the response of neutrophils between biomaterials.

The proposed approach analyzing multiple neutrophil functions is of benefit towards understanding the possible consequences of biomaterial properties for tissue repair. Based on our results, metabolic activity of neutrophils was highest in PCL and TCP after 1 and 3 hours, in conjunction with elevated levels of LDH release in PCL, TCP and PVA and lower cell viability after 24 hours. Serum was not added to cell culture media to prevent possible effects of serum proteins on neutrophil activation, that could mask the specific biomaterials effect. The role of serum in influencing the interaction between neutrophils and biomaterials is a crucial point requiring further investigation. Previous studies investigated the effects of physicochemical properties like size, shape, surface topography, wettability and surface charge on neutrophils, suggesting that these features might play a role in neutrophil survival and activation¹⁴. The low viability of neutrophils on PCL might be due to low adhesion on the hydrophobic surface because of the serum-free conditions, implying lower levels of protein coating on all substrates. Interestingly, in presence of serum hydrophobic surfaces are prone to marked protein absorption, fostering survival or activation of neutrophils^{14, 30}. Although TCP is also intrinsically hydrophobic, plates for tissue culture

are surface treated to increase hydrophilicity and thereby cell adhesion. Unlike for other cell types, identifying a standard substrate for neutrophil cell culture to study their interaction with materials is not straightforward, because every material will inevitably influence neutrophils activation. Consequently, our experiments and data analysis compared the response on different materials rather than against a chosen standard. After 24 hours the survival of neutrophils on a hydrophilic PVA (hydrogel) surface was lower than on hydrogels consisting of naturally derived macromolecules with matched mechanical properties. Therefore, chemical composition of materials also plays a role in neutrophil survival. This difference in response is further supported by the elevated levels of LDH that were found in the supernatant of neutrophils cultured on the aforementioned synthetic materials. After 24 hours, LDH levels were significantly increased indicating higher levels of cell membrane damage or cell death for neutrophils cultured on synthetic materials in comparison to naturally derived materials. The high levels of LDH in PCL, PVA and TCP indicate that the prevalent form of cell death is necrosis rather than apoptosis or other types of programmed cell death. In apoptosis the cell-membrane is still intact in contrast with necrosis where a damaged cell-membrane results in the release of LDH ³¹. Whether a cell will undergo necrosis, or the more regulated apoptosis depends on what stimulus the neutrophil receives ^{32, 33}. Neutrophil death by necrosis is usually a trigger for inflammation and a major cause of tissue damage ^{33, 34}. This may fuel an unwanted inflammatory response after the implantation of a biomaterial. After 24 hours on the natural materials, almost all neutrophils were alive and released little LDH indicating that they might be in an activated but still living state.

The present study was limited to investigating the early response to biomaterials because, *in vivo*, at later time points, neutrophils recruit and activate additional leukocytes, such as macrophages by releasing pro-inflammatory mediators and thereby promote tissue repair ³⁵. Therefore, neutrophils that are cultured on substrates from naturally derived materials might still be secreting factors to attract cells needed for the repair to the material and thereby eventually promote tissue repair. The aforementioned examples highlight the importance to compare different assays related to viability, only the entire panel of assays will allow to understand the neutrophil response over time.

Once activated, neutrophils do not necessarily directly undergo cell death. Instead, they may respond with other effector functions such as cytokine release, degranulation and pathogen destruction by the release of ROS ³⁵. ROS production, i.e. oxidative burst, is an important and powerful mechanism in the defense against bacterial and fungal infections ³⁶. Besides their role in antimicrobial clearing, ROS are also important

in the regulation of inflammation³⁷. The oxidative burst released by neutrophils can also help in the degradation of particles previously internalized. In our model, we observed clear differences between materials in the production of superoxide anion, a prominent specie within the ROS family. Neutrophils seeded on the naturally derived materials showed higher ROS secretion compared to synthetic ones, especially after 3 hours. If the oxidative burst is sustained for an extended period of time, it can also contribute to inflammatory damage of the tissue surrounding the implanted material¹⁷. It has also been shown that ROS production leads to neutrophil apoptosis, indicating that neutrophils releasing high amounts of ROS might undergo this form of programmed cell-death³⁸. Neutrophil death by apoptosis in turn is critical for the resolution of inflammation by the polarization of pro-inflammatory macrophages into anti-inflammatory macrophages^{14, 39}. This process is essential for the final outcome of tissue healing and biomaterial integration. Future studies should determine whether the high levels of ROS produced by neutrophils on natural materials indeed lead to this change in polarization state. One limitation of our study is that superoxide anion is only one of several ROS, and future studies should investigate a broader spectrum of ROS production. Given the inherent ROS instability and the lack of off-the-shelf assays, this might prove non-trivial.

Besides cell survival and producing an oxidative burst, neutrophils can release NETs in response to a variety of stimuli that can activate them. NETs are composed of a network of chromatin fibers that are covered with proteins such as neutrophil elastase and myeloperoxidase (MPO)⁴⁰. NET formation is one of the most interesting and unique aspects of neutrophil behavior. In our setup, neutrophils that were cultured on the synthetic materials PCL and PVA secreted 8-10 times higher levels of both MPO and neutrophil elastase. This might be indicative of increased neutrophils activation and NET formation on synthetic in comparison to natural materials, although other techniques such as direct imaging of the genetic material should be carried out to confirm NETosis. This finding is in line with a recent study that reported that coating PCL fibers with a HA based hydrogel alleviated the neutrophil elastase response compared to PCL fibers without coating⁴¹. At the same time, this highlights the potential to modulate the neutrophil response by selection of the biomaterials, therefore, it is important to understand the consequences of the response to different immune cells to biomaterials before we can actively modulate the neutrophil response. Besides being important as an antimicrobial defense, neutrophil elastase also acts as a protease and can cleave components of the extracellular matrix such as elastin⁴². High levels of neutrophil elastase can lead to degradation of the extracellular matrix of tissues surrounding the biomaterial and thereby compromise the integration and final outcome when a biomaterial is used. Next to neutrophil elastase MPO is

also an important molecule involved in the formation of NETS. MPO is known as an important neutrophil attractant ⁴³. This means that MPO secretion attracts more neutrophils to the implant site eventually leading to chronic inflammation that might impair tissue repair or stimulate the foreign body reaction. Furthermore, MPO has been demonstrated to be involved in tissue damage, and as such it plays a role in many inflammatory diseases ⁴⁴. For this reason, MPO is even considered as a new biomarker of inflammation in chronic inflammatory diseases like rheumatoid arthritis and ulcerative colitis ⁴⁵. Regarding the synthetic materials that demonstrated a higher release of MPO in our study, this could mean more inflammation and eventually even a risk of tissue damage at the implantation site. Given the clear difference between the two classes of materials in the neutrophil elastase and MPO response, these assays can be used to distinguish between the response a biomaterial elicits and eventually be helpful in choosing the biomaterial with the preferred immune response.

Neutrophils are increasingly acknowledged for their role in the regulation and development of inflammatory and immune responses. Besides the release of an oxidative burst, release of enzymes and the formation of NETs, neutrophils also secrete a large variety of cytokines and play a significant role in the development of inflammatory diseases and the foreign body reaction ¹⁹. It was, however, unclear if all these cytokines would also be involved in the response of neutrophils exposed to different biomaterials. For this reason, we screened a panel of 92 cytokines related to inflammation. In total, we found 19 cytokines to be secreted by neutrophils that were cultured on different materials. Amongst them common neutrophil cytokines such as VEGF-A, MMP9 and IL-8, but also less commonly studied proteins such as HGF, EN-RAGE, and uPA. Interestingly, further cytokine analysis showed a distinctive response between neutrophils cultured on synthetic materials and on natural materials. Four out of the six cytokines that were overall highest expressed in our set-up follow the trend in neutrophil response discussed before. Neutrophils on synthetic materials secrete higher amounts of VEGF-A, HGF, EN-RAGE, OSM compared to natural materials. The higher release of cytokines is accompanied by reduced cell survival and the release of MPO and elastase on these synthetic materials compared to natural materials. The difference in cytokine release on synthetic compared to natural materials might be even more pronounced considering the increase in dead cells in the synthetic materials. The lower cell viability in the synthetic materials (PCL and TCP) supports this assumption.

The high level of VEGF-A released by neutrophils indicate that neutrophils contribute to angiogenesis often related to inflammation and tissue injury. In a mouse model it was shown that VEGF-A expressing neutrophils are actors in inflammatory angiogenesis.

In an *in vitro* experiment the authors demonstrated that the release of VEGF from murine neutrophils was only present upon activation with phorbol-12-myristate 13-acetate ⁴⁶. VEGF-A released by activated neutrophils might recruit monocytes, stimulate macrophage polarization and thus contributing to the inflammatory response. Depending on the cytokines released by the neutrophils during the initial response, the foreign body reaction might be modulated. The mechanistic reasons for this behavior and the implications of these findings in tissue repair are still unclear, and should be subject of further investigations. Based on our results, cytokines commonly associated with neutrophils such as IL-6, IL-10, IL-17A, MCP-1, TNF ^{19, 47} were low or absent in the conditioned media, including the groups with the highest endotoxin level. This might suggest that under our experimental conditions the materials did not significantly activate neutrophils resulting in release of pro- or anti-inflammatory cytokines. More knowledge is needed on the role of the specific cytokines in tissue healing, as well as a potential synergistic or antagonistic effect they could have. A thorough understanding of these mechanisms could lead to a classification system for neutrophil function analog to what is commonly recognized for macrophages, whose phenotype can be classified as classically activated M1 (pro-inflammatory) or alternatively activated M2 (anti-inflammatory/repair) ⁴⁸. Attempts to introduce neutrophils classification in “N1 and N2 phenotype” have already been described, underlining a spectrum of specific neutrophil functions. Most of this research has been undertaken in the field of oncology identifying N1 as anti-tumoral and N2 as pro-tumoral neutrophils. However, this classification is still debated, together with the set of parameters that could be used to indicate neutrophil ^{11, 49}. A classification system to discriminate between a more pro- or anti-inflammatory response of neutrophils would help in the development and selection of biomaterials for specific applications. The prolonged release of pro-inflammatory cytokines and chemokines might stimulate chronic inflammation, and trigger macrophage recruitment and fusion on materials, which in turn may lead to an increased foreign body reaction. The extent to which *in vitro* response of neutrophils can predict the foreign body reaction can only be speculated and needs more studies *in vitro* and *in vivo* in future. One additional aspect to consider is the preservation of neutrophils phagocytic activity, and the role which could be played.

One possible bias in evaluating neutrophil behavior *in vitro* is the endotoxin content of the substrates analyzed. Our endotoxin assay revealed higher endotoxins for GelMa and THA. This is to be expected since their natural origin. Collagen is also of natural origin, however the strong acidic environment and thorough dialysis used for its extraction might have deactivated or removed the endotoxins. Despite the comparative higher level, the endotoxins in GelMa and THA are still at a low level

according to FDA guidelines⁵⁰. GelMA, which was the material displaying the highest endotoxins amount, could be safely administered up to 0.36 ml/kg with parenteral administration, corresponding to 25 ml for an individual weighing 70 kg in a single administration. Taking as a reference other recent FDA regulations for endotoxin levels in medical devices, the endotoxin level of the products should be below 0.5 EU/mL when the device is rinsed with 40 mL of non-pyrogenic water. Based on this, the endotoxin concentration of GelMA is approximately 0.067 EU/mL, which is less than the acceptable level⁵¹. Also, the maximum level in our experiments of 2.7 EU/ml (equal to 0.27 ng/ml) was lower than the 100 ng/ml described in literature for potential activation of neutrophils⁵². Additionally, GelMa and THA did not trigger a higher inflammatory response compared to the other materials, indicating that the results in our study should not have been biased by the endotoxin level.

In summary, there is a gap of knowledge concerning neutrophils interaction with biomaterials, what this means for foreign body response and tissue regeneration, and how to design biomaterials to modulate this process. This study is a step towards further investigations in this direction, and introduces a series of experimental methods to assess initial response of neutrophils to different biomaterials. This method was applied to a selection of naturally derived and synthetic polymeric biomaterials, identifying clear differences between the substances tested. The overall trend showed increased neutrophil survival on naturally derived constructs, together with higher oxidative burst, decreased MPO and elastase release, and cytokine secretion compared to neutrophils on synthetic materials. Neutrophils have the potential to be exploited in foreign body reaction biomaterial guided tissue repair strategies with the ability to modulate inflammation based on their response to biomaterials. Neutrophils are an under-investigated target in this context, and further studies are necessary to unravel mechanistic aspects of their response to materials and the biological implications for tissue healing. Future studies should address the complex interaction of neutrophils with other immune cells in innate and adaptive immunity. Unraveling these mechanisms, has the potential to open new avenues in biomaterial design.

Supplementary Table S1. All proteins analyzed by OLINK technology

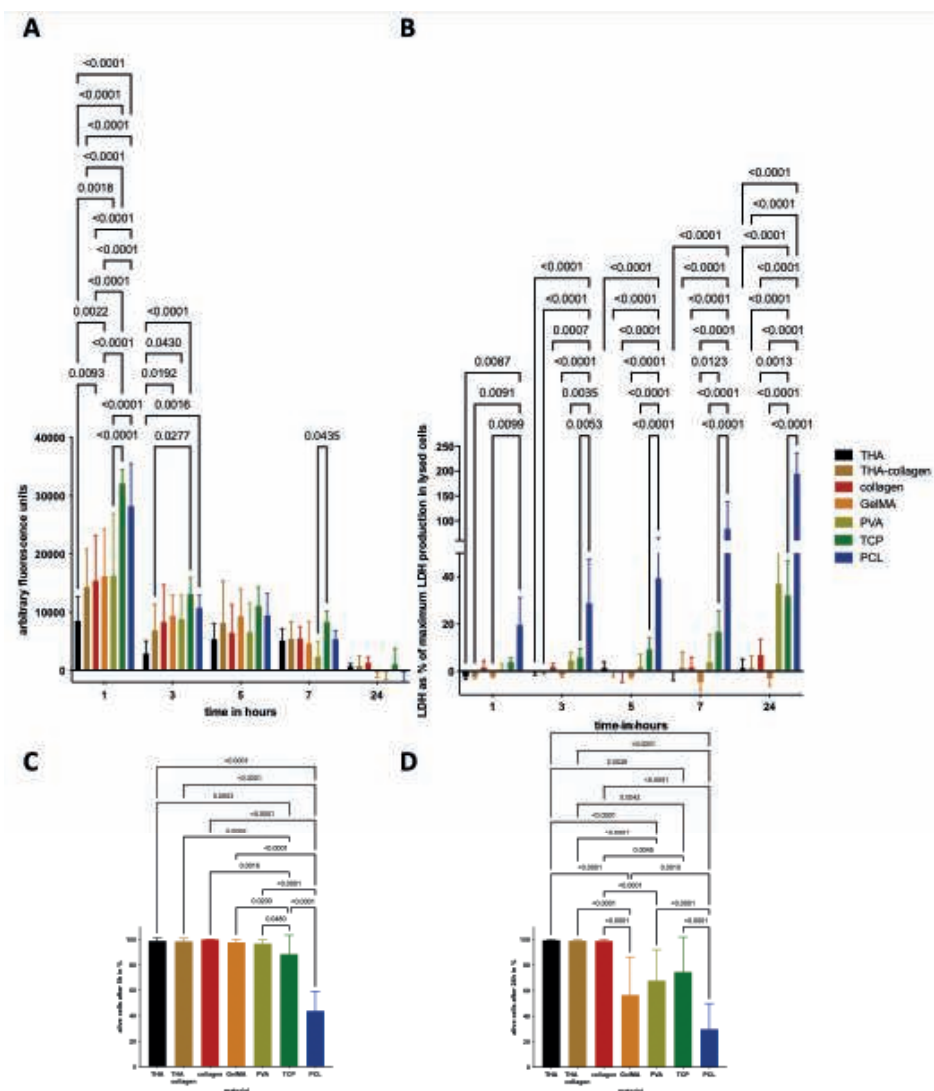
Adenosine Deaminase (ADA)	Fibroblast growth factor 19 (FGF-19)	Interleukin-17C (IL-17C)	Osteoprotegerin (OPG)
Artemin (ARTN)	Fibroblast growth factor 21 (FGF-21)	Interleukin-18 (IL-18)	Programmed cell death 1 ligand 1 (PD-L1)
Beta-nerve growth factor (Beta-NGF)	Fibroblast growth factor 23 (FGF-23)	Interleukin-18 receptor 1 (IL-18R1)	Protein S100-A12 (EN-RAGE)
Caspase 8 (CASP-8)	Fms-related tyrosine kinase 3 ligand (Flt3L)	Interleukin-20 (IL-20)	Signaling lymphocytic activation molecule (SLAMF1)
C-C motif chemokine 4 (CCL4)	Fractalkine (CX3CL1)	Interleukin-20 receptor subunit alpha (IL-20RA)	SIR2-like protein (SIRT2)
C-C motif chemokine 19 (CCL19)	Glial cell line-derived neurotrophic factor (GDNF)	Interleukin-22 receptor subunit alpha-1 (IL-22RA1)	STAM-binding protein (STAMPB)
C-C motif chemokine 20 (CCL20)	Hepatocyte growth factor (HGF)	Interleukin-24 (IL-24)	Stem cell factor (SCF)
C-C motif chemokine 23 (CCL23)	Interferon gamma (IFN-gamma)	Interleukin-33 (IL-33)	Sulfotransferase 1A1 (ST1A1)
C-C motif chemokine 25 (CCL25)	Interleukin-1 alpha (IL-1 alpha)	Latency-associated peptide transforming growth factor beta 1 (LAP TGF-beta-1)	T-cell surface glycoprotein CD5 (CD5)
C-C motif chemokine 28 (CCL28)	Interleukin-2 (IL-2)	Leukemia inhibitory factor (LIF)	T-cell surface glycoprotein CD6 isoform (CD6)
CD40L receptor (CD40)	Interleukin-2 receptor subunit beta (IL-2RB)	Leukemia inhibitory factor receptor (LIF-R)	T-cell surface glycoprotein CD8 alpha chain (CD8A)
CUB domain-containing protein 1 (CDCP1)	Interleukin-4 (IL-4)	Macrophage colony-stimulating factor 1 (CSF-1)	Thymic stromal lymphopoietin (TSLP)
C-X-C motif chemokine 1 (CXCL1)	Interleukin-5 (IL-5)	Macrophage inflammatory protein 1-alpha (CCL3)	TNF-beta (TNFB)
C-X-C motif chemokine 5 (CXCL5)	Interleukin-6 (IL-6)	Matrix metalloproteinase-1 (MMP-1)	TNF-related activation-induced cytokine (TRANCE)
C-X-C motif chemokine 6 (CXCL6)	Interleukin-7 (IL-7)	Matrix metalloproteinase-10 (MMP-10)	TNF-related apoptosis-inducing ligand (TRAIL)
C-X-C motif chemokine 9 (CXCL9)	Interleukin-8 (IL-8)	Monocyte chemotactic protein 1 (MCP-1)	Transforming growth factor alpha (TGF-alpha)
C-X-C motif chemokine 10 (CXCL10)	Interleukin-10 (IL-10)	Monocyte chemotactic protein 2 (MCP-2)	Tumor necrosis factor (Ligand) superfamily, member 12 (TWEAK)
C-X-C motif chemokine 11 (CXCL11)	Interleukin-10 receptor subunit alpha (IL-10RA)	Monocyte chemotactic protein 3 (MCP-3)	Tumor necrosis factor (TNF)

Supplementary Table S1. All proteins analyzed by OLINK technology (*continued*)

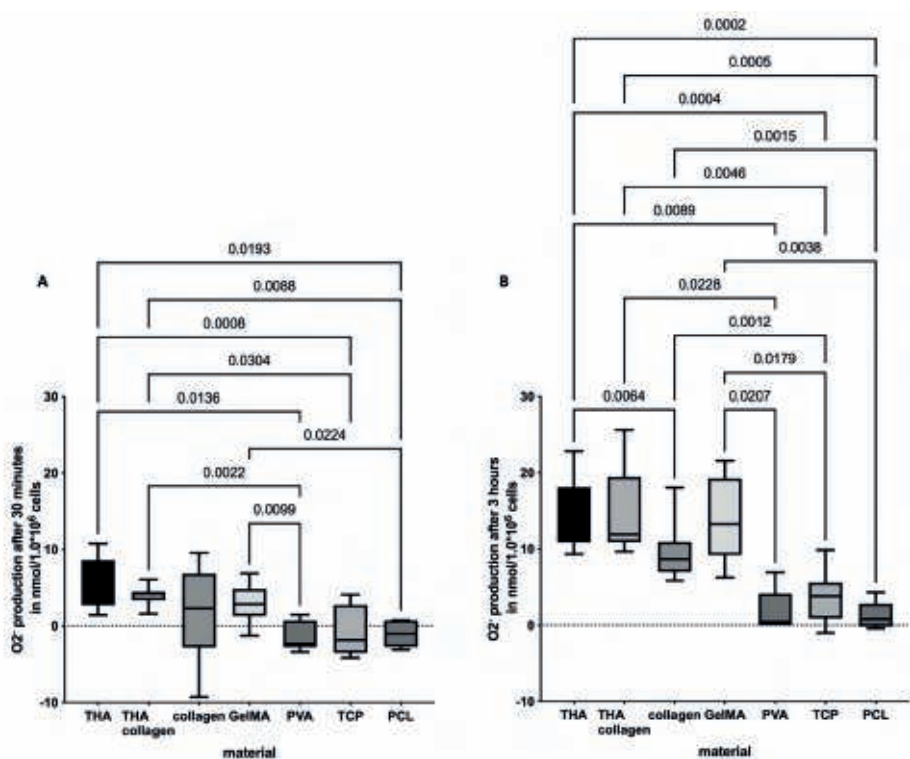
Cystatin D (CST5)	Interleukin-10 receptor subunit beta (IL-10RB)	Monocyte chemotactic protein 4 (MCP-4)	Tumor necrosis factor ligand superfamily member 14 (TNFSF14)
Delta and Notch-like epidermal growth factor-related receptor (DNER)	Interleukin-12 subunit beta (IL-12B)	Natural killer cell receptor 2B4 (CD244)	Tumor necrosis factor receptor superfamily member 9 (TNFRSF9)
Eotaxin-1 (CCL11)	Interleukin-13 (IL-13)	Neurotrophin-3 (NT-3)	Urokinase-type plasminogen activator (uPA)
Eukaryotic translation initiation factor 4E-binding protein 1 (4E-BP1)	Interleukin-15 receptor subunit alpha (IL-15RA)	Neurturin (NRTN)	Vascular endothelial growth factor A (VEGF-A)
Fibroblast growth factor 5 (FGF-5)	Interleukin-17A (IL-17A)	Oncostatin-M (OSM)	

Supplementary Table S2. Proteins detected in >75% of the samples

Protein detected in >75% of samples	
IL8	MMP1
VEGF-A	IL18R1
uPA	CXCL5
IL6	HGF
MCP1	CCL3
OSM	EN-RAGE
CXCL1	CD40
CCL4	ADA
IL18	CSF1
TNFSF14	

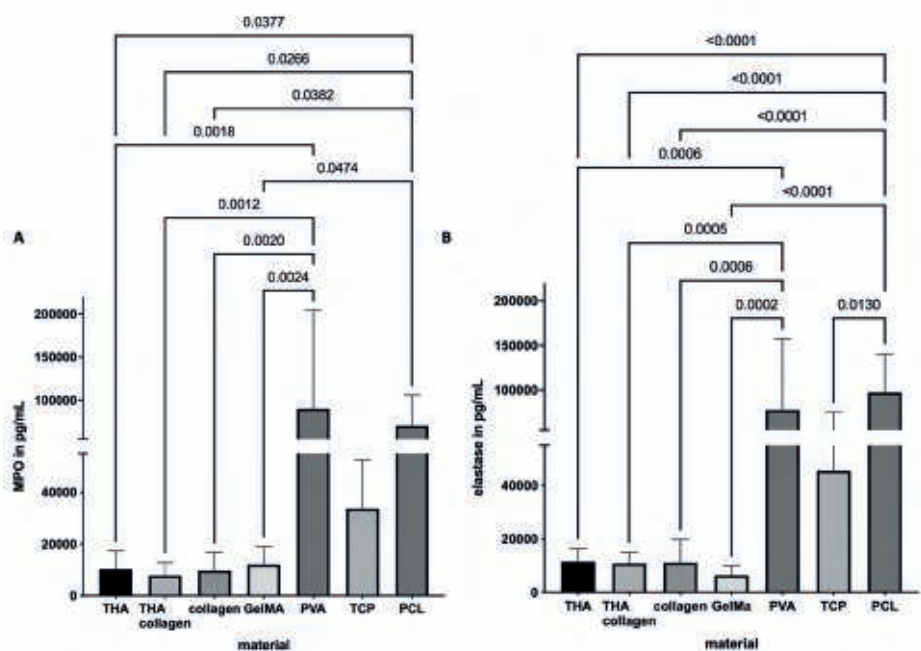


Supplementary Figure 1. Neutrophil activity and cell survival on different materials
A) Metabolic activity of neutrophils expressed as fluorescence units over time and among different materials. B) LDH release by neutrophils cultured on different materials expressed as a percentage of the maximum amount of LDH release after cell lysis. C) The percentage of alive cells after 5 hours. D) The percentage of alive cells after 24 hours. Each bar represents the mean of 5 donors + SD. Abbreviations: LDH, lactate dehydrogenase.



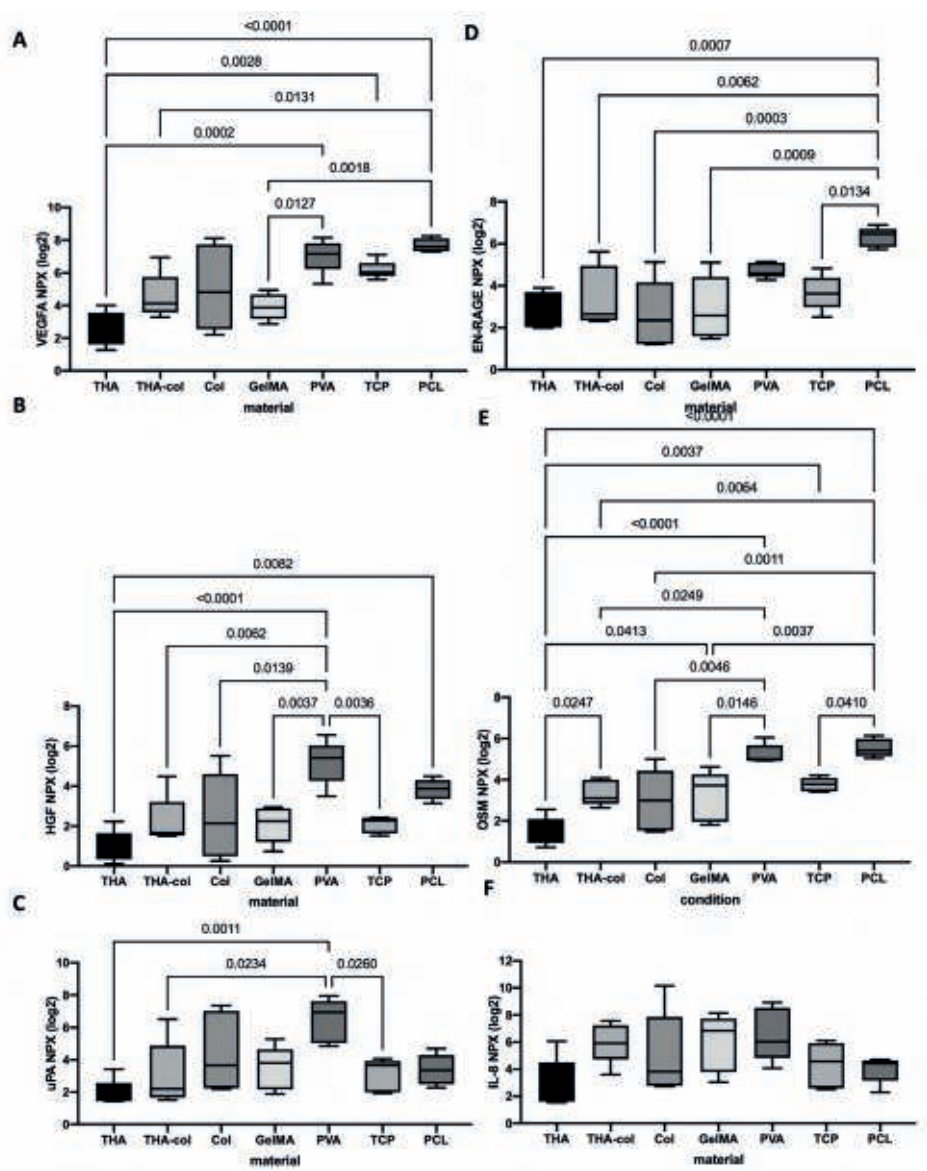
Supplementary Figure 2. Superoxide anion production by neutrophils cultured on different materials

Superoxide anion production after A) 30 minutes and B) 3 hours of culture. Box plots represent the 25th and 75th percentile with the median, the whiskers indicate the maximum and minimum.



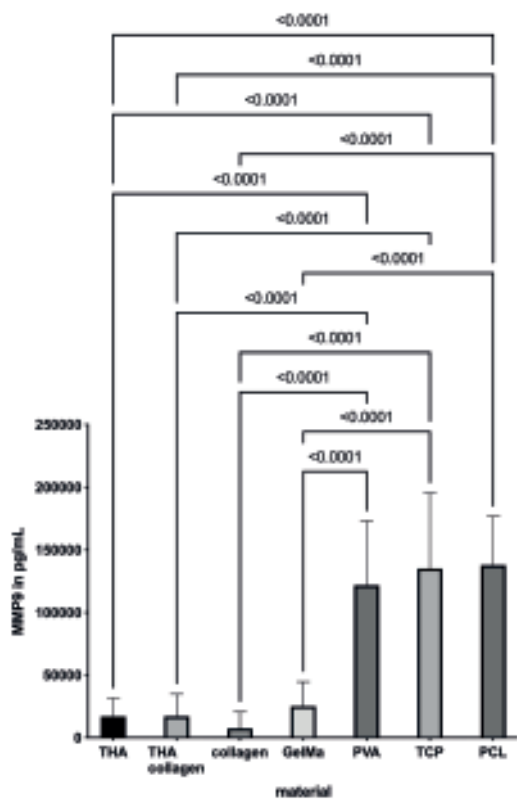
Supplementary Figure 3. The release of neutrophil extracellular trap components on different materials

The release of A) MPO in pg/ml and B) neutrophil elastase in pg/ml by neutrophils cultured on different materials. Each bar represents the mean level + SD. Abbreviations: MPO, myeloperoxidase.



Supplementary Figure 4. Analysis of cytokine secretion by neutrophils using the OLINK technology

A-F) Box plots showing the level of A) VEGFA, B) HGF, C) uPA, D) EN-RAGE, E) OSM, and F) IL-8. Box plots represent the 25th and 75th percentile with the median, the whiskers indicate the maximum and minimum.



Supplementary Figure 5. MMP9 secretion by neutrophils
The secretion of MMP9 in pg/ml by neutrophils cultured on different materials. Each bar represents the mean level of MMP-9 + SD.

REFERENCES

1. Hench LL, Thompson I. Twenty-first century challenges for biomaterials. *J R Soc Interface*. 2010;7 Suppl 4(Suppl 4):S379-91.
2. Anderson JM, Rodriguez A, Chang DT. Foreign body reaction to biomaterials. *Seminars in Immunology*. 2008;20(2):86-100.
3. Dziki JL, Badylak SF. Immunomodulatory biomaterials. *Current Opinion in Biomedical Engineering*. 2018;6:51-7.
4. Elisseeff SFBaJH. *Immunomodulatory Biomaterials*. Cambridge: Woodhead Publishing; 2021.
5. Summers C, Rankin SM, Condliffe AM, Singh N, Peters AM, Chilvers ER. Neutrophil kinetics in health and disease. *Trends Immunol*. 2010;31(8):318-24.
6. Fetz AE, Radic MZ, Bowlin GL. Neutrophils in Biomaterial-Guided Tissue Regeneration: Matrix Reprogramming for Angiogenesis. *Tissue Eng Part B Rev*. 2021;27(2):95-106.
7. Franz S, Rammelt S, Scharnweber D, Simon JC. Immune responses to implants-a review of the implications for the design of immunomodulatory biomaterials. *Biomaterials*. 2011;32(28):6692-709.
8. Sridharan R, Cameron AR, Kelly DJ, Kearney CJ, O'Brien FJ. Biomaterial based modulation of macrophage polarization: a review and suggested design principles. *Materials Today*. 2015;18(6):313-25.
9. Dancey JT, Deubelbeiss KA, Harker LA, Finch CA. Neutrophil kinetics in man. *J Clin Invest*. 1976;58(3):705-15.
10. Jaillon S, Ponzetta A, Di Mitri D, Santoni A, Bonecchi R, Mantovani A. Neutrophil diversity and plasticity in tumour progression and therapy. *Nature Reviews Cancer*. 2020;20(9):485-503.
11. Ohms M, Möller S, Laskay T. An Attempt to Polarize Human Neutrophils Toward N1 and N2 Phenotypes in vitro. *Front Immunol*. 2020;11:532.
12. Kovtun A, Bergdolt S, Wiegner R, Radermacher P, Huber-Lang M, Ignatius A. The crucial role of neutrophil granulocytes in bone fracture healing. *Eur Cell Mater*. 2016;32:152-62.
13. Bastian OW, Kuijper A, Koenderman L, Stellato RK, van Solinge WW, Leenen LP, et al. Impaired bone healing in multitrauma patients is associated with altered leukocyte kinetics after major trauma. *Journal of Inflammation Research*. 2016;9:69.
14. Ode Boni BO, Lamboni L, Souho T, Gauthier M, Yang G. Immunomodulation and cellular response to biomaterials: the overriding role of neutrophils in healing. *Materials Horizons*. 2019;6(6):1122-37.
15. Selders GS, Fetz AE, Radic MZ, Bowlin GL. An overview of the role of neutrophils in innate immunity, inflammation and host-biomaterial integration. *Regen Biomater*. 2017;4(1):55-68.
16. Kohno K, Koya-Miyata S, Harashima A, Tsukuda T, Katakami M, Ariyasu T, et al. Inflammatory M1-like macrophages polarized by NK-4 undergo enhanced phenotypic switching to an anti-inflammatory M2-like phenotype upon co-culture with apoptotic cells. *J Inflamm (Lond)*. 2021;18(1):2.

17. Mittal M, Siddiqui MR, Tran K, Reddy SP, Malik AB. Reactive oxygen species in inflammation and tissue injury. *Antioxid Redox Signal*. 2014;20(7):1126-67.
18. Papayannopoulos V, Metzler KD, Hakkim A, Zychlinsky A. Neutrophil elastase and myeloperoxidase regulate the formation of neutrophil extracellular traps. *J Cell Biol*. 2010;191(3):677-91.
19. Tecchio C, Micheletti A, Cassatella MA. Neutrophil-derived cytokines: facts beyond expression. *Front Immunol*. 2014;5:508.
20. Chang S, Popowich Y, Greco RS, Haimovich B. Neutrophil survival on biomaterials is determined by surface topography. *J Vasc Surg*. 2003;37(5):1082-90.
21. Kaplan SS, Basford RE, Jeong MH, Simmons RL. Mechanisms of biomaterial-induced superoxide release by neutrophils. *J Biomed Mater Res*. 1994;28(3):377-86.
22. Szponder T, Wessely-Szponder J, Sobczyńska-Rak A. The Neutrophil Response to Rabbit Antimicrobial Extract After Implantation of Biomaterial into a Bone/Cartilage Defect. In *Vivo*. 2018;32(6):1345-51.
23. Velard F, Laurent-Maquin D, Braux J, Guillaume C, Bouthors S, Jallot E, et al. The effect of zinc on hydroxyapatite-mediated activation of human polymorphonuclear neutrophils and bone implant-associated acute inflammation. *Biomaterials*. 2010;31(8):2001-9.
24. Loebel C, D'Este M, Alini M, Zenobi-Wong M, Eglin D. Precise tailoring of tyramine-based hyaluronan hydrogel properties using DMTMM conjugation. *Carbohydr Polym*. 2015;115:325-33.
25. Van Den Bulcke AI, Bogdanov B, De Rooze N, Schacht EH, Cornelissen M, Berghmans H. Structural and rheological properties of methacrylamide modified gelatin hydrogels. *Biomacromolecules*. 2000;1(1):31-8.
26. Pelletier M, Maggi L, Micheletti A, Lazzeri E, Tamassia N, Costantini C, et al. Evidence for a cross-talk between human neutrophils and Th17 cells. *Blood*. 2010;115(2):335-43.
27. Heissig B, Nishida C, Tashiro Y, Sato Y, Ishihara M, Ohki M, et al. Role of neutrophil-derived matrix metalloproteinase-9 in tissue regeneration. *Histol Histopathol*. 2010;25(6):765-70.
28. Rhee SH. Lipopolysaccharide: basic biochemistry, intracellular signaling, and physiological impacts in the gut. *Intest Res*. 2014;12(2):90-5.
29. Lakschevitz FS, Hassanpour S, Rubin A, Fine N, Sun C, Glogauer M. Identification of neutrophil surface marker changes in health and inflammation using high-throughput screening flow cytometry. *Exp Cell Res*. 2016;342(2):200-9.
30. Christo SN, Bachhuka A, Diener KR, Mierczynska A, Hayball JD, Vasilev K. The Role of Surface Nanotopography and Chemistry on Primary Neutrophil and Macrophage Cellular Responses. *Adv Healthc Mater*. 2016;5(8):956-65.
31. Chan FK, Moriwaki K, De Rosa MJ. Detection of necrosis by release of lactate dehydrogenase activity. *Methods Mol Biol*. 2013;979:65-70.
32. Turina M, Miller FN, McHugh PP, Cheadle WG, Polk HC, Jr. Endotoxin inhibits apoptosis but induces primary necrosis in neutrophils. *Inflammation*. 2005;29(1):55-63.
33. Presbitero A, Mancini E, Castiglione F, Krzhizhanovskaya VV, Quax R. Game of neutrophils: modeling the balance between apoptosis and necrosis. *BMC Bioinformatics*. 2019;20(6):475.

34. Grecian R, Whyte MKB, Walmsley SR. The role of neutrophils in cancer. *Br Med Bull*. 2018;128(1):5-14.
35. Brostjan C, Oehler R. The role of neutrophil death in chronic inflammation and cancer. *Cell death discovery*. 2020;6(1):1-8.
36. Nguyen GT, Green ER, Mecsas J. Neutrophils to the ROScUE: Mechanisms of NADPH Oxidase Activation and Bacterial Resistance. *Frontiers in Cellular and Infection Microbiology*. 2017;7(373).
37. Dröge W. Free radicals in the physiological control of cell function. *Physiol Rev*. 2002;82(1):47-95.
38. Clément MV, Ponton A, Pervaiz S. Apoptosis induced by hydrogen peroxide is mediated by decreased superoxide anion concentration and reduction of intracellular milieu. *FEBS Lett*. 1998;440(1-2):13-8.
39. Diwanji N, Bergmann A. The beneficial role of extracellular reactive oxygen species in apoptosis-induced compensatory proliferation. *Fly (Austin)*. 2017;11(1):46-52.
40. Kaplan MJ, Radic M. Neutrophil extracellular traps: double-edged swords of innate immunity. *J Immunol*. 2012;189(6):2689-95.
41. Blum C, Taskin MB, Shan J, Schilling T, Schlegelmilch K, Teßmar J, et al. Appreciating the First Line of the Human Innate Immune Defense: A Strategy to Model and Alleviate the Neutrophil Elastase-Mediated Attack toward Bioactivated Biomaterials. *Small*. 2021;17(13):e2007551.
42. Korkmaz B, Moreau T, Gauthier F. Neutrophil elastase, proteinase 3 and cathepsin G: physicochemical properties, activity and physiopathological functions. *Biochimie*. 2008;90(2):227-42.
43. Klinke A, Nussbaum C, Kubala L, Friedrichs K, Rudolph TK, Rudolph V, et al. Myeloperoxidase attracts neutrophils by physical forces. *Blood*. 2011;117(4):1350-8.
44. Aratani Y. Myeloperoxidase: Its role for host defense, inflammation, and neutrophil function. *Archives of Biochemistry and Biophysics*. 2018;640:47-52.
45. Khan AA, Alsahli MA, Rahmani AH. Myeloperoxidase as an Active Disease Biomarker: Recent Biochemical and Pathological Perspectives. *Med Sci (Basel)*. 2018;6(2).
46. Gong Y, Koh DR. Neutrophils promote inflammatory angiogenesis via release of preformed VEGF in an in vivo corneal model. *Cell Tissue Res*. 2010;339(2):437-48.
47. Tamassia N, Bianchetto-Aguilera F, Arruda-Silva F, Gardiman E, Gasperini S, Calzetti F, et al. Cytokine production by human neutrophils: Revisiting the “dark side of the moon”. *Eur J Clin Invest*. 2018;48 Suppl 2:e12952.
48. Italiani P, Boraschi D. From monocytes to M1/M2 macrophages: phenotypical vs. functional differentiation. *Frontiers in immunology*. 2014;5:514.
49. Fridlender ZG, Sun J, Kim S, Kapoor V, Cheng G, Ling L, et al. Polarization of tumor-associated neutrophil phenotype by TGF-beta: “N1” versus “N2” TAN. *Cancer Cell*. 2009;16(3):183-94.
50. Administration UFaD. Bacterial Endotoxins/Pyrogens 1985 [Available from: <https://www.fda.gov/inspections-compliance-enforcement-and-criminal-investigations/inspection-technical-guides/bacterial-endotoxinspyrogens>].

51. FDA Limits Medical Devices [Available from: https://www.fda.gov/regulatory-information/search-fda-guidance-documents/guidance-industry-pyrogen-and-endotoxins-testing-questions-and-answers#_Toc315937935].
52. Soler-Rodriguez AM, Zhang H, Lichenstein HS, Qureshi N, Niesel DW, Crowe SE, et al. Neutrophil activation by bacterial lipoprotein versus lipopolysaccharide: differential requirements for serum and CD14. *J Immunol.* 2000;164(5):2674-83.

7

Discussion

The research described in this thesis focused on the use of an endogenous approach to stimulate the cell free repair of osteochondral defects, and sought to understand the complex interactions between mesenchymal stromal cell migration, inflammation and biomaterials. This understanding is crucial for the optimization of endogenous repair strategies for osteochondral defects.

The complex relationship between inflammation and osteochondral repair

The repair of osteochondral defects is a complex process that occurs in a tissue environment generally characterised by inflammation ^{1,2}. In joints with cartilage damage, the intra-articular environment is frequently disturbed and accompanied by synovial inflammation ³. Acute joint trauma leads to an increase in cytokine levels, which remain elevated if the damage is not fully repaired ^{4,5}. Synovial fluid obtained from patients with rheumatoid arthritis (RA), an autoimmune disorder characterized by high levels of inflammatory cytokines was found to inhibit chondrogenesis in subchondral MSCs ⁶. Similar, synovium conditioned medium from OA patients (a more 'chronic' inflammatory situation) inhibited MSC chondrogenesis ⁷. In contrast, synovial fluid collected from controls did not exhibit such inhibitory effects ⁶. Similar to the inflammatory situation in RA and OA, synovial fluid from injured knee joints also inhibited cartilage-related matrix synthesis ⁸. Apparently, synovial fluid contains chondrogenesis promoting factors. However, the positive effect of these factors may be inhibited by the concurrent presence of inflammation in the joint environment. Interestingly, studies in mice have shown that the absence of pro-inflammatory molecules like TNF- α and COX-2 can delay bone healing, implying that inflammation is essential for tissue repair ^{9,10}. This idea is supported by a previous study showing that exposure of human MSCs to TNF- α in the early phase of *in vitro* culture, can boost chondrogenesis ¹¹. However, excessive inflammation may inhibit MSC chondrogenesis in models of OA and traumatically injured joints ^{12,13}. This stresses the need to resolve or reduce inflammation at some point for optimal tissue repair. The importance of anti-inflammatory cytokines in cartilage repair has been widely documented ^{14,15}. It is important, to note that joint inflammation is a multifaceted phenomenon and cannot be attributed to a single factor. It is likely the result of a complex interplay between both pro-inflammatory and anti-inflammatory cytokines. As such, targeting a single cytokine for inhibition or stimulation may not be the most effective approach ¹⁶. Instead, for optimal joint repair, efforts should be directed towards modulating the cytokine "cocktail". One strategy for modulating the composition of the "cocktail" of pro- and anti-inflammatory factors contributing to joint inflammation is the administration of anti-inflammatory drugs, such as triamcinolone acetonide (TAA).

As demonstrated in **chapter 2** the application of TAA *in vitro* led to the inhibition of multiple pro-inflammatory markers and stimulation of anti-inflammatory markers in the synovium. Additionally, results in **chapter 3** from an osteochondral defect mouse model showed that intra-articular TAA injection resulted in less synovial inflammation compared to saline-injected mice, which aligns with findings from previous studies in arthritis rodent models ^{17,18}. In some cases, TAA injection even reduced inflammation to levels comparable to those observed in healthy, non-operated joints, which is consistent with reports of reduced mononuclear cell infiltration and intimal hyperplasia in response to TAA ¹⁹⁻²¹. These changes in pro- and anti-inflammatory factors may promote a more favorable joint environment.

Most studies on inflammation and osteochondral tissue repair have focused on chondrogenesis or osteogenesis. For endogenous osteochondral repair to happen, the first stages should involve attracting progenitor cells capable of generating new tissue. MSCs have been observed to migrate towards sites of inflammation in various studies covering wounds and tumor environments ^{22,23}. The migratory capacity of MSCs has been shown to be stimulated by several factors present in joints with cartilage defects ²⁴. These factors have been extensively studied individually and have collectively been demonstrated to have a positive impact on MSC migration. However, the impact of modulating inflammation on MSC migration towards the defect site has not been widely studied. In **chapter 2**, we evaluated MSC migration in response to conditioned medium from synovium modulated with TAA. The data collected showed that MSC migration was higher in response to medium conditioned by TAA-modulated synovium compared to unmodulated synovium. In **chapter 3**, we observed infiltration of undifferentiated spindle-shaped cells into the defect site in an osteochondral defect model in mice, indicating migration of bone marrow-residing MSCs. However, no difference was observed in cell density or defect filling between the saline and TAA group after 10 days, suggesting TAA did not impact cell migration or proliferation in the defect. This discrepancy may be due to the (length of) exposure to TAA, which has been shown in previous studies to reduce chondrocyte viability and inhibit cell migration after a longer exposure period ²⁵⁻²⁸. In those studies, the exposure to TAA varied from 4 to 14 days and was thereby very likely comparable to the exposure time applied in **chapter 3**, but much longer than the 16 hours used in the study described in **chapter 2**, possibly explaining the discrepancy between the observed results. The exposure of MSCs/chondrocytes to TAA for a longer period might have overruled the beneficial effect of modulating inflammation that could be beneficial in the migration process. This knowledge should be taken into consideration when using TAA in a clinical setting, especially since in human joints TAA can be detected in the joint up to 2-3 weeks after injection ²⁹.

The findings in **chapter 3** further support this idea. The tissue filling the osteochondral defect consisted of chondrocyte-like cells encased in a thionine-stained matrix. Although the median Pineda cartilage repair score was comparable between mice treated with TAA after 1 day and the control mice injected with saline, a significantly smaller percentage of the defect area was filled in the TAA-treated mice. Additionally, a significantly lower proportion of the filled defect area stained positively for type II collagen in TAA-treated mice, suggesting that intra-articular TAA injection inhibits osteochondral repair. Previous studies have demonstrated that the use of anti-inflammatory compounds, such as a protein kinase inhibitor or TNF- α inhibitor, during the early stages of chondrogenesis can inhibit cartilage formation^{30,31}. This could explain the decrease in type II collagen deposition observed in our study, as we administered the anti-inflammatory compound during the early stages of new cartilage formation in the defect site. Further investigation, including serological measurements of synovial fluid and analysis of the composition of inflammatory cells within the synovial membrane over time, is necessary to better understand the role of modulating joint inflammation in osteochondral repair and determine the optimal timing of this step.

The impact of TAA on articular cartilage remains a subject of ongoing debate in the field of orthopaedics. Studies examining the effect of TAA on cartilage in both healthy and OA joints have produced conflicting results. One study reported dose-dependent degenerative changes in the cartilage of healthy rabbit knees following weekly injections of 3 mg TAA for 2-6 weeks³². Another study found increased cartilage degeneration, as indicated by higher Mankin scores, in surgically anterior cruciate ligament and meniscus destabilized rat knees treated with the extended-release form of TAA²⁷. These findings align with the reduced type II collagen deposition and decreased filling of the defect observed in **chapter 3**. However, in a collagenase-induced OA rat model, TAA in either bolus or extended-release form had no effect on cartilage degeneration¹⁸. Frisbie and colleagues found less cartilage degeneration, as indicated by lower Mankin scores, following two intra-articular doses of 12 mg TAA administered 13 and 27 days after surgical induction of osteochondral fractures in equine carpal bones¹⁹. Notably, the effects were most pronounced when TAA was injected into the contralateral (uninjured) joint rather than the diseased joint, indicating that low concentrations of TAA may have beneficial effects. The extended presence of TAA in the joint and higher concentrations of TAA may have detrimental effects on the cartilage, as seen in the study of Rudnik et al.²⁷, although this may vary depending on the joint pathology. The current evidence is conflicting and suggests both beneficial and harmful impacts on the cartilage³³. Further research is necessary to explore whether other drugs can effectively reduce inflammation and improve MSC migration.

The role of anti-inflammatory and repair macrophages in osteochondral repair and its potential as therapeutic target

Chapter 2 presents the impact of modulation of synovial inflammation on MSC migration. The synovium, a critical component in joint inflammation and wound healing, contains a high number of macrophages, which play a vital role in osteochondral repair³⁴⁻³⁶. To create a more favorable cartilage repair environment, we aimed to target and modulate the macrophages in the synovium using TAA. Our results showed that secreted factors released by all macrophage phenotypes stimulate MSC migration. Additionally, we observed a shift in the synovium towards an anti-inflammatory state. This shift in phenotype is consistent with previous studies that have shown that glucocorticoids, such as dexamethasone and methylprednisolone, can modify the polarization state of pro-inflammatory macrophages into a more anti-inflammatory phenotype³⁷⁻³⁹. Moreover, glucocorticoids have been shown to promote the differentiation of naïve monocytes into an anti-inflammatory macrophage phenotype, which could further enhance the effect seen⁴⁰. It is yet to be determined whether these mechanisms play a role when glucocorticoids are applied to the joint rather than in an *in vitro* setting.

In **chapter 2**, we observed that modulation of repair- and anti-inflammatory macrophages led to a two- to three-fold increase in MSC migration. Conversely, modulation of pro-inflammatory macrophages and synovial fibroblasts did not show any significant effect on MSC migration. These findings suggest that the enhancement of MSC migration is attributed specifically to the role of repair- and anti-inflammatory macrophages. Hence, shifting the polarization state from pro-inflammatory to anti-inflammatory macrophages could represent a promising avenue for boosting MSC migration during endogenous osteochondral repair. However, the suitability of TAA as a modulatory tool for this purpose remains controversial as outlined earlier in this discussion. As an alternative approach to TAA, BMP-2 can be used as research has suggested that BMP-2 may lower the expression of pro-inflammatory macrophage markers and encourage macrophages transition towards a tissue repair phenotype⁴¹. In our semi-orthotopic model in **chapter 5**, the number of pro-inflammatory macrophages was found to be lower in the BMP-2 condition compared to the scaffold-only condition after 4 weeks. In addition to regulating the immune system, BMP-2 may also promote cell migration, chondrogenesis, and osteogenesis^{41,42}. Given the significance of shifting from a pro-inflammatory to an anti-inflammatory macrophage phenotype, the regulatory effect of BMP-2 may serve as another potential mechanism for promoting early-phase osteochondral repair by both stimulating migration of MSC and enhancing tissue formation through the transitioning of macrophage phenotype. Future research should focus on exploring therapeutic strategies that can specifically

target repair- and anti-inflammatory macrophages without negatively impacting the overall cartilage homeostasis.

In addition to their positive impact on MSC migration, anti-inflammatory and repair macrophages can also increase the cartilage-forming capacity of MSCs⁴³. These macrophages produce anti-inflammatory factors, such as IL-4, IL-10, and IL-1RA, as well as pro-chondrogenic factors like TGF- β and IGF^{7,44,45}. Meanwhile, pro-inflammatory macrophages from the synovium produce factors like TNF- α and IL-1 β , that inhibit MSC chondrogenesis and contribute to synovial tissue catabolism by promoting production of matrix degrading enzymes^{7,46,47}. Anti-inflammatory cytokines, such as IL-4 that can block TNF- α and IL-1 β production, and IL-10 that can enhance expression of type II collagen and glycosaminoglycan, have been shown to play a crucial role in cartilage repair promoting chondrogenesis^{14,48}. Previous studies have highlighted the potential of using IL-4 for cartilage protection. By overexpressing IL-4 locally, the activation of MMPs precursors can be blocked, thereby preventing the destruction of cartilage caused by MMPs⁴⁹. This further supports the idea of modulating pro-inflammatory macrophages towards a more anti-inflammatory and repair phenotype to improve the outcome of endogenous cartilage repair strategies. Overall, our results provide insight into the potential of modulation of inflammation and specifically modulating pro-inflammatory macrophages towards an anti-inflammatory phenotype to create a favorable environment for osteochondral repair.

Modification of biomaterials to improve osteochondral repair

Biomaterials have played a crucial role in the advancement of orthopedic surgery, offering novel solutions for the repair of osteochondral defects⁵⁰⁻⁵². The development of scaffolds that mimic the natural extracellular matrix has paved the way for the regeneration of osteochondral tissue. Cell-free material-based approaches to treat defects are desirable due to the scarcity of autologous chondrocytes and the benefits of performing a single-stage procedure. In cell-free approaches, the infiltration of surrounding cells into the biomaterial is essential for matrix deposition and effective osteochondral repair⁵³. However, the limited invasion of MSCs into cell-free biomaterials remains a challenge⁵⁴⁻⁵⁶. To address this issue, we explored two strategies: modifying the properties of biomaterials and incorporating biologic factors into the biomaterial.

Hydrogels have emerged as a promising material in cartilage repair due to their cartilage-like features, including three-dimensional hydrophilic polymer networks that can absorb large amounts of water, high mechanical strength, good reproducibility, and

biocompatibility when used in combination with natural polymers such as hyaluronan, gelatin, collagen, chitosan, and alginate^{57,58}. The mechanical properties, swelling rate, degree of functionalization, pore size, and biodegradability of hydrogels can be modified to suit a variety of biomedical applications. The most important aspect in cell-free therapeutic approaches for osteochondral repair is to allow the migration of surrounding MSCs and chondrocytes and induce their participation in repair^{59,60}.

In **chapter 4** we investigated the effect of different modifications of three hydrogels on osteochondral repair. We found that the use of a MMP degradable crosslinker in NorHA hydrogels resulted in significantly more tissue formation than a DTT crosslinker. Additionally, the addition of collagen to hyaluronan hydrogels demonstrated a trend towards enhanced migration of MSCs and chondrocytes compared to pure hyaluronan, likely due to the cell adhesion sites present in collagen that facilitate cell infiltration into the material⁶¹. This concept of adding collagen to enhance cell adhesion may be relevant to other materials facing limitations with cell adhesion, such as synthetic biodegradable polymers. The combination of natural and synthetic materials in composite biomaterials can result in a material with superior mechanical properties, bio-functionality, and controllable degradability, thus providing the benefits of both synthetic polymeric and natural materials. In the studies in **chapter 4**, the repair tissue formed within the osteochondral defect was insufficient, with a low overall percentage of the defect that was filled and a particularly low amount of cartilage and bone-like tissue. The observed inadequate tissue formation may be attributed to challenges in cellular infiltration into the material. Our findings suggest that the difficulty of cells invading the material might be due to the small mesh size of the hydrogels used. The mesh size and pore connectivity of the network are critical parameters in 3D cell migration, as they directly affect the physical presence and mobility of cells⁶². A previous study has shown that a larger mesh size leads to more cell migration⁶³. An earlier *in vitro* investigation comparing GelMA with diverse degrees of functionalization demonstrated that more functionalization was associated with lower cell migration^{64,65}. As a higher degree of functionalization can lead to smaller pore sizes, this might be an important factor to keep in mind in biomaterial design⁶⁶. Based on a study utilizing PLGA scaffolds, it was found that the optimal pore size for cartilage falls within the range of 100-200 μm , and for bone it is between 300-450 μm ⁶⁷. This data suggests that hydrogels may not be the most suitable choice for osteochondral repair without the use of cells, due to their smaller pore/mesh size which prevents optimal infiltration and tissue formation of MSCs. Moreover, in the context of osteochondral repair, it is essential to design a biomaterial construct that can address the unique requirements of both cartilage and subchondral bone repair. One possible strategy to achieve this is to use a hybrid or biphasic biomaterial construct, in

which the component responsible for cartilage repair has a highly elastic modulus that can withstand pressure and resist friction, thereby facilitating extracellular matrix deposition. This can also promote chondrogenesis of MSCs while preventing undesired hypertrophic differentiation and contributing to chondrocyte mineralization. The other component of the construct responsible for subchondral bone repair should be capable of promoting the development of a vascular network within the biomaterial. This can help to facilitate nutrient transport, stimulate osteoblast proliferation, and provide robust support for the regeneration of the overlying cartilage. An example of such a scaffold is the one we employed in **chapter 5**, that contains a collagen layer for the cartilage region and a collagen-hydroxyapatite layer for the calcified tissue layers.

Another strategy to enhance cell migration within cell-free materials involves the use of chemotactic and growth factors. Recombinant human SDF-1 α is an example of a factor that has improved cell migration in fibrin and HA gels⁶⁸ and also the incorporation of IGF-1, and TGF- β 3 have been shown to improve cell migration into hydrogels⁶⁹⁻⁷¹. BMP-2 and PDGF-BB have also been observed to stimulate cell ingrowth⁷²⁻⁷⁸. These factors have been shown to enhance chondrogenesis, improve osteoblast function, and facilitate bone integration, making them suitable candidates for osteochondral repair⁷⁹⁻⁸³. In **chapter 5**, we incorporated these factors in a clinically-applied Col/Col-Mg-Hap scaffold used for osteochondral repair. In the *ex vivo* osteochondral defect model, the cell ingrowth into the scaffold was improved by both BMP-2 and PDGF-BB compared to the scaffold alone. Additionally, both BMP-2 and PDGF-BB addition resulted in a slightly greater amount of osteochondral tissue within the scaffold at the early repair phase of 4 weeks albeit still very limited. At the more mature stage of 8 weeks, there was no difference in osteochondral repair between the scaffold-only and BMP-2 or PDGF-BB-adsorbed conditions. This discrepancy could be due to the fact that the scaffold-only condition already demonstrated very good integrative repair, leaving little room for further improvement with the addition of BMP-2 and PDGF-BB. In the hydrogel setting, however, the incorporation of these chemotactic factors could be a valuable tool to further evaluate their potential in stimulating osteochondral repair, as in these acellular hydrogels there is still much room for improvement. Another example of a potential solution to improve cell infiltration and tissue repair is the use of a platelet-rich plasma (PRP), which has demonstrated improved chemotaxis and chondrogenesis of MSCs in a GelMA hydrogel⁸⁴. Besides the improvement in chemotaxis and chondrogenesis, the addition of PRP to GelMA polarized macrophages from a more pro-inflammatory to a more anti-inflammatory state which could have been the reason for improved osteochondral repair in line with the concept earlier in this discussion providing a very interesting candidate to

improve hydrogel assisted cell-free osteochondral repair. However, there are many techniques to produce PRP and the content of PRP is not very well controllable, which may lead to significant difference per application. Other strategies include adding chondro- and osteoinductive biochemical cues ⁸⁵, incorporating mineral ions such as calcium, magnesium, and zinc into biomaterial design ⁸⁶, gene targeting factors such as mRNA ⁸⁷, anti-inflammatory agents, and small compound drugs ⁸⁸, which have been demonstrated to have positive effects on osteochondral repair. Modifying biophysical properties of biomaterials alone, as done in this thesis, may be only the first step towards a fully controlled process of osteochondral repair. It is important to note that cell migration is a complex process regulated by multiple factors, including cell signaling pathways, extracellular matrix composition, and mechanical properties of the environment. In fact, biophysical modifications to biomaterials may influence some of these factors, they may not fully replicate the complexity of the native tissue environment. Nonetheless, it is important to evaluate small modifications to biomaterials as both biophysical and biochemical cues function synergistically to facilitate cartilage and bone regeneration ⁸⁹.

Another critical aspect of successful osteochondral repair is achieving strong interfacial adhesion between the biomaterial construct and the surrounding defect edges. Enhancing this adhesion is crucial to promote integration and ensure the long-term stability of the repair.

The inflammatory response in biomaterial-guided tissue repair

The outcome of tissue repair guided by biomaterials is closely tied to the body's innate immune response as biomaterials are recognized as foreign bodies upon implantation ⁹⁰. This leads to activation of the innate immune system and recruitment of immune cells such as neutrophils, monocytes, and macrophages ^{90,91}. The inflammatory response elicited by biomaterials can vary widely, and various design factors can modulate this response to foster functional tissue healing or regeneration ⁹².

In **chapters 4 and 5**, we evaluated the inflammatory response towards different implanted biomaterials *in vivo*. The results showed that hydrogels elicited only a minor foreign body reaction as demonstrated by only a few inflammatory cells on and within the hydrogels. Also, additional staining with F4/80 and MPO (data not shown) confirmed that implantation of the different hydrogels did not result in massive activation of macrophages and neutrophils. Notably, in **chapter 5**, four weeks following collagen/hydroxyapatite scaffold implantation, a marked inflammatory response was observed, characterized by the presence of neutrophils and macrophages surrounding and within

the scaffold. At this time point, there was limited osteochondral tissue formation, but after eight weeks, inflammation had fully subsided, and tissue repair was evident in all scaffolds, indicating that the resolution of inflammation over time may be essential for successful biomaterial-assisted tissue repair. One of our preliminary, unpublished experiments revealed that the absence of inflammation following implantation of the collagen-only layer of the Col/Col-Mg-Hap scaffold did not lead to cell infiltration nor tissue repair in the semi-orthotopic osteochondral defect model in mice after 8 weeks, while the collagen/HA layer, which induced more inflammation, demonstrated clear signs of tissue repair. This supports the notion that inflammation is necessary for successful osteochondral repair. Inflammation is known to influence cell migration as well as matrix degradation and therefore can be a factor influencing the ingrowth of cells in the biomaterial^{56,93-95}. To better understand the inflammatory response to biomaterials, it would be valuable to have tools to pre-screen the response prior to *in vivo* experiments. By doing so, we can ultimately tune the inflammatory response and improve the outcome of osteochondral repair.

After considerable focus on macrophages, the role of neutrophils in biomaterial-guided tissue repair has gained increasing attention⁹⁶. Neutrophils play a critical role in recruiting macrophages and facilitating the transition from pro-inflammatory to anti-inflammatory macrophages, a key factor in resolving inflammation and promoting tissue repair^{97,98}. This transition has been previously described in this thesis as an essential aspect for improving cell migration. Understanding the impact of neutrophils on osteochondral repair is crucial as they have been found to both aid and impair the repair process. Activated neutrophils can damage cartilage by releasing ROS and elastase, which degrade the GAG, suppress the proliferation and migration of chondrocytes, and induce cell death⁹⁹. In contrast, neutrophil-derived vesicles can counteract inflammation and promote cartilage protection by stimulating the production of TGF- β , a key player in chondrogenesis^{100,101}. These findings highlight the dual role of neutrophils in osteochondral repair and underscore the importance of understanding their impact. Despite their prominence as the most prevalent immune cells in the body, their function in response to biomaterial implantation remains poorly understood. In **chapter 6**, we established an *in vitro* model to assess various functions of human primary neutrophils in response to different materials. In comparison to natural materials, synthetic materials induce rapid neutrophil death, leading to high levels of LDH, ROS production, and the release of NET components such as MPO and neutrophil elastase. The high levels of LDH suggest that necrosis is the prevalent form of cell death, which can trigger inflammation and contribute to tissue damage^{102,103}. In addition, high levels of ROS and the release of neutrophil elastase can degrade the extracellular matrix surrounding the biomaterial and high

levels of MPO lead to chronic inflammation by replenishing neutrophils at the implant site¹⁰⁴⁻¹⁰⁶. These findings suggest that synthetic materials tend to activate neutrophils to a greater extent, potentially leading to tissue damage and increased inflammation when compared to natural materials. This knowledge can also be used to modulate the immune response for successful repair. For example, in biomaterials where there is limited inflammation, the addition of a synthetic material can induce inflammation and promote repair. Nevertheless, maintaining a balance is critical, as excessive inflammation can be detrimental.

Future research could focus on different biophysical properties of biomaterials, such as material topography, surface chemistry, and stiffness, and understanding their impact on the immune response and osteochondral repair. This will be essential for actively modulating the neutrophil and macrophage response and improving tissue repair.

The importance of model selection for relevant and applicable osteochondral repair research

The results obtained in the studies described in **chapters 2-5** across various experiments were not supporting the same conclusions. The differences obtained between *in vitro*, *ex vivo*, and *in vivo* models may be attributed to biological environment that each model represents. The environmental differences among these models can impact the experimental results. Additionally, the effects of incorporating BMP-2 and PDGF-BB into a biomaterial demonstrated disparate outcomes in *ex vivo* and *in vivo* models, which could be influenced by the chosen time-point and species for each experiment. Furthermore, the discrepancy in osteochondral repair was also dependent on the site of implantation of the scaffold. The addition of BMP-2 seems to have a beneficial effect on repair in the non-weight bearing semi-orthotopic mouse model and in the caprine trochlear groove, whilst BMP-2 addition worsened the repair in the weight bearing caprine femoral condyle. This indicates that the role of loading could also have a significant impact on the final results observed in **chapter 5**. These conflicting results highlight the importance of performing both *in vitro* and *in vivo* testing of all biomaterials, as the results may be affected by the specific model used. When selecting an animal model, it is important to consider several factors, including the size and shape of the osteochondral defect to be created, the biomechanical properties of the joint, the healing potential of the animal, and the ethical considerations involved in using animals for research purposes. A suitable animal model should mimic the biological processes and pathologies of the human condition being studied to ensure that the results obtained are relevant and applicable to the human population.

Ultimately, the selection of an appropriate animal model for osteochondral repair should be based on a careful evaluation of the research question, the biomaterial being tested, and the ethical considerations involved in using animals for research purposes.

FUTURE DIRECTIONS

Immunomodulation in osteochondral repair: a promising approach

Throughout this thesis, the significance of immunomodulation has been emphasized and found to be critical for enhancing cell migration. The data in this thesis showed that a shift from pro- to anti-inflammatory macrophages can be influenced by a currently available drug, chemotactic factors such as IL-4, IL-10, and BMP-2. A previous study also found that physical exercise can contribute to this shift, highlighting the importance of postoperative physiotherapy for ultimate success¹⁰⁷. Numerous biomaterials have been shown to affect macrophage polarization. For instance, Dai et al. used squid-derived type II collagen in a scaffold and demonstrated the polarization of pro-inflammatory macrophages towards anti-inflammatory macrophages, leading to the expression of cartilage matrix associated genes by chondrocytes, the suppression of pathological apoptosis and hypertrophy of chondrocytes⁴⁵.

Developing a biomaterial with immunomodulatory properties is an effective and practical approach. In one study, a biomimetic with a bone-like staggered nano interface was examined for its immunomodulatory properties during bone regeneration, and it was observed that the hierarchical nano interface facilitated anti-inflammatory macrophage polarization, which promoted endogenous bone regeneration¹⁰⁸. Incorporating TGF- β 1 into a hydrogel was found to increase anti-inflammatory macrophage polarization and enhance chondrogenesis¹⁰⁹. These findings illustrate the potential for modifying a biomaterial to modulate the immune response and promote osteochondral repair by influencing the interaction between the biomaterial and immune cells involved in the host response. However, it should be noted that all of these studies only focused on the effect of biomaterials on macrophage polarization, neglecting other immune cells that may work in either a synergistic or antagonistic manner. Thus, it is important for future studies to comprehensively evaluate the involvement of the entire immune system, including neutrophils and macrophages, and their interplay.

The approach used in this thesis to modulate the macrophage phenotype had some limitations with negative effects on the formation of new osteochondral tissue. Exploring

other therapeutic options that specifically polarize pro-inflammatory macrophages towards more anti-inflammatory and repair macrophages without having negative effects on the formation of new osteochondral tissue may result in more effective strategies for promoting endogenous cartilage repair. One option could be the use of MSC injections. These MSC-based injections can exert an immunomodulatory effect on the affected joint and potentially provide a source of growth factor stimulation¹¹⁰. The efficacy of stem cell injections in polarizing the macrophage phenotype towards a more anti-inflammatory state is unclear and might be the subject of future research. The optimal timing of the anti-inflammatory treatment relative to the processes involved in osteochondral repair should also be studied to gain insights into the potential benefits and drawbacks of these treatments. Understanding the mechanisms underlying joint inflammation modulation and its impact on osteochondral repair may lead to the development of new and more effective treatments for osteochondral defects. Overall, investigating the effect of modulation of inflammation presents a promising avenue for future research in the field of orthopedics.

Exploring cell-based approaches in a single procedure for osteochondral repair

A key aspect of cell-free osteochondral repair is focused on promoting the migration of cells to the site of injury or defect. However, cell migration is limited by several factors, such as the presence of physical barriers like scar tissue, inadequate blood supply to the damaged area, and the absence of specific signaling molecules or growth factors necessary for cell migration and proliferation⁵⁶. Additionally, the age and overall health of the individual can also impact the ability of cells to migrate and effectively repair the affected tissue¹¹¹. Literature suggests that a large number of chondrogenic progenitor cells are required for successful osteochondral repair^{112,113}.

The drawback of limited cell availability and difficulty in promoting cell migration and proliferation in biomaterial-based cell-free approaches might be overcome by applications that involve the use of harvested cells in combination with other strategies. With the application of cells, a source of new and functional tissue can be provided that can integrate with the surrounding environment and promote healing. The challenge remains to obtain a sufficient number of cells as a substantial quantity is required to initiate a proper osteochondral repair response. Future therapies could focus on incorporating cells into the repair process to promote the regeneration of functional cartilage tissue while still enabling one-stage procedures, which is a significant benefit in clinical practice. This can be addressed by combining directly isolated chondrocytes or chondrons with autologous MSCs or allogenic MSCs, which has

been shown to enhance the chondrogenic effect ^{114,115}. An alternative involves the use of *in vitro* cultured and expanded allogeneic chondrocytes as a one-stage procedure. Research suggests that juvenile human chondrocytes have a higher potential to restore articular cartilage than adult cells and can be transplanted without the risk of rejection ¹¹⁶. Clinical studies have shown that *in vitro* expanded allogeneic chondrocytes transplanted in biodegradable, alginate-based, biocompatible scaffolds have produced satisfactory results and a good safety profile in the treatment of chondral and osteochondral lesions in the knee, with results reported up to 6 years post-treatment ¹¹⁷. The use of viable chondrocytes from cadaveric human donors has also been demonstrated and the chondrogenic capacity is not altered by cryopreservation, providing another large pool of cells that can be used in osteochondral repair ¹¹⁸. Another emerging technique in the field of osteochondral repair involves the use of cartilage fragments, which has been shown to improve cell migration, proliferation, and GAG content compared to chondrocytes alone ¹¹⁹. Further studies are needed to determine the optimal cell source to use or whether a combination of cell sources will be best in osteochondral repair. A combination of these therapies may provide the best results by utilizing both the benefits of chondroprogenitor cells and cartilage fragments to promote the growth and regeneration of functional tissue. The best approach may depend on the individual patient and specific conditions being treated. Artificial intelligence-based software could in the future hopefully determine the best treatment strategy for the individual patient. Since there is still no ideal solution, further research in both the field of cell free-approaches and cell-based approaches is necessary.

Towards more effective osteochondral repair through biomaterials and 3D printing

The current methods for repairing osteochondral defects are limited by their inability to recreate the complex spatial distribution of cell types and tissue organization that is required for successful repair ¹²⁰. To address this challenge, there is a growing interest in 3D printing technology to produce highly precise 3D structures that mimic the morphology and function of both cartilage and subchondral bone. This technology involves the use of hydrogel as a temporary extracellular matrix and layer-by-layer printing of various matrices. Furthermore, these structures can be printed in the exact dimensions of a patient's osteochondral defect. The implementation of MRI-guided 3D printing or trans-arthroscopic direct 3D printing could significantly enhance the accuracy and efficacy of repairing osteochondral defects ¹²¹. Another option in 3D printing is incorporating different cell types also known as bioprinting. The potential utilization of a combination of chondrocytes, mesenchymal stromal cells,

cartilage fragments, and even induced pluripotent stem cells (iPSCs) in the field of osteochondral repair could be an interesting possibility in the future ¹²². Looking towards the future, 3D printing technology holds great potential for the repair of osteochondral defects. In fact, by mimicking the intricate spatial distribution of cells and tissue organization in native cartilage and subchondral bone.

Therapeutic options should focus on producing stable hyaline-like cartilage for long-term integrative repair. To produce stable hyaline-like cartilage the subchondral bone plays a key role in mechanically and metabolically supporting the articular cartilage ¹²³. The functional conditions of the articular cartilage and its supporting bone are closely linked, and injuries to either can have adverse effects on the entire joint environment ¹²⁴. The subchondral bone serves not only as a shock absorber, but also contains cavities that harbor blood vessels that provide vital nutrients and signaling molecules for the deeper layers of the cartilage ^{125,126}. It is important to acknowledge that the cartilage and subchondral bone are highly interdependent, and together form a functional unit. The field of osteochondral repair should focus on improving our understanding of the interplay between biomaterials, the immune system, and repair cells. Studies should particularly concentrate on the comprehensive involvement of the immune system, including neutrophils and macrophages, and their interplay in order to create more biocompatible biomaterials and develop new therapeutic targets for tissue repair. Ultimately, this should lead to functional osteochondral repair and integration, that can be guided by biomaterials that elicit the right immune response. With continued advancements in the field, it is hoped that future treatments will provide a more successful and long-lasting solution for the repair of osteochondral defects.

REFERENCES

1. Heard BJ, Achari Y, Chung M, Shrive NG, Frank CB. Early joint tissue changes are highly correlated with a set of inflammatory and degradative synovial biomarkers after ACL autograft and its sham surgery in an ovine model. *Journal of Orthopaedic Research*. 2011;29(8):1185-1192.
2. Swärd P, Struglics A, Englund M, Roos HP, Frobell RB. Soft tissue knee injury with concomitant osteochondral fracture is associated with higher degree of acute joint inflammation. *The American journal of sports medicine*. 2014;42(5):1096-1102.
3. Tsuchida AI, Beekhuizen M, t Hart MC, Radstake TRDJ, Dhert WJA, Saris DBF, van Osch GJVM, Creemers LB. Cytokine profiles in the joint depend on pathology, but are different between synovial fluid, cartilage tissue and cultured chondrocytes. *Arthritis Research & Therapy*. 2014;16(5):441.
4. Larsson S, Englund M, Struglics A, Lohmander L. Interleukin-6 and tumor necrosis factor alpha in synovial fluid are associated with progression of radiographic knee osteoarthritis in subjects with previous meniscectomy. *Osteoarthritis and cartilage*. 2015;23(11):1906-1914.
5. Åhlén M, Roshani L, Lidén M, Struglics A, Rostgård-Christensen L, Kartus J. Inflammatory cytokines and biomarkers of cartilage metabolism 8 years after anterior cruciate ligament reconstruction: results from operated and contralateral knees. *The American journal of sports medicine*. 2015;43(6):1460-1466.
6. Krüger JP, Endres M, Neumann K, Stuhlmüller B, Morawietz L, Häupl T, Kaps C. Chondrogenic differentiation of human subchondral progenitor cells is affected by synovial fluid from donors with osteoarthritis or rheumatoid arthritis. *Journal of Orthopaedic Surgery and Research*. 2012;7(1):1-10.
7. Fahy N, de Vries-van Melle ML, Lehmann J, Wei W, Grotenhuis N, Farrell E, van der Kraan PM, Murphy JM, Bastiaansen-Jenniskens YM, van Osch GJ. Human osteoarthritic synovium impacts chondrogenic differentiation of mesenchymal stem cells via macrophage polarisation state. *Osteoarthritis Cartilage*. 2014;22(8):1167-1175.
8. Yang KA, Saris D, Verbout A, Creemers L, Dhert W. The effect of synovial fluid from injured knee joints on in vitro chondrogenesis. *Tissue engineering*. 2006;12(10):2957-2964.
9. Gerstenfeld LC, Cho T-J, Kon T, Aizawa T, Cruceta J, Graves B, Einhorn T. Impaired intramembranous bone formation during bone repair in the absence of tumor necrosis factor-alpha signaling. *Cells Tissues Organs*. 2001;169(3):285-294.
10. Xie C, Ming X, Wang Q, Schwarz EM, Guldborg RE, O'Keefe RJ, Zhang X. COX-2 from the injury milieu is critical for the initiation of periosteal progenitor cell mediated bone healing. *Bone*. 2008;43(6):1075-1083.
11. Voskamp C, Koevoet WJLM, Somoza RA, Caplan AI, Lefebvre V, van Osch GJVM, Narcisi R. Enhanced Chondrogenic Capacity of Mesenchymal Stem Cells After TNF α Pre-treatment. *Frontiers in Bioengineering and Biotechnology*. 2020;8(658).
12. Heldens GT, Blaney Davidson EN, Vitters EL, Schreurs BW, Piek E, van den Berg WB, van der Kraan PM. Catabolic factors and osteoarthritis-conditioned medium inhibit chondrogenesis of human mesenchymal stem cells. *Tissue Eng Part A*. 2012;18(1-2):45-54.

13. Wei W, Rudjito E, Fahy N, Verhaar JA, Clockaerts S, Bastiaansen-Jenniskens YM, van Osch GJ. The infrapatellar fat pad from diseased joints inhibits chondrogenesis of mesenchymal stem cells. *Eur Cell Mater.* 2015;30:303-314.
14. Assirelli E, Pulsatelli L, Dolzani P, Platano D, Olivotto E, Filardo G, Trisolino G, Facchini A, Borzi RM, Meliconi R. Human osteoarthritic cartilage shows reduced in vivo expression of IL-4, a chondroprotective cytokine that differentially modulates IL-1 β -stimulated production of chemokines and matrix-degrading enzymes in vitro. *PLoS one.* 2014;9(5):e96925.
15. Zhang Y, Pizzute T, Pei M. Anti-inflammatory strategies in cartilage repair. *Tissue Eng Part B Rev.* 2014;20(6):655-668.
16. van der Kraan PM. The Interaction between Joint Inflammation and Cartilage Repair. *Tissue Eng Regen Med.* 2019;16(4):327-334.
17. Kumar A, Bendele AM, Blanks RC, Bodick N. Sustained efficacy of a single intra-articular dose of FX006 in a rat model of repeated localized knee arthritis. *Osteoarthritis and cartilage.* 2015;23(1):151-160.
18. Rudnik-Jansen I, Colen S, Berard J, Plomp S, Que I, van Rijen M, Woike N, Egas A, van Osch G, van Maarseveen E, Messier K, Chan A, Thies J, Creemers L. Prolonged inhibition of inflammation in osteoarthritis by triamcinolone acetonide released from a polyester amide microsphere platform. *J Control Release.* 2017;253:64-72.
19. Frisbie DD, Kawcak CE, Trotter GW, Powers BE, Walton RM, McIlwraith CW. Effects of triamcinolone acetonide on an in vivo equine osteochondral fragment exercise model. *Equine Vet J.* 1997;29(5):349-359.
20. Krenn V, Morawietz L, Burmester GR, Kinne RW, Mueller-Ladner U, Muller B, Haupt T. Synovitis score: discrimination between chronic low-grade and high-grade synovitis. *Histopathology.* 2006;49(4):358-364.
21. Sieker JT, Ayturk UM, Proffen BL, Weissenberger MH, Kiapour AM, Murray MM. Immediate Administration of Intraarticular Triamcinolone Acetonide After Joint Injury Modulates Molecular Outcomes Associated With Early Synovitis. *Arthritis Rheumatol.* 2016;68(7):1637-1647.
22. Rustad KC, Gurtner GC. Mesenchymal Stem Cells Home to Sites of Injury and Inflammation. *Adv Wound Care (New Rochelle).* 2012;1(4):147-152.
23. Spaeth E, Klopp A, Dembinski J, Andreeff M, Marini F. Inflammation and tumor microenvironments: defining the migratory itinerary of mesenchymal stem cells. *Gene Ther.* 2008;15(10):730-738.
24. Fu X, Liu G, Halim A, Ju Y, Luo Q, Song AG. Mesenchymal Stem Cell Migration and Tissue Repair. *Cells.* 2019;8(8).
25. Syed HM, Green L, Bianski B, Jobe CM, Wongworawat MD. Bupivacaine and triamcinolone may be toxic to human chondrocytes: a pilot study. *Clinical Orthopaedics and Related Research®.* 2011;469(10):2941-2947.
26. Drago JL, Danial CM, Braun HJ, Pouliot MA, Kim HJ. The chondrotoxicity of single-dose corticosteroids. *Knee Surgery, Sports Traumatology, Arthroscopy.* 2012;20(9):1809-1814.
27. Rudnik-Jansen I, Tellegen AR, Pouran B, Schrijver K, Meij BP, Emans PJ, de Gendt E, Thomas RE, Kik MJL, de Visser HM, Weinans H, Egas A, van Maarseveen E, Woike N, Mihov G, Thies J, Tryfonidou MA, Creemers LB. Local controlled release of corticosteroids

- extends surgically induced joint instability by inhibiting tissue healing. *Br J Pharmacol*. 2019;176(20):4050-4064.
28. Tempfer H, Gehwolf R, Lehner C, Wagner A, Mtsariashvili M, Bauer HC, Resch H, Tauber M. Effects of crystalline glucocorticoid triamcinolone acetone on cultured human supraspinatus tendon cells. *Acta Orthop*. 2009;80(3):357-362.
 29. Derendorf H, Möllmann H, Grüner A, Haack D, Gyselby G. Pharmacokinetics and pharmacodynamics of glucocorticoid suspensions after intra-articular administration. *Clinical Pharmacology & Therapeutics*. 1986;39(3):313-317.
 30. van Beuningen HM, de Vries-van Melle ML, Vitters EL, Schreurs W, van den Berg WB, van Osch GJ, van der Kraan PM. Inhibition of TAK1 and/or JAK can rescue impaired chondrogenic differentiation of human mesenchymal stem cells in osteoarthritis-like conditions. *Tissue Eng Part A*. 2014;20(15-16):2243-2252.
 31. Kawaguchi A, Nakaya H, Okabe T, Tensho K, Nawata M, Eguchi Y, Imai Y, Takaoka K, Wakitani S. Blocking of tumor necrosis factor activity promotes natural repair of osteochondral defects in rabbit knee. *Acta Orthop*. 2009;80(5):606-611.
 32. Moskowitz RW, Davis W, Sammarco J, Mast W, Chase SW. Experimentally induced corticosteroid arthropathy. *Arthritis and rheumatism*. 1970;13(3):236-243.
 33. Wernecke C, Braun HJ, Dragoo JL. The Effect of Intra-articular Corticosteroids on Articular Cartilage: A Systematic Review. *Orthop J Sports Med*. 2015;3(5):2325967115581163.
 34. Smith MD. Suppl 1: the normal synovium. *The open rheumatology journal*. 2011;5:100.
 35. Sellam J, Berenbaum F. The role of synovitis in pathophysiology and clinical symptoms of osteoarthritis. *Nature Reviews Rheumatology*. 2010;6(11):625.
 36. Fernandes TL, Gomoll AH, Lattermann C, Hernandez AJ, Bueno DF, Amano MT. Macrophage: A Potential Target on Cartilage Regeneration. *Front Immunol*. 2020;11:111.
 37. Utomo L, van Osch GJ, Bayon Y, Verhaar JA, Bastiaansen-Jenniskens YM. Guiding synovial inflammation by macrophage phenotype modulation: an in vitro study towards a therapy for osteoarthritis. *Osteoarthritis Cartilage*. 2016;24(9):1629-1638.
 38. Tu GW, Shi Y, Zheng YJ, Ju MJ, He HY, Ma GG, Hao GW, Luo Z. Glucocorticoid attenuates acute lung injury through induction of type 2 macrophage. *J Transl Med*. 2017;15(1):181.
 39. Siebelt M, Korthagen N, Wei W, Groen H, Bastiaansen-Jenniskens Y, Müller C, Waarsing JH, de Jong M, Weinans H. Triamcinolone acetone activates an anti-inflammatory and folate receptor-positive macrophage that prevents osteophytosis in vivo. *Arthritis Res Ther*. 2015;17:352.
 40. Yona S, Gordon S. Inflammation: Glucocorticoids turn the monocyte switch. *Immunol Cell Biol*. 2007;85(2):81-82.
 41. Wu DH, Hatzopoulos AK. Bone morphogenetic protein signaling in inflammation. *Exp Biol Med (Maywood)*. 2019;244(2):147-156.
 42. The Immunomodulatory Role of BMP-2 on Macrophages to Accelerate Osteogenesis. *Tissue Engineering Part A*. 2018;24(7-8):584-594.
 43. Sesia SB, Duhr R, Medeiros da Cunha C, Todorov A, Schaeren S, Padovan E, Spagnoli G, Martin I, Barbero A. Anti-inflammatory/tissue repair macrophages enhance the cartilage-

- forming capacity of human bone marrow-derived mesenchymal stromal cells. *J Cell Physiol.* 2015;230(6):1258-1269.
44. Manferdini C, Paoletta F, Gabusi E, Gambari L, Piacentini A, Filardo G, Fleury-Cappellesso S, Barbero A, Murphy M, Lisignoli G. Adipose stromal cells mediated switching of the pro-inflammatory profile of M1-like macrophages is facilitated by PGE2: in vitro evaluation. *Osteoarthritis and cartilage.* 2017;25(7):1161-1171.
 45. Dai M, Sui B, Xue Y, Liu X, Sun J. Cartilage repair in degenerative osteoarthritis mediated by squid type II collagen via immunomodulating activation of M2 macrophages, inhibiting apoptosis and hypertrophy of chondrocytes. *Biomaterials.* 2018;180:91-103.
 46. Wehling N, Palmer GD, Pilapil C, Liu F, Wells JW, Muller PE, Evans CH, Porter RM. Interleukin-1beta and tumor necrosis factor alpha inhibit chondrogenesis by human mesenchymal stem cells through NF-kappaB-dependent pathways. *Arthritis Rheum.* 2009;60(3):801-812.
 47. Harrell CR, Markovic BS, Fellabaum C, Arsenijevic A, Volarevic V. Mesenchymal stem cell-based therapy of osteoarthritis: current knowledge and future perspectives. *Biomedicine & pharmacotherapy.* 2019;109:2318-2326.
 48. Zhang T, Yao Y. Effects of inflammatory cytokines on bone/cartilage repair. *Journal of Cellular Biochemistry.* 2019;120(5):6841-6850.
 49. Van Lent P, Holthuysen A, Slöetjes A, Lubberts E, Van Den Berg W. Local overexpression of adeno-viral IL-4 protects cartilage from metallo proteinase-induced destruction during immune complex-mediated arthritis by preventing activation of pro-MMPs. *Osteoarthritis and cartilage.* 2002;10(3):234-243.
 50. Brittberg M. Cellular and Acellular Approaches for Cartilage Repair: A Philosophical Analysis. *Cartilage.* 2015;6(2 Suppl):4S-12S.
 51. Ricci M, Tradati D, Maione A, Uboldi FM, Usellini E, Berruto M. Cell-free osteochondral scaffolds provide a substantial clinical benefit in the treatment of osteochondral defects at a minimum follow-up of 5 years. *J Exp Orthop.* 2021;8(1):62.
 52. Kon E, Filardo G, Perdisa F, Venieri G, Marcacci M. Acellular Matrix-Based Cartilage Regeneration Techniques for Osteochondral Repair. *Operative Techniques in Orthopaedics.* 2014;24(1):14-18.
 53. Pabbruwe MB, Esfandiari E, Kafienah W, Tarlton JF, Hollander AP. Induction of cartilage integration by a chondrocyte/collagen-scaffold implant. *Biomaterials.* 2009;30(26):4277-4286.
 54. Wei F, Liu S, Chen M, Tian G, Zha K, Yang Z, Jiang S, Li M, Sui X, Chen Z, Guo Q. Host Response to Biomaterials for Cartilage Tissue Engineering: Key to Remodeling. *Front Bioeng Biotechnol.* 2021;9:664592.
 55. Sennett ML, Friedman JM, Ashley BS, Stoeckl BD, Patel JM, Alini M, Cucchiari M, Eglin D, Madry H, Mata A, Semino C, Stoddart MJ, Johnstone B, Moutos FT, Estes BT, Guilak F, Mauck RL, Dodge GR. Long term outcomes of biomaterial-mediated repair of focal cartilage defects in a large animal model. *Eur Cell Mater.* 2021;41:40-51.
 56. Qu F, Guilak F, Mauck RL. Cell migration: implications for repair and regeneration in joint disease. *Nat Rev Rheumatol.* 2019;15(3):167-179.

57. Zhang YS, Khademhosseini A. Advances in engineering hydrogels. *Science*. 2017;356(6337):eaaf3627.
58. Li L, Yu F, Zheng L, Wang R, Yan W, Wang Z, Xu J, Wu J, Shi D, Zhu L, Wang X, Jiang Q. Natural hydrogels for cartilage regeneration: Modification, preparation and application. *Journal of Orthopaedic Translation*. 2019;17:26-41.
59. Guo T, Noshin M, Baker HB, Taskoy E, Meredith SJ, Tang Q, Ringel JP, Lerman MJ, Chen Y, Packer JD. 3D printed biofunctionalized scaffolds for microfracture repair of cartilage defects. *Biomaterials*. 2018;185:219-231.
60. Sharma B, Fermanian S, Gibson M, Unterman S, Herzka DA, Cascio B, Coburn J, Hui AY, Marcus N, Gold GE. Human cartilage repair with a photoreactive adhesive-hydrogel composite. *Science translational medicine*. 2013;5(167):167ra166-167ra166.
61. Gavenis K, Schneider U, Maus U, Mumme T, Muller-Rath R, Schmidt-Rohlfing B, Andereya S. Cell-free repair of small cartilage defects in the Goettinger minipig: which defect size is possible? *Knee Surgery, Sports Traumatology, Arthroscopy*. 2012;20(11):2307-2314.
62. Pathak A, Kumar S. Biophysical regulation of tumor cell invasion: moving beyond matrix stiffness. *Integrative Biology*. 2011;3(4):267-278.
63. Vainieri ML, Lolli A, Kops N, D'Atri D, Eglin D, Yayon A, Alini M, Grad S, Sivasubramanian K, van Osch G. Evaluation of biomimetic hyaluronic-based hydrogels with enhanced endogenous cell recruitment and cartilage matrix formation. *Acta Biomater*. 2020;101:293-303.
64. Klotz BJ, Lim KS, Chang YX, Soliman BG, Pennings I, Melchels FPW, Woodfield TBF, Rosenberg AJ, Malda J, Gawlitta D. Engineering of a complex bone tissue model with endothelialised channels and capillary-like networks. *Eur Cell Mater*. 2018;35:335-348.
65. Pepelanova I, Kruppa K, Scheper T, Lavrentieva A. Gelatin-Methacryloyl (GelMA) Hydrogels with Defined Degree of Functionalization as a Versatile Toolkit for 3D Cell Culture and Extrusion Bioprinting. *Bioengineering (Basel)*. 2018;5(3).
66. Chen YC, Lin RZ, Qi H, Yang Y, Bae H, Melero-Martin JM, Khademhosseini A. Functional Human Vascular Network Generated in Photocrosslinkable Gelatin Methacrylate Hydrogels. *Adv Funct Mater*. 2012;22(10):2027-2039.
67. Duan P, Pan Z, Cao L, He Y, Wang H, Qu Z, Dong J, Ding J. The effects of pore size in bilayered poly (lactide-co-glycolide) scaffolds on restoring osteochondral defects in rabbits. *Journal of Biomedical Materials Research Part A: An Official Journal of The Society for Biomaterials, The Japanese Society for Biomaterials, and The Australian Society for Biomaterials and the Korean Society for Biomaterials*. 2014;102(1):180-192.
68. Yu Y, Brouillette MJ, Seol D, Zheng H, Buckwalter JA, Martin JA. Use of recombinant human stromal cell-derived factor 1 α -loaded fibrin/hyaluronic acid hydrogel networks to achieve functional repair of full-thickness bovine articular cartilage via homing of chondrogenic progenitor cells. *Arthritis Rheumatol*. 2015;67(5):1274-1285.
69. Nixon AJ, Fortier LA, Williams J, Mohammed H. Enhanced repair of extensive articular defects by insulin-like growth factor-I-laden fibrin composites. *J Orthop Res*. 1999;17(4):475-487.

70. Lee CH, Cook JL, Mendelson A, Moiola EK, Yao H, Mao JJ. Regeneration of the articular surface of the rabbit synovial joint by cell homing: a proof of concept study. *Lancet*. 2010;376(9739):440-448.
71. Luo Z, Jiang L, Xu Y, Li H, Xu W, Wu S, Wang Y, Tang Z, Lv Y, Yang L. Mechano growth factor (MGF) and transforming growth factor (TGF)- β 3 functionalized silk scaffolds enhance articular hyaline cartilage regeneration in rabbit model. *Biomaterials*. 2015;52:463-475.
72. Enhancement of BMP-2 Induced Bone Regeneration by SDF-1 α Mediated Stem Cell Recruitment. *Tissue Engineering Part A*. 2014;20(3-4):810-818.
73. Liu S, Liu Y, Jiang L, Li Z, Lee S, Liu C, Wang J, Zhang J. Recombinant human BMP-2 accelerates the migration of bone marrow mesenchymal stem cells via the CDC42/PAK1/LIMK1 pathway in vitro and in vivo. *Biomater Sci*. 2018;7(1):362-372.
74. Zhang W, Zhu C, Wu Y, Ye D, Wang S, Zou D, Zhang X, Kaplan DL, Jiang X. VEGF and BMP-2 promote bone regeneration by facilitating bone marrow stem cell homing and differentiation. *Eur Cell Mater*. 2014;27:1-11; discussion 11-12.
75. Nash TJ, Howlett CR, Martin C, Steele J, Johnson KA, Hicklin DJ. Effect of platelet-derived growth factor on tibial osteotomies in rabbits. *Bone*. 1994;15(2):203-208.
76. Heldin CH, Westermark B. Mechanism of action and in vivo role of platelet-derived growth factor. *Physiol Rev*. 1999;79(4):1283-1316.
77. Phipps MC, Xu Y, Bellis SL. Delivery of platelet-derived growth factor as a chemotactic factor for mesenchymal stem cells by bone-mimetic electrospun scaffolds. *PLoS One*. 2012;7(7):e40831.
78. Hankenson KD, Dishowitz M, Gray C, Schenker M. Angiogenesis in bone regeneration. *Injury*. 2011;42(6):556-561.
79. Kim SE, Yun YP, Lee JY, Shim JS, Park K, Huh JB. Co-delivery of platelet-derived growth factor (PDGF-BB) and bone morphogenic protein (BMP-2) coated onto heparinized titanium for improving osteoblast function and osteointegration. *Journal of tissue engineering and regenerative medicine*. 2015;9(12):E219-228.
80. Keceli HG, Bayram C, Celik E, Ercan N, Demirbilek M, Nohutcu RM. Dual delivery of platelet-derived growth factor and bone morphogenetic factor-6 on titanium surface to enhance the early period of implant osseointegration. *Journal of periodontal research*. 2020;55(5):694-704.
81. Taniyama T, Masaoka T, Yamada T, Wei X, Yasuda H, Yoshii T, Kozaka Y, Takayama T, Hirano M, Okawa A, Sotome S. Repair of Osteochondral Defects in a Rabbit Model Using a Porous Hydroxyapatite Collagen Composite Impregnated With Bone Morphogenetic Protein-2. *Artificial Organs*. 2015;39(6):529-535.
82. Zhou N, Li Q, Lin X, Hu N, Liao JY, Lin LB, Zhao C, Hu ZM, Liang X, Xu W, Chen H, Huang W. BMP2 induces chondrogenic differentiation, osteogenic differentiation and endochondral ossification in stem cells. *Cell Tissue Res*. 2016;366(1):101-111.
83. Kieswetter K, Schwartz Z, Alderete M, Dean DD, Boyan BD. Platelet derived growth factor stimulates chondrocyte proliferation but prevents endochondral maturation. *Endocrine*. 1997;6(3):257-264.

84. Jiang G, Li S, Yu K, He B, Hong J, Xu T, Meng J, Ye C, Chen Y, Shi Z, Feng G, Chen W, Yan S, He Y, Yan R. A 3D-printed PRP-GelMA hydrogel promotes osteochondral regeneration through M2 macrophage polarization in a rabbit model. *Acta Biomater.* 2021;128:150-162.
85. Zhu M, Zhong W, Cao W, Zhang Q, Wu G. Chondroinductive/chondroconductive peptides and their-functionalized biomaterials for cartilage tissue engineering. *Bioact Mater.* 2022;9:221-238.
86. Mouriño V, Cattalini JP, Boccaccini AR. Metallic ions as therapeutic agents in tissue engineering scaffolds: an overview of their biological applications and strategies for new developments. *J R Soc Interface.* 2012;9(68):401-419.
87. Bartel DP. MicroRNAs: genomics, biogenesis, mechanism, and function. *Cell.* 2004;116(2):281-297.
88. Li T, Liu B, Chen K, Lou Y, Jiang Y, Zhang D. Small molecule compounds promote the proliferation of chondrocytes and chondrogenic differentiation of stem cells in cartilage tissue engineering. *Biomed Pharmacother.* 2020;131:110652.
89. Li J, Liu Y, Zhang Y, Yao B, Enhejirigala, Li Z, Song W, Wang Y, Duan X, Yuan X, Fu X, Huang S. Biophysical and Biochemical Cues of Biomaterials Guide Mesenchymal Stem Cell Behaviors. *Front Cell Dev Biol.* 2021;9:640388.
90. Anderson JM, Rodriguez A, Chang DT. Foreign body reaction to biomaterials. *Seminars in Immunology.* 2008;20(2):86-100.
91. Franz S, Rammelt S, Scharnweber D, Simon JC. Immune responses to implants-a review of the implications for the design of immunomodulatory biomaterials. *Biomaterials.* 2011;32(28):6692-6709.
92. Dziki JL, Badyalak SF. Immunomodulatory biomaterials. *Current Opinion in Biomedical Engineering.* 2018;6:51-57.
93. Zhang S, Hu B, Liu W, Wang P, Lv X, Chen S, Liu H, Shao Z. Articular cartilage regeneration: The role of endogenous mesenchymal stem/progenitor cell recruitment and migration. *Semin Arthritis Rheum.* 2020;50(2):198-208.
94. Li M, Yin H, Yan Z, Li H, Wu J, Wang Y, Wei F, Tian G, Ning C, Li H, Gao C, Fu L, Jiang S, Chen M, Sui X, Liu S, Chen Z, Guo Q. The immune microenvironment in cartilage injury and repair. *Acta Biomaterialia.* 2022;140:23-42.
95. van der Kraan PM. The Interaction between Joint Inflammation and Cartilage Repair. *Tissue Engineering and Regenerative Medicine.* 2019;16(4):327-334.
96. Sridharan R, Cameron AR, Kelly DJ, Kearney CJ, O'Brien FJ. Biomaterial based modulation of macrophage polarization: a review and suggested design principles. *Materials Today.* 2015;18(6):313-325.
97. Dancey JT, Deubelbeiss KA, Harker LA, Finch CA. Neutrophil kinetics in man. *J Clin Invest.* 1976;58(3):705-715.
98. Kohno K, Koya-Miyata S, Harashima A, Tsukuda T, Katakami M, Ariyasu T, Ushio S, Iwaki K. Inflammatory M1-like macrophages polarized by NK-4 undergo enhanced phenotypic switching to an anti-inflammatory M2-like phenotype upon co-culture with apoptotic cells. *J Inflamm (Lond).* 2021;18(1):2.

99. Wang G, Jing W, Bi Y, Li Y, Ma L, Yang H, Zhang Y. Neutrophil elastase induces chondrocyte apoptosis and facilitates the occurrence of osteoarthritis via caspase signaling pathway. *Frontiers in Pharmacology*. 2021;12:666162.
100. Gasser O, Schifferli JrA. Activated polymorphonuclear neutrophils disseminate anti-inflammatory microparticles by ectocytosis. *Blood*. 2004;104(8):2543-2548.
101. Headland SE, Jones HR, Norling LV, Kim A, Souza PR, Corsiero E, Gil CD, Nerviani A, Dell'Accio F, Pitzalis C. Neutrophil-derived microvesicles enter cartilage and protect the joint in inflammatory arthritis. *Science translational medicine*. 2015;7(315):315ra190-315ra190.
102. Grecian R, Whyte MKB, Walmsley SR. The role of neutrophils in cancer. *Br Med Bull*. 2018;128(1):5-14.
103. Presbitero A, Mancini E, Castiglione F, Krzhizhanovskaya VV, Quax R. Game of neutrophils: modeling the balance between apoptosis and necrosis. *BMC Bioinformatics*. 2019;20(6):475.
104. Korkmaz B, Moreau T, Gauthier F. Neutrophil elastase, proteinase 3 and cathepsin G: physicochemical properties, activity and physiopathological functions. *Biochimie*. 2008;90(2):227-242.
105. Janusz M, Durham S. Inhibition of cartilage degradation in rat collagen-induced arthritis but not adjuvant arthritis by the neutrophil elastase inhibitor MDL 101,146. *Inflammation research*. 1997;46:503-508.
106. Aratani Y. Myeloperoxidase: Its role for host defense, inflammation, and neutrophil function. *Archives of Biochemistry and Biophysics*. 2018;640:47-52.
107. Castrogiovanni P, Di Rosa M, Ravalli S, Castorina A, Guglielmino C, Imbesi R, Vecchio M, Drago F, Szychlińska MA, Musumeci G. Moderate physical activity as a prevention method for knee osteoarthritis and the role of synoviocytes as biological key. *International journal of molecular sciences*. 2019;20(3):511.
108. Jin S-S, He D-Q, Luo D, Wang Y, Yu M, Guan B, Fu Y, Li Z-X, Zhang T, Zhou Y-H. A biomimetic hierarchical nanointerface orchestrates macrophage polarization and mesenchymal stem cell recruitment to promote endogenous bone regeneration. *ACS nano*. 2019;13(6):6581-6595.
109. Ji X, Lei Z, Yuan M, Zhu H, Yuan X, Liu W, Pu H, Jiang J, Zhang Y, Jiang X, Xiao J. Cartilage repair mediated by thermosensitive photocrosslinkable TGFβ1-loaded GM-HPCH via immunomodulating macrophages, recruiting MSCs and promoting chondrogenesis. *Theranostics*. 2020;10(6):2872-2887.
110. Saw K-Y, Anz A, Merican S, Tay Y-G, Ragavanaidu K, Jee CS, McGuire DA. Articular cartilage regeneration with autologous peripheral blood progenitor cells and hyaluronic acid after arthroscopic subchondral drilling: a report of 5 cases with histology. *Arthroscopy: The Journal of Arthroscopic & Related Surgery*. 2011;27(4):493-506.
111. Collins-Hooper H, Woolley TE, Dyson L, Patel A, Potter P, Baker RE, Gaffney EA, Maini PK, Dash PR, Patel K. Age-related changes in speed and mechanism of adult skeletal muscle stem cell migration. *Stem Cells*. 2012;30(6):1182-1195.
112. Puelacher W, Kim S, Vacanti J, Schloo B, Mooney D, Vacanti C. Tissue-engineered growth of cartilage: the effect of varying the concentration of chondrocytes seeded onto synthetic

- polymer matrices. *International journal of oral and maxillofacial surgery*. 1994;23(1):49-53.
113. Chahla J, Dean CS, Moatshe G, Pascual-Garrido C, Serra Cruz R, LaPrade RF. Concentrated bone marrow aspirate for the treatment of chondral injuries and osteoarthritis of the knee: a systematic review of outcomes. *Orthopaedic journal of sports medicine*. 2016;4(1):2325967115625481.
 114. Słynarski K, de Jong WC, Snow M, Hendriks JAA, Wilson CE, Verdonk P. Single-stage autologous chondrocyte-based treatment for the repair of knee cartilage lesions: two-year follow-up of a prospective single-arm multicenter study. *The American Journal of Sports Medicine*. 2020;48(6):1327-1337.
 115. Saris TF, de Windt TS, Kester EC, Vonk LA, Custers RJ, Saris DB. Five-year outcome of 1-stage cell-based cartilage repair using recycled autologous chondrons and allogenic mesenchymal stromal cells: a first-in-human clinical trial. *The American Journal of Sports Medicine*. 2021;49(4):941-947.
 116. Adkisson IV HD, Martin JA, Amendola RL, Milliman C, Mauch KA, Katwal AB, Seyedin M, Amendola A, Streeter PR, Buckwalter JA. The potential of human allogeneic juvenile chondrocytes for restoration of articular cartilage. *The American journal of sports medicine*. 2010;38(7):1324-1333.
 117. Dhollander AA, Verdonk PC, Lambrecht S, Verdonk R, Elewaut D, Verbruggen G, Almqvist KF. Midterm results of the treatment of cartilage defects in the knee using alginate beads containing human mature allogenic chondrocytes. *The American journal of sports medicine*. 2012;40(1):75-82.
 118. Olivos-Meza A, Velasquillo Martínez C, Olivos Díaz B, Landa-Solís C, Brittberg M, Pichardo Bahena R, Ortega Sanchez C, Martínez V, Alvarez Lara E, Ibarra-Ponce de León JC. Co-culture of dedifferentiated and primary human chondrocytes obtained from cadaveric donor enhance the histological quality of repair tissue: an in-vivo animal study. *Cell and Tissue Banking*. 2017;18:369-381.
 119. Lu Y, Dhanaraj S, Wang Z, Bradley DM, Bowman SM, Cole BJ, Binette F. Minced cartilage without cell culture serves as an effective intraoperative cell source for cartilage repair. *Journal of Orthopaedic Research*. 2006;24(6):1261-1270.
 120. Daly AC, Freeman FE, Gonzalez-Fernandez T, Critchley SE, Nulty J, Kelly DJ. 3D bioprinting for cartilage and osteochondral tissue engineering. *Advanced Healthcare Materials*. 2017;6(22):1700298.
 121. Di Bella C, Duchi S, O'Connell CD, Blanchard R, Augustine C, Yue Z, Thompson F, Richards C, Beirne S, Onofrillo C. In situ handheld three-dimensional bioprinting for cartilage regeneration. *Journal of tissue engineering and regenerative medicine*. 2018;12(3):611-621.
 122. Nguyen D, Hägg DA, Forsman A, Ekholm J, Nimkingratana P, Brantsing C, Kalogeropoulos T, Zaunz S, Concaro S, Brittberg M. Cartilage tissue engineering by the 3D bioprinting of iPS cells in a nanocellulose/alginate bioink. *Scientific reports*. 2017;7(1):1-10.
 123. Oláh T, Madry H. The Osteochondral Unit: The Importance of the Underlying Subchondral Bone. In: Farr J, Gomoll AH, eds. *Cartilage Restoration: Practical Clinical Applications*. Cham: Springer International Publishing; 2018:13-22.

124. Gomoll AH, Madry H, Knutsen G, van Dijk N, Seil R, Brittberg M, Kon E. The subchondral bone in articular cartilage repair: current problems in the surgical management. *Knee surgery, sports traumatology, arthroscopy : official journal of the ESSKA*. 2010;18(4):434-447.
125. Robling AG, Castillo AB, Turner CH. Biomechanical and molecular regulation of bone remodeling. *Annu Rev Biomed Eng*. 2006;8:455-498.
126. Li G, Yin J, Gao J, Cheng TS, Pavlos NJ, Zhang C, Zheng MH. Subchondral bone in osteoarthritis: insight into risk factors and microstructural changes. *Arthritis research & therapy*. 2013;15:1-12.

8

Summary

SUMMARY

Osteochondral defects involve both the articular cartilage and the subchondral bone, and may lead to disability in the aging population. Osteochondral defects are accompanied by joint inflammation. Inflammation plays a crucial role in the wound healing response and is characterised by various factors that are important regulators in the attraction and migration of mesenchymal stromal cells (MSCs) towards sites of injury. MSC migration is an important step in the repair process, as MSCs must first migrate to the site of the defect before they can begin the process of osteochondral tissue repair. Excessive or prolonged inflammation, however, can hinder tissue repair and may lead to the formation of inferior quality repair tissue. Early inhibition or reduction of inflammation may improve tissue formation, but it was unknown whether this would have a negative effect on the migration of MSCs to the defect site in the early phases of the repair process. In **chapter 2**, we investigated the effect of synovial inflammation on MSC migration *in vitro* and tested whether the modulation of inflammation using triamcinolone acetate (TAA), a corticosteroid, would affect migration. The results showed that synovial inflammation promoted MSC migration and that TAA further enhanced this process by increasing the ability of anti-inflammatory and repair macrophages to stimulate MSC migration. Specifically, TAA decreased the percentage of pro-inflammatory macrophages and increased the percentage of anti-inflammatory macrophages. Because of these positive effects we decided to use this clinically applied drug in a setting that more closely resembles the actual situation in an osteochondral defect. In **chapter 3** we evaluated the effect of intra-articular injection of TAA in an osteochondral repair mouse model and found that it reduced synovial inflammation, had no effect on cell migration, but negatively affected cartilage repair. Although our findings suggested that modulation of inflammation might be a promising strategy for enhancing the endogenous repair of osteochondral defect, TAA seems not to be the right tool to do so. Future therapies targeting anti-inflammatory macrophages may improve MSC migration and should have no negative effect on the developing osteochondral tissue, thereby promoting osteochondral regeneration.

Another approach to repair osteochondral defects is the use of biomaterials such as hydrogels and scaffolds. These biomaterials have demonstrated to support osteochondral repair *in vitro* but face challenges *in vivo* related to limited cellular invasion. In **chapter 4** we investigated the effect of three different modifications to three cell-free hydrogels on cell migration and related tissue formation for the repair of osteochondral defects. We found that modification of hydrogels by reducing the crosslinking density, use of a degradable crosslinker or including fibrillar collagen

can control and improve cell migration and tissue formation. In **chapter 5** we aimed to improve migration and thereby osteochondral repair by adsorbing BMP-2 and/or PDGF-BB onto a bi-layered collagen/collagen-magnesium-hydroxyapatite scaffold. We found that adding BMP-2 or PDGF-BB increased migration of cells into the biomaterial in an early stage of repair.

The implantation of a biomaterial, as we did in **chapters 4 and 5**, elicits an inflammatory response, and the resolution of inflammation is crucial for optimal repair. The type of biomaterial and its design can impact the intensity and duration of the inflammatory response, and it is therefore important to carefully design and select biomaterials that elicit an appropriate inflammatory response for optimal osteochondral repair. In general, the hydrogels used in **chapter 4** induced a minor inflammatory response with limited invasion of inflammatory cells. Conversely, the collagen/hydroxyapatite scaffold used in **chapter 5** showed more inflammation, and it was found that this inflammatory response is necessary for successful osteochondral repair. Interestingly, preliminary experiments showed that absence of inflammation after implantation of a scaffold did not lead to tissue repair, supporting the idea that inflammation is critical for successful biomaterial-assisted tissue repair. Pre-screening tools to evaluate the inflammatory response could help to improve the outcome of biomaterial-assisted tissue repair. While macrophages are well-studied for their role in the inflammatory response, neutrophils also play an important role in this process. In **chapter 6**, we focused specifically on the set-up to study the response of human primary neutrophils to a range of naturally- and synthetically-derived materials *in vitro*. We showed that neutrophils had increased survival on naturally derived constructs and exhibited a higher oxidative burst, decreased myeloperoxidase and neutrophil elastase, and decreased cytokine secretion compared to neutrophils on synthetic materials. This culture model can be used to pre-screen the response to biomaterials prior to *in vivo* experiments.

Further studies should concentrate on the comprehensive involvement of the immune system, including neutrophils and macrophages, in osteochondral repair and their interplay rather than focusing on one immune cell type only. By doing so, we can ultimately tune the inflammatory response and improve the outcome of osteochondral repair. Biomaterial-guided osteochondral repair should focus on improving our understanding of the interplay between biomaterials, the immune system, and repair cells. Understanding the impact of these factors on osteochondral repair will be essential for actively modulating inflammation and designing biomaterials to achieve successful functional osteochondral repair and integration of the repair tissue with the original tissue at the defect edges.

9

Nederlandse samenvatting

NEDERLANDSE SAMENVATTING

Osteochondrale defecten omvatten zowel het gewrichtskraakbeen als het onderliggende subchondrale bot en kunnen leiden tot invaliditeit. Osteochondrale defecten gaan gepaard met gewrichtsontsteking. Ontsteking speelt een cruciale rol in de wondgenezing en wordt gekenmerkt door verschillende factoren die belangrijk zijn in het aantrekken en de migratie van mesenchymale stromale cellen (MSCs) naar plaatsen waar weefselschade is opgetreden. MSC-migratie is een belangrijke stap in het reparatieproces, aangezien MSCs eerst naar de plaats van het defect moeten migreren voordat ze het proces van weefselherstel kunnen starten. Overmatige of langdurige ontsteking kan echter het weefselherstel belemmeren en kan leiden tot de vorming van weefsel van matige kwaliteit. Vroege remming of vermindering van ontsteking kan de weefselvorming verbeteren, maar het was onbekend of dit een negatief effect zou hebben op de migratie van MSCs naar de plaats van het osteochondraal defect in de vroege fasen van het reparatieproces. In **hoofdstuk 2** hebben we het effect van synoviale ontsteking op MSC-migratie middels celkweek onderzocht en getest of de remming van ontsteking met triamcinolonacetonide (TAA), een corticosteroïd, de migratie beïnvloedde. De resultaten toonden aan dat synoviale ontsteking MSC-migratie stimuleerde en dat TAA dit proces verder stimuleerde via “ontstekingsremmende” en “reparatie” macrofagen. Specifiek verminderde TAA het percentage ontstekingsbevorderende macrofagen en verhoogde het percentage ontstekingsremmende macrofagen. Op basis van deze positieve effecten besloten we dit medicijn dat ook in de klinische praktijk al wordt toegepast, te gebruiken in een situatie die meer lijkt op de werkelijke situatie bij een osteochondraal defect. In **hoofdstuk 3** hebben we daarom het effect van injectie van TAA in het kniegewricht geëvalueerd in een muismodel voor osteochondraal herstel. We ontdekten dat TAA de synoviale ontsteking verminderde, geen effect had op celmigratie, maar een negatief effect had op het kraakbeenherstel. Hoewel onze bevindingen suggereren dat modulatie van ontsteking een veelbelovende strategie zou kunnen zijn om het lichaamseigen herstel van osteochondrale defecten te verbeteren, lijkt TAA niet het juiste middel te zijn om dit te doen. Toekomstige behandelingen gericht op ontstekingsremmende macrofagen kunnen de MSC-migratie verbeteren, maar mogen geen negatief effect hebben op het zich ontwikkelende osteochondrale weefsel, waardoor herstel wordt bevorderd.

Het herstel van osteochondrale defecten kan ook verbeterd worden door het gebruik van biomaterialen. Deze biomaterialen hebben aangetoond het osteochondrale herstel in celkweek experimenten te ondersteunen, maar worden in dierstudies en klinische studies geconfronteerd met uitdagingen gerelateerd aan beperkte celingroei. In

hoofdstuk 4 onderzochten we het effect van drie verschillende aanpassingen van hydrogels, op celmigratie en gerelateerde weefselvorming voor het herstel van osteochondrale defecten. Hydrogels zijn biomaterialen met een grote hoeveelheid water. We ontdekten dat aanpassingen van hydrogels door het verminderen van de crosslink-dichtheid, het gebruik van een afbreekbare crosslinker of het toevoegen van collageen, de celmigratie en weefselvorming kunnen verbeteren. In **hoofdstuk 5** richtten we ons op het verbeteren van defectherstel door BMP-2 en/of PDGF-BB te adsorberen op een uit twee lagen bestaand biomateriaal van collageen/collageen-magnesium-hydroxyapatiet. We ontdekten dat het toevoegen van BMP-2 of PDGF-BB de migratie van cellen in het biomateriaal in een vroeg stadium van herstel mogelijk kan verhogen.

De implantatie van een biomateriaal, zoals we deden in **hoofdstukken 4 en 5**, veroorzaakte een ontstekingsreactie en het verdwijnen van deze ontsteking is cruciaal voor optimaal herstel van het defect. Het type biomateriaal en het ontwerp ervan kunnen de intensiteit en duur van de ontstekingsreactie beïnvloeden, en het is daarom belangrijk om zorgvuldig biomaterialen te ontwerpen en selecteren die een geschikte ontstekingsreactie opwekken voor optimaal herstel van een osteochondraal defect. Over het algemeen veroorzaakten de hydrogelen die in **hoofdstuk 4** werden gebruikt een minimale ontstekingsreactie en een beperkte invasie van ontstekingscellen. In tegenstelling hiermee gaf het collageen/hydroxyapatiet biomateriaal dat in **hoofdstuk 5** werd gebruikt meer ontsteking, en vonden we dat deze ontstekingsreactie noodzakelijk is voor succesvol herstel van het osteochondrale defect. Interessant genoeg toonden nog niet gepubliceerde experimenten aan dat bij implantatie van een biomateriaal dat geen ontsteking gaf, er geen weefselherstel optrad, wat de gedachte ondersteunt dat ontsteking cruciaal is voor succesvol biomateriaal- ondersteund weefselherstel. Hulpmiddelen om deze ontstekingsreactie te evalueren vóór gebruik, kunnen helpen bij het verbeteren van de uitkomst van biomateriaal-ondersteund weefselherstel.

Hoewel macrofagen goed bestudeerd zijn vanwege hun rol in de ontstekingsreactie, hebben neutrofielen, die ook een belangrijke rol spelen in dit proces, veel minder aandacht gehad. In **hoofdstuk 6** hebben we ons specifiek gericht op het bestuderen van de reactie van neutrofielen geïsoleerd uit menselijk bloed in het laboratorium, op een reeks van biomaterialen gemaakt van natuurlijke of synthetische componenten. We hebben aangetoond dat neutrofielen langer overleven op natuurlijke materialen en een hogere oxidatieve burst, lagere myeloperoxidase en neutrofiel elastase en lagere cytokine-secretie hadden, in vergelijking met neutrofielen op synthetische materialen.

Dit laboratoriummodel kan worden gebruikt om de reactie op biomaterialen te testen vóór dat deze geïmplantéerd worden in een dier of mens.

Toekomstige onderzoeken zouden zich moeten concentreren op de betrokkenheid van het complete immuunsysteem, inclusief neutrofielen en macrofagen, bij het herstel van osteochondrale defecten, in plaats van zich te richten op één type ontstekingscel. Door dit te doen, kunnen we uiteindelijk de ontstekingsreactie afstemmen en de uitkomst van osteochondraal defectherstel verbeteren. Herstel van osteochondrale defecten met behulp van biomaterialen zou zich moeten richten op het verbeteren van ons begrip van de interactie tussen biomaterialen, het immuunsysteem en de cellen verantwoordelijk voor het herstel. Het begrijpen van de impact van deze factoren op het herstel van osteochondrale defecten is essentieel voor het actief moduleren van ontsteking en het ontwerpen van biomaterialen om functioneel herstelweefsel te krijgen en integratie van het herstelweefsel met het oorspronkelijke weefsel aan de defectranden te bereiken.

A large, bold, dark gray letter 'A' is positioned on the right side of the page. To its right is a solid gray square that extends to the right edge of the page. The letter 'A' is partially overlaid by the gray square.

Appendices

A large, bold, dark gray letter 'A' is positioned on the right side of the page. To its right is a solid gray square that extends to the right edge of the page. The letter 'A' is partially overlaid by the gray square.

List of publications

LIST OF PUBLICATIONS

Schwab A*, Wesdorp MA*, Xu J, Abinzano F, Loebel C, Falandt M, Levato R, Eglin D, Narcisi R, Stoddart MJ, Malda J, Burdick JA, D'Este M, van Osch GJVM. Modulating design parameters to drive cell invasion into hydrogels for osteochondral tissue formation.

Journal of Orthopedic Translation. 2023 Sep 4:41;42-53.

Xu J, Fahmy-Garcia S, Wesdorp MA, Kops N, Forte L, De Luca C, Misciagna MM, Dolcini L, Filardo G, Labberté M, Vancíková K, Kok J, van Rietbergen B, Nickel J, Farrell E, Brama PAJ, van Osch GJVM. Effectiveness of BMP-2 and PDGF-BB Adsorption onto a Collagen/Collagen-Magnesium-Hydroxyapatite Scaffold in Weight-Bearing and Non-Weight-Bearing Osteochondral Defect Bone Repair: In Vitro, Ex Vivo and In Vivo Evaluation.

Journal of Functional Biomaterials. 2023 Feb 16;14(2):111.

Nieboer MF, Reijman M, Wesdorp MA, Bastiaansen-Jenniskens YM, Meuffels DE. Improved Understanding of the Inflammatory Response in Synovial Fluid and Serum after Traumatic Knee Injury, Excluding Fractures of the Knee: A Systematic Review.

Cartilage. 2023 Jan 20:19476035221141417

Wesdorp MA, Schwab A, Bektas EI, Narcisi R, Eglin D, Stoddart MJ, Van Osch GJVM, D'Este M. A culture model to analyze the acute biomaterial-dependent reaction of human primary neutrophils in vitro.

Bioactive Materials. 2022 Jul 2;20:627-637

Wesdorp MA, Moerman S, Vochteloo AJH, Mathijssen NMC. External validation of the Almelo Hip Fracture Score, a prediction model for early mortality following hip fracture surgery.

European Journal of Trauma and Emergency Surgery. 2022 Jun;48(3):1871-1877

Wesdorp MA, Capar S, Bastiaansen-Jenniskens YM, Kops N, Creemers LB, Verhaar JAN, Van Osch GJVM, Wei W. Intra-articular Administration of Triamcinolone Acetonide in a Murine Cartilage Defect Model Reduces Inflammation but Inhibits Endogenous Cartilage Repair.

The American Journal of Sports Medicine. 2022 May;50(6):1668-1678

Wesdorp MA, Bastiaansen-Jenniskens YM, Capar S, Verhaar JAN, Narcisi R, Van Osch GJVM. Modulation of Inflamed Synovium Improves Migration of Mesenchymal Stromal Cells in Vitro Through Anti-Inflammatory Macrophages. *Cartilage*. 2022 Jan-Mar;13(1):19476035221085136

Wesdorp MA, Eijgenraam SM, Meuffels DE, Bierma-Zeinstra SMA, Kleinrensink GJ, Bastiaansen-Jenniskens YM, Reijman M. Traumatic Meniscal Tears Are Associated With Meniscal Degeneration. *The American Journal of Sports Medicine*. 2020 Aug;48(10):2345-2352

Eijgenraam SM, Bovendeert FAT, Verschueren J, van Tiel J, Bastiaansen-Jenniskens YM, Wesdorp MA, Nasserinejad K, Meuffels DE, Guenoun J, Klein S, Reijman M, Oei EHG. T2 mapping of the meniscus is a biomarker for early osteoarthritis. *European Radiology*. 2019 Oct;29(10):5664-5672



A

PhD Portfolio

PHD PORTFOLIO

Personal details

Name	Marinus Anthonie Wesdorp
Department	Orthopaedics and Sports Medicine, Erasmus MC University Medical Center, Rotterdam, The Netherlands
Research school	Postgraduate school Molecular Medicine / Erasmus MC Graduate School
PhD period	May 2018 - December 2021
Promotors	Prof. Gerjo J.V.M. van Osch, PhD and Prof. Jan A.N. Verhaar, MD, PhD
Co-promotor	Roberto Narcisi, PhD

Workload (ECTS)

Courses

Nov 2018	SCORE course MolMed	1.0
Jan 2019	Systematisch literatuuronderzoek PubMed/ Embase. Reviews: project management Endnote	1.0
Apr 2019	Laboratory Animal Science	3.0
Jun 2019	Scientific Integrity	0.3
Nov 2020	Biomedical writing course	2.0
Mar 2019	23 rd Molecular Medicine Day, Rotterdam. Poster	0.5

(Inter)national Conferences

Oct 2019	15 th ICRS World Congress, Vancouver, Canada. Oral	1.0
May 2020	TERMIS-EU Manchester, United Kingdom. Oral	covid-19
Nov 2020	29 th annual meeting NBTE, @home, Online. Oral	1.0
Feb 2021	ORS annual meeting, @home, Online. Oral	1.0
Okt 2021	NOV jaarcongres 2021, Den Bosch. Oral	1.0
Nov 2021	6th TERMIS World Congress @home, Online. 2 Orals	2.0
Dec 2021	eCM Biofabrication for Orthopaedics Davos, Switzerland. Oral	covid-19

Department/consortium presentations and meetings

2018-2021	Lab meetings department of Orthopaedics (weekly)	2.0
2018-2021	Research meetings department of internal medicine/ Skeleton meetings	2.0

2018-2021	Journal Club (monthly)	1.0
2018-2021	AOCD consortium meetings	1.0
2018-2021	Lab-clinic meeting (quarterly)	0.5
2018-2021	Orthopaedics and Sports Medicine Science Day (annually)	0.5

Teaching and student supervision

2018-2021	Teaching minor orthopedic sports traumatology	1.0
2018-2021	Supervising bachelor students writing assignment minor orthopedic sports traumatology	1.0
2018-2019	Supervising bachelor student systematic review elective disorders of the musculoskeletal system	0.5
2020-2021	Supervising bachelor students systematic review elective regenerative medicine	0.5
2020-2021	Supervising PhD student Jietao Xu	4.0

Miscellaneous

2018-2021	Organization lab-clinic meetings Orthopaedics and Sports Medicine	0.5
Oct 2019 - Sep 2020	Research Fellowship at AO Research Institute Davos, Switzerland	8.0
Jan 2020	Organization ski trip Orthopaedics and Sports Medicine	0.5
2020-2022	Organization sporthopedie	0.5
Jan 2021	Organization science day Orthopaedics and Sports Medicine	0.5

Awards

Apr 2021	EuroNanoMed3 Review Seminar, Best Poster Award	
----------	--	--

Total 37.8



A

Dankwoord

DANKWOORD

De afgelopen jaren zijn voorbij gevlogen. In het begin klonk het als een utopie dat ik ooit een boekwerk als proefschrift zou produceren en twijfelde ik wel eens of het ooit wel af zou komen. Gelukkig sta je er niet alleen voor en zijn er veel personen die ieder op hun eigen wijze hebben bijgedragen aan dit boek. Een aantal van hen wil ik in het bijzonder bedanken.

Prof. dr. G. J.V.M. van Osch, beste Gerjo, tijdens mijn masteronderzoek leek het jou een goed idee een keer koffie te drinken en voor ik het wist begon ik driekwart jaar later met dit promotietraject. Ik wil graag mijn oprechte dankbaarheid en waardering uitspreken voor de onschatbare begeleiding die je me gedurende mijn hele promotietraject hebt geboden, en de mogelijkheden die je me hebt gegeven om mijn dromen na te jagen. Ik begrijp nog steeds niet hoe iemand met jouw agenda het voor elkaar krijgt om binnen een dag na het versturen van een nieuw manuscript hierop te reageren met minimaal 500 comments, ik vind het bewonderenswaardig hoe je zoveel ballen in de lucht weet te houden en altijd voor iedereen tijd hebt. Dank ook voor alle lichtpuntjes die je steeds zag in mijn data als ik weer eens dacht dat het waardeloos was. Ik durf met trots te zeggen dat ik me geen betere promotor had kunnen wensen. Dank voor alles!

Prof. dr J.A.N. Verhaar, beste professor Verhaar, dank voor uw kostbare tijd, begeleiding, adviezen en onze gezellige gesprekken over skiën en Davos. U heeft niet alleen als mijn promotor gefungeerd, maar ook als een voorbeeld. Dankuwel dat u mij de kans heeft geboden om na mijn promotietraject mijn eerste stappen in de kliniek te zetten om ervaring op te doen binnen de orthopedie.

Ik wil graag mijn oprechte dank uitspreken aan **Dr. Bastiaansen-Jenniskens**, beste Yvonne, dank voor het vertrouwen wat je in me had tijdens mijn masteronderzoek en de kans die je me hebt geboden om dit promotietraject te starten. Hoewel onze samenwerking slechts een jaar heeft geduurd, heeft jouw begeleiding en oprechte betrokkenheid bijgedragen aan de kwaliteit van mijn werk en geholpen om mijn academische doelen te bereiken. I would also like to express my gratitude to **Dr. Roberto Narcisi**, who seamlessly stepped into the role of co-promotor after Yvonne's departure. I am thankful for his willingness to take on this responsibility and for his role in shaping the final stages of my work. I hope that one day we will run a marathon together. Grazie!

Prof. dr. Bouten, prof. dr. Dolhain en prof. dr. Karperien, leden van de beoordelingscommissie. Hartelijk dank voor jullie tijd en voor het kritisch lezen en beoordelen van dit proefschrift.

Dr. van der Windt, beste Anna, mijn allereerste kennismaking met de orthopedie was bij jou op de poli kamer tijdens het coschap heelkunde, wat ontzettend leuk dat je nu onderdeel uitmaakt van de grote commissie, zo is de cirkel weer rond. **Prof. dr. Alini**, the famous football player from Locarno who has his own Panini sticker and became a great scientist. Thank you for being part of the committee, it is an honour to have you here.

Mijn oprechte dank gaat uit naar de onmisbare ‘labmoeders’, **Nicole, Wendy, Janneke en Sandra**. Jullie toewijding en zorgzaamheid zijn de fundering van het lab. Jullie vrolijkheid, bereidheid om te helpen en de wijze raad die jullie voor me hadden als ik even op het krukje kwam zitten en het niet meer zag zitten, hebben mijn onderzoekservaring verrijkt.

Alle collega’s van het lab **Niamh, Andrea, Letizia, Chantal, Mauricio, Yannick, Enrique, Virginia, Sohrab, Lizette, Shorouk, Kavitha, Mike, Pedro, Encheng, Jietao, Judith** en alle anderen, dankjewel, thank you, grazie, gracias, danke, धन्यवाद, 謝謝 voor de mooie tijd, lab meetings, lab days en biertjes. **Eric**, working with you, has been a delightful experience, and I hold in high regard the valuable insights and guidance you’ve offered. Alle collega’s van het klinische onderzoek **Eline, Annika, Rintje, Michiel, Abigael, Britt, Floris, Lichelle, Joshua, Mark, Tjerk, Fleur, Noortje**, en alle anderen, heel veel dank voor jullie samenwerking, gezelligheid en de potjes tafelvoetbal. In het bijzonder dank aan **Max**, dank dat ik bij jou de eerste orthopedische stappen in het onderzoek mocht zetten en onze eindeloze gesprekken over fietsen en voetbal, inmiddels is jou vast duidelijk wat nu de beste club van Nederland is;)

The incredible experience of my research fellowship in Davos I will never forget. First of all, thank you **prof. dr. David Eglin** and **prof. dr. Geoff Richards** for letting me be part of the AO Family. This journey wouldn’t have been as enriching and successful without the unwavering support and guidance of **dr. Matteo d’Este** and **dr. Andrea Schwab**. My time in Davos taught me to be a ‘real’ scientist and successfully create a new research line and be in charge from start to finish. Danke, **Jan**, für all unsere Langlauf- und Radabenteuer. Vielen Dank an die Budag-Alumni, **Nadine, Andrea, Teresa, Johannes und Maja** für das Teilen der Wohnung, die gemütlichen Aperos und die gemeinsam verbrachte Zeit auf der Dachterrasse. Also, thanks to all other people

from the AO Research Institute who helped me with my research and enrich my life by spending another year in the mountains.

Orthopedisch chirurgen en AIOS van het Erasmus MC dank voor jullie betrokkenheid en de leerzame tijd tijdens mijn eerste klinische stappen binnen de orthopedie. **Prof. Dr. Eygendaal**, mijn eerste stappen in de kliniek waren onder uw begeleiding, dank voor het vertrouwen en de onschatbare lessen in zowel klinisch als bestuurlijk opzicht. Tevens wil ik mijn dank uitspreken aan **dr. Koen Bos**, wiens betrokkenheid bij de voortgang van dit traject erg belangrijk was. Dank voor het vertrouwen dat je in me hebt als toekomstig orthopedisch chirurg. Daarnaast ook een speciale dank aan **dr. Duncan Meuffels**, dank voor het geloof en de begeleiding bij mijn allereerste paper, dit heeft mijn enthousiasme voor de wetenschap aangewakkerd. Als ik weer terug ben in het Erasmus MC hoop ik nog meer van jullie te leren!

Chirurgen en arts-assistenten van het Franciscus Gasthuis & Vlietland, en in het bijzonder opleider **dr. Marijn Poelman**, dank voor de fijne en warme omgeving waarin ik terecht ben gekomen. Dank voor jullie begeleiding en de goede basis die ik bij jullie mag leggen voor mijn verdere carrière, jullie zijn een mooie club.

Het harde werk voor dit proefschrift was nooit mogelijk geweest zonder voldoende ontspanning. Deze ontspanning gaf altijd weer nieuwe energie om door te gaan. Mannen van **Old Times** en de **Raad der Stokken**, dank voor onze bijzondere vriendschap, de jaarlijkse tripjes en mooie momenten die we beleefd hebben. Ondanks dat we over het hele land verspreid zijn, zien we elkaar nog regelmatig. Ik hoop dat onze band nog jarenlang zo sterk en trouw blijft en er nog vele poepchique diners, wintersporten en borrels volgen. **Thomas, Dex en Rico**, dank voor de vele avonturen die wij in de sneeuw en in de lucht hebben beleefd, ik hoop snel weer met jullie op de ski's te staan. **Calvin**, dankjewel voor het weekenden lang beachvolleyballen aan de Nederlandse kust. **Joppe**, bedankt voor de spannende avonden RISK tot diep in de nacht en het proeven van jouw culinaire avonturen. De **Eetclub**, ik ken jullie al vanaf jaar 1 van geneeskunde, dank dat jullie er altijd voor me zijn geweest en voor de nodige ontspanning en Eetclub avonden en weekenden. Ook al ben ik er niet altijd bij, ik weet dat ik altijd bij jullie terecht kan. **Axel en Ghislaine**, dank dat ik ooit bij jullie in huis mocht komen wonen, de vele reizen die we samen gemaakt hebben en de vriendschap die we daardoor hebben ontwikkeld. Ik hoop dat we nog veel mooie avonden bij de Vrienden van Amstel Live gaan beleven. **Nando**, dank dat ik jou via Axel heb leren kennen, onze wekelijkse hardlooprondjes en de vele middagen Formule 1 in de mancave. **Pim**, dank voor onze eindeloze uren op de racefiets na weer een dag promoveren. Ik kom snel weer naar Zwolle om te fietsen.

Lieve **Anke** en **Alain**, **Sanne** en **Kevin**, ik ben gezegend met zo'n geweldige schoonfamilie. Dank dat ik me vanaf het eerste moment ontzettend welkom voelde. Ik ben ontzettend gelukkig met dit warme bad en de nodige afleiding met mooie weekendjes op Vlie. Ik hoop dat we in de toekomst nog veel mooie momenten zullen beleven.

Opa en **oma Wesdorp**, dank voor jullie interesse en support tijdens dit traject. Ik kan nu zeggen dat ik echt 'bijna' klaar ben met studeren;)

Opa Ton en **Oma Corrie**, dank voor jullie steun en in het bijzonder ons wekelijkse woensdag 'kroketengesprek' tijdens mijn jaar in Davos. Ik mis jullie.

Lieve **Joost** en **Koen**, kleine broers. Ook al zien en spreken we elkaar niet regelmatig, ik weet dat ik altijd bij jullie terecht kan. Dank voor jullie onvoorwaardelijke steun gedurende mijn leven en dat ik altijd op jullie kan rekenen. Ik ben trots op jullie en trots dat jullie vandaag mijn paranimf willen zijn.

Lieve **Mam** en **Pap**, woorden kunnen niet beschrijven hoe dankbaar ik ben voor jullie liefde, steun en opofferingen die jullie me gedurende mijn hele leven hebben geschonken. Jullie zijn mijn rotsen, mijn gidsen en mijn grootste supporters. Zonder jullie zou ik niet de persoon zijn die ik vandaag ben. Jullie hebben me geleerd altijd in jezelf te geloven en overal het maximale uit te halen, en voor dat en nog veel meer ben ik jullie eeuwig dankbaar. Mijn succes is jullie succes, en ik draag dit proefschrift op aan jullie beiden met alle liefde en waardering. Ik hoop nog lang van jullie te mogen genieten.

Lieve **Kris**, woorden schieten tekort om mijn dankbaarheid voor jouw onvoorwaardelijke steun en liefde te uiten. Ik ben ontzettend dankbaar voor de bijzondere momenten die we hebben gedeeld en de herinneringen die we samen hebben gemaakt. Ik kijk vol enthousiasme uit naar de toekomst en naar alle avonturen die nog voor ons liggen. Ik hou van je.



A

Curriculum Vitae

CURRICULUM VITAE

Marinus Anthonie Wesdorp was born on July 5th 1993 in Bergen op Zoom, The Netherlands, and was named Tim by his parents. He graduated from the Regionale Scholen Gemeenschap 't Rijks in Bergen op Zoom with honors in 2011. That same year, he moved to Rotterdam to study Medicine at the Erasmus University Rotterdam. During multiple winter seasons, he worked as a skiing instructor in Fiss, Austria, which was his biggest passion. After that, he completed a research internship at the dept. of Orthopedics at the Erasmus MC University Medical Center, which sparked his interest in fundamental research. He finished his medical internships at the department of Orthopedics of the Reinier de Graaf



hospital in Delft and the department of Trauma surgery in the Tygerberg Hospital in Cape Town, South Africa. He started his PhD-project in May 2018 at the department of Orthopaedics and Sports Medicine under the supervision of dr. Yvonne Bastiaansen-Jenniskens, dr. Roberto Narcisi, Prof. dr. Jan Verhaar and Prof. dr. Gerjo van Osch. During this period as PhD candidate, he spent a year in the mountains, combining research at the AO Research Institute Davos with his passion for skiing and cycling, under the supervision of dr. Andrea Schwab, dr. David Eglin and dr. Matteo D'Este. He began his career in orthopedic surgery as a resident not in training at the Erasmus MC University Medical Center in January 2022, under the supervision of dr. Koen Bos. He was accepted into the orthopedic training program in the ROGO Rotterdam in that same year. In March 2023, he started his training program at the department of Surgery in the Franciscus Gasthuis & Vlietland hospital under the supervision of dr. Marijn Poelman.

